

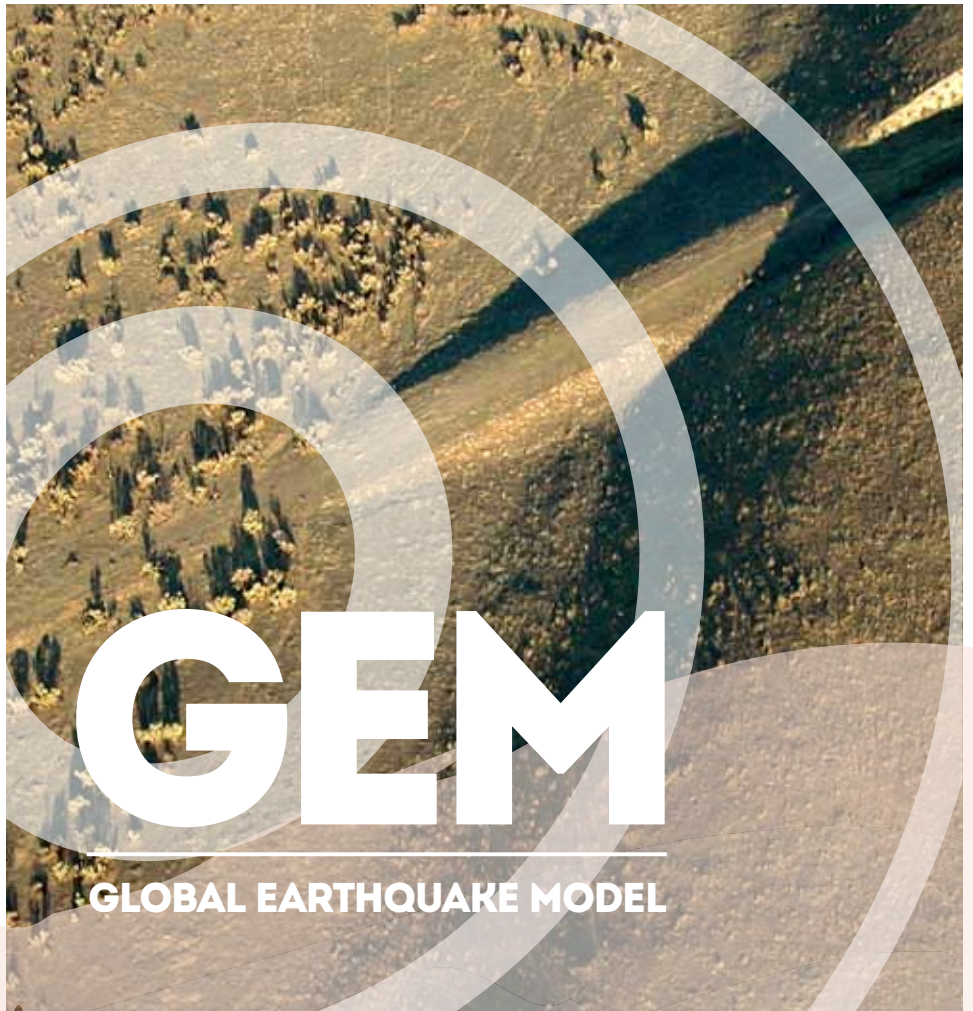
The GEM Faulted Earth Project

GEM TECHNICAL REPORT
2015-02 V1.0.0



Christophersen, A., Berryman,
K., Litchfield, N.

GEOLOGICAL,
EARTHQUAKE AND
GEOPHYSICAL DATA



GLOBAL EARTHQUAKE MODEL

The GEM Faulted Earth Project

The GEM Faulted Earth Global Component Project

Version: 1.0

Author(s): Christophersen, A., Berryman, K., Litchfield, N.

Date: April, 2015

Copyright © 2015 **Christophersen, A., Berryman, K., Litchfield, N.** Except where otherwise noted, this work is made available under the terms of the [Creative Commons license CC BY 3.0 Unported](#)

The views and interpretations in this document are those of the individual author(s) and should not be attributed to the GEM Foundation. With them also lies the responsibility for the scientific and technical data presented. The authors do not guarantee that the information in this report is completely accurate.

Citation: **Christophersen, A., Berryman, K., Litchfield, N. (2015) The GEM Faulted Earth Project, Version 1.0, April 2015, GEM Faulted Earth Project, 8-U 8-8) uk**

www.globalquakemodel.org

ACKNOWLEDGEMENTS

For the review of database schema and report documents we thank Marco Pagani (GEM Foundation, Pavia, Italy), Kathy Haller (USGS, Denver, U.S.), Ross Stein (USGS, Menlo Park, U.S.), Carlos Costa (Universidad Nacional de San Luis, Argentina), Kerry Sieh (Earth Observatory of Singapore), Pilar Villamor (GNS Science, New Zealand), William Ries (GNS Science, New Zealand), Rob Langridge (GNS Science, New Zealand), and Bob Yeats (Oregon State University, U.S.).

For the IT development of the database schema, the database exchange formats, and the up-load of existing databases, we acknowledge Richard Thomas (GNS Science, New Zealand).

For the webtool development we thank Ben Wyss (GEM Foundation, Pavia, Italy), Paul Henshaw (GEM Foundation, Pavia, Italy), Marco Pagani (GEM Foundation, Pavia, Italy), Josh McKenty (formerly GEM Foundation, Pavia, Italy) and John Tartar (formerly GEM Foundation, Pavia, Italy).

For participating in the workshop on subduction zones and contributing to the development of the database of subduction zones, and the accompanying report, we acknowledge Laura Wallace (University of Texas at Austin, U.S.), Gavin Hayes (USGS, Denver, U.S.), Peter Bird (University of California, Los Angeles, U.S.), Kelin Wang (Pacific Geoscience Centre, Sidney, Canada), Roberto Basili (Istituto Nazionale di Geofisica e Vulcanologia, Rome, Italy), Thorne Lay (University of California Santa Cruz, U.S.), Ross Stein (USGS, Menlo Park, U.S.), Takeshi Sagiya (Nagoya University, Japan), Charles Rubin (Earth Observatory of Singapore), Sergio Barrientos (Seismological Service, University of Chile, Chile), Corne Kreemer (University of Nevada, Reno, U.S.), Marco Pagani (GEM Foundation, Pavia, Italy), Ken Gledhill (GNS Science, New Zealand), Kathy Haller (USGS, Denver, U.S.), Carlos Costa (Universidad Nacional de San Luis, Argentina), Tom Parsons (USGS, Menlo Park, U.S.), and Pat McCrory (USGS, Menlo Park, U.S.).

For the contribution of existing databases we thank Dan Clarke (Geoscience Australia), Andrew McPherson (Geoscience Australia), Richard Koehler (State of Alaska, Division of Geological Surveys, U.S.), Kathy Haller (USGS, Denver, U.S.), Monica Wolfson-Schwehr (University of New Hampshire, U.S.), Margaret Boettcher (University of New Hampshire, U.S.), Yoshioka Toshikazu (National Institute of Advanced Industrial Science and Technology, Tsukuba, Japan).

For compiling the data on the Himalaya Frontal Thrust system and contributing to the report we acknowledge William Ries (GNS Science, New Zealand) and Steve Wesnousky (University of Nevada, Reno, U.S.).

For the compilation and review of scaling relationships we thank Mark Stirling (GNS Science, New Zealand) and Tatiana Goded (GNS Science, New Zealand).

For the participation and contributions to the Southeast Asia Workshop we acknowledge Pilar Villamor (GNS Science, New Zealand), Nick Horspool (GNS Science, New Zealand), Teraphan Ornthammarath (Department of Civil and Environmental Engineering, Mahidol University, Thailand, formerly RIMES, the Regional Integrated Multi-Hazard Early Warning System for Africa and Asia, and AIT, the Asian Institute of Technology, Thailand), Danny Hilman Natawidjaja (Indonesian Institute of Sciences), Mudrik Daryono (Indonesian Institute of Sciences), Asdani Soehaimi (Indonesian Geological Agency), Cipta Athanasius (Indonesian Geological Agency), Thura Aung (Myanmar Earthquake Committee), Mathew Moihoi (Department of Mineral Policy & Geohazards Management, Papua New Guinea), Marie Etchebes (Earth Observatory of Singapore, Nanyang Technical University, Singapore), Phan Trong Trinh (Institute of Geological Science, Vietnam), Maria Isabel T. Abigania (PHIVOLCS, The Philippines), Mabelline T. Cahulogan (PHIVOLCS, The Philippines), Passakorn Pananont (Kasetsart University, Thailand), Suwith Kosuwan (Department of Mineral Resources,

Thailand), Prinya Putthapiban (Mahidol University, Thailand), Kruawun Jankaew (Chulalongkorn University, Thailand), Thanu Harnpattanapanich (Panya Consultant, Thailand), Anuthep Chaovanalikit (Panya Consultant, Thailand), Barry Abonales (RIMES, the Regional Integrated Multi-Hazard Early Warning System for Africa and Asia, and AIT, the Asian Institute of Technology, Thailand), Pichapon Robru (RIMES, the Regional Integrated Multi-Hazard Early Warning System for Africa and Asia, and AIT, the Asian Institute of Technology, Thailand), Songkhun Boonchaisuk (Mahidol University, Thailand), Sutthipong Noisagool (Mahidol University, Thailand), Acharah Photisom (Department of Mineral Resources, Thailand), Kyle Bradley (Earth Observatory of Singapore Singapore, Nanyang Technical University, Singapore), and Pennung Warnitchai (Asian Institute of Technology, Thailand).

For the participation and contributions to the Mexico Workshop we acknowledge Pilar Villamor (GNS Science, New Zealand), Ramon Zuñiga (Centro de Geociencias de Juriquilla, Universidad Nacional Autónoma de Mexico), Rob Langridge (GNS Science, New Zealand), Victor Hugo Garduno-Monroy (Universidad de Michoacana de Sam Nicolas de Hidalgo, Morelia, Mexico), Diana C. Soria Caballero (Universidad de Michoacana de Sam Nicolas de Hidalgo, Morelia, Mexico), Maria Magdalena Vazquez Bucio (Universidad de Michoacana de Sam Nicolas de Hidalgo, Morelia, Mexico), Avith Mendoza (Universidad de Michoacana de Sam Nicolas de Hidalgo, Morelia, Mexico), Ana Paula Hernández (CICESE, Ensenada, Baja California, Mexico), Tania Gonzalez (Earth Consultants International, Santa Ana, CA, USA), Aníbal Godoy (Universidad Politécnica de Ingeniería, Honduras), Luis Eveline (Universidad Politécnica de Ingeniería, Honduras), Manuel Rodriguez Maradiaga, Jose J. Diaz Martinez (Universidad Complutense de Madrid, Spain), Antonio Alvarez (INETER, Managua, Nicaragua), Ing. Marisol Echaverry López (INETER, Managua, Nicaragua), Carlos Rubi (Centro de Estudios Geológicos de la Univ. de Managua, Panama), Walter Montero (Centro de Investigaciones en Ciencias Geológicas, Universidad de Costa Rica), Esteban Chaves (Ovsicori, Universidad Nacional de Costa Rica), Allan López (ICE, Costa Rica), Arkin Tapia (Geosciences Institute of the University of Panamá), Benjamin Ponce (Geoambiente SA, Mexico DF), Gerardo Aguirre (Centro de Geociencias, UNAM Juriquilla, Queretaro), Pierre Lacan (Centro de Geociencias, UNAM Juriquilla, Queretaro), Rodrigo Portillo (Centro de Geociencias, UNAM Juriquilla, Queretaro), Jorge Arzate (Centro de Geociencias, UNAM Juriquilla, Queretaro), Ivan Sune (Centro de Geociencias, UNAM Juriquilla, Queretaro), Gonzalo Cid (Centro de Geociencias, UNAM Juriquilla, Queretaro), Jorge Nieto (Facultad de Ingeniería, UNAM, Mexico DF), Daniele Dell'Erba (Centro de Geociencias, UNAM Juriquilla, Queretaro), Rodrigo Leon (Centro de Geociencias, UNAM Juriquilla, Queretaro).

For the book *Active Faults of the World* we thank Bob Yeats (Oregon State University, U.S.) and Kristine Weber (Cartographic Services, Portland, Oregon, U.S.).

ABSTRACT

This is the final report of the GEM Faulted Earth Project (GFE), which was active between 2010 and 2013. GFE set out to build a global active fault database with a common set of strategies, standards and formats, to be placed in the public domain. Nearly 100 individuals from 43 institutions in 21 countries contributed to GFE by providing feedback on the database design and the compilation tool, as well as the documents describing them, contributing data and participating in several workshops.

The highlights of GFE are:

- A database schema for neotectonic faults, folds and fault sources, accompanied by a Data Dictionary, and IT documentation.
- Upload of six pre-existing national databases as well as a global mid-ocean ridge transform database to the database.
- In collaboration with GEM the development of the GFE compilation tool, which is fully integrated into the OpenQuake platform, and is accompanied by guidelines.
- Characterisation of the world's subduction plate interfaces as basis for generating earthquake event sets for inclusion in earthquake hazard and risk.
- Characterisation of the Himalayan Frontal Thrust largely following the methods developed for oceanic subduction zones as basis for generating earthquake event sets for inclusion in earthquake hazard and risk.
- A review of magnitude scaling relationships and publication of the recommendations.
- The publication of the book 'Active Faults of the world'.
- Regional workshops in Southeast Asia and Central America to train geologists in the use of the compilation tool and general aspects of active fault mapping and characterisation.

The development of a modern neotectonic fault database structure and a unique graphical interface for the compilation of new fault data is a generational advance on previous databases. The GFE database utilises the best aspects of national databases currently in existence around the world and condenses these into a minimum set of requirements that drive a globally consistent procedure for characterising fault data inputs to seismic hazard and risk assessment in the GEM platform.

Achieving global coverage data coverage has been a challenge for many reasons. Data that were promised at the stage of proposal writing were not available during the project. Many regions of the world have only limited capability to compile fault data and building capability requires more resources than available in the GFE budget. Some countries have concerns about information on active faults being in the public domain. However, GFE has laid a good foundation in developing the database structure and a series of guidelines and reports, and in collaboration with GEM in developing the online data compilation tool. For parts of the world with no or only partly coverage of neotectonic fault data, we recommend the establishment of national programmes to map, compile and synthesise neotectonic fault data under the auspices of a database manager. In this way, consistently compiled neotectonic faults can contribute to seismic hazard assessment. The availability of international standards will help collaboration across national borders.

Keywords: Neotectonic faults; fault sources; database design; OpenQuake webtool

TABLE OF CONTENTS

	Page
ACKNOWLEDGEMENTS.....	ii
ABSTRACT	iv
TABLE OF CONTENTS	v
LIST OF FIGURES.....	xv
LIST OF TABLES.....	xvii
1 Introduction.....	1
2 Inventory of existing fault databases and data attributes.....	3
2.1 Introduction.....	3
2.2 Description and inventory of existing fault databases and data attributes.....	3
2.2.1 The INGV Database of Individual Seismogenic Sources (DISS)	3
2.2.2 The USGS Quaternary faults and folds Database.....	4
2.2.3 The AIST RIO-DB Active Fault Database of Japan.....	4
2.2.4 The Map and Database of Quaternary Deformation for Andean Countries	4
2.2.5 The New Zealand Active Faults Database of GNS Science	4
2.2.6 The New Zealand National Seismic Hazard Model of GNS Science	5
2.2.7 Taiwan Active Fault Database	5
2.2.8 Afghanistan Fault Database	5
2.2.9 Global subduction zones, mid-ocean ridges, transforms, and diffuse deformation zones	5
2.2.10 Seismic Hazard Harmonization in Europe (SHARE)	6
2.2.11 Earthquake Model in the Middle East Region (EMME)	6
2.2.12 Inventory of data attributes.....	6
2.3 Critical review of accessible databases for use in the design of the GEM Faulted Earth.....	10
2.3.1 Database types.....	10
2.3.2 Data accessibility and database documentation	11
2.3.3 Review of database attributes	11
2.3.4 Specific review comments the INGV Database of Individual Seismogenic Sources (DISS)	11
2.3.5 Specific review comments the USGS Quaternary faults and folds Database	11
2.3.6 Specific review comments the AIST RIO-DB Active Fault Database of Japan	11
2.3.7 Specific review comments the GNS New Zealand Active Faults Database.....	12
2.3.8 Specific review comments global subduction zones, oceanic ridges, transforms, and diffuse deformation zones	12

3	Database design process, philosophies and structure	13
3.2	Database design philosophies and structure	13
3.2.4	Neotectonic folds – blind faults	17
3.2.5	Automatic derivation or calculation of fault sources.....	17
3.2.6	Data completeness factors	17
3.2.7	Uncertainties.....	18
4	Data Dictionary	19
4.1	Introduction.....	19
4.2	Neotectonic faults	20
4.2.1	Accuracy (Traces, Observations: Events, Observations: Displacement, Observations: Slip Rates, Observations: Fault Geometry)	20
4.2.2	Age of last movement (Fault Sections, Faults; Observations: Events).....	20
4.2.3	Age of last movement category (Fault Sections, Observations: Events)	20
4.2.4	Aseismic-slip factor (Fault Sections, Faults).....	20
4.2.5	Aseismic-slip factor completeness (Fault Sections, Faults).....	20
4.2.6	Compiled by (Fault Sections, Faults).....	21
4.2.7	Contributed by (Fault Sections, Faults).....	21
4.2.8	Created at (Fault Sections, Faults*)	21
4.2.9	Dip (Fault Sections, Faults).....	21
4.2.10	Dip completeness (Fault Sections, Faults)	21
4.2.11	Dip direction (Fault Sections, Faults, Observation: Fault Geometry)	22
4.2.12	Dip direction completeness (Fault Sections, Faults)	22
4.2.13	Dip displacement (Fault Sections, Observations: Displacement)	22
4.2.14	Dip slip rate (Fault Sections, Observations: Slip rates)	23
4.2.15	Displacement (Fault Sections, Faults)	23
4.2.16	Displacement category (Fault Sections, Observations: Displacement)	23
4.2.17	Downthrown side (Fault Sections, Faults, Observations: Fault geometry).....	23
4.2.18	Episodic behaviour (Fault Sections, Faults).....	24
4.2.19	Geomorphic Expression (Traces)	24
4.2.20	Historical earthquake (Fault Sections, Observations: Events)	25
4.2.21	Horizontal displacement (Fault Sections, Observations: Displacement)	25
4.2.22	H:V ratio (Fault Sections, Observations: Slip rates)	25
4.2.23	Last updated	25
4.2.24	Length (Fault Sections, Faults)	25
4.2.25	Location Method (Traces)	25
4.2.26	Lower seismogenic depth (Fault Sections, Faults)	26
4.2.27	Lower seismogenic depth completeness (Fault sections, Faults).....	26

4.2.28	Marker age (Fault Sections, Observations: Slip rates, Observations: Displacement, Observations: Events).....	26
4.2.29	Name (Traces, Fault Sections, Faults)	27
4.2.30	Net displacement (Fault Sections, Observations: Displacement).....	27
4.2.31	Net slip rate (Fault Sections, Faults, Observations: Slip rates)	27
4.2.32	Net slip rate completeness (Fault Sections, Faults)	27
4.2.33	Notes (Traces, Fault Sections*, Faults*, Observations: Events, Observations: Displacement, Observations: Slip Rates, Observations: Fault Geometry)	27
4.2.34	Overall completeness (Fault Sections, Faults)	27
4.2.35	Pre-historical earthquake (Fault Sections, Observations: Events).....	28
4.2.36	Rake (Fault Sections, Faults, Observations: Slip rates)	28
4.2.37	Recurrence interval (Fault Sections, Faults, Observations: Events).....	28
4.2.38	Recurrence interval category (Fault Sections, Observations: Events)	29
4.2.39	References *	29
4.2.40	Scale (Traces, Observations: Events, Observations: Displacement, Observations: Slip Rates, Observations: Fault Geometry)	29
4.2.41	Site feature (Observations: Events, Observations: Displacement, Observations: Slip Rates, Observations: Fault Geometry)	29
4.2.42	Slip rate category (Fault Sections, Observations: Slip rates)	29
4.2.43	Slip type (Fault Sections, Faults, Observations: Slip rates)	30
4.2.44	Slip type completeness (Fault Sections, Faults)	31
4.2.45	Strike (Fault Sections, Faults, Observations: Fault geometry)	31
4.2.46	Strike slip rate (Fault Sections, Faults, Observations: Slip rates).....	31
4.2.47	Surface dip (Observations: Fault geometry)	31
4.2.48	Total displacement (Fault Sections, Observations: Displacement).....	32
4.2.49	Upper seismogenic depth (Fault Sections, Faults).....	32
4.2.50	Upper seismogenic depth completeness (Fault Sections, Faults).....	32
4.2.51	Vertical displacement (Fault Sections, Observations: Displacement)	32
4.2.52	Vertical slip rate (Fault Sections, Faults, Observations: Slip rates).....	32
4.3	Neotectonic Folds*	33
4.3.1	Accuracy (Axial traces, Observations) *	33
4.3.2	Age of last movement (Folds, Blind Faults) *	33
4.3.3	Age of last movement category (Folds) *	33
4.3.4	Aseismic-slip factor (Folds, Blind Faults) *	33
4.3.5	Axial plane dip (Folds) *	33
4.3.6	Axial plane dip direction (Folds) *	34
4.3.7	Compiled by (Folds, Blind Faults) *	34
4.3.8	Contributed by (Folds, Blind Faults) *	34

4.3.9 Created at (Folds, Blind Faults) *	34
4.3.10 Dip (Blind Faults) *	34
4.3.11 Dip completeness (Blind Faults) *	35
4.3.12 Dip direction (Blind Faults) *	35
4.3.13 Dip direction completeness (Blind Faults) *	35
4.3.14 Displacement (Folds) *	35
4.3.15 Episodic behaviour (Folds, Blind Faults) *	35
4.3.16 Fold type (Folds) *	36
4.3.17 Geomorphic Expression (Axial traces) *	36
4.3.18 Growth rate – vertical (Folds) *	36
4.3.19 Growth rate – horizontal (Folds) *	37
4.3.20 Last updated *	37
4.3.21 Length (Folds, Blind Faults) *	37
4.3.22 Limb dip – shallow limb (Folds) *	37
4.3.23 Limb dip – steep limb (Folds) *	37
4.3.24 Limb dip direction – shallow limb (Folds) *	37
4.3.25 Limb dip direction – steep limb (Folds) *	38
4.3.26 Location Method (Axial traces) *	38
4.3.27 Lower seismogenic depth (Blind Faults) *	38
4.3.28 Lower seismogenic depth completeness (Blind Faults) *	39
4.3.29 Marker age (Folds) *	39
4.3.30 Name (Axial traces, Folds, Blind Faults) *	39
4.3.31 Net slip rate (Blind Faults) *	39
4.3.32 Net slip rate completeness (Blind Faults) *	39
4.3.33 Notes (Axial traces, Folds, Blind Faults) *	40
4.3.34 Overall completeness (Folds, Blind Faults) *	40
4.3.35 Plunge (Folds) *	40
4.3.36 Plunge direction (Folds) *	40
4.3.37 Recurrence interval (Folds, Blind Faults) *	41
4.3.38 References *	41
4.3.39 Scale (Axial traces, Observations) *	41
4.3.40 Site feature (Observations) *	41
4.3.41 Slip type (Blind Faults) *	41
4.3.42 Slip type completeness (Blind Faults) *	42
4.3.43 Strike (Blind Faults) *	42
4.3.44 Strike slip rate (Blind Faults) *	43
4.3.45 Tilt rate – shallow limb (Folds) *	43

4.3.46	Tilt rate – steep limb (Folds) *	43
4.3.47	Upper seismogenic depth (Blind Faults) *	43
4.3.48	Upper seismogenic depth completeness (Blind Faults) *	43
4.3.49	Vertical slip rate (Blind Faults)	44
4.4	Fault Sources	44
4.4.1	Age of last movement (Fault Sources)	44
4.4.2	Area (Fault Sources)	44
4.4.3	Aseismic-slip factor (Fault Sources)	44
4.4.4	Aseismic-slip factor completeness (Fault Sources)	44
4.4.5	Compiled by (Fault Sources)	45
4.4.6	Contributed by (Fault Sources)	45
4.4.7	Created at (Fault Sources) *	45
4.4.8	Dip (Fault Sources)	45
4.4.9	Dip completeness (Fault Sources)	45
4.4.10	Dip direction (Fault Sources)	46
4.4.11	Dip direction completeness (Fault Sources)	46
4.4.12	Last updated	46
4.4.13	Length (Fault Sources)	46
4.4.14	Lower seismogenic depth (Fault Sources)	46
4.4.15	Lower seismogenic depth completeness (Fault Sources)	47
4.4.16	Maximum magnitude (Fault Sources)	47
4.4.17	Name (Fault Sources)	47
4.4.18	Net slip rate (Fault Sources)	47
4.4.19	Net slip rate completeness (Fault Sources)	47
4.4.20	Notes (Fault Sources) *	48
4.4.21	Overall completeness (Fault Sources)	48
4.4.22	Rake (Fault Sources)	48
4.4.23	Recurrence interval (Fault Sources)	49
4.4.24	References (Fault Source) *	49
4.4.25	Slip type (Fault Sources)	49
4.4.26	Slip type completeness (Fault Sources)	50
4.4.27	Tectonic region (Fault Sources) *	50
4.4.28	Upper seismogenic depth (Fault Sources)	50
4.4.29	Upper seismogenic depth completeness (Fault Sources)	50
4.4.30	Width (Fault Sources)	51
4.5	Maximum magnitude calculation	51
4.6	Recurrence interval calculation	53

5	The database design	54
5.1	Background.....	54
5.2	UML Model.....	54
5.2.1	Gem-Core	55
5.2.2	Gem-Metadata.....	55
5.3	Implementation.....	56
5.3.1	Composite Data values	56
5.3.2	Spatial Characteristics	56
5.3.3	Redundancy	57
5.3.4	Ubiquitous language	57
5.3.5	Version Management.	57
5.3.6	GEM Faulted Earth ERD	57
5.4	Table Descriptions	58
5.5	Interchange Mechanisms	60
5.6	Appendix 1. Sample queries	61
6	The database XML interchange	63
6.1	Introduction.....	63
6.2	Interchange Content	63
6.2.1	XML Entities.	63
6.2.2	Interchange Hierarchy	64
6.2.3	Null values.....	65
6.2.4	Composite data values.....	65
6.2.5	Attribute value descriptions	65
6.2.6	Normalisation.....	66
6.2.7	Recording Lineage.....	66
6.2.8	QualityAssurance	66
6.2.9	Lookup Values	67
6.3	Appendix A Gem Faulted Earth Interchange Entities.....	69
6.4	Appendix B GEM FaultedEarth Observation elements	74
7	Magnitude scaling relationships.....	80
7.1	Introduction.....	80
7.2	Methodology	81
7.2.1	Tectonic Regime.....	81
7.2.2	Quality Score.....	81
7.3	Recommended Regressions	82
7.3.1	Regression Tabulation.....	82
7.3.2	Hanks and Bakun (2008) relationship	86

7.3.3	UCERF2 relationship.....	86
7.3.4	Wesnousky (2008) relationships.....	86
7.3.5	Leonard (2010) relationships.....	87
7.3.6	Yen and Ma (2011) relationships.....	89
7.3.7	Stirling et al. (2008) relationship (New Zealand oblique slip).....	89
7.3.8	Anderson et al. (1996) relationship.....	90
7.3.9	Nuttli (1983) relationship.....	90
7.3.10	Villamor et al. (2007) relationship (New Zealand normal slip).....	91
7.3.11	Strasser et al. (2010) relationships.....	91
7.3.12	Blaser et al. (2010) relationship.....	92
7.3.13	Ichinose et al. (2006) relationship.....	92
7.4	Conclusions.....	93
7.5	Recommendations.....	93
7.6	Other Regressions.....	94
7.6.1	Shaw (2009) relationship.....	94
7.6.2	Ellsworth-B relationship.....	95
7.6.3	Bonilla et al. (1984) relationships.....	95
7.6.4	Stirling et al. (2002) relationship.....	96
7.6.5	Stock and Smith (2000) relationship.....	96
7.6.6	Vakov (1996) relationship.....	97
7.6.7	Stirling et al. (1996) relationships.....	98
7.6.8	Mai and Beroza (2000) relationships.....	98
7.6.9	Somerville et al. (1999) relationship.....	99
7.6.10	Wells and Coppersmith (1994) relationships.....	99
7.6.11	Dowrick and Rhoades (2004) relationship.....	100
7.6.12	Wyss (1979) relationship.....	100
7.6.13	Somerville (2006) relationship.....	100
7.6.14	Ambraseys and Jackson (1998) relationship.....	101
8	Fault compilation tool.....	102
8.1	Introduction and tool overview.....	102
8.1.1	Access and login.....	102
8.1.2	Tool design philosophy.....	103
8.1.3	Tool layout.....	103
8.1.4	Adding and uploading base layers.....	105
8.2	Guidelines for entering new data.....	108
8.2.1	Step 1 – Traces.....	108
8.2.2	Step 2 – Sections.....	111

8.2.3	Step 3 – Faults	113
8.2.4	Step 4 – Fault sources	115
8.2.5	Step 5 – Review fault sources	116
8.2.6	Optional step – Site observations	116
9	Bulk upload of national and global databases	119
9.1	Introduction.....	119
9.2	New Zealand active faults database.....	120
9.3	New Zealand National Seismic Hazard Model.....	121
9.4	Active fault database of Japan	121
9.5	Alaska Quaternary faults and folds database.....	122
9.6	USA Quaternary fault and fold database	123
9.7	Australia neotectonic feature database.....	124
9.8	Mid-ocean ridge transform database.....	125
9.9	New Zealand active faults database (afdb) – attribute mapping, formatting and upload.....	126
9.10	New Zealand National Seismic Hazard Model (NSHM) – attribute mapping, formatting and upload	128
9.11	Active fault database (afdb) of Japan – attribute mapping, formatting and upload	130
9.12	Alaska Quaternary fault and fold database (Qfdb) – attribute mapping, formatting and upload.....	131
9.13	USA Quaternary fault and fold database (Qfdb) – attribute mapping, formatting and upload	133
9.14	Australia neotectonic feature database (nfdb) – attribute mapping, formatting and upload.....	134
9.15	Mid-ocean ridge transform database (Mortdb) – attribute mapping, formatting and upload	137
10	Characterisation of subduction zones	139
10.1	Introduction.....	139
10.2	Procedure	143
10.3	Results	144
10.4	Discussion and Conclusions	160
10.5	Definition of Database Parameters	160
10.6	Additional notes on parameter choices for specific subduction zones/segments	162
10.6.1	Alaska/Aleutian	162
10.6.2	Cascadia	163
10.6.3	Japan	163
10.6.4	Kanto	163
10.6.5	Nankai	163
10.6.6	Kurile	163
10.6.7	Ryukyu.....	163
10.6.8	Izu-Bonin	164
10.6.9	Mariana	164
10.6.10	North Yap, and Palau/South Yap.....	164

10.6.11	Hikurangi	164
10.6.12	Kermadec	164
10.6.13	Tonga.....	165
10.6.14	Puysegur.....	165
10.6.15	Hjort	165
10.6.16	Northwest Solomon	165
10.6.17	Southeast Solomon	166
10.6.18	New Hebrides.....	166
10.6.19	New Britain.....	166
10.6.20	New Guinea.....	167
10.6.21	Manus (east and west).....	167
10.6.22	Andaman	167
10.6.23	Sumatra	167
10.6.24	Java.....	168
10.6.25	Calabria	168
10.6.26	Hellenic.....	168
10.6.27	Cyprus.....	169
10.6.28	Makran	169
10.6.29	Ecuador/Columbia segment of the Andean margin.....	169
10.6.30	Peru segment of the Andean margin	169
10.6.31	Northern Chile segment of the Andean margin.....	169
10.6.32	Central Chile segment of the Andean margin	169
10.6.33	Patagonia (north and south segments).....	169
10.6.34	South Shetland Islands	170
10.6.35	South Sandwich.....	170
10.6.36	Jalisco segment of Middle America.....	170
10.6.37	Michoacan to Guatemala portion of Middle America	170
10.6.38	Middle America – El Salvador to Nicaragua	170
10.6.39	Middle America – Costa Rica to west Panama.....	171
10.6.40	Lesser Antilles.....	171
10.6.41	Manila	171
10.6.42	Philippine.....	171
10.6.43	East Luzon	171
10.6.44	Cotabato.....	172
10.6.45	Sulu.....	172
10.6.46	Minahassa	172
10.6.47	Seram	172

10.6.48	Timor	173
10.6.49	Manokwari	173
10.6.50	Molucca Sea	173
11	Characterisations of the Himalaya frontal thrust system.....	174
11.1	Introduction.....	174
11.2	Method.....	176
11.2.1	Digitising and characterising the HFT trace	176
11.2.2	Defining and characterising segments.....	177
11.2.3	Defining and characterising floating segment	178
11.3	Results	179
11.3.1	HFT traces	179
11.3.2	Segment characterisation	180
11.3.3	HFT Paleoseismology	183
11.4	Conclusions.....	185
12	Towards new neotectonic fault data.....	186
12.1	Overview of the two regional workshops	186
12.2	Overview of the status of active faults in the participating countries in Southeast Asia.....	186
12.2.1	Thailand.....	186
12.2.2	Vietnam.....	187
12.2.3	Myanmar.....	187
12.2.4	The Philippines.....	187
12.2.5	Indonesia.....	187
12.2.6	Papua New Guinea.....	188
12.3	Overview of the status of active faults in the participating countries in Central America	188
12.3.1	Mexico.....	188
12.3.2	Guatemala.....	189
12.3.3	Honduras.....	189
12.3.4	El Salvador	189
12.3.5	Nicaragua	189
12.3.6	Costa Rica	190
12.3.7	Panama	190
12.4	Conclusions and recommendations resulting from the workshops.....	190
12.4.1	Recommendations going forward	191
13	Summary and outlook	193
	REFERENCES.....	194

LIST OF FIGURES

	Page
Figure 3.1 The GEM Faulted Earth conceptual database structure.....	14
Figure 3.2 Schematic maps showing the relationship between traces, sections, faults and fault sources for a) neotectonic faults consisting of more than one section and trace, b) neotectonic faults consisting of one section and one trace.	16
Figure 4.1 Aki and Richards (1980) conventions for noting strike, dip direction, and rake	22
Figure 5.1 GEM-Core UML model.....	55
Figure 5.2 Faulted Earth Observation/Metadata UML.....	56
Figure 5.3 Faulted Earth ERD	58
Figure 6.1 Top level fearth_fault_export element	64
Figure 6.2 Observations child element for NeotectonicSection.....	65
Figure 6.3 Fold length composite attribute values.....	65
Figure 6.4 Attribute group for lower seismogenic depth	66
Figure 6.5 fearth_blind_fault_summary element	69
Figure 6.6 fearth_fault_summary element	70
Figure 6.7 fearth_fold element.....	71
Figure 6.8 fearth_fault_source element.....	72
Figure 6.9 fearth_neotectonic_section element.....	73
Figure 6.10 Dip observation element	74
Figure 6.11 Displacement observation element.....	75
Figure 6.12 Event observation element	76
Figure 6.13 RecurrenceInterval observation element.....	77
Figure 6.14 SectionPlaneGeometry observation element	78
Figure 6.15 Slip observation element.....	79
Figure 7.1 The Darfield earthquake compared to some commonly used regression relationships.....	80
Figure 8.1 Accessing the tool on the OpenQuake website.....	103
Figure 8.2 Layout of the tool with the three main panels labelled in red.....	104
Figure 8.3 Upload a base map layer.	105
Figure 8.4 Upload a GeoTIFF base map layer.	106
Figure 8.5 Upload a Shapefile base map layer.	107
Figure 8.6 Add Metadata to a new base map layer.....	107
Figure 8.7 Display an uploaded base map layer in the map window.....	108
Figure 8.8 Draw a trace.....	109

Figure 8.9 Upload traces.....	110
Figure 8.10 Edit or delete traces.....	111
Figure 8.11 Join traces to form a section.....	112
Figure 8.12 Edit section attributes.	113
Figure 8.13 Join sections to form a fault.	114
Figure 8.14 Enter fault attributes	115
Figure 8.15 Generate a fault source	116
Figure 8.16 Draw a site and enter site observations	117
Figure 8.17 Upload a site and edit site observations	118
Figure 9.1 Active fault and fold traces, and fault source polygons (red) uploaded to the GFE database as at 31 May 2013	119
Figure 9.2 New Zealand active fault traces (red) uploaded to the GFE database	120
Figure 9.3 New Zealand fault source polygons (red) uploaded to the GFE database	121
Figure 9.4 Active fault database of Japan traces uploaded to the GFE database	122
Figure 9.5 Alaska fault and fold traces (red) uploaded to the GFE database. Traces not uploaded are shown in black	123
Figure 9.6 USA active fault and fold traces uploaded to the GFE database (red). Traces not uploaded are shown in black, and fault areas not uploaded in yellow.	124
Figure 9.7 Australia active fault traces (red) uploaded to the GFE database.....	125
Figure 9.8 Mid-ocean ridge transform traces and sources (red) uploaded to the GFE database.	126
Figure 10.1 Location of the subduction zones identified in this database modified from Hayes et al. (2012) reproduced with permission of John Wiley and Sons.	140
Figure 10.2 Subduction zone interface seismicity and trench segmentation, from Heuret et al. (2011) reproduced with permission of John Wiley and Sons.	143
Figure 10.3 Plot showing relationships between maximum magnitude, rupture area, coupling coefficient and relative velocity across the interface for each of the 79 subduction interface zones and their possible segments considered in this study.	146
Figure 11.1 Synopsis of historical and paleoseismic history along the HFT from Kumar et al. (2010) reproduced with permission of John Wiley and Sons.	174
Figure 11.2 Overview of the mapped traces.	180
Figure 11.3 Elevation, coupling coefficient, seismicity rate, temperature on the main Himalayan Thrust (MHT) HFT from Ader et al. (2012) reproduced with permission of John Wiley and Sons.	183

LIST OF TABLES

	Page
Table 2.1 Neotectonic fault and fold attributes in existing databases.....	6
Table 2.2 Fault source attributes in existing databases.	9
Table 2.3 Databases classified into neotectonic fault and fold and fault source types.	10
Table 4.1 Magnitude scaling relationships for calculation of fault source maximum magnitude. From Stirling and Goded (2012) and Stirling et al. (2013).	51
Table 7.1 Tectonic regimes, sub regimes, and mechanisms (slip types) used as a basis for sorting regressions for appropriate use in seismic hazard studies.....	81
Table 7.2 Shortlisted regressions for each combination of tectonic environment, sub-environment and slip-type (underlined = highest priority).....	82
Table 10.1 Subduction Interface Zone Parameters as defined in Section 10.5.....	147
Table 10.2 Compilation of published subduction interface zone b-values.	159
Table 11.1 Definition of the subduction zone parameters used for characterising the HFT segments.....	177
Table 11.2 Attributes of the three HFT segments	181
Table 11.3 Attributes of the segment HFT Paleoseismology.....	184
Table 12.1 Seismic stations and accelerometers in Central America (Rose et al., 2004).....	188

1 Introduction

GEM, the Global Earthquake Model, is a global collaboration that brings together state-of-the-art science, national, regional and international organisations and individuals with the aim to build ‘a uniform, independent standard to calculate and communicate earthquake risk worldwide’ (<http://www.globalquakemodel.org>, Pinho 2012; Crowley et al. 2013). In 2010 GEM commissioned four global projects to assemble complementary sources of data to characterise future earthquake occurrence: A strain rate model to capture future earthquake potential (Kreemer et al., 2014) and three projects to collect data on past earthquakes: An historical earthquake catalogue (Albini et al., 2013), an instrumental earthquake catalogue (Storchak, et al., 2013) and a global fault database. This report describes the GEM Faulted Earth (GFE) project and the development of the GEM neotectonic fault database. This report consists mainly of the reproduction of reports that were written as part of the deliverables during the course of the GFE project. Collated in this way, the reports present a good summary of the GFE project.

The GFE project aimed ‘to build a global active fault and seismic source database with a common set of strategies, standards and formats, to be placed in the public domain’ (Berryman, et al., 2010). The primary goal of the database is to capture all observations that a geologist would make about a neotectonic¹ fault, such as surface traces, as well as derived attributes, such as slip rate. As such, the database can be seen as an electronic field notebook. The database can accommodate sparse as well as abundant data to be applicable in different regions of the world. The database contains two layers, one for fault and fold observations, and the other for fault sources which are simplified characteristics of the fault that can generate earthquakes and thus can contribute to seismic hazard assessment. Initially the fault source layer meant to include information on data other than fault observations (Berryman, et al., 2010). This was amended during the project; now fault sources are calculated directly from fault observations. This ensures that formulas are used consistently; that any changes made to neotectonic fault or fold attributes are also reflected in the fault source; and that there is an audit trail of where the fault source attributes come from.

The GFE project consisted of six work packages:

1. Data specification
2. Global fault database development
3. Global fault and source database
4. GEM Faulted Earth portal
5. New active fault data
6. Final report and dissemination.

The key deliverable of ‘Data specification’ (1) was a report on the review of existing databases, which is reproduced in Section 2. The database development (2) included the conceptual design process as outlined in Section 3, as well as the IT development (Section 5). To describe all database attributes in detail, a Data Dictionary has been written (Section 4). An XML database schema has been developed to facilitate transferring bulk datasets or entire fault databases (Section 6).

¹ Neotectonic faults and folds are those that have been active in the current tectonic regime of a region. The time period will vary from region to region with longer times required to characterise fault activity in low strain regions.

To provide tools for the calculations required to derive fault sources from fault data, the GFE has undertaken a comprehensive review of scaling relationships (Stirling et al., 2012, 2013). The report on this is reproduced in Section 7.

In parallel, to the database development process, the GFE project team worked with the GEM model facility to develop a webtool to compile new fault data (4). Section 8 provides user guidelines for the tool.

Work package 3, global fault and source database, includes the bulk upload of existing databases (Section 9), and the characterisation of subduction zones (Section 10) and the characterisation of the Himalaya frontal thrust system (Section 11).

The efforts undertaken under work package 5, 'new active fault data' is described in Section 12. Work package 6 includes this report, as well as the book 'Active faults of the work' by Robert Yeats, which was published in April 2012. This report closes with a summary and outlook in Section 13.

2 Inventory of existing fault databases and data attributes

This section is a reproduction of the report Litchfield, Berryman, Stein and Willis (2011) with minor adjustment to the section referencing, up-dating of references and modification to the text to reflect the time that has passed since the report came out. The numbers in squared brackets refer to the web links in the reference list. The references are merged with the references in the other sections.

2.1 Introduction

This report forms deliverable D1 of the GEM Faulted Earth project: Inventory of existing fault databases and data attributes. Much of the work for deliverable D1 was undertaken in preparation for, and then included in, the GEM Faulted Earth proposal. The contents from the proposal are included here and then built upon with updates since the time of the writing of the proposal (July 2009), as well as a critical review undertaken during the building of the GEM Faulted Earth database (Task 2).

2.2 Description and inventory of existing fault databases and data attributes

Sections 2.2.1 to 2.2.10 contain a description of existing databases that were assessed for the GEM Faulted Earth proposal, prepared in July 2009. Much of the text is reproduced directly from the proposal with some minor modifications to correct grammar and minor content errors, as well as the addition of published references and websites, and any significant updates. Sections 2.11 and 2.12 contain a description of databases, which have become available subsequent to the submission of the GEM Faulted Earth proposal. Section 2.2.13 consists of two tables listing the data attributes in these databases, which are discussed further in section 2.3.

The databases included sections 2.2.1 to 2.2.11 generally exist online, downloadable, and/or published national, regional, or global fault databases, which were readily accessible during the design phase of the GEM Faulted Earth database. Some countries (e.g., New Zealand, Japan) have more detailed versions of their databases, which are not available for public viewing and download, and are not included in this review.

2.2.1 *The INGV Database of Individual Seismogenic Sources (DISS)*

The INGV Database of Individual Seismogenic Sources (DISS) (Basili et al., 2008, 2009; Haller and Basili, 2011) [1] can be viewed either in web map or in Google Earth. It has over 200 seismogenic sources and individual faults. When queried they provide links to a website with information including location and geometry, maximum magnitude, and slip rates, all with quality ratings and citation. There is also a list of most recent and penultimate earthquakes, as well as associated active faults and folds. There is then a large comments section with multiple paragraphs about the structure, open questions about the feature, and a brief summary of several cited works on the feature. There is a large reference list for each fault and a section with both pictures of the structure and figures from papers about the area. It is also possible to perform a search or sort by any category using the online database. All of the data is downloadable into ESRI products, AutoCAD, and MapInfo Interchange Format. The website claims to be under development so that the files can also be exported into GMT, 3D-Move, as well as allowing the application to be more customizable with different grid formats and fault features. The website claims that the software is designed to readily incorporate other fault databases.

2.2.2 The USGS Quaternary faults and folds Database

The USGS Quaternary Faults and Folds Database (Haller et al., 2003; Machette et al., 2004) [2] is based in an interactive web map with the ability to load it into Google Earth. Fault data for more than 1900 faults and several hundred seismic sources (Petersen et al., 2008; Haller and Basili, 2011) [3] is accessible when a fault is selected by providing a link to that fault's information on the USGS website. This information is provided in various report levels, with complete reports providing detailed information on geometry, a small synopsis, fault name history, location reliability, geologic setting, paleoseismology studies, geomorphic expressions, surficial deposit faulting, historic and prehistoric deformation history, and recurrence rate. Faults are color-coded by activity, with warmer colors representing more recent activity. Export capabilities include whole map and localized area downloads into the ESRI product suite. A separate database for Alaska has been published since the initial review of available databases (Koehler et al., 2012). Both of the USGS and Alaska databases were uploaded to the GFE database (see Sections 9.5, 9.6, 9.12 and 9.13).

2.2.3 The AIST RIO-DB Active Fault Database of Japan

The AIST (Geological Survey of Japan) RIO-DB Active Fault Database of Japan (Yoshioka et al., 2005) is a GIS database and a summary version is available on the web [4]. The web version has information on almost 550 faults and can be operated either using Google Maps or using a web map like software. One issue with the program is that Japan is broken up into roughly 30 sections, and only the faults from each section can be seen at once. The database does have a good search function, which allows up to three different search values to be entered based on available data (i.e., values for slip rate, geometry, location, etc.), and allows the search results to be sorted based on importance of each value. Data for each fault includes both field and historical age of last faulting and rupture probability in next 30 years using the BPT and Poisson model. There is no export ability for the database and no way to upload new fault information. The AIST database was uploaded to the GFE database (see Sections 9.4 and 9.11).

2.2.4 The Map and Database of Quaternary Deformation for Andean Countries

The Map and Database of Quaternary Deformation for Andean Countries contains information for over 1500 faults in ArcGIS format for all of the South American Andean nations. The database is accompanied by a book, Atlas de deformaciones cuaternarias de los Andes (Proyecto Multinacional Andino: Geociencia para les Comunidades Andinas, 2008) as well as a series of maps and reports for individual countries (Monetro et al., 1998; Cowan et al., 1998; Audemard et al., 2000; Costa et al., 2000; Cowan et al., 2000; Laevnu et al., 2000; Paris et al., 2000; Saadi et al., 2002; Eguez et al., 2003; Machare et al., 2003). These data were supposed to be developed into a database but unfortunately this was never completed.

In January 2014 the South America Risk Assessment (SARA) project started, organised by GEM and with support of the SwissRe Foundation (<http://www.globalquakemodel.org/what/regions/south-america/>). One component of SARA is to compile active fault data for South America.

2.2.5 The New Zealand Active Faults Database of GNS Science

The GNS Science New Zealand Active Faults Database (Jongens and Dellow, 2003; Litchfield and Jongens, 2006) is a GIS database and a summary version is available on the web [6]. The web map has the ability to pan and zoom, with the choice of a DEM background or a topographic contour map. It is possible to have different visible and active layers simultaneously. Data uploading is theoretically possible with a GNS user account, although it has not been tested. Roberto Basili of INGV, Rome has the New Zealand fault database and seismic source model (2.1.7) in GIS format, and has converted the file for view in Google Earth, although

it is not an integrated functioning database at this time. Database query allows one to search for faults based on slip sense, recurrence interval, last event, slip rate, and single event displacement (e.g., high, medium, low, very low slip rate). Each fault page contains a small inset map of the fault overlaying the DEM, as well as a small list of references with links to their abstracts. Images of the fault may be included as well. The New Zealand active faults database was uploaded to the GFE database (See Sections 9.2 and 9.9).

2.2.6 The New Zealand National Seismic Hazard Model of GNS Science

Fault sources for New Zealand are contained in the GNS Science New Zealand National Seismic Hazard Model (Stirling et al., 1998, 2002, 2012). The fault sources are currently not available for public viewing or download from a website. The most recent (2010) version (Stirling et al., 2012) contains 536 fault sources which are shown as simplified lines delineating the upper edge. Attributes include fault type, length, dip, dip direction, depth to top and base, slip rate, M_{max} , single event displacement, and references. The fault source upper edge lines were converted to polygons and the New Zealand National Seismic Hazard Model was uploaded to the GFE database (See Sections 9.3 and 9.10).

2.2.7 Taiwan Active Fault Database

Some active fault information is available for 42 faults on the island of Taiwan in ArcGIS shape file format from the Central Geologic Survey of Taiwan (Shyu et al., 2005). The active fault parameters include fault type, length, dip down-dip limit and some fault source parameters have been calculated (e.g., Moment magnitude and slip).

2.2.8 Afghanistan Fault Database

This was constructed by the USGS in 2007 (Ruleman et al., 2007), largely on the basis of imagery analysis. Faults are classified into three slip-rate (>10 mm/yr, 1-10 mm/yr, and indeterminate slip rate) and three rake (strike-slip, thrust, and normal) categories. There is an associated seismic source database. This is an instructive example of what the fault reconnaissance studies might be able to accomplish in other regions.

2.2.9 Global subduction zones, mid-ocean ridges, transforms, and diffuse deformation zones

Subduction zone earthquakes release approximately 90% of the long-term seismic moment outside of orogens (Bird and Kagan, 2004), and so it is essential that they are included in GEM Faulted Earth with as much detail and precision as possible. Hayes et al. (2009, 2012) created SLAB 1.0 [7], a 3D representation of subducting slabs. Through focal mechanisms and Peter Bird's (2003) global plate boundary file, they determine the strike, dip, and rake of subducting slabs at given latitude and longitude. This database will be publically released soon. The subduction zones are generated from a series of regularly-spaced 2D profiles that are then extrapolated into the 3D structure, segmented based on geometry. Issues may arise because rake generally changes down-dip, and slip rate and seismic coupling coefficient is not included. Multiple formats are possible for surface projection including iso-depth contours. Available download formats will be ASCII and GMT.

Files containing global plate boundaries and diffuse deformation zones are available from Bird (2003) and DeMets et al. (2010). These are ASCII format files and contain 52 global plates and diffuse deformation polygons. MORVEL, the plate model of DeMets et al. (2010) also includes high resolution coordinates for trenches, transforms and spreading centers. Many of these files are available in GMT format.

Mid-ocean ridge transform fault slip rates, seismogenic depth, seismic coupling coefficient, and length can be found from Boettcher and Jordan (2004).

An up-dated version of the mid-ocean ridge transform fault database was uploaded as fault sources to the GFE database (Section 9.8 and 9.15). Subduction zones have been characterised separately (Section 10).

2.2.10 Seismic Hazard Harmonization in Europe (SHARE)

SHARE is a GEM Regional Programme, which commenced in June 2009, with the objective to provide a community-based seismic hazard model for the Euro-Mediterranean region with update mechanisms [8]. One of the work packages is to develop a European database of active faults and seismogenic sources. The database is hosted on a website [9], which is currently (Oct 2011) only accessible by SHARE partners, but will be made available to the public before the end of the SHARE programme (31 May 2012). The data are stored in 7 regions: Central Mediterranean, Northern Africa, Iberia, Central Europe, Eastern Europe, Greece, Turkey (Basili and Kastelic, 2011).

The database design is adopted from the Italy (DISS) database, taking into account input from the USGS and New Zealand databases (Basili and Kastelic, 2011). Four types of seismogenic sources are stored: (1) individual, (2) composite, (3) debated, and (4) subduction sources. The separation of subduction sources is new to the SHARE database, and although preliminary subduction sources have been compiled, they are still undergoing development (R. Basili pers. comm., Sept 2011). Source attributes include: length, width, depth, strike, dip, rake, displacement, slip rate, recurrence interval, latest earthquake, elapsed time, penultimate earthquake and magnitude (Basili et al., 2008; Basili and Kastelic, 2011). The database also contains some limited active fault attributes: type, name, and references, and can also store comments and pictures. Only seismogenic sources are compulsory, and the amount of active fault data stored in the SHARE database varies between the partners. The database is now published (Basili et al., 2013).

2.2.11 Earthquake Model in the Middle East Region (EMME)

EMME [10] is a GEM Regional Programme which commenced in January 2010 and finished in 2014. It aimed to assess seismic hazard, the associated risk in terms of structural damage, casualties and economic losses. The project also included an evaluation of the effects of relevant mitigation measures in the Middle East region. One of the work packages was to develop seismic sources, which includes a regional compilation of active faults. The fault attributes which are being compiled are: type, length, strike, dip, rake, dip direction, horizontal slip rate (with error), vertical slip rate (with error), aseismic slip rate, top depth, bottom depth, maximum horizontal and vertical displacement, and references (Sesetyan, 2011).

2.2.12 Inventory of data attributes

Tables 2.1 and 2.2 contain the data attributes within the databases listed in sections 2.1 and 2.2. The databases are split into: (1) neotectonic fault and fold (Table 2.1), and (2) fault source (Table 2.2) attributes, which are defined and discussed further in section 3.1.

Table 2.1 Neotectonic fault and fold attributes in existing databases.

Italy (DISS) Euro-Mediterranean (SHARE)	USA (Quaternary faults and folds)	Japan (RIO-DB)	Andean countries	New Zealand (web version)	Taiwan	Afghanistan
Name	Name	Name	Name	Name	Name	Name
	Name comments					
	County and States					
	AMS sheets					

Italy (DISS) Euro-Mediterranean (SHARE)	USA (Quaternary faults and folds)	Japan (RIO-DB)	Andean countries	New Zealand (web version)	Taiwan	Afghanistan
	Synopsis		Synopsis			
	Physiographic provinces					
	Reliability of location					
	Geologic setting					
	Length	Length				
	Sense of movement	Sense of faulting	Fault type	Fault sense	Type	Rake
	Strike	Trend	Average strike			
	Dip		Dip		Dip	
			Dip direction			
		Uplifted side	Downthrown block			
			Fold axis dip			
			Fold limb dip			
	Geomorphic expression		Geomorphic expression			Activity category
	Slip-rate category	Slip rate	Slip rate	Slip rate		
		Recurrence Interval	Recurrence interval	Recurrence Interval		
	Historic earthquake		Historic earthquake			
	Most recent prehistoric deformation	Age of last faulting	Last movement	Last event		
		Slip per event		Single event displacement		
			Reliability of the information			
	Paleoseismology studies					
	Age of faulted surficial deposits					
		Elapsed time rate				
		Rupture probability in the next 30 years				

Italy (DISS) Euro-Mediterranean (SHARE)	USA (Quaternary faults and folds)	Japan (RIO-DB)	Andean countries	New Zealand (web version)	Taiwan	Afghanistan
Reference	References			Selected references		
Comments			Other information			
	Date		Date			
	Compilers		Last updated			
			Compiler			
			Organisation			
			Email address			

Table 2.2 Fault source attributes in existing databases.

Italy (DISS) Euro-Mediterranean (SHARE)	USA (NSHMP)	New Zealand (NSHM)	Taiwan	Mid-ocean ridges
Name	Name	Name	Fault name	Fault name
Location	Fault trace	Fault trace (list of coordinates)		Centrepoin latitude, longitude
Length	Length	Length	Length	Length
Min depth	Rupture top	Top		
Max depth	Rupture bottom	Depth	Downdip limit	Depth
Strike				
Width	Down dip width	Width	Width	
		Area	Area	Area
Dip	Dip	Dip	Fault dip	
	Dip direction	Dip direction		
Rake	Rake			
	Sense of slip	Type	Fault type	
Slip rate	Slip rate	Slip rate		Tectonic slip rate
	Slip rate rank			
Magnitude	Magnitude	Magnitude	Magnitude	Expected M_{max}
			Seismic moment	
Recurrence		Recurrence Interval		
Slip		Displacement	Displacement	
	Aseismic-slip factor			Seismic coupling
Latest earthquake	Last event			
Penultimate earthquake				
Elapsed time				
	Probability of activity			
				Maximum observed M_b since 1964
				Maximum observed M_s since 1964
				Maximum observed M_w since 1964
Compiled by				
Latest update				

2.3 Critical review of accessible databases for use in the design of the GEM Faulted Earth

2.3.1 Database types

One of the clear distinctions apparent from the inventory of existing databases is that they can be separated into two main types, which we call: (1) neotectonic fault and fold, and (2) fault source databases. Neotectonic fault and fold databases are those, which contain detailed, often field-derived, data of faults and folds which have evidence of activity during the current tectonic regime (the length of which varies around the globe). Fault source databases contain summary data of faults or fault systems, which are considered capable of generating earthquakes. Fault sources are typically defined in 3-dimensions, whereas neotectonic faults and folds are generally represented by their surface traces (2-dimensions). The classification of the existing databases into these two types is shown in Table 2.3.

The existence of separate neotectonic fault and fold and fault source databases is likely to be for a variety of reasons, including the history of development of some of the earliest developed databases (US, New Zealand, Japan), and/or that they are housed in different organisations (Japan). The possible exceptions are the Italy (DISS), Euro-Mediterranean (SHARE), and Middle East (EMME) databases, which do contain a neotectonic (active) fault and fold layer, but with only limited attributes. The Taiwan active fault database also has some fault source attributes.

Having separate databases is not ideal, as they require manual (i.e., non-automated) linkages and updates. It also means that accessing the primary fault and fold data and uncertainties, which underlie the fault sources, is not a simple process. This is why an important component of the GEM Faulted Earth project is to build a database with two linked layers, a neotectonic fault and fold layer, and a fault source layer.

Table 2.3 Databases classified into neotectonic fault and fold and fault source types.

Geographic location	Neotectonic fault and fold database	Fault source database
Italy	Database of Individual Seismogenic Sources*	Database of Individual Seismogenic Sources
USA	Quaternary fault and fold database	National Seismic Hazard Map
New Zealand	New Zealand active fault database	National Seismic Hazard Model
Japan	Active fault database of Japan	Japan Seismic Hazard Information Station
Andean Countries	Map and Database of Quaternary Deformation for Andean Countries	
Taiwan	Taiwan active fault database	Taiwan active fault database
Afghanistan	Afghanistan fault database	Afghanistan seismic source database
Euro-Mediterranean	European database of active faults and seismogenic sources*	European database of active faults and seismogenic sources
Middle East	Middle East database of active faults and seismogenic sources*	Middle East database of active faults and seismogenic sources

* Limited active fault attributes

2.3.2 Data accessibility and database documentation

Despite most of these databases being available on the web and/or published, only the Italy (DISS), Japan, USA, and global subduction zones (SLAB1.0) databases currently allow data downloads. The data are generally available in two formats, GIS shapefile or Google Earth kml files. The accessibility of this data has influenced some of the design and export features of the database GEM Faulted Earth.

The Italy (DISS), USA, and New Zealand databases have documentation describing design concepts and formats (Haller and Machette, 1993; Jongens and Dellow, 2003; Basili et al., 2008, 2009). This, along with discussions with the administrators of the Italy (Roberto Basili), USA (Kathy Haller), and Australia (Dan Clark) databases has also influenced the design of the GEM Faulted Earth database.

2.3.3 Review of database attributes

Tables 2.1 and 2.2 show that there are several attributes, which are common to several databases. For the neotectonic faults and folds databases (Table 2.1), the most common attributes are name, sense of movement, dip, slip rate, recurrence interval, last event, and references. Several of these are key parameters required for seismic hazard assessment and GEM Faulted Earth will definitely include all these attributes in the database. The Japanese database also has elapsed time since most recent surface rupture and rupture probability in the next 30 years. The USA database also has a number of extra attributes describing the location, as well as paleoseismology studies, age of faulted surficial deposits, and geologic setting. The latter could be useful for informing choice of earthquake magnitude scaling relationships and ground motion prediction equations in the seismic hazard analysis.

The fault source databases (Table 2.2) have even more attributes in common (see also Haller and Basili, 2011), which reflects their requirement for seismic hazard calculations. GEM Faulted Earth will of course need to include all these attributes. Some differences reflect their requirement in only certain tectonic settings, such as aseismic-slip factor, which is important for creeping faults in California. GEM Faulted Earth will therefore need to include such attributes for a global database.

2.3.4 Specific review comments the INGV Database of Individual Seismogenic Sources (DISS)

As mentioned previously, the Italy (DISS) database is primarily a fault source database. The web map does however, show both neotectonic fault and folds and fault sources in a clear and effective way, and GEM Faulted Earth is likely to adopt a similar form of presentation.

2.3.5 Specific review comments the USGS Quaternary faults and folds Database

The USA Quaternary Faults and Folds database is probably the largest existing database, and is also one of the earliest developed. One of the negative features for seismic hazard purposes however, is that it contains a lot of text, and some of the numerical value fields (e.g., slip rate) are grouped into categories. While it is desirable to document data sources, it is considered that the time to enter this level of documentation would be a barrier to people entering data into the GEM Faulted Earth database.

2.3.6 Specific review comments the AIST RIO-DB Active Fault Database of Japan

Faults in the Japanese database are currently broken into 2 km long segments and will need to be combined into longer faults for seismic hazard analysis. The Japanese database also includes site-specific data attributes (i.e., data collected at a particular site, such as a fault trench). The inclusion of this provides a useful documentation of the level of data available for particular faults and attributes.

2.3.7 Specific review comments the GNS New Zealand Active Faults Database

Like the Japanese database, the web version of the New Zealand database only provides a summary of a more detailed version. This more detailed database is available to the developers of the GEM Faulted Earth database and is a major influence on the design of the GEM Faulted Earth database. One particular aspect of the New Zealand database which is not apparent on the web version and which is proving unavoidable in the design of the GEM Faulted Earth database is a hierarchy of fault data on faults, sections, and traces, and at specific sites (point data) (Jongens and Dellow, 2003).

2.3.8 Specific review comments global subduction zones, oceanic ridges, transforms, and diffuse deformation zones

Examination of the SLAB1.0 and Mid-ocean ridge files show significantly different attributes from fault seismic sources. Therefore, like the SHARE database, GEM Faulted Earth treated them separately from neotectonic fault and fold derived sources.

3 Database design process, philosophies and structure

This section is a reproduction of Section 2 of the Guidelines for compilation report by Litchfield, Wyss, Christophersen, Thomas, Berryman, Henshaw, Villamor, and Pagani (2013b); the remainder of that report is contained in section 8. Minor adjustments have been made to the section numbering, and removal of a table that is already included in Section 2. The references are merged with the references in the other sections.

3.1 Database design process

The first step in the design of the GEM Faulted Earth database was a review of existing, publicly available regional or national databases (Litchfield et al., 2011). Databases reviewed are listed in Table 2.3 in section 2 of this report. Key findings included that many databases can be classified as either: (1) neotectonic fault and fold, or (2) fault source databases (Table 2.1), although some more recent databases (DISS, SHARE, EMME) do contain some data of both. These recent databases reflect a growing recognition that for seismic hazard modeling purposes a combined database is desirable, and this is an important design concept of the GEM Faulted Earth database (Section 3.2). Comparison of existing database attributes shows that many are common to all databases, particularly fault source databases. Thus these common, as well as region-specific, attributes must be included in the GEM Faulted Earth database. Specific features of some databases were also briefly discussed and result in recommendations such as using a web map display such as the DISS database, and the need to include subduction zones and mid ocean ridge transforms as a separate type of fault source. These key findings were then used to design the GEM Faulted Earth database.

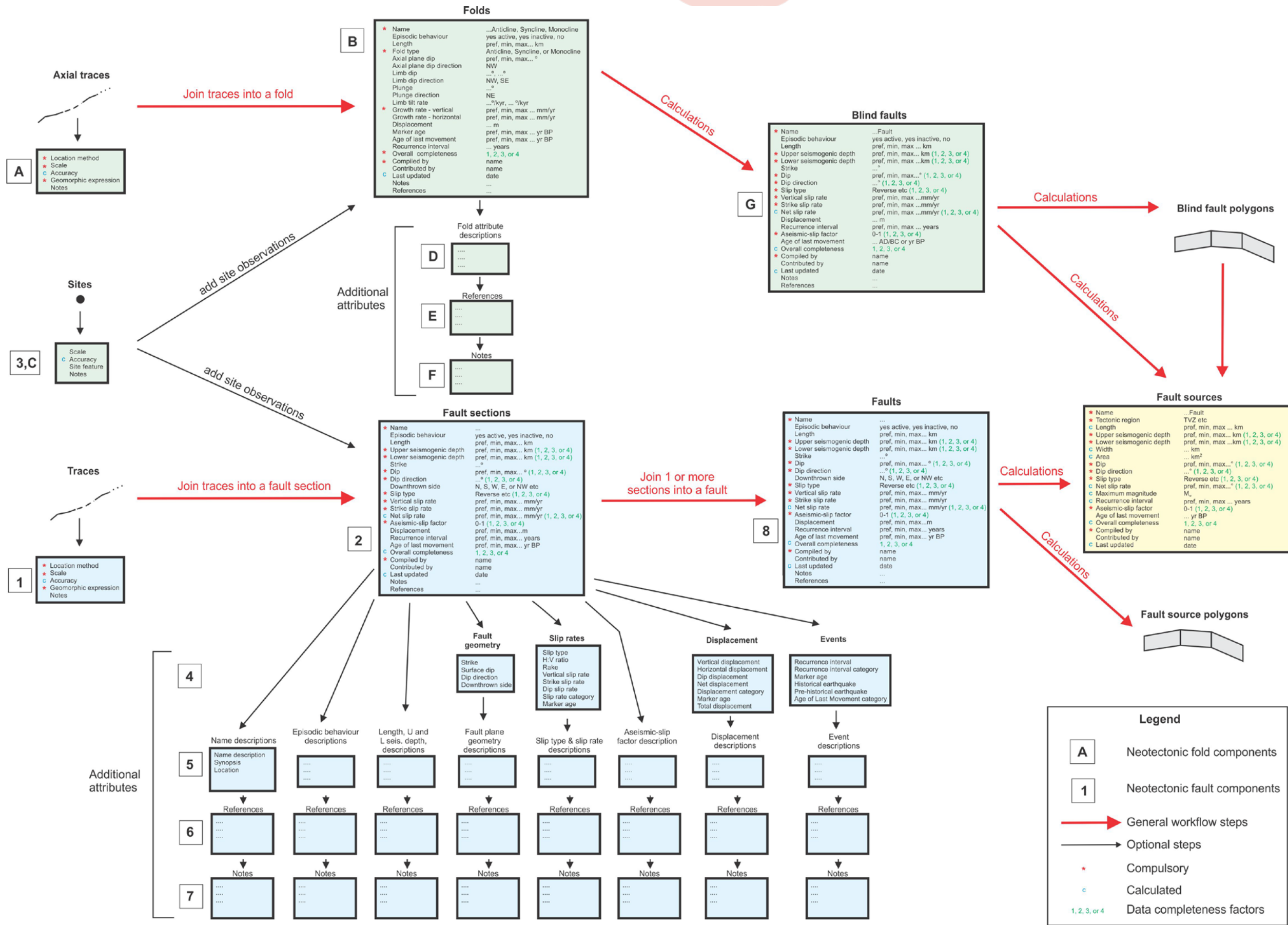
The next step was to develop a preliminary database design and to test it with example data. The first version of the database was developed at the Earth Observatory of Singapore by Nicola Litchfield and Mary Anne McKittrick, and it was tested on New Zealand and Southeast Asia data, as examples of faults with abundant and limited data (attributes) respectively.

From there the design was an iterative process of design, testing, and feedback. The database structure was circulated among the authors of this report and other members of the GEM Faulted Earth consortium, with particular mention of Mary Anne McKittrick, Mudrik Daryono, Afroz Shah (EOS, Singapore), Dan Clark (Geoscience Australia), Roberto Basili (INGV), Kathy Haller, Ned Field, Gavin Hayes (USGS).

A final important component of the design process was development of the fault compilation tool described in section 3. The concurrent development of the tool resulted in a number of changes to the database design, which was useful in conceptualising how the database is to be populated in practise. The tool was developed by the GEM Foundation, and so we would like to acknowledge others who contributed to the project, including John Tarter who was involved in the early stages.

3.2 Database design philosophies and structure

The conceptual database structure resulting from the above process is shown in Figure 3.1. This is not the technical structure of the database, which is described by Thomas et al. (2012). Instead, it shows the general concepts of the main components (spatial data and attribute tables), linkages (black and red arrows), and workflow (red arrows) of entering data into the database. In this section we describe the overall design philosophies and structure.



Version 1.2.1

Figure 3.1 The GEM Faulted Earth conceptual database structure.

3.2.1 Database components

The database has three main components: (1) Neotectonic faults (blue boxes 1-8 on Figure 3.1); (2) Neotectonic folds (green boxes A-G); and (3) Fault sources (yellow box).

The neotectonic fault and fold components (blue and green boxes) contain the detailed field observations and derived attributes for neotectonic faults and folds. This component is similar to reviewed neotectonic fault and fold databases (middle column of Table 2.3).

Fault sources (yellow box) are simplified faults with key attributes for seismic hazard modelling. This component is similar to reviewed fault source databases (right column of Table 2.3).

3.2.2 Database levels; compulsory and optional attributes

A key database design philosophy of the neotectonic fault and fold component of the database is that it is multi-levelled, with summary tables (boxes 2, 8, B and G on Figure 3.1) stored at upper levels and additional attributes (boxes 4-7 and D-F on Figure 3.1) stored at lower levels. This serves several purposes: (1) reducing the number of attributes in individual tables to a manageable level; (2) facilitating prioritisation of attribute compilation to key attributes for seismic hazard analysis (see next paragraph); and (3) grouping together similar attributes to ease searching.

The summary tables (2, 8, B, G) include some of the key attributes needed for seismic hazard analysis. Since this GEM Faulted Earth database is designed primarily for input into seismic hazard models, entering these key attributes are designated compulsory. The compulsory attributes are marked with a red asterisk on Figure 3.1. Many of the compulsory attributes also require a data completeness factor (green numbers 1-4 on Figure 4.1), described in section 3.2.6.

Any attributes not marked with a red asterisk are optional. These include some summary attributes (e.g., episodic behaviour, strike, downthrown side, axial plane dip; boxes 2, B), additional attributes for neotectonic fault sections and folds (boxes 4-7 and D-F), and site observations. Site observations are attributes which have been collected at a specific site, and can include any of the attributes in the summary tables (2, B) and the additional attribute tables (4-7, D-F). Although these additional attributes are not required for seismic hazard assessment, they are useful for a variety of other purposes, such as documenting the number and uncertainties in observations to derive key attributes (e.g., slip rate).

It should be noted that the fault compilation tool has a slightly different structure to that shown in Figure 3.1. In general, it includes multiple forms and tables that broadly match to the upper level summary tables (2, 8, B, G, fault sources), as well as traces (1, A) and the site observations (3, C). A key difference however, is that when these tables are first opened, they only show the compulsory fields. Optional fields (including boxes 4-7 and D-F) can then be shown by expanding the table after selecting a “more fields” button. The tool structure is described further in Section 7.

3.2.3 Neotectonic faults – traces, sections, faults

Another important design philosophy is that neotectonic faults are stored in three components – traces, sections, and faults. The purpose of this is to facilitate the simplification of often complex active fault data into fault sources for seismic hazard modelling. Thus, detailed locations of faults are stored as traces, which are grouped together into sections with attributes such as slip rate and dip. Faults are defined as those that could rupture the ground surface in a single maximum magnitude earthquake, and can consist of one or more sections. Faults are then further simplified into fault sources (and ultimately seismic sources) for input into a seismic hazard model. The workflow from traces to sections, faults and ultimately fault sources is shown by the red arrows in the conceptual database structure in Figure 3.1, and in map view in Figure 3.2a.

Traces, sections, and faults are described in more detail below, and it is important to note that in the fault compilation tool, it is necessary to first define all of traces, sections, and faults before a fault source can be generated. This is still the case even if a fault consists of just one section and trace (Figure 3.2b).

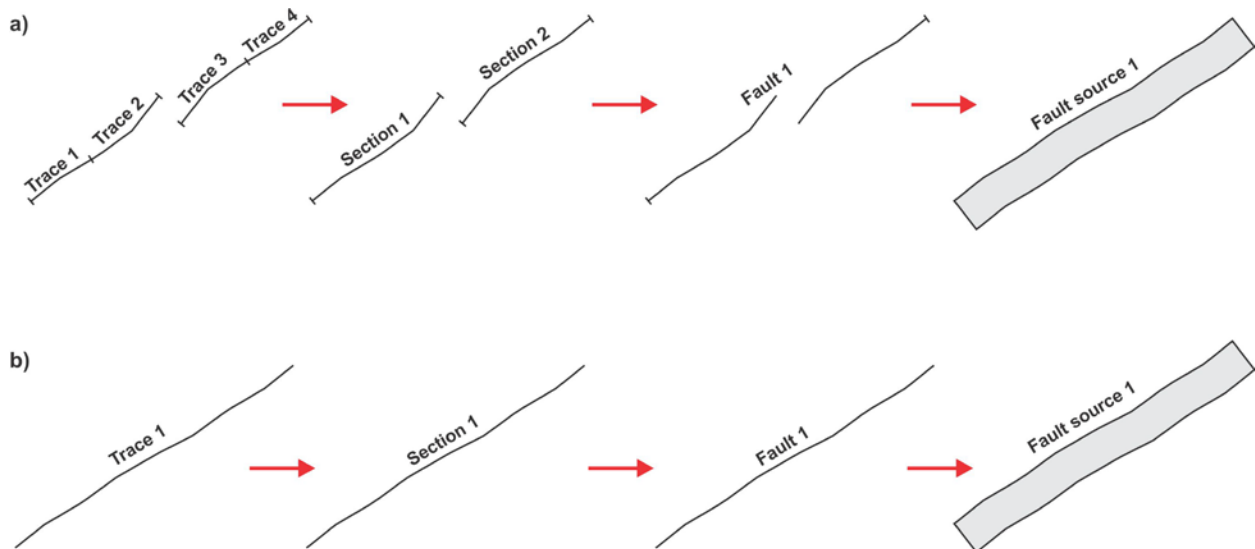


Figure 3.2 Schematic maps showing the relationship between traces, sections, faults and fault sources for a) neotectonic faults consisting of more than one section and trace, b) neotectonic faults consisting of one section and one trace.

Traces are the locations of where faults are interpreted to rupture the ground surface. They may be represented by a distinct fault scarp with a particular geomorphic expression, or may be inferred surface locations based on geophysical imaging of a fault at depth. For example, immediately after a ground surface rupture a fault is likely to be represented by a sharp scarp, but with time, the scarp is likely to be eroded or possibly buried by younger deposits (e.g., tephra or alluvium). In the latter case, the existence of a trace can be inferred and classified as having a geomorphic expression of “concealed”. Furthermore, because erosion and burial are unlikely to be uniform along a fault, the expression of originally geographically distinct traces may also vary along-strike. For example, an originally sharp scarp may now be eroded at one end. In this database, this would be mapped as two traces with different geomorphic expressions.

A trace in this database is therefore defined as one with a particular geomorphic expression. This serves two main purposes: (1) to indicate the uncertainty of the location of a fault on the ground surface; and (2) to determine the display of traces on a map. For example, a sharp scarp may be displayed as a solid line, whereas an eroded scarp may be displayed as a dashed line, and a concealed fault as a dotted line. As well as geomorphic expression, the other attributes entered for traces are a name, the scale at which it was mapped, the location method (generally the type of map on which it was captured – e.g., Google Earth), and notes.

Sections are faults or portions of faults that have particular attributes (e.g., slip rate, dip, recurrence interval, age of last movement), and are represented in map view by one or more traces (Figure 3.2). Sections are typically geographically or geomorphologically distinct, separated from other sections by step-overs, or by changes in geometry (strike, dip, dip direction). The size of step-overs between sections is not defined in this database, but sections should not be shorter than 5 km. Multiple attributes can be stored for sections (boxes

2 and 4 in Figure 3.1), and site-specific attributes (observations; boxes 2 and 4 at sites located in box 3 in Figure 3.1) can also be linked to a section.

Faults are those that can rupture the ground surface in a single maximum magnitude earthquake. Faults consist of one or more sections, and are represented in map view by one or more traces (Figure 3.2). For example, if a fault is composed of two sections, it is also made up of all the traces for each of those two sections (Figure 3.2a). Only summary attributes are stored for faults (box 8 on Figure 3.1). If a fault is only comprised of one section, then the section and fault summary attributes will be identical. If a fault is comprised of two or more sections, the fault summary attributes are a composite of the section summary attributes, as defined by the user.

3.2.4 Neotectonic folds – blind faults

In order to convert folds into fault sources for seismic hazard analysis, this database makes the assumption (common in many seismic hazard models) that all anticlines and monoclines are the surface expression of blind faults. As a result, there is a requirement to define a blind fault polygon (which will become the fault source polygon) and blind fault attributes (box G in Figure 3.1). The blind fault attributes are similar to the summary section (box 2 in Figure 2.1) or fault attributes (box 8 in Figure 3.1). Folds cannot be composed of sections in this database.

3.2.5 Automatic derivation or calculation of fault sources

Another key design philosophy is that most of the fault source attributes (yellow box on Figure 3.1) are derived from fault (box 8) or blind fault (box G) attributes, or are calculated from other attributes (those marked with a blue c in the yellow box). For example, dip is derived from neotectonic fault or blind fault dip, and width is calculated from upper and lower seismogenic depth and dip. The purpose of this is to ensure: (1) formulas are used consistently; (2) any changes made to neotectonic fault or fold attributes are also reflected in the fault source; and (3) there is an audit trail of where the fault source attribute comes from.

An important implication of this is that if automatically derived or calculated fault source attributes are not consistent with other data, then the only way to alter these attributes is to alter either: (1) neotectonic fault or fold attributes; or (2) change the length of the fault source through different combinations of fault sections. For example, if the fault source recurrence interval (calculated from displacement divided by slip rate) is significantly shorter than the recurrence interval derived from field data, then a higher value could be obtained by decreasing the slip rate, or increasing fault length (e.g., by combining more sections), or both.

3.2.6 Data completeness factors

An important requirement in the database is an assessment of the quality of data or level of knowledge of some of the key attributes. This is quantified as a data completeness factor, a relative number from 1 to 4 (1 being the highest) which are assigned to seven compulsory neotectonic section, fault and blind fault attributes. An overall data completeness factor is then calculated as a combination of the individual data completeness factors, with a higher weighting given to the slip rate data completeness factor.

3.2.7 *Uncertainties*

As well as an assessment of the quality or level of knowledge, it is important to quantify uncertainties of numerical attributes such as dip and slip rate. These uncertainties are stored in the form of a preferred value, accompanied by a minimum and maximum value. The minimum and maximum values are inferred to represent a 95% level of confidence. For compulsory attributes all three of the preferred, minimum, and maximum values are required.

4 Data Dictionary

This section is a reproduction of the report by Litchfield, Berryman and Thomas (2013a). Minor adjustments have been made to the section numbering. The references are merged with the references in the other sections.

4.1 Introduction

This report provides definitions, formats, and guidelines for compilation of each attribute in the GEM Faulted Earth neotectonic fault, fold and fault source database. The report is primarily for use when uploading new data using the web-based fault compilation tool (Litchfield et al., 2013b), and descriptions of each attribute from this report are included as help windows in the tool. It will also assist mapping and converting attributes in existing national and global databases for bulk upload into the GEM Faulted Earth Database (Litchfield and Thomas, 2013). The database design is described by Thomas (2012) and Litchfield et al. (2013b).

The report is divided into three sections: (a) Neotectonic faults (Section 4.2); (b) Neotectonic folds (Section 4.3); and (c) Fault sources (Section 4.4). Within each section the attributes are described in alphabetical order (using the name in the fault compilation tool, which may differ slightly from that in the database for the national and global dataset uploads). The description for each attribute typically contains:

- Whether the attribute is compulsory, optional, or calculated
- The format (e.g., a value, a range)
- The expression of uncertainties (generally as preferred, minimum, and maximum values)
- A definition of the attribute
- Hints about how to enter the attribute where data may be lacking or the user is lacking experience

In brackets beside the names of each attribute are the names of the tables in the fault compilation tool where each attribute is stored. Some of the attributes in the tool are split out as only one value can be stored in each field. For example, dip is stored in three fields, maximum dip, minimum dip, preferred dip. For the sake of efficiency in this report all three are combined into one description.

At the time of writing of this part of this report (May 2013), the fault compilation tool (v1.12.11) does not contain all of the attributes in the GEM Faulted Earth Database, most notably neotectonic folds (green boxes A-G in Figure 3.1). These attributes are included in this report because they may be included in the tool in the future and many have been populated during the bulk upload of national and regional databases (Litchfield and Thomas, 2013). These attributes are denoted with an *, and it should be noted that some details of the descriptions (e.g., names and formats) may change during further development of the tool. Some other features in the tool which are not currently working, such as calculations, are also denoted by an *.

Appendices contain descriptions of the calculations of magnitude and recurrence interval.

4.2 Neotectonic faults

4.2.1 Accuracy (*Traces, Observations: Events, Observations: Displacement, Observations: Slip Rates, Observations: Fault Geometry*)

- Calculated
- Reported as a number – i.e., 1:200,000 is reported as 200000

Conservative definition of the location accuracy of the trace or a site on the ground surface, calculated from twice the scale at which the trace was mapped. For example, if a trace was mapped at 1:100,000 scale then the accuracy is calculated to be 1:200,000.

4.2.2 Age of last movement (*Fault Sections, Faults; Observations: Events*)

- Optional
- Reported as years before 1950 AD
- Expressed as preferred, minimum, and maximum

Timing of the most recent maximum magnitude earthquake on the fault. Generally derived from historical or field data, but may be inferred from geomorphic expression, analogous faults, expert opinion, etc. Historical earthquakes for which the date is well constrained (i.e., to within one year) should be reported as a preferred value only, relative to 1950 AD. For example 1940 AD is reported as 10 and 1987 AD as -37. Ages obtained by radiocarbon dating must be reported as calibrated ages.

4.2.3 Age of last movement category (*Fault Sections, Observations: Events*)

- Optional
- Reported as a range of years before present
- Chosen one category from a list:
 - 0 – <1000
 - 1000 – <11,700 (Holocene)
 - 11,700 – <50,000
 - 50,000 – <100,000
 - 100,000 – <1,000,000
 - 1,000,000 – <10,000,000

An inferred age or timing of the last maximum magnitude earthquake on the fault, selected from one of 6 categories. Only to be used if there is no data available to quantify a more precise age.

4.2.4 Aseismic-slip factor (*Fault Sections, Faults*)

- Compulsory
- Reported as a value from 0 (fully locked) to 1 (fully creeping), up to 2 decimal places

Fraction of fault slip released by creep. For most faults this is likely to be 0.

4.2.5 Aseismic-slip factor completeness (*Fault Sections, Faults*)

- Compulsory
- Reported as 1, 2, 3, or 4

Relative ranking of the completeness of the data constraining the Aseismic-slip factor.

- 1 = well constrained from multiple field data
- 2 = moderately constrained from field data
- 3 = poorly constrained from field or geological data
- 4 = inferred

4.2.6 Compiled by (Fault Sections, Faults)

- Compulsory
- Free text up to 64 characters long
- Only one person can be entered

The name of the person who compiled the data for entry into the database.

4.2.7 Contributed by (Fault Sections, Faults)

- Optional
- Free text up to 64 characters long

The name of the person who contributed most of the data.

4.2.8 Created at (Fault Sections, Faults*)

- Optional
- Reported as a date (yyyy-mm-dd)

The date at which data for a particular table was entered or modified. In the fault compilation tool this is chosen from a calendar.

4.2.9 Dip (Fault Sections, Faults)

- Compulsory
- Reported in decimal degrees, from 0° (horizontal) to 90° (vertical), rounded to the nearest degree
- Expressed as preferred, minimum, and maximum

Downward inclination of the fault plane from the horizontal, averaged across the entire fault plane (which may or not be the same as the surface dip). Generally derived from a combination of field and subsurface geophysical data (e.g., seismic reflection profile), but may be inferred from nearby faults or typical values from faults of the same style. If uncertainties cannot be quantified, a default value of $\pm 10^\circ$ should be used.

4.2.10 Dip completeness (Fault Sections, Faults)

- Compulsory
- Reported as 1, 2, 3, or 4

Relative ranking of the completeness of the data constraining the fault dip.

- 1 = well constrained from multiple field data and/or high resolution seismic profile data
- 2 = moderately constrained from field or seismic profile data
- 3 = poorly constrained from subsurface geophysical data
- 4 = inferred

4.2.11 Dip direction (Fault Sections, Faults, Observation: Fault Geometry)

- Compulsory
- Reported in decimal degrees from 1° to 360°, rounded to the nearest degree, whereby:
 - 90° = east
 - 180° = south
 - 270° = west
 - 360° = north

The compass direction towards which the fault dips. If the strike and downthrown side are known it can be calculated from 90° to the strike following the Aki and Richards (1980) convention (or the right-hand rule) (Figure 4.1), but an independently derived value can also be entered.

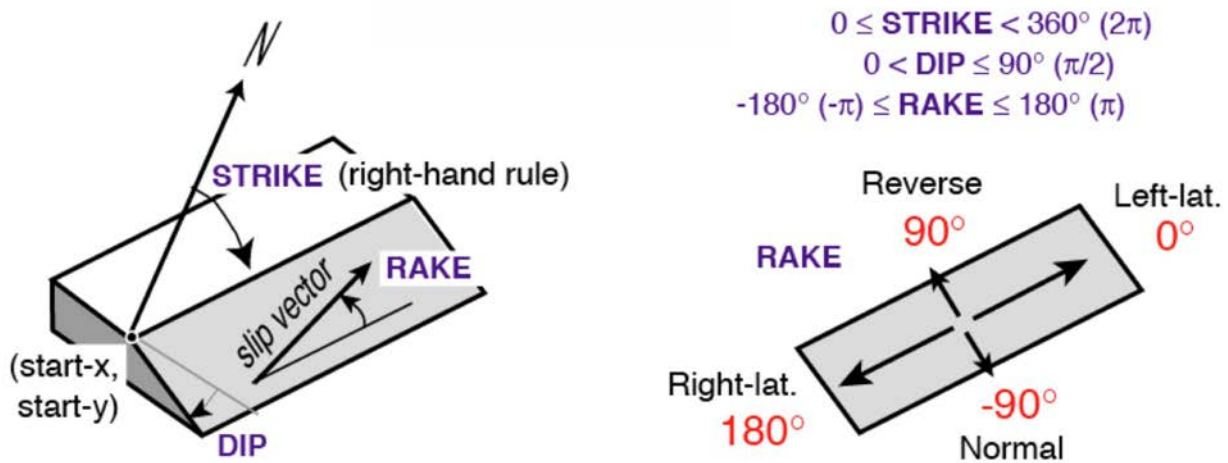


Figure 4.1 Aki and Richards (1980) conventions for noting strike, dip direction, and rake

4.2.12 Dip direction completeness (Fault Sections, Faults)

- Compulsory
- Reported as 1, 2, 3, or 4

Relative ranking of the completeness of the data constraining the fault dip direction.

1 = well constrained from multiple field data and/or high resolution seismic profile data

2 = moderately constrained from field or seismic profile data

3 = poorly constrained from subsurface geophysical data

4 = inferred

4.2.13 Dip displacement (Fault Sections, Observations: Displacement)

- Optional
- Reported in metres, up to 2 decimal places
- Expressed as preferred, minimum, maximum

Displacement per event measured down the dip of the fault plane. May be calculated from field measurements of displacement of dated markers down the fault plane, or from vertical displacement and the fault dip.

4.2.14 Dip slip rate (Fault Sections, Observations: Slip rates)

- Optional
- Reported in millimetres per year, up to 3 decimal places
- Expressed as preferred, minimum, maximum

The dip-parallel (or straight down-dip) component of slip rate on the fault plane (see also slip rate). May be calculated from field measurements of displacement of dated markers down the fault plane or from vertical slip rate and the fault dip.

4.2.15 Displacement (Fault Sections, Faults)

- Optional
- Reported in metres, up to 2 decimal places
- Expressed as preferred, minimum, maximum

Average net slip or displacement during a single maximum magnitude earthquake on the fault plane (i.e., single event displacement). This may be the average of multiple values from different sites along each fault or fault section. Generally derived from field data, but may be inferred from analogous faults, expert opinion, scaling relations, etc.

4.2.16 Displacement category (Fault Sections, Observations: Displacement)

- Optional
- Reported in metres
- Chosen one category from a list:
 - 0.1 – <0.5
 - 0.5 – <1
 - 1 – <5
 - 5 – <10
 - 10 – <30

An inferred net displacement per event, selected from a limited number of categories. To be used when there is no available data.

4.2.17 Downthrown side (Fault Sections, Faults, Observations: Fault geometry)

- Optional
- Reported as one of:
 - N
 - S
 - W
 - E
 - NW
 - SW
 - NE

- SE

Geographic quadrant of the side of the fault that has been displaced downwards.

4.2.18 Episodic behaviour (Fault Sections, Faults)

- Optional
- Choose one of:
 - Yes Active
 - Yes Inactive
 - No

Is there any evidence for episodic behaviour (i.e., periods of activity and inactivity) on the section or fault within the current tectonic regime? If there is evidence for episodic behaviour, is it currently in an active period?

4.2.19 Geomorphic Expression (Traces)

- Compulsory
- Chosen one expression from a list:
 - Surface trace
 - Eroded scarp
 - Sharp feature
 - Topographic feature
 - Bedrock extension
 - Concealed
 - No trace

Expression of the fault on the ground or on digital imagery (e.g., Google Earth).

1. Surface Trace = Clearly defined trace of a recent or well preserved fault rupture trace mapped in the field or from high resolution imagery (e.g., LiDAR, aerial photographs).
2. Eroded scarp = Eroded or naturally degraded faultline scarp mapped in the field or from high resolution imagery (e.g., LiDAR, aerial photographs).
3. Sharp feature = Well defined, distinct, feature (e.g., faultline scarp) mapped from remote sensing (e.g., SRTM data, Google Earth).
4. Topographic feature = Non-scarp feature e.g., changes in gradient, alignment of saddles, springs, etc.
5. Bedrock extension = Inferred extension of a neotectonic fault along a bedrock fault.
6. Subtle feature = Moderately – poorly defined feature mapped from remote sensing (e.g., SRTM data, Google Earth).
7. Concealed = Inferred trace buried beneath deposits younger than the last fault rupture (e.g., alluvium) or a water body (river, lake, sea).
8. No trace = No geomorphic expression of the fault exists, but it is inferred from other datasets.

This attribute determines the linetypes used to display the faults in map view:

1 – 3 = solid line

4 – 6 = dashed line

7 – 8 = dotted line

4.2.20 Historical earthquake (Fault Sections, Observations: Events)

- Optional
- Reported in years relative to 1950 AD

Year of the most recent maximum magnitude earthquake that occurred during the historical period (time of written records). May be derived from instrumental or historical data. The definition of the historical period will vary globally. Reported relative to 1950 AD, e.g., 1940 AD is reported as 10 and 1987 AD as -37.

4.2.21 Horizontal displacement (Fault Sections, Observations: Displacement)

- Optional
- Reported in metres, up to 2 decimal places
- Expressed as preferred, minimum, maximum

Displacement per event measured along the strike of the fault plane (i.e., horizontal displacement). Generally calculated from field measurements of horizontal displacements.

4.2.22 H:V ratio (Fault Sections, Observations: Slip rates)

- Optional
- Reported as a ratio
- Expressed as preferred, minimum, maximum

Ratio of Horizontal to Vertical displacement per event on the fault plane (e.g., 1:3 means 1 m horizontal displacement and 3 m vertical displacement). Generally derived from field or geological data.

4.2.23 Last updated

- Calculated
- Reported as a date (yyyy-mm-dd)

Date when the fault attributes were last updated. In the fault compilation tool this is automatically calculated and does not appear in the tables.

4.2.24 Length (Fault Sections, Faults)

- Optional
- Reported in kilometres, rounded to the nearest kilometre

Length of the section or fault, measured along its strike. Generally measured manually along an approximate midpoint of the fault traces.

4.2.25 Location Method (Traces)

- Compulsory
- Choose one method from a list:

- GPS survey
- LiDAR
- Aerial photographs
- Topographic Map
- Google Earth
- Digital Elevation Model *
- Digital Elevation Model (SRTM) *
- Geological Map *
- Personal Communication *
- Report *
- Composite

The source map or base map on which the trace was digitised. Composite can be used where traces were digitised on more than one base map.

4.2.26 Lower seismogenic depth (Fault Sections, Faults)

- Compulsory
- Reported in kilometres, rounded to the nearest kilometre
- Expressed as preferred, minimum, maximum

Vertical distance below the ground surface to the bottom edge (base) of the fault or fault section. For historical fault ruptures, this may be obtained from seismological data (e.g., earthquake hypocentre, aftershock seismicity). For remaining faults it may be inferred from the base of the seismogenic zone, as defined by instrumental seismicity, or from locking depths derived from geodesy. If uncertainties cannot be quantified, a default value of $\pm 10\%$ should be used.

4.2.27 Lower seismogenic depth completeness (Fault sections, Faults)

- Compulsory
- Reported as 1, 2, 3, or 4

Relative ranking of the completeness of the data constraining the lower seismogenic depth.

1 = well constrained from field data or high resolution seismic profile data

2 = moderately constrained from seismic profile or instrumental seismicity data

3 = poorly constrained from instrumental seismicity data

4 = inferred

4.2.28 Marker age (Fault Sections, Observations: Slip rates, Observations: Displacement, Observations: Events)

- Optional
- Reported as years before 1950 AD
- Expressed a preferred, minimum, maximum

Age of the geomorphic or geological marker used to calculate slip rate or displacement. Ages obtained by radiocarbon dating must be reported as calibrated ages.

4.2.29 Name (Traces, Fault Sections, Faults)

- Compulsory
- Free text up to 96 characters long

The name of a feature. Traces, sections and faults can all have the same name, and there multiple traces, sections and faults can also have the same name. For unnamed traces or sections, it is suggested a name is assigned followed by a number (e.g., Alpine Fault – Section 1).

4.2.30 Net displacement (Fault Sections, Observations: Displacement)

- Optional
- Reported in metres, up to 2 decimal places
- Expressed as preferred, minimum, maximum

Average net slip or displacement during a single maximum magnitude earthquake on the fault plane (i.e., single event displacement). Calculated from the vertical and horizontal displacements.

4.2.31 Net slip rate (Fault Sections, Faults, Observations: Slip rates)

- Calculated *
- Reported in millimetres per year, up to 3 decimal places
- Expressed as preferred, minimum, maximum

The slip (displacement or movement) rate on the fault plane along the direction of maximum slip, averaged over a time period involving at least two large earthquakes.

4.2.32 Net slip rate completeness (Fault Sections, Faults)

- Compulsory
- Reported as 1, 2, 3, or 4

Relative ranking of the completeness of the data constraining the slip rate.

1 = well constrained from multiple field data

2 = moderately constrained from field data

3 = poorly constrained from field or geological data

4 = inferred

4.2.33 Notes (Traces, Fault Sections*, Faults*, Observations: Events, Observations: Displacement, Observations: Slip Rates, Observations: Fault Geometry)

- Optional
- Free text

Brief notes of important information about any attribute for a trace, section or fault. It is recommended this includes descriptions of the derivations of the compulsory attributes.

4.2.34 Overall completeness (Fault Sections, Faults)

- Calculated *
- Reported as 1, 2, 3, or 4, rounded to the nearest whole number

Relative ranking of the overall completeness of the fault data, weighted towards the key parameter slip rate. Calculated from a combination of all the fault data completeness rankings, whereby the slip rate ranking contributes 5 times the others, i.e.:

upper seismogenic depth data completeness +
 lower seismogenic depth data completeness +
 dip data completeness +
 dip direction data completeness +
 slip type data completeness +
 5 x slip rate data completeness +
 aseismic-slip data completeness

divided by the total, 11.

4.2.35 Pre-historical earthquake (Fault Sections, Observations: Events)

- Optional
- Reported as years before 1950 AD
- Expressed as preferred, minimum, and maximum

Age of the most recent maximum magnitude earthquake, and that occurred prior to the historical period (time of written records). Derived from field data. Ages obtained by radiocarbon dating must be reported as calibrated ages.

4.2.36 Rake (Fault Sections, Faults, Observations: Slip rates)

- Optional
- Reported in decimal degrees, from -180° to 180° , rounded to the nearest degree, whereby:
 - -90° = normal
 - 0° = left lateral (sinistral)
 - 90° = reverse
 - 180° = -180° = right lateral (dextral)
- Expressed as preferred, minimum, maximum

The direction of hanging wall slip, measured relative to the horizontal (strike). May be defined from field or seismological data. May be calculated from H:V ratios or inferred from slip type. Is defined using the Aki and Richards (1980) convention (or the right-hand rule; Figure 4.1).

4.2.37 Recurrence interval (Fault Sections, Faults, Observations: Events)

- Optional
- Reported in years, rounded to the nearest year
- Expressed as preferred, minimum, maximum

Average time between successive maximum magnitude earthquakes. Generally derived from field data, but may be calculated from D/SR (Displacement divided by Slip Rate), or inferred from analogous faults, expert opinion, etc.

4.2.38 Recurrence interval category (Fault Sections, Observations: Events)

- Optional
- Reported in years
- Chosen one category from a list:
 - 10 – <100
 - 100 – <1000
 - 1000 – <2000
 - 2000 – <5000
 - 5000 – <10,000
 - 10,000 – <100,000
 - 100,000 – <500,000
 - 500,000 – <1,000,000
 - 1,000,000 – <10,000,000

An inferred recurrence interval selected from a limited number of categories. To be used only when there is no available data.

4.2.39 References *

- Optional
- Free text
- Bulletin of the Seismological Society of America format

List of references noted for a particular trace, fault section, fault or site observation.

4.2.40 Scale (Traces, Observations: Events, Observations: Displacement, Observations: Slip Rates, Observations: Fault Geometry)

- Compulsory
- Reported as a number – i.e., 1:200,000 is reported as 200000

Scale at which the trace spatial data was digitised (e.g., 1:100000). For new traces digitised in the fault compilation tool, this is automatically populated from the scale on the screen at the time the attribute is entered. For traces uploaded this should be entered as the average scale at which the trace was digitised.

4.2.41 Site feature (Observations: Events, Observations: Displacement, Observations: Slip Rates, Observations: Fault Geometry)

- Optional
- Free text up to 24 characters long

Brief description of the site. For example, fault in trench, displaced riser, displaced fan, line of springs.

4.2.42 Slip rate category (Fault Sections, Observations: Slip rates)

- Optional
- Reported in millimetres per year
- Chosen one category from a list:

- 0.001 – <0.01
- 0.01 – <0.1
- 0.1 – <1
- 1 – <5
- 5 – <10
- 10 – <50
- 50 – <100
- 100 – <200

An inferred net slip rate, selected from a limited number of categories. To be used only when there is no available data.

4.2.43 Slip type (*Fault Sections, Faults, Observations: Slip rates*)

- Compulsory
- Choose one type from a list:
 - Reverse
 - Thrust (dip <45°)
 - Normal
 - Dextral
 - Sinistral
 - Strike slip *
 - Normal dextral
 - Normal sinistral
 - Reverse dextral *
 - Reverse sinistral *
 - Dextral normal
 - Dextral reverse
 - Sinistral reverse
 - Sinistral normal
 - Thrust dextral *
 - Thrust sinistral *
 - Thrust strike slip *
 - Dextral thrust *
 - Sinistral thrust *
 - Strike slip thrust *
 - Strike slip normal *
 - Normal strike slip *
 - Reverse strike slip *
 - Strike slip reverse *

Dominant and, if applicable, secondary type (sense) of relative slip (displacement or movement) on the fault plane. For the latter, the secondary sense is listed first, followed by the dominant slip. For example a dominantly normal fault with a minor component of dextral slip would be classified as a dextral normal fault.

4.2.44 Slip type completeness (Fault Sections, Faults)

- Compulsory
- Reported as 1, 2, 3, or 4

Relative ranking of the completeness of the data constraining the slip type.

1 = well constrained from multiple field data and/or high resolution seismic profile data

2 = moderately constrained from field or seismic profile data

3 = poorly constrained from subsurface geophysical data

4 = inferred

4.2.45 Strike (Fault Sections, Faults, Observations: Fault geometry)

- Optional
- Reported in decimal degrees from 1° to 360°, rounded to the nearest degree, whereby:
 - 90° = east
 - 180° = south
 - 270° = west
 - 360° = north
- Expressed as preferred, minimum, maximum

The compass direction of the intersection of the fault plane with a horizontal plane (usually simplified as the ground surface). Is defined using the Aki and Richards (1980) convention (or the right-hand rule), whereby the fault dips to the right side (Figure 4.1). For example a fault with a strike of 0° dips to the east, whereas a fault of 180° dips to the west. Defined as an average value for the entire fault or section.

4.2.46 Strike slip rate (Fault Sections, Faults, Observations: Slip rates)

- Optional
- Reported in millimetres per year, up to 3 decimal places
- Expressed as preferred, minimum, maximum

The horizontal, or strike-parallel, component of slip on the fault (see also slip rate). Generally calculated from field measurements of horizontal displacement of dated markers.

4.2.47 Surface dip (Observations: Fault geometry)

- Optional
- Reported in decimal degrees, from 0° (horizontal) to 90° (vertical), rounded to the nearest degree
- Expressed as preferred, minimum, and maximum

Downward inclination of the fault plane from the horizontal, measured at or near the ground surface (e.g., in natural exposures or trenches).

4.2.48 Total displacement (Fault Sections, Observations: Displacement)

- Optional
- Reported in kilometres, up to 2 decimal places

The total displacement across the fault or fault section during the current tectonic regime.

4.2.49 Upper seismogenic depth (Fault Sections, Faults)

- Compulsory
- Reported in kilometres, rounded to the nearest kilometre
- Expressed as preferred, minimum, maximum

Vertical distance below the ground surface to the top edge (tip) of the fault or fault section. For sections or faults with a surface trace this will be 0 and the minimum and maximum will also be 0. If uncertainties cannot be quantified, a default value of $\pm 10\%$ should be used.

4.2.50 Upper seismogenic depth completeness (Fault Sections, Faults)

- Compulsory
- Reported as 1, 2, 3, or 4

Relative ranking of the completeness of the data constraining the upper seismogenic depth.

1 = well constrained from field data or high resolution seismic profile data

2 = moderately constrained from field, seismic profile, or instrumental seismicity data

3 = poorly constrained from field, seismic profile, or instrumental seismicity data

4 = inferred

4.2.51 Vertical displacement (Fault Sections, Observations: Displacement)

- Optional
- Reported in metres, up to 2 decimal places
- Expressed as preferred, minimum, maximum

The vertical component of displacement per event. Generally averaged from field displacement measurements.

4.2.52 Vertical slip rate (Fault Sections, Faults, Observations: Slip rates)

- Compulsory
- Reported in millimetres per year, up to 3 decimal places
- Expressed as preferred, minimum, maximum

The vertical component of slip (displacement or movement) rate on the fault plane averaged over a time period involving at least two large earthquakes. Generally calculated from field or geological measurements of vertical displacement of dated markers. If uncertainties can't be quantified then they must be estimated to encompass the most likely range of values within a 95% confidence interval.

4.3 Neotectonic Folds*

4.3.1 Accuracy (Axial traces, Observations) *

- Calculated
- Reported as a number – i.e., 1:200,000 is reported as 200000

Conservative definition of the location accuracy of the fold axial trace on the ground surface, calculated from twice the scale at which the trace was mapped. For example, if a trace was mapped at 1:100,000 scale then the accuracy is calculated to be 1:200,000.

4.3.2 Age of last movement (Folds, Blind Faults) *

- Optional
- Reported as years before 1950 AD
- Expressed as preferred, minimum, and maximum

Timing of the most recent maximum magnitude earthquake on the fault. Generally derived from historical or field data, but may be inferred from geomorphic expression, analogous faults, expert opinion, etc. Historical earthquakes for which the date is well constrained (i.e., to within one year) should be reported as a preferred value only, relative to 1950 AD. For example 1940 AD is reported as 10 and 1987 AD as -37. Ages obtained by radiocarbon dating must be reported as calibrated ages.

4.3.3 Age of last movement category (Folds) *

- Optional
- Reported as a range of years before present
- Chosen one category from a list:
 - 0 – <1000
 - 1000 – <11,700 (Holocene)
 - 11,700 – <50,000
 - 50,000 – <100,000
 - 100,000 – <1,000,000
 - 1,000,000 – <10,000,000

An inferred age or timing of the last maximum magnitude earthquake on the fault, selected from one of 6 categories. Only to be used if there is no data available to quantify a more precise age.

4.3.4 Aseismic-slip factor (Folds, Blind Faults) *

- Compulsory
- Reported as a value from 0 (fully locked) to 1 (fully creeping), up to 2 decimal places

Fraction of blind fault slip released by creep. For most faults this is likely to be 0.

4.3.5 Axial plane dip (Folds) *

- Optional
- Reported in decimal degrees, from 0° (horizontal) to 90° (vertical), rounded to the nearest degree

- Expressed as preferred, minimum, and maximum

Downward inclination of the fold axial plane from the horizontal, measured in a direction perpendicular to its strike, averaged over the entire axial plane. Generally derived from subsurface geophysical data (e.g., seismic reflection profile), but may be inferred from nearby folds or typical values from folds of the same style.

4.3.6 Axial plane dip direction (Folds) *

- Optional
- Reported in decimal degrees from 1° to 360°, rounded to the nearest degree, whereby:
 - 90° = east
 - 180° = south
 - 270° = west
 - 360° = north

The compass direction towards which the axial plane dips. If the strike and downthrown side are known it can be calculated from 90° to the strike following the Aki and Richards (1980) convention (or the right-hand rule) (Figure 4.1), but an independently derived value can also be entered.

4.3.7 Compiled by (Folds, Blind Faults) *

- Compulsory
- Free text up to 64 characters long
- Only one person can be entered

The name of the person who compiled the data for entry into the database.

4.3.8 Contributed by (Folds, Blind Faults) *

- Optional
- Free text up to 64 characters long.

The name of the person who contributed most of the data.

4.3.9 Created at (Folds, Blind Faults) *

- Optional
- Reported as a date (yyyy-mm-dd)

The date at which data for a particular table was entered or modified. In the fault compilation tool this is chosen from a calendar.

4.3.10 Dip (Blind Faults) *

- Compulsory
- Reported in decimal degrees, from 0° (horizontal) to 90° (vertical), rounded to the nearest degree
- Expressed as preferred, minimum, and maximum

Downward inclination of the fault plane from the horizontal, averaged across the entire fault plane (which may or not be the same as the surface dip). Generally derived from subsurface geophysical data (e.g., seismic reflection profile), but may be inferred from nearby faults or typical values from faults of the same style. If uncertainties cannot be quantified, a default value of $\pm 10^\circ$ should be used.

4.3.11 Dip completeness (Blind Faults) *

- Compulsory
- Reported as 1, 2, 3, or 4

Relative ranking of the completeness of the data constraining the fault dip.

1 = well constrained from high resolution seismic profile data

2 = moderately constrained seismic profile data

3 = poorly constrained from subsurface geophysical data

4 = inferred

4.3.12 Dip direction (Blind Faults) *

- Compulsory
- Reported in decimal degrees from 1° to 360°, rounded to the nearest degree, whereby:
 - 90° = east
 - 180° = south
 - 270° = west
 - 360° = north

The compass direction towards which the blind fault dips. If the strike and downthrown side are known it can be calculated from 90° to the strike following the Aki and Richards (1980) convention (or the right-hand rule) (Figure 4.1), but an independently derived value can also be entered.

4.3.13 Dip direction completeness (Blind Faults) *

- Compulsory
- Reported as 1, 2, 3, or 4

Relative ranking of the completeness of the data constraining the fault dip direction.

1 = well constrained from high resolution seismic profile data

2 = moderately constrained seismic profile data

3 = poorly constrained from subsurface geophysical data

4.3.14 Displacement (Folds) *

- Optional
- Reported in metres, up to 2 decimal places
- Expressed as preferred, minimum, maximum

Average net slip or displacement during a single maximum magnitude earthquake resulting in fold growth (i.e., single event displacement). Generally derived from field data, but may be inferred from analogous folds, expert opinion, scaling relations, etc.

4.3.15 Episodic behaviour (Folds, Blind Faults) *

- Optional
- Choose one of:

- Yes Active
- Yes Inactive
- No

Is there any evidence for episodic behaviour (i.e., periods of activity and inactivity) on the fold or blind fault within the current tectonic regime? If there is evidence for episodic behaviour, is it currently in an active period?

4.3.16 Fold type (Folds) *

- Compulsory
- Choose one type from a list:
 - Anticline
 - Syncline
 - Monocline

Type of fold, defined by its cross-sectional shape.

4.3.17 Geomorphic Expression (Axial traces) *

- Compulsory
- Choose one expression from a list:
 - Sharp feature
 - Broad warp
 - Topographic feature
 - Limb defined
 - Concealed
 - No trace

Expression of the fold axial trace on the ground or on digital imagery (e.g., SRTM data, Google Earth).

1. Sharp feature = Well defined, distinct, feature (fold scarp)
2. Broad warp = Wide, moderately well defined topographic warp or bulge, where the position of the axial trace is moderately defined.
3. Topographic feature = ridge crest or depression which might represent an eroded axial trace.
4. Bedrock extension = Inferred extension of a fault along a bedrock fold.
- 4 Limb defined = axial trace inferred between two limbs, but the exact position is poorly defined.
5. Concealed = Inferred fold buried beneath deposits younger than the last phase of deformation (e.g., alluvium) or a water body (river, lake, sea).
6. No trace = No geomorphic expression of the fold exists, but it is inferred from other datasets.

4.3.18 Growth rate – vertical (Folds) *

- Compulsory
- Reported in millimetres per year, up to 3 decimal places
- Expressed as preferred, minimum, and maximum

The rate of vertical growth of the fold (fold amplitude growth). Generally derived from field data, but may be inferred from geomorphic expression, geodetic data, plate motion budgets etc.

4.3.19 Growth rate – horizontal (Folds) *

- Optional
- Reported in millimetres per year, up to 3 decimal places
- Expressed as preferred, minimum, and maximum

The rate of horizontal growth (elongation) of the fold, measured parallel to its strike. Generally derived from field or geological data.

4.3.20 Last updated *

- Calculated
- Reported as a date (yyyy-mm-dd)

Date when the fold or blind fault attributes were last updated. In the fault compilation tool this is automatically calculated and does not appear in the tables.

4.3.21 Length (Folds, Blind Faults) *

- Optional
- Reported in kilometres, rounded to the nearest kilometre
- Expressed as preferred, minimum, and maximum

Length of the fold measured along its axial trace; inferred length of the blind fault.

4.3.22 Limb dip – shallow limb (Folds) *

- Optional
- Reported in decimal degrees, from 0° (horizontal) to 90° (vertical), rounded to the nearest degree.
- Expressed as preferred, minimum, and maximum

Downward inclination of the shallow limb of the fold from the horizontal. Generally derived from field or subsurface geophysical data (e.g., seismic reflection profile).

4.3.23 Limb dip – steep limb (Folds) *

- Optional
- Reported in decimal degrees, from 0° (horizontal) to 90° (vertical), rounded to the nearest degree.
- Expressed as preferred, minimum, and maximum

Downward inclination of the steep limb of the fold from the horizontal. Generally derived from field or subsurface geophysical data (e.g., seismic reflection profile).

4.3.24 Limb dip direction – shallow limb (Folds) *

- Optional
- Reported in decimal degrees from 1° to 360°, rounded to the nearest degree, whereby:
 - 90° = east
 - 180° = south

- 270° = west
- 360° = north

The compass direction towards which the shallow limb of the fold dips. If the strike and downthrown side are known it can be calculated from 90° to the strike following the Aki and Richards (1980) convention (or the right-hand rule) (Figure 4.1), but an independently derived value can also be entered.

4.3.25 Limb dip direction – steep limb (Folds) *

- Optional
- Reported in decimal degrees from 1° to 360°, rounded to the nearest degree, whereby:
 - 90° = east
 - 180° = south
 - 270° = west
 - 360° = north

The compass direction towards which the steep limb of the fold dips. If the strike and downthrown side are known it can be calculated from 90° to the strike following the Aki and Richards (1980) convention (or the right-hand rule) (Figure 2.1), but an independently derived value can also be entered.

4.3.26 Location Method (Axial traces) *

- Compulsory
- Choose one method from a list:
 - GPS survey
 - LiDAR
 - Aerial photographs
 - Topographic Map
 - Google Earth
 - Digital Elevation Model *
 - Digital Elevation Model (SRTM) *
 - Geological Map *
 - Personal Communication *
 - Report *
 - Composite

The base map on which the fold axial trace was digitised. Composite can be used where traces were digitised on more than one base map.

4.3.27 Lower seismogenic depth (Blind Faults) *

- Compulsory
- Reported in kilometres, rounded to the nearest kilometre
- Expressed as preferred, minimum, maximum

Vertical distance below the ground surface to the bottom edge (base) of the blind fault. For historical fault ruptures, this may be obtained from seismological data (e.g., earthquake hypocentre, aftershock seismicity). For remaining faults it may be inferred from the base of the seismogenic zone, as defined by instrumental seismicity, or from locking depths derived from geodesy. If uncertainties cannot be quantified, a default value of $\pm 10\%$ should be used.

4.3.28 Lower seismogenic depth completeness (Blind Faults) *

- Compulsory
- Reported as 1, 2, 3, or 4

Relative ranking of the completeness of the data constraining the lower seismogenic depth.

1 = well constrained from field data or high resolution seismic profile data

2 = moderately constrained from seismic profile or instrumental seismicity data

3 = poorly constrained from instrumental seismicity data

4 = inferred

4.3.29 Marker age (Folds) *

- Optional
- Reported as years before 1950 AD
- Expressed as preferred, minimum, maximum

Age of the dominant geomorphic or geological marker which is folded and used to calculate key attributes such as fold vertical growth rate. Ages obtained by radiocarbon dating must be reported as calibrated ages.

4.3.30 Name (Axial traces, Folds, Blind Faults) *

- Compulsory
- Free text up to 96 characters long

The name of a known or inferred trace, fold, or blind fault. For unnamed features, a name will need to be assigned, such as from a nearby place name.

4.3.31 Net slip rate (Blind Faults) *

- Compulsory
- Reported in millimetres per year, up to 3 decimal places
- Expressed as preferred, minimum, maximum

The net slip (displacement or movement) rate on the blind fault plane averaged over a time period involving at least two large earthquakes.

4.3.32 Net slip rate completeness (Blind Faults) *

- Compulsory
- Reported as 1, 2, 3, or 4

Relative ranking of the completeness of the data constraining the slip rate.

- 1 = well constrained from multiple fold vertical growth rate field data
- 2 = moderately constrained from fold vertical growth rate field data
- 3 = poorly constrained from fold vertical growth rate field or geological data
- 4 = inferred

4.3.33 Notes (Axial traces, Folds, Blind Faults) *

- Optional
- Free text

Brief notes of any important neotectonic fold information which are not included elsewhere in the database.

4.3.34 Overall completeness (Folds, Blind Faults) *

- Compulsory, Calculated
- Reported as 1, 2, 3, or 4, rounded to the nearest whole number

Relative ranking of the overall completeness of the fold or blind fault data, weighted towards the key parameter slip rate. For folds this needs to be assigned qualitatively. For blind faults it is calculated from a combination of all the fault data completeness rankings, whereby the slip rate ranking contributes 5 times the others, i.e.:

upper seismogenic depth data completeness +
 lower seismogenic depth data completeness +
 dip data completeness +
 dip direction data completeness +
 slip type data completeness +
 5 x slip rate data completeness +
 aseismic-slip data completeness

divided by the total, 11.

4.3.35 Plunge (Folds) *

- Optional
- Reported in decimal degrees, from 0° (horizontal) to 90° (vertical), rounded to the nearest degree
- Expressed as preferred, minimum, and maximum

Downward inclination of the fold axial trace from the horizontal, measured along its strike. Generally measured at the ground surface.

4.3.36 Plunge direction (Folds) *

- Optional
- Reported in decimal degrees from 1° to 360°, rounded to the nearest degree, whereby:
 - 90° = east
 - 180° = south
 - 270° = west
 - 360° = north

The compass direction towards which the fold plunges. Generally measured at the ground surface or from geological data.

4.3.37 Recurrence interval (Folds, Blind Faults) *

- Optional
- Reported in years, rounded to the nearest year
- Expressed as preferred, minimum, maximum

Average time between successive maximum magnitude earthquakes on the fold or blind fault. Generally derived from fold field data, but may be calculated from D/SR (Displacement divided by Slip Rate), or inferred from analogous faults, expert opinion, etc.

4.3.38 References *

- Optional
- Free text
- Bulletin of the Seismological Society of America format

List of references noted for a particular axial trace, fold, blind fault or site observation.

4.3.39 Scale (Axial traces, Observations) *

- Compulsory
- Reported as a number – i.e., 1:200,000 is reported as 200000

Scale at which the fold axial trace spatial data was digitised (e.g., 1:100,000). For new traces digitised in the fault compilation tool or in a GIS programme, this is the average scale at which the digitiser is working.

4.3.40 Site feature (Observations) *

- Optional
- Free text up to 24 characters long

Brief description of the site. For example, fault in trench, displaced riser, displaced fan, line of springs.

4.3.41 Slip type (Blind Faults) *

- Compulsory
- Choose one type from a list:
 - Reverse
 - Thrust (dip <45°)
 - Normal
 - Dextral
 - Sinistral
 - Strike slip *
 - Normal dextral
 - Normal sinistral
 - Reverse dextral *

- Reverse sinistral *
- Dextral normal
- Dextral reverse
- Sinistral reverse
- Sinistral normal
- Thrust dextral *
- Thrust sinistral *
- Thrust strike slip *
- Dextral thrust *
- Sinistral thrust *
- Strike slip thrust *
- Strike slip normal *
- Normal strike slip *
- Reverse strike slip *
- Strike slip reverse *

Dominant and, if applicable, secondary type (sense) of relative slip (displacement or movement) on the blind fault plane. For the latter, the secondary sense is listed first, followed by the dominant slip. For example a dominantly normal fault with a minor component of dextral slip would be classified as a dextral normal fault.

4.3.42 Slip type completeness (Blind Faults) *

- Compulsory
- Reported as 1, 2, 3, or 4

Relative ranking of the completeness of the data constraining the slip type.

1 = well constrained from multiple field data and/or high resolution seismic profile data

2 = moderately constrained from field or seismic profile data

3 = poorly constrained from subsurface geophysical data

4 = inferred

4.3.43 Strike (Blind Faults) *

- Optional
- Reported in decimal degrees from 1° to 360°, rounded to the nearest degree, whereby:
 - 90° = east
 - 180° = south
 - 270° = west
 - 360° = north
- Expressed as preferred, minimum, maximum

The compass direction of the intersection of the fault plane with a horizontal plane. Is defined using the Aki and Richards (1980) convention (the right-hand rule), whereby the fault dips to the right side (Figure 4.1). For example a fault with a strike of 0° dips to the east, whereas a fault of 180° dips to the west. Defined as an average value for the entire blind fault.

4.3.44 Strike slip rate (Blind Faults) *

- Optional
- Reported in millimetres per year, up to 3 decimal places
- Expressed as preferred, minimum, maximum

The horizontal, or strike-parallel, component of slip (displacement or movement) rate on the fault plane averaged over a time period involving at least two large earthquakes. Generally calculated from field measurements of horizontal displacement of dated markers.

4.3.45 Tilt rate – shallow limb (Folds) *

- Optional
- Reported in degrees per thousand years (°/kyr), up to 3 decimal places
- Expressed as preferred, minimum, and maximum

The rate of tilt (differential uplift or subsidence from the horizontal) of the shallow fold limb.

4.3.46 Tilt rate – steep limb (Folds) *

- Optional
- Reported in degrees per thousand years (°/kyr), up to 3 decimal places
- Expressed as preferred, minimum, and maximum

The rate of tilt (differential uplift or subsidence from the horizontal) of the steep fold limb.

4.3.47 Upper seismogenic depth (Blind Faults) *

- Compulsory
- Reported in kilometres, rounded to the nearest kilometre
- Expressed as preferred, minimum, maximum

Vertical distance below the ground surface to the top edge (tip) of the blind fault. If uncertainties cannot be quantified, a default value of ±10% should be used.

4.3.48 Upper seismogenic depth completeness (Blind Faults) *

- Compulsory
- Reported as 1, 2, 3, or 4

Relative ranking of the completeness of the data constraining the upper seismogenic depth.

1 = well constrained from high resolution seismic profile data

2 = moderately constrained from seismic profile, or instrumental seismicity data

3 = poorly constrained from seismic profile, or instrumental seismicity data

4 = inferred

4.3.49 Vertical slip rate (*Blind Faults*)

- Compulsory
- Reported in millimetres per year, up to 3 decimal places
- Expressed as preferred, minimum, maximum

The vertical component of slip (displacement or movement) rate on the blind fault plane averaged over a time period involving at least two large earthquakes. Generally assigned from the fold vertical growth rate. If uncertainties can't be quantified then they must be estimated to encompass the most likely range of values within a 95% confidence interval.

4.4 Fault Sources

In the fault compilation tool all of the fault sources attributes are automatically populated from the fault attributes.

4.4.1 Age of last movement (*Fault Sources*)

- Optional
- Reported as years before 1950 AD
- Obtained automatically from fault or blind fault age of last movement
- Expressed as preferred, minimum, and maximum

Year or age of the most recent maximum magnitude earthquake on the fault source. Ages obtained by radiocarbon dating must be reported as calibrated ages.

4.4.2 Area (*Fault Sources*)

- Calculated
- Reported in square kilometres (km²), rounded to the nearest km²
- Expressed as preferred, minimum, maximum

Area of the fault source as measured on the fault plane. Calculated from length and width, and their uncertainties.

4.4.3 Aseismic-slip factor (*Fault Sources*)

- Compulsory
- Reported as a value from 0 (fully locked) to 1 (fully creeping), up to 2 decimal places
- Obtained automatically from the fault or blind fault aseismic-slip factor

Fraction of the fault source slip released by creep.

4.4.4 Aseismic-slip factor completeness (*Fault Sources*)

- Compulsory
- Reported as 1, 2, 3, or 4.
- Obtained automatically from the fault or blind fault aseismic-slip data completeness

Relative ranking of the completeness of the data constraining the Aseismic-slip factor.

1 = well constrained from multiple field data

2 = moderately constrained from field data

3 = poorly constrained from field or geological data

4 = inferred

4.4.5 *Compiled by (Fault Sources)*

- Compulsory
- Free text up to 64 characters long
- Only one person can be entered
- Obtained directly from the fault or blind fault Compiled by

The name of the person who compiled the data for entry into the database.

4.4.6 *Contributed by (Fault Sources)*

- Optional
- Free text up to 64 characters long
- Obtained directly from the fault or blind fault compiled by.

The name of the person who contributed most of the fault source attributes.

4.4.7 *Created at (Fault Sources) **

- Optional
- Reported as a date (yyyy-mm-dd)

The date at which data for a particular table was entered or modified. In the fault compilation tool this is chosen from a calendar.

4.4.8 *Dip (Fault Sources)*

- Compulsory
- Reported in decimal degrees, from 0° (horizontal) to 90° (vertical), rounded to the nearest degree
- Expressed as preferred, minimum, and maximum.
- Obtained automatically from the fault or blind fault dip

Downward inclination of the fault plane from the horizontal, averaged for the entire fault plane (i.e., not just the surface dip).

4.4.9 *Dip completeness (Fault Sources)*

- Compulsory
- Reported as 1, 2, 3, or 4.
- Obtained automatically from the fault or blind fault dip data completeness

Relative ranking of the completeness of the data constraining the fault dip.

1 = well constrained from multiple field data and/or high resolution seismic profile data

2 = moderately constrained from field or seismic profile data

3 = poorly constrained from subsurface geophysical data

4 = inferred

4.4.10 *Dip direction (Fault Sources)*

- Compulsory
- Reported in decimal degrees from 1° to 360°, rounded to the nearest degree, whereby:
 - 90° = east
 - 180° = south
 - 270° = west
 - 360° = north
- Obtained automatically from the fault or blind fault dip direction

The compass direction towards which the fault dips. Could be calculated from the strike following the Aki and Richards (1980) convention (or the right-hand rule; Figure 4.1), but can also be entered manually.

4.4.11 *Dip direction completeness (Fault Sources)*

- Compulsory
- Reported as 1, 2, 3, or 4
- Obtained automatically from the neotectonic fault or blind fault dip direction data completeness

Relative ranking of the completeness of the data constraining the fault dip direction.

- 1 = well constrained from multiple field data and/or high resolution seismic profile data
- 2 = moderately constrained from field or seismic profile data
- 3 = poorly constrained from subsurface geophysical data
- 4 = inferred

4.4.12 *Last updated*

- Calculated
- Reported as a date (yyyy-mm-dd)

Date when the fault source attributes were last updated. In the fault compilation tool this is automatically calculated and does not appear in the tables.

4.4.13 *Length (Fault Sources)*

- Calculated
- Reported in kilometres, rounded to the nearest kilometre
- Expressed as preferred, minimum, maximum

Length of the fault source, measured along its strike. The minimum and maximum lengths are $\pm 10\%$ of the preferred value.

4.4.14 *Lower seismogenic depth (Fault Sources)*

- Compulsory
- Reported in kilometres, rounded to the nearest kilometre
- Expressed as preferred, minimum, maximum
- Obtained automatically from the fault or blind fault lower seismogenic depth

Vertical distance below the ground surface to the bottom edge (base) of the fault source.

4.4.15 Lower seismogenic depth completeness (Fault Sources)

- Compulsory
- Reported as 1, 2, 3, or 4
- Obtained automatically from the fault or blind fault lower seismogenic depth

Relative ranking of the completeness of the data constraining the lower seismogenic depth.

1 = well constrained from field data or high resolution seismic profile data

2 = moderately constrained from seismic profile or instrumental seismicity data

3 = poorly constrained from instrumental seismicity data

4 = inferred

4.4.16 Maximum magnitude (Fault Sources)

- Calculated
- Moment magnitude (M_w), to 1 decimal place
- Choose one magnitude scaling relation from a list (Appendix A)
- Expressed as preferred, minimum, maximum

Moment magnitude of the maximum size earthquake that the fault source could produce.

4.4.17 Name (Fault Sources)

- Compulsory
- Free text up to 96 characters long

The name of the fault source. This will generally be the same as the corresponding neotectonic fault, fold, and/or blind fault. For sources without corresponding fault or fold data, the source may be named from an earthquake, nearby place name, etc.

4.4.18 Net slip rate (Fault Sources)

- Compulsory
- Reported in millimetres per year, up to 3 decimal places
- Expressed as preferred, minimum, maximum
- Obtained automatically from the fault or blind fault slip rate

The net slip (displacement or movement) rate on the fault plane averaged over a time period involving at least two large earthquakes.

4.4.19 Net slip rate completeness (Fault Sources)

- Compulsory
- Reported as 1, 2, 3, or 4
- Obtained automatically from the fault or blind fault slip rate data completeness.

Relative ranking of the completeness of the data constraining the slip rate.

- 1 = well constrained from multiple field data
- 2 = moderately constrained from field data
- 3 = poorly constrained from field or geological data
- 4 = inferred

4.4.20 Notes (Fault Sources) *

- Optional
- Free text

Brief notes of any important information about the fault source not included elsewhere in the database.

4.4.21 Overall completeness (Fault Sources)

- Calculated
- Reported as 1, 2, 3, or 4, rounded to the nearest whole number
- Obtained directly from fault or blind fault data completeness

Relative ranking of the overall completeness of the fault source data, weighted towards the key parameter slip rate. Calculated from a combination of all the fault data completeness rankings, whereby the slip rate ranking contributes 5 times the others, i.e.:

upper seismogenic depth data completeness +
 lower seismogenic depth data completeness +
 dip data completeness +
 dip direction data completeness +
 slip type data completeness +
 5 x slip rate data completeness +
 aseismic-slip data completeness

divided by the total, 11.

4.4.22 Rake (Fault Sources)

- Optional
- Reported in decimal degrees, from -180° to 180° , rounded to the nearest degree, whereby:
 - -90° = normal
 - 0° = left lateral (sinistral)
 - 90° = reverse
 - $180^\circ = -180^\circ$ = right lateral (dextral)
- Expressed as preferred, minimum, maximum
- Obtained from the fault rake.

The direction of hanging wall slip, measured relative to the horizontal (strike).

4.4.23 *Recurrence interval (Fault Sources)*

- Calculated
- Reported in years, rounded to the nearest year
- Expressed as preferred, minimum, maximum

Average recurrence interval calculated from displacement divided by slip rate, whereby displacement is calculated from scaling relations (see Appendix B).

4.4.24 *References (Fault Source) **

- Optional
- Free text
- Bulletin of the Seismological Society of America format

List of references for the fault source data.

4.4.25 *Slip type (Fault Sources)*

- Compulsory
- Choose one type from a list:
 - Reverse
 - Thrust (dip <45°)
 - Normal
 - Dextral
 - Sinistral
 - Strike slip *
 - Normal dextral
 - Normal sinistral
 - Reverse dextral *
 - Reverse sinistral *
 - Dextral normal
 - Dextral reverse
 - Sinistral reverse
 - Sinistral normal
 - Thrust dextral *
 - Thrust sinistral *
 - Thrust strike slip *
 - Dextral thrust *
 - Sinistral thrust *
 - Strike slip thrust *
 - Strike slip normal *
 - Normal strike slip *

- Reverse strike slip *
- Strike slip reverse *
- Obtained automatically from the neotectonic fault or blind fault slip type

Dominant and, if applicable, secondary type (sense) of relative slip (displacement or movement) on the fault plane. For the latter, the secondary sense is listed first, followed by the dominant slip. For example a dominantly normal fault with a minor component of dextral slip would be classified as a dextral normal fault.

4.4.26 Slip type completeness (Fault Sources)

- Compulsory
- Reported as 1, 2, 3, or 4
- Obtained directly from the fault or blind fault slip type data completeness.

Relative ranking of the completeness of the data constraining the slip type.

- 1 = well constrained from multiple field data and/or high resolution seismic profile data
- 2 = moderately constrained from field or seismic profile data
- 3 = poorly constrained from subsurface geophysical data
- 4 = inferred

4.4.27 Tectonic region (Fault Sources) *

- Optional
- Free text up to 254 characters

Brief description of the tectonic region in which the fault source is located. Is useful in selecting the magnitude scaling relationship to be used for calculating the magnitude.

4.4.28 Upper seismogenic depth (Fault Sources)

- Compulsory
- Reported in kilometres, rounded to the nearest kilometre
- Expressed as preferred, minimum, maximum
- Obtained automatically from the fault or blind fault upper seismogenic depth

Vertical distance below the ground surface to the top edge (tip) of the fault source.

4.4.29 Upper seismogenic depth completeness (Fault Sources)

- Compulsory
- Reported as 1, 2, 3, or 4
- Obtained automatically from the fault or blind fault upper seismogenic depth data completeness.

Relative ranking of the completeness of the data constraining the upper seismogenic depth.

- 1 = well constrained from field data or high resolution seismic profile data
- 2 = moderately constrained from field, seismic profile, or instrumental seismicity data
- 3 = poorly constrained from field, seismic profile, or instrumental seismicity data
- 4 = inferred

4.4.30 Width (Fault Sources)

- Calculated
- Reported in kilometres, rounded to the nearest kilometre
- Expressed as preferred, minimum, maximum

Width of the fault source, measured on the fault plane, in a down-dip direction (i.e., perpendicular to the strike). Calculated from dip, and upper and lower seismic depths, and their uncertainties.

4.5 Maximum magnitude calculation

Maximum magnitude is calculated from fault source polygon Length or Area using magnitude-length or magnitude-area scaling relationships. The appropriate magnitude scaling relationships should be selected from Table A.1 on the basis of tectonic regime.

At the time of writing (May 2013) the fault compilation tool (v.12.11) automatically calculates maximum magnitude from a single magnitude scaling relationship.

Table 4.1 Magnitude scaling relationships for calculation of fault source maximum magnitude. From Stirling and Goded (2012) and Stirling et al. (2013).

Tectonic regime	Name ¹	Relationship	Units	Quality score ²
Fast (> 10 mm/yr), plate boundary crustal, strike-slip faults	<u>Hanks and Bakun (2008) – A</u> $\leq 537\text{km}^2$	$M_w = \text{Log}A + (3.98 \pm 0.03)$	A: Area (km ²)	1
	<u>Hanks and Bakun (2008) – A</u> $> 537\text{km}^2$	$M_w = 4/3\text{Log}A + (3.07 \pm 0.04)$		1
	UCERF2	$M_w = 4.2775A^{0.0726}$	A: Area (km ²)	1
	Wesnousky (2008) – strike slip	$M_w = 5.56 + 0.87\text{Log}L$ sig=0.24 (in M_w)	L: surface rupture length (km)	1
	Leonard (2010)	$M_w = 3.99 + \text{Log}A$	A: Area (km ²)	1
Slow (<10 mm/yr) plate boundary crustal faults (all slip types)	<u>Yen and Ma (2011) – all</u>	$\text{Log}A_e = -13.79 + 0.87\text{Log}M_o$ sig=0.41 (in A_e) $\text{Log}M_o = 16.05 + 1.5M_w$	A_e : effective area (m ²)	1
Slow (<10 mm/yr) plate boundary crustal strike-slip faults	Hanks and Bakun (2008) – A $\leq 537\text{km}^2$	$M_w = \text{Log}A + (3.98 \pm 0.03)$	A: Area (km ²)	1
	<u>Stirling et al. (2008) (New Zealand – oblique-slip)</u>	$M_w = 4.18 + 2/3\text{log}W + 4/3\text{log}L$ sig=0.18 (in M_w)	L: subsurface rupture length (km) W: Width (km)	1
	Wesnousky (2008) – strike slip	$M_w = 5.56 + 0.87\text{Log}L$ sig=0.24 (in M_w)	L: surface rupture length (km)	1
	Yen and Ma (2011) – strike slip	$\text{Log}A_e = -14.77 + 0.92\text{Log}M_o$ sig=0.40 (in A_e) $\text{Log}M_o = 16.05 + 1.5M_w$	A_e : effective area (m ²)	1

Tectonic regime	Name ¹	Relationship	Units	Quality score ²
Slow (<10 mm/yr) plate boundary crustal normal faults	<u>Wesnousky (2008) – normal</u>	$M_w = 6.12 + 0.47\text{Log}L$ sig=0.27 (in M_w)	L: surface rupture length (km)	1
Slow (<10 mm/yr) plate boundary crustal reverse faults	Stirling <i>et al.</i> (2008) (New Zealand – oblique-slip)	$M_w = 4.18 + 2/3\text{log}W + 4/3\text{log}L$ sig=0.18 (in M_w)	W: Width (km) L: Subsurface rupture length (km)	1
	Wesnousky (2008) – reverse	$M_w = 4.11 + 1.88\text{Log}L$ sig=0.24 (in M_w)	L: surface rupture length (km)	1
	<u>Yen and Ma (2011) – dip slip</u>	$\text{Log}A_e = -12.45 + 0.80\text{Log}M_o$ sig=0.43 (in A_e) $\text{Log}M_o = 16.05 + 1.5M_w$	A_e : effective area (m ²)	1
Stable continental reverse faults	Anderson <i>et al.</i> (1996)	$M_w = 5.12 + 1.16\text{Log}L - 0.20\text{Log}S$ sig=0.26 (in M_w)	L: surface fault length (km) S: slip rate (mm/yr) M_o : seismic moment (dyne-cm)	2
	<u>Nuttli (1983)</u>	$\text{Log} M_o = 3.65\text{Log}L + 21.0$ $\text{Log}M_o = 16.05 + 1.5M_w$	L: subsurface fault length (km)	3
	<u>Johnston (1994)</u>	$M_w = 1.36 * \text{Log}L + 4.67$	L=surface rupture length (km)	3
Stable continental strike-slip faults	<u>Anderson <i>et al.</i> (1996)</u>	$M_w = 5.12 + 1.16\text{Log}L - 0.20\text{Log}S$ sig=0.26 (in M_w)	L: surface fault length (km) S: slip rate (mm/yr) M_o : seismic moment (dyne-cm)	2
	<u>Nuttli (1983)</u>	$\text{Log} M_o = 3.65\text{Log}L + 21.0$ $\text{Log}M_o = 16.05 + 1.5M_w$	L: subsurface fault length (km)	3
Continental subduction thrust faults	<u>Strasser <i>et al.</i> (2010) Interface events</u>	$M_w = 4.441 + 0.846 \log_{10} (A)$ sig=0.286 (in M_w)	A: Rupture Area (km ²)	1
Marine subduction thrust faults	<u>Strasser <i>et al.</i> (2010) Interface events</u>	$M_w = 4.441 + 0.846 \log_{10} (A)$ sig=0.286 (in M_w)	A: Rupture Area (km ²)	1
	Blaser <i>et al.</i> (2010) Oceanic/subduction Reverse	$\text{Log}_{10}L = -2.81 + 0.62M_w$ $S_{xy} = 0.16$ (orthogonal standard deviation)	L: subsurface fault length (km)	1

Tectonic regime	Name ¹	Relationship	Units	Quality score ²
Intraslab subduction normal faults	<u>Ichinose <i>et al.</i> (2006)</u>	$\text{Log}_{10}(A_a) = 0.57 (\pm 0.06) M_0 - 13.5$ $(\pm 1.5) \text{sig} = 16.1$ (in A_a)	A_a : combined area of asperities (km ²) M_0 =seismic moment (dyne-cm)	1
Thin (<10 km) volcanic crust normal faults	<u>Villamor <i>et al.</i> (2001) (New Zealand – normal)</u>	$M_w = 3.39 + 1.33 \text{Log} A$ $\text{sig} = 0.195$ (in M_w)	A: Area (km ²)	1
Thick (>10 km) volcanic crust normal faults	<u>Wesnousky (2008) – normal</u>	$M_w = 6.12 + 0.47 \text{Log} L$ $\text{sig} = 0.27$ (in M_w)	L: surface fault length (km)	1

¹ Underlined relationships are recommended (highest Quality score and/or most suitable regressions for the given tectonic regimes).

Regressions not underlined provide close alternatives to the shortlisted regressions for the given tectonic regimes.

² 1 = best available, 2 = good, 3 = fair

4.6 Recurrence interval calculation

Fault source recurrence interval is calculated automatically using the following steps and equations:

1. Calculate seismic moment (M_0) from maximum magnitude (M_w) using:

$$\log M_0 = 16.05 + 1.5 M_w \quad (1.1)$$

(Hanks and Kanamori, 1977).

2. Calculate displacement (per event, or single event displacement; D) using:

$$M_0 = \mu L W D \quad (1.2)$$

(Aki and Richards, 1980). Where μ is rigidity modulus (assumed to be 3×10^{11} dyne/cm²), L is fault source length in centimetres, W is fault source width in centimetres.

3. Calculate recurrence interval from:

$$RI = D/SR \quad (1.3)$$

Where RI is recurrence interval in years, D is displacement in millimetres, SR is slip rate in millimetres per year.

The calculated displacement (D) and recurrence interval (RI) can then be compared with the field-based data stored for neotectonic faults or blind faults. If there are major discrepancies, changes can be made to the fault source length, or dip (in the neotectonic fault and blind fault parts of the data), until the recalculated values match within uncertainty.

5 The database design

This section is a reproduction of the Database Design report (Thomas et al., 2012), skipping part of the introduction and with minor adjustment to the section numbering and removal of a figure that is included as Figure 3.1. The original Appendix 1 is included as further sub-section.

This Section aims to describe the GEM Faulted Earth database schema. The GEM Faulted Earth database is designed to provide a new standard for recording neotectonic fault and fault source information, and to serve as a centralised repository for the aggregation of existing national datasets.

5.1 Background

The database design is based on a thorough review of existing databases (Litchfield et al., 2011, and Section 2). The scientific aspects are not addressed in this document. Earth Science has a very parametric view towards capturing data and the GFE database is no different. Some design concepts were incorporated from previous work in this area (Morrison et al., 2003).

Litchfield et al. (2013b) (and Section 3) furnished a conceptual fault, fold, and fault source model (Figure 3.1). Further object modelling and robustness analysis using UML (Figures 5.1, 5.2) helped to confirm the roles and responsibilities.

Some key elements that existed within the conceptual model were:

- High level summary information
- Fine grain detailed information
- Companion Metadata
- Data Quality Assurance
- Geometric Representation
- Composite data values

The challenge was to incorporate these, at times, conflicting aspects within a spatially enabled RDBMS. Where possible the domain integrity or identity of entities was preserved or at least visible from the outside. Normalisation techniques were applied where appropriate and these influenced later design versions of the schema.

5.2 UML Model

The UML model is presented here in two parts for ease of printing: 1) the summary information and spatial trace part; and 2) the combined observational and metadata part. The separation is also a slight historical legacy due to a more complete understanding of the nature of observation data.

5.2.1 Gem-Core

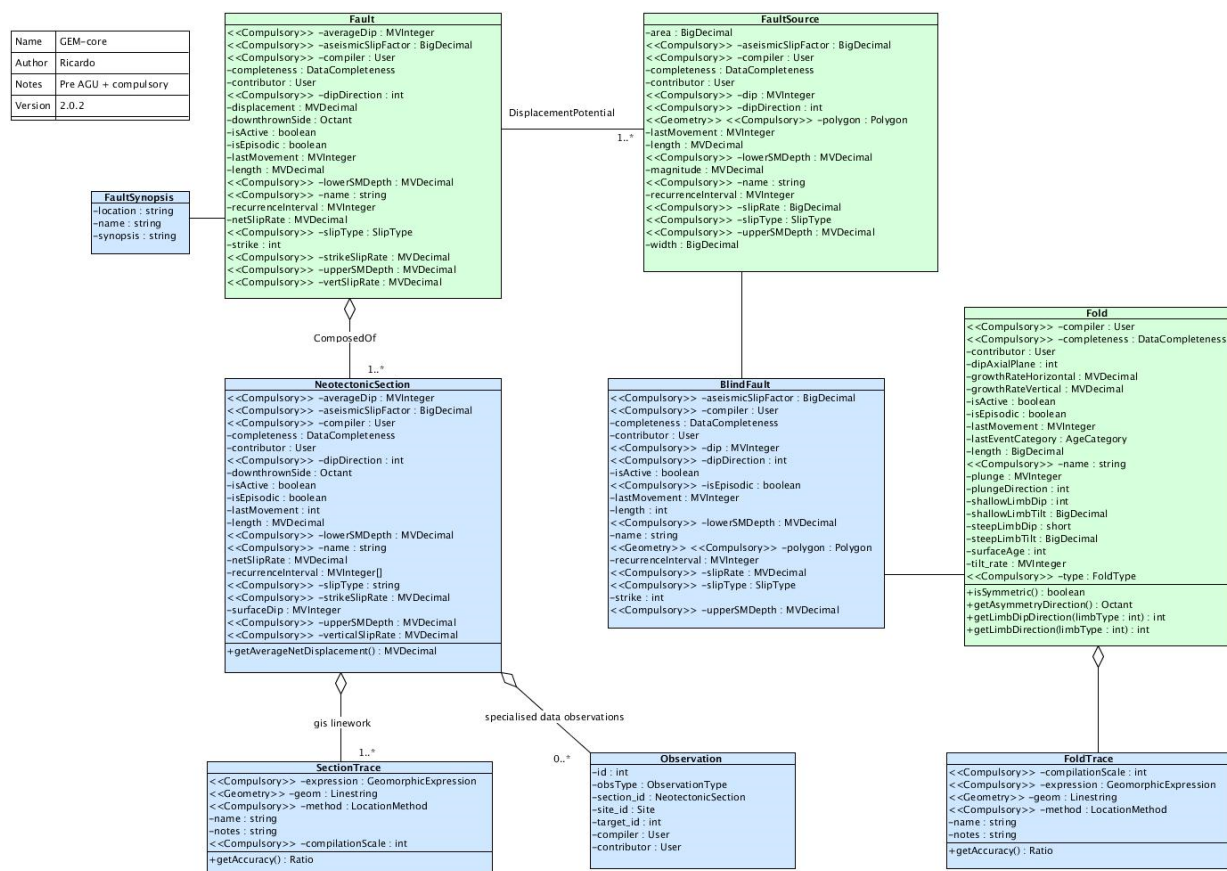


Figure 5.1 GEM-Core UML model

Figure 5.1 represents a domain object model for the high level entities from the conceptual model. Compulsory stereotypes have been added to indicate mandatory status of object properties. This is to assist business rule implementation for user interfaces (UIs). The stereotypes are noted here because it is not always possible to enforce this at a database level.

5.2.2 Gem-Metadata

Figure 5.2 illustrates the domain model for the combined observational and metadata component.

The high definition observations extracted from Figure 3.1 are generalised into a common Observation. An Observation handles speciality through the use of an ObservationType, which in turn is used to define collections of Parameters and Results. Observations may be recorded at spatial sites of interest, but are not required to be exclusively “spatial”. Section 4.6 (former Appendix 1) provides some working example SQL queries, based on New Zealand data, to reconstitute Observation and Observation related data.

The GEM Faulted Earth database has a requirement for the recording of very fine grained metadata. This is partially shown in Figure 3.1. Litchfield et al. (2013a) itemise this in more detail. Suffice to say that metadata needs to be captured at both a record and individual field level.

Field level metadata can be stored directly against a result, in the form of a description property termed the derivation, or a categorical derivation type. Record level metadata is stored in the form of a compilation note.

Name	GEM-metadata
Author	Ricardo
Notes	Post Obsvn review
Version	2.0.1

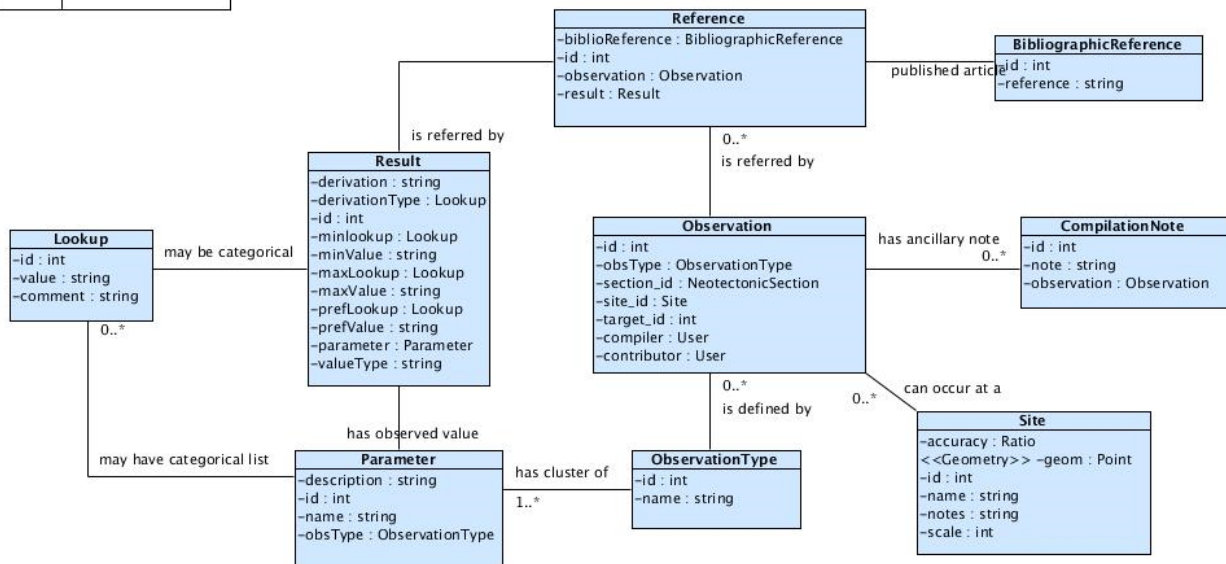


Figure 5.2 Faulted Earth Observation/Metadata UML

5.3 Implementation

The implementation has been performed using the open source Postgresql database. The current installation is based on Version 9.1.2. Spatial data has been managed using the PostGis extension for Postgresql. The current version is 1.5.3.

5.3.1 Composite Data values

One data characteristic of the earthquake domain is that some particular properties or parameters do not have a single value. These are instead recorded as 3-value tuples, which express the minimum, maximum and preferred values.

The Postgresql RDBMS allowed us to create composite data types for these multi-value tuples. Insertions or updates are performed using Row Constructor expressions (<http://www.postgresql.org/docs/9.1/static/sql-expressions.html/SQL-SYNTAX-ROW-STRUCTORS>). These are expressed by the types:

- gem.mv_date
- gem.mv_decimal
- gem.mv_integer
- gem.mv_smallint

5.3.2 Spatial Characteristics

Emphasis has been placed on the storage of spatial locations for the Faulted Earth database. To support that Sites locations are recorded as POINTS, FoldTraces and SectionTraces are recorded as LINESTRINGS,

FaultSources are recorded as POLYGONS which effectively project the outline of the rupture plane to the Earths' surface.

For the linear features, requirements of the scientists and local New Zealand conditions within the data preclude the use of MULTILINESTRING geometry types. All geometries are recorded using the WGS84 Coordinate Reference System (CRS).

Using spatial technological characteristics such as MULTILINESTRING geometry types, and linear referencing were examined, but discarded when local conditions proved them to be either inadequate or inappropriate.

5.3.3 Redundancy

All tables with the GEM Faulted Earth database can essentially be reduced to a series of Observations. Thus the high level summary tables will also contain an additional Observation record. Providing this behaviour was to facilitate handling numeric data in a consistent way.

Another reason was to allow the machine-generation of summary records, using an automated process, without overwriting existing data. This process would aggregate values from the fine-grained Observation-Parameter-Results under a series of different aggregation rules to simulate "modelling" behaviour.

Normalising data into the Observation table does make some aspects of the database harder to work with. Retaining the high level summary tables allows them to act as convenient facades and permit some business rules to be implemented in the form of triggers and check constraints. They also make spatially enabled columns a lot easier to implement.

5.3.4 Ubiquitous language

Throughout the process multi-disciplinary team members have used terms quite interchangeably when sometimes they are not. For example, a "Geometry" represents something very different to an Earthquake Geologist compared to a Spatial Information practitioner. This discrepancy was identified quite early on and addressed to avoid ambiguity. Changes agreeable to all parties were applied to entity names throughout the database, and this will be evident in the different versions that represent the evolution of the database structure.

5.3.5 Version Management.

Right from the inception of the project version management of the database schema was central to the project. Maven for java technologies was used as a complete project management tool. The Liquibase Maven plugin project (www.liquibase.org) was used solely for managing and performing changes to the schema, and has proved extremely beneficial by ensuring a consistent structure during changes.

The ability to update and subsequently rollback changes ad-nauseum guarantees schema integrity and the ability to restore the schema at any point in time. Changes across major version releases can be encountered, but are easily overcome.

5.3.6 GEM Faulted Earth ERD

Figure 5.3 illustrates the Entity-Relationship Diagram as implemented. At this stage the schema name is "gem". Tables are prefixed with "fearth_".

What will be immediately apparent is the discrepancy between NULLable constraints in the schema and the <<compulsory>> stereotypes of the logical UML model. The process of loading existing data sets highlighted where the data was incomplete. This forced relaxing of several NOT NULL constraints.

fearth_bibliographic_reference

Records bibliographic references for published scientific papers.

fearth_blind_fault_summary

Records summaries for faults that have no visible surface expression

fearth_compilation_note

Records anecdotal comments for observation records.

fearth_completion

Records the level of data completion and optionally description why, for individual parameter results of an observation.

fearth_data_completion

A lookup table recording possible data completion values.

fearth_fault_source

Records potential fault ruptures for known fault summaries.

fearth_fault_summary

Top level fault summary table. This may be populated interactive or as the result of aggregating underlying data.

fearth_fault_synopsis

A table containing a brief synopsis for Fault Summaries.

fearth_fold

High level Fold summary table.

fearth_fold_trace

Stores geometry linework and associated attributes for Folds.

fearth_gem_role

Stores activity roles for the FaultedEarth project such as Compiler, Contributor, Administrator etc.

fearth_gem_user

GEM Faulted Earth project members

fearth_gem_user_role

Many to many join table for users and roles.

fearth_geomorphic_expression

A lookup table for the trace spatial tables.

fearth_location_method

A table containing location method lookup values for the trace spatial tables.

fearth_lookup

A central table containing all raw lookup values for non-spatial records.

fearth_neotectonic_section

High level Neotectonic Section summary table.

fearth_observation

A table containing fine-grained observation records.

fearth_observation_type

A list of potential observation types.

fearth_parameter

Individual field definitions for a specific summary or observation type.

fearth_parameter_lookup

A join table defining a discrete range of lookup values, for individual parameters.

fearth_reference

A join table storing published bibliographic references for high level summary or observation records.

fearth_result

Stores data for individual fields of an observation. Data may be raw values or categorical lookup values retrieved from *fearth_lookup*.

fearth_section_trace

Stores the geometry linework and corresponding attributes for Neotectonic Sections.

fearth_site

Stores location geometries for sites or places of activity.

5.5 Interchange Mechanisms

Population of the database is anticipated to occur via: 1) bulk loading of entire national databases, and 2) individual transactions corresponding to updates from a web based User Interface.

An XML interchange format has been created to satisfy the requirement of transferring bulk databases. The document structure resembles the conceptual model produced by Earthquake Geologists. The XML format is described in more detail in a companion document (Thomas, 2012).

While not a direct requirement of the project, the structure of the interchange format could also permit exchange of data from the user Interface database, and provide a temporary offline storage capability for when field conditions do not have network connectivity.

5.6 Appendix 1. Sample queries

Example 1. List the range of lookup values for the slip type attribute of a FaultSummary:

```
select fl.value
from gem.fearth_lookup fl
  inner join gem.fearth_parameter_lookup fpl
    on fl.lookup_id=fpl.lookup_id
  inner join gem.fearth_parameter p
    on fpl.parameter_id=p.parameter_id
  inner join gem.fearth_observation_type ot
    on p.observation_type_id=ot.observation_type_id
where p.name='slip_type' and ot.name='fault_summary'
```

Example 2. List all slip type observations:

```
select r.*
from gem.fearth_result r
  inner join gem.fearth_parameter p
    on r.parameter_id = p.parameter_id
  inner join gem.fearth_observation_type ot
    on p.observation_type_id = ot.observation_type_id
  inner join gem.fearth_observation o
    on o.observation_type_id = ot.observation_type_id
where ot.name='slip'
```

Example 3. List recorded observations by section for the named Wellington Fault.

```
select section_id,
  (select name from gem.fearth_neotectonic_section where
  neotectonic_section_id = o.section_id) as section_name,
  o.observation_id,
  ot.name,
  (select name from gem.fearth_gem_user where user_id=o.compiler_id)as
  compiler,
  (select name from gem.fearth_gem_user where user_id = o.contributor_id) as
  contributor,
  o.created_date,
  o.modified_date
from gem.fearth_observation_type ot
  inner join gem.fearth_observation o
    on o.observation_type_id = ot.observation_type_id
where o.target_id in
  (select neotectonic_section_id
  from gem.fearth_neotectonic_section s
    inner join gem.fearth_fault_summary as f
      on f.fault_summary_id = s.fault_summary_id
    where f.name like '%Wellington%')
  and o.observation_type_id<>2;
```

Example 4 List all observation results for the Wellington Fault

```
select distinct
  (select name from gem.fearth_neotectonic_section where
  neotectonic_section_id = o.section_id) as section_name,
  o.observation_id,
  ot.name as obsn_name,
  p.name,
  r.result_id,
  r.min_value as min,
```

```
    r.max_value as max,
    r.pref_value as pref,
    r.min_lookup,r.max_lookup,
    r.pref_lookup,
    (select name from gem.fearth_gem_user where
user_id=o.compiler_id)as compiler,
    (select name from gem.fearth_gem_user where user_id =
o.contributor_id) as contributor

from gem.fearth_observation_type ot
    inner join gem.fearth_observation o
        on o.observation_type_id = ot.observation_type_id
    inner join gem.fearth_parameter p
        on p.observation_type_id=ot.observation_type_id
    inner join gem.fearth_result r
        on r.parameter_id = p.parameter_id
where o.target_id in
    (select neotectonic_section_id from
gem.fearth_neotectonic_section s
    inner join gem.fearth_fault_summary as f
        on f.fault_summary_id = s.fault_summary_id
    where f.name like '%Wellington%')
and o.observation_type_id <>2
order by o.observation_id;
```

6 The database XML interchange

This section is a reproduction of the XML Interchange report (Thomas, 2012) with minor adjustment to the section numbering, and including the appendices as further sub-section.

6.1 Introduction

As part of the GEM Faulted Earth project (<http://www.globalquakemodel.org/hazard-global-components/active-faults>), an XML interchange format has been created to facilitate transferring bulk datasets or entire fault databases. This document explains the document format, some of the reasoning behind it, and techniques to streamline the process.

The hierarchical nature of the interchange format, enables the GEM Faulted Earth database (Thomas et al., 2012) to receive external data supplies, and subsequently process the data in accordance with its internal structure, in a totally independent manner from how the data may be stored by the contributing organisation.

Where possible the document structure resembles the conceptual model produced by Earthquake Geologists Litchfield et al. (2013b). The reasons for this were:

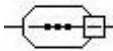
- to create the simplest format possible,
- to avoid vendor specific DBMS issues,
- to avoid exposing the underlying Faulted Earth DBMS schema
- to avoid foreign key relationships by prescribing a hierarchical structure
- to facilitate uploading of disparate databases in a consistent and repeatable manner
- to present a series of high-level entities to the interchange contributors.

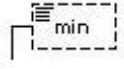
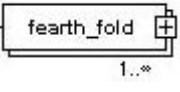
6.2 Interchange Content

6.2.1 XML Entities.

GEM Faulted Earth entities will be modelled as complex XML Elements. Each of these elements will contain the necessary data, either directly as element text values, or as nested complex XML Elements, some of which may be complex elements themselves. In general the use of XML Attributes is avoided, with the exception of flagging known NULL values which is addressed further on.

The figures presented in this document were created using Regis Cosnier's *XSD Diagram* utility for visualising XSD documents (<http://regis.cosnier.free.fr/?page=XSDDiagram>). The following legend can be used as a brief guide:

	Octagon shape denotes a complex child element
	Solid enclosure denotes a mandatory element

	Dashed enclosure denotes an optional element
	Multiple leaves denote a collection of child elements

6.2.2 Interchange Hierarchy

Figure 5.1 stylistically represents an xml interchange document conforming to the published schema (gem_fe.xsd). The document contains a single top level element named fearth_fault_export. fearth_fault_export will contain four children:

- blind_faults,
- faults,
- folds, and
- sources,

Each of these elements act as a “container” element to group collections of the high level database entity records. Each of the “container” elements can be empty to allow independent data exchange within an organisation. For example FaultSources and Faults may be contributed by separate teams within an organisation and therefore not be compiled at the same time.

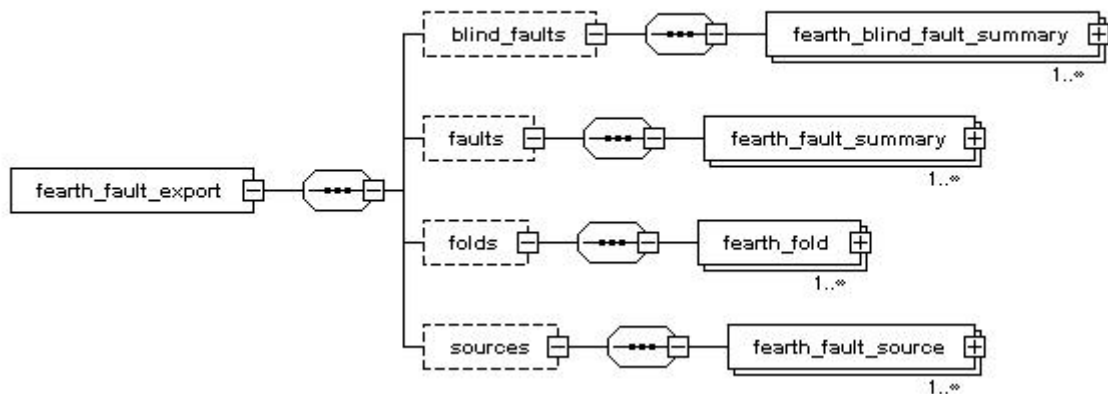


Figure 6.1 Top level fearth_fault_export element

Note the fifth high level entity which represents Neotectonic Fault Sections is contained as a child element within the fearth_fault_summary hierarchy, and is not shown above.

NeotectonicSection is one of the more complex elements as it also contains fine-grained observation records as child elements. These are illustrated in Figure 6.2.

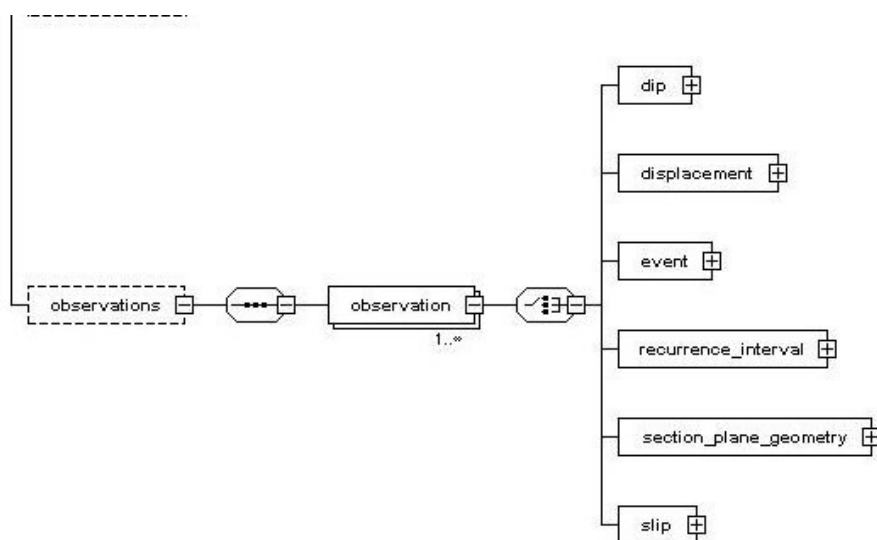


Figure 6.2 Observations child element for NeotectonicSection

Appendix A in Section 6.3 Provides a listing for each of the high-level entities, and Appendix B in Section 6.4 lists the observation elements

6.2.3 Null values

Not all XMLElements require a value to be present. Those elements allowed to be empty must be marked accordingly. To do this the xml attribute `xsd:nil="true"` should be supplied. This is required for correct operation of the xml parser by the receiving party.

6.2.4 Composite data values

Many of the parameters in the conceptual model have a requirement to store 3 values (if known). These correspond to minimum, maximum and preferred values. Any element required to have provision for minimum, maximum and preferred values will be modelled accordingly. Figure 6.3 shows an example taken from the length attribute of a Fold record

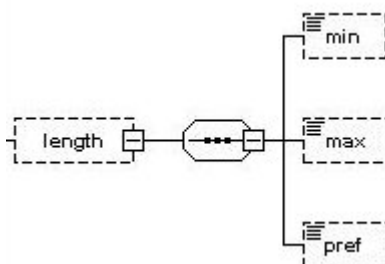


Figure 6.3 Fold length composite attribute values

6.2.5 Attribute value descriptions

In accordance with the Data Dictionary (Litchfield et al., 2013a), values provided for entity records are often accompanied with a brief description explaining why or how the particular value was determined. In a few cases an additional attribute is required to indicate the level of completion for the data. The interchange

document satisfies this need by defining attributes in groups where necessary. Figure 6.4 shows an example taken from a fault_summary record for the lower seismogenic depth.

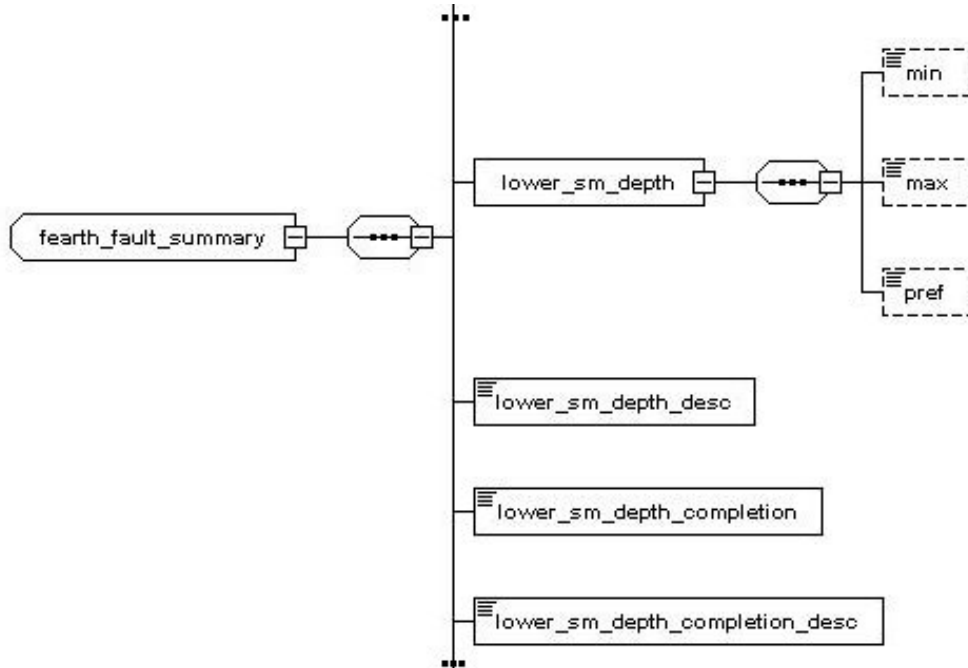


Figure 6.4 Attribute group for lower seismogenic depth

6.2.6 Normalisation

Any form of foreign key linking within the xml document is avoided, and values may be repeated freely. A good example of this is the use of bibliographic references. There may be several repeated values for the same reference throughout the document. This does increase the overall size of the transfer document, but simplifies processing and is considered an acceptable form of redundancy. When uploaded into GEM FaultedEarth the data will be properly normalised.

6.2.7 Recording Lineage

Contributing organisations are entitled to supply their internal record identifiers. These elements will be visible as having an “_id” suffix to their name. When provided these will be processed and converted to CompilationNotes as a way of providing lineage for the data.

6.2.8 Quality Assurance

To ensure data Quality Assurance at point-of-supply, the interchange format is self validating. An XML Schema (xsd) document has been published (http://data.gns.cri.nz/xsd/gem/gem_fe.xsd) to accompany the interchange file. The ability to receive immediate feedback will streamline the exchange between organisations by minimising feedback cycles related to data discrepancies when performing the data mapping exercise.

Experience with the New Zealand active fault database indicates that idiosyncrasies within neotectonic fault databases are commonplace. These may be data type inconsistencies, differences in modelled structures, and the meaning of data values. Successful navigation of these issues requires the hands-on expertise of the contributing organisation and not third party mediators.

It is possible for several feedback cycles to occur between Earthquake Geologists and IT staff within each contributing organisation. This self-governance enables the contributors to make the correct assumptions when mapping internal structures and various lookup codes to the GEM Faulted Earth model. The XSD schema is provided to assist this process.

6.2.9 Lookup Values

The XSD schema also defines discrete ranges of potential lookup values for a particular database attribute or “element” in the interchange document. Each lookup type will be defined as a Simple XMLElement and have a restricted range of values. The current list of lookup types and values are:

age_category

- "0-1000"
- "1000-11,700"
- "11,700-50,000"
- "50,000-100,000"
- "100,000-1,000,000"
- "1,000,000-10,000,000"

data_completion

- "well-constrained"
- "moderately-constrained"
- "poorly-constrained"
- "inferred"

fold_type

- "Anticline"
- "Monocline"
- "Syncline"

octant

- "E"
- "N"
- "NE"
- "NW"
- "S"
- "SE"
- "SW"
- "W"

recurrence_interval_category

- "10-100"
- "100-1000"
- "1000-2000"
- "2000-5000"
- "5000-10000"
- "1000-100000"
- "10000-500000"
- "50000-1000000"
- "100000-1000000"

recurrence_interval_type

- "EQ"
- "Calculated"

slip_rate_category

- "0.001-0.01"
- "0.01-0.1"
- "0.1-1"
- "1-5"
- "5-10"
- "10-50"
- "50-100"
- "100-200"

slip_type

- "Reverse"
- "Thrust"
- "Normal"
- "Dextral"
- "Sinistral"
- "Normal-dextral"
- "Normal-sinistral"
- "Reverse-dextral"
- "Reverse-sinistral"
- "Dextral-normal"
- "Dextral-reverse"
- "Sinistral-reverse"
- "Sinistral-normal"

6.3 Appendix A Gem Faulted Earth Interchange Entities

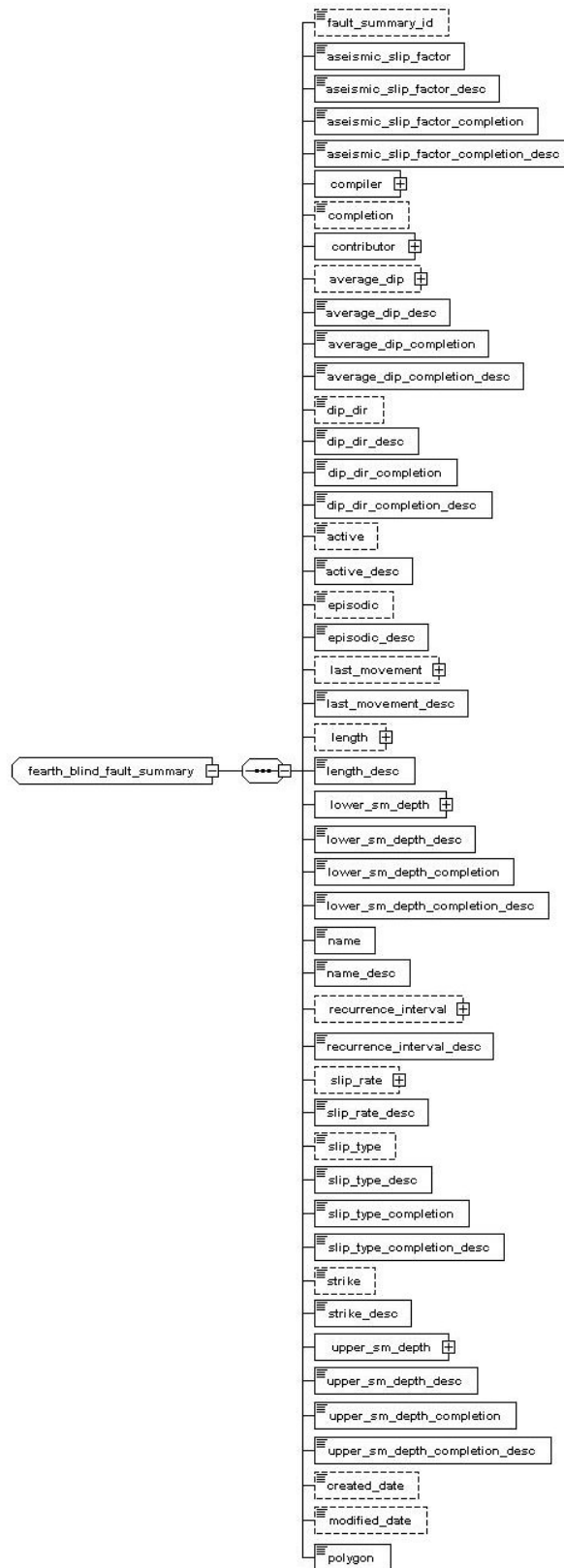


Figure 6.5 fearth_blind_fault_summary element

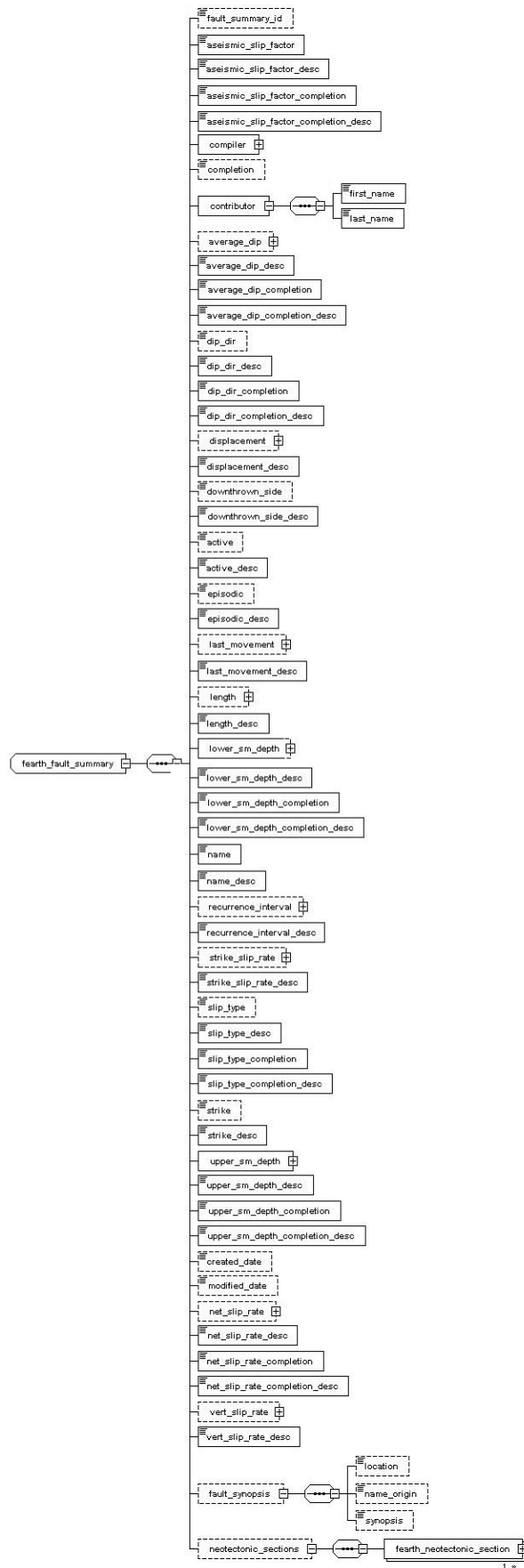


Figure 6.6 fearth_fault_summary element

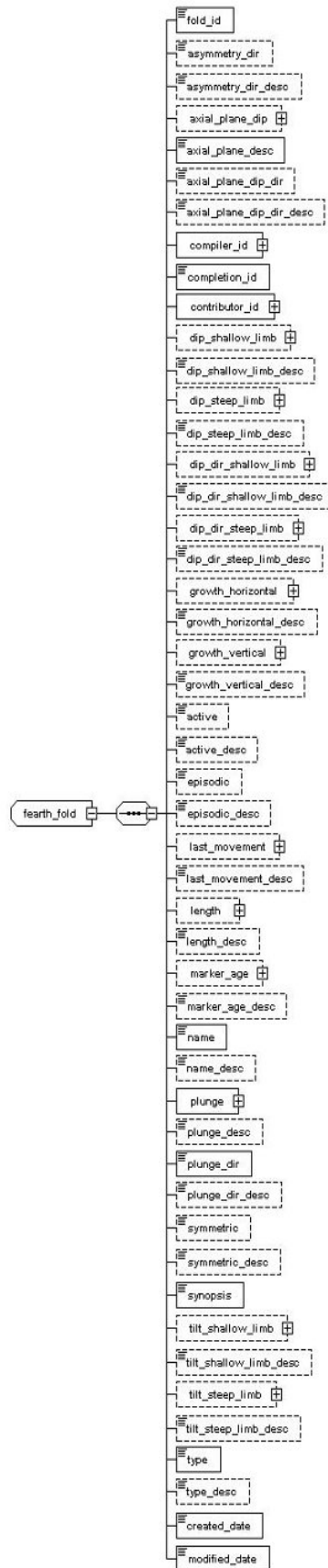


Figure 6.7 fearth_fold element

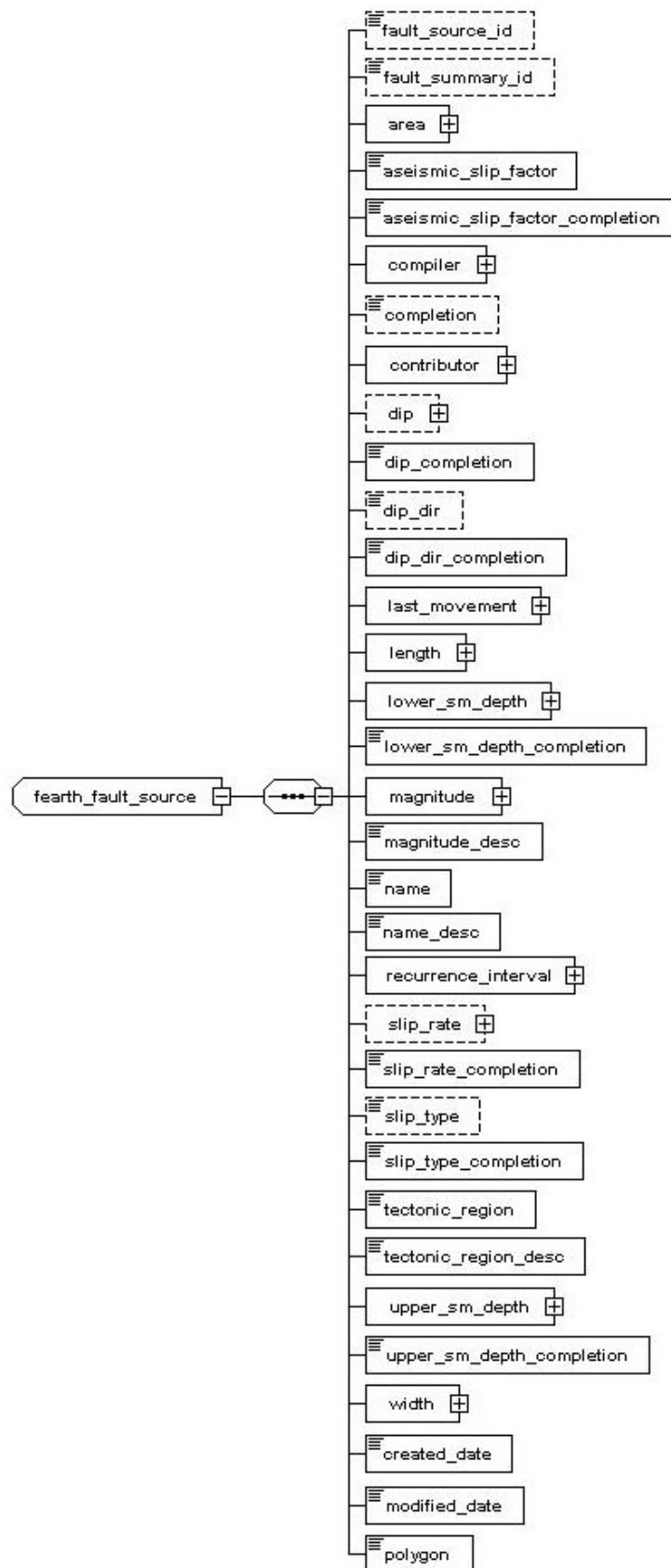


Figure 6.8 fearth_fault_source element

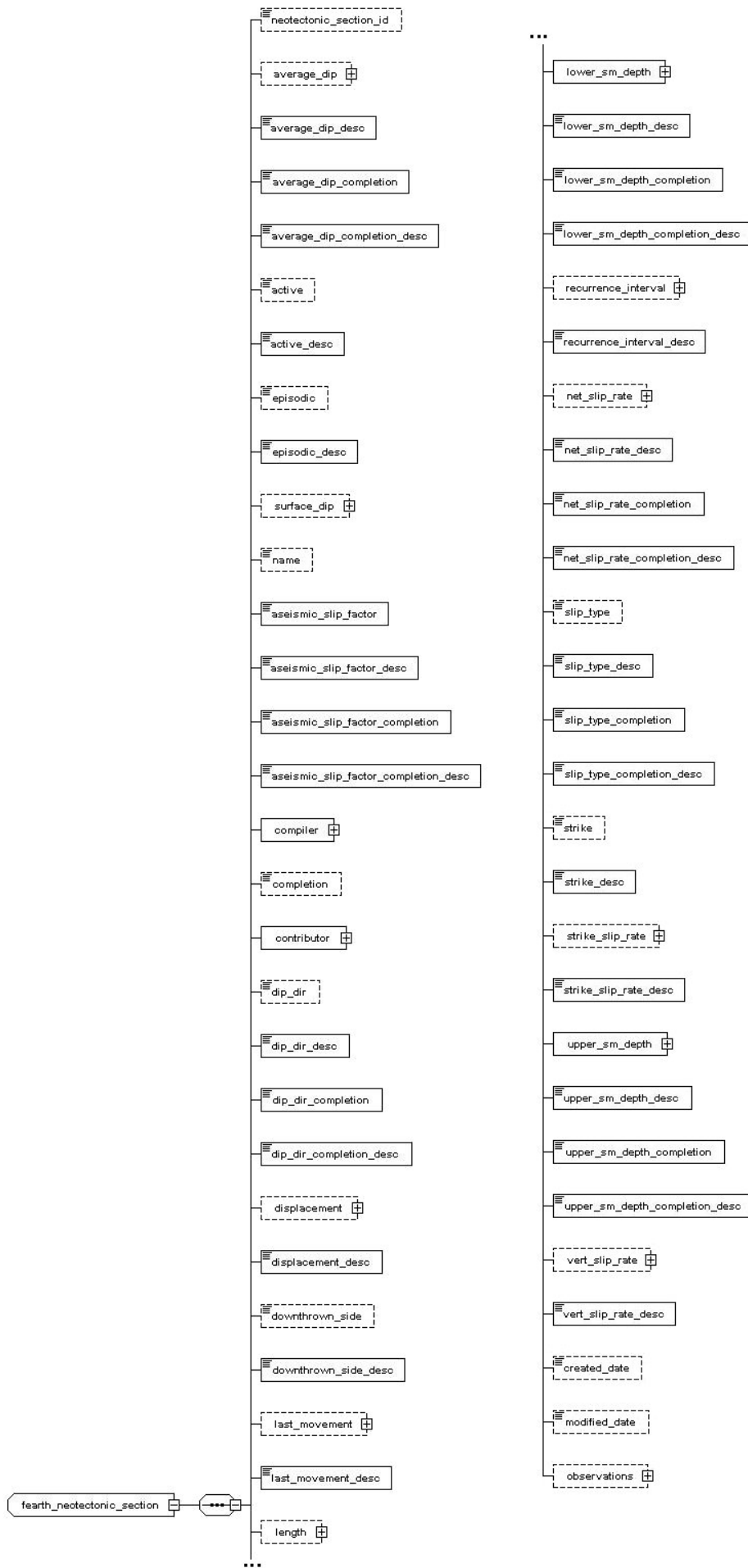


Figure 6.9 fearth_neotectonic_section element

6.4 Appendix B GEM FaultedEarth Observation elements

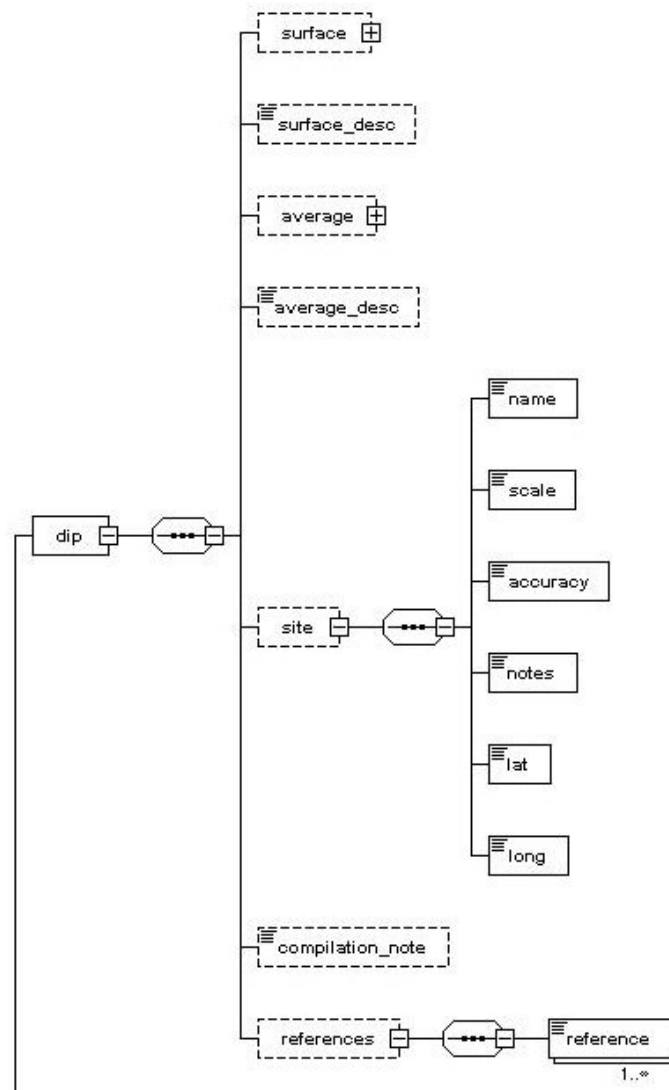


Figure 6.10 Dip observation element

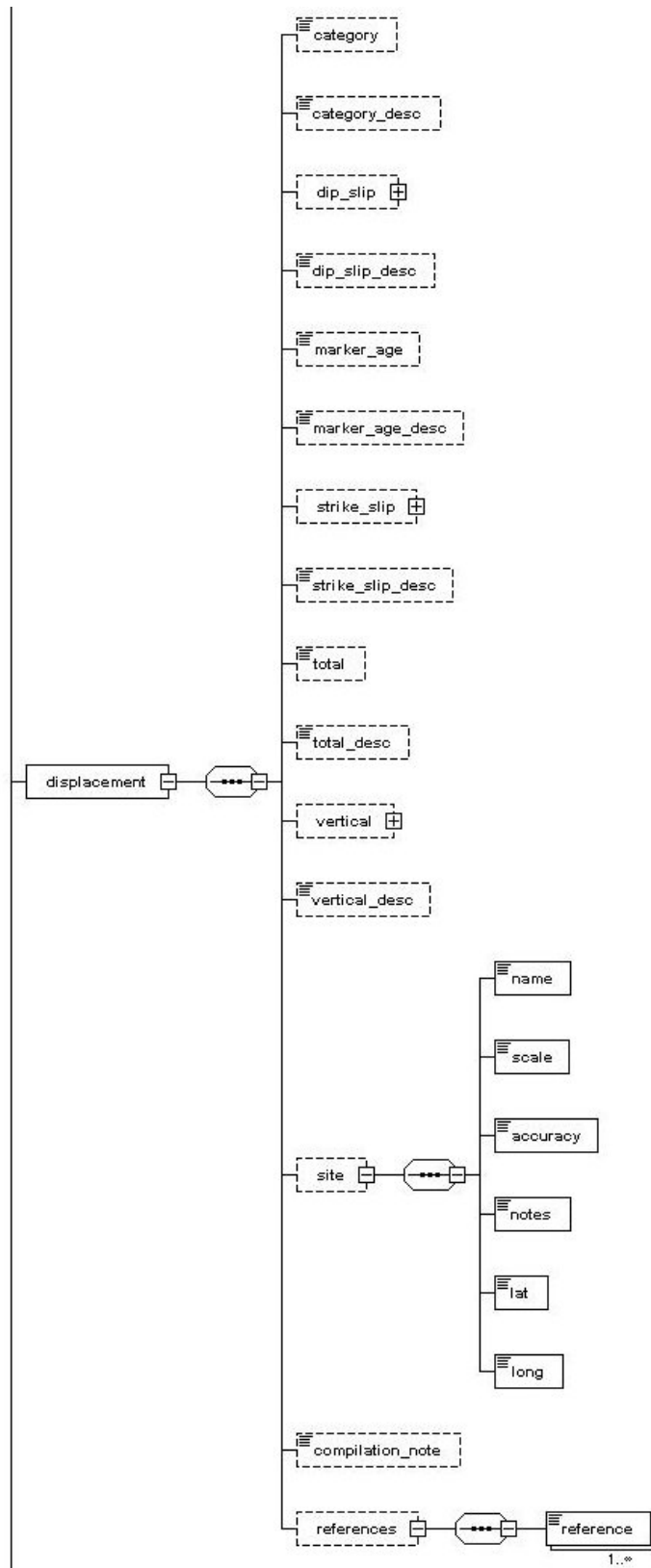


Figure 6.11 Displacement observation element

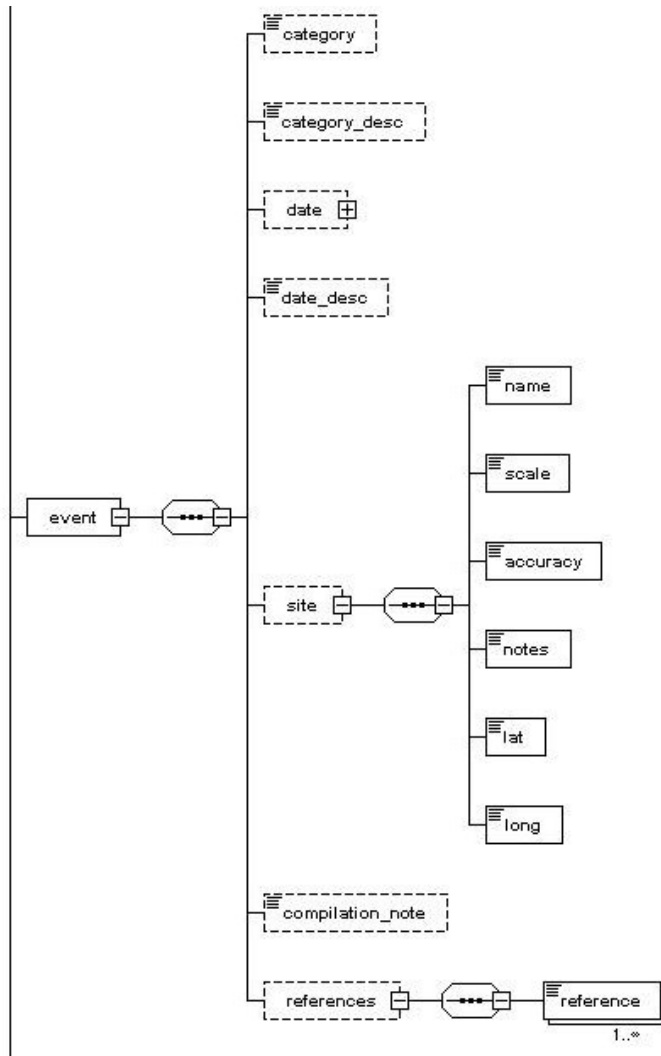


Figure 6.12 Event observation element

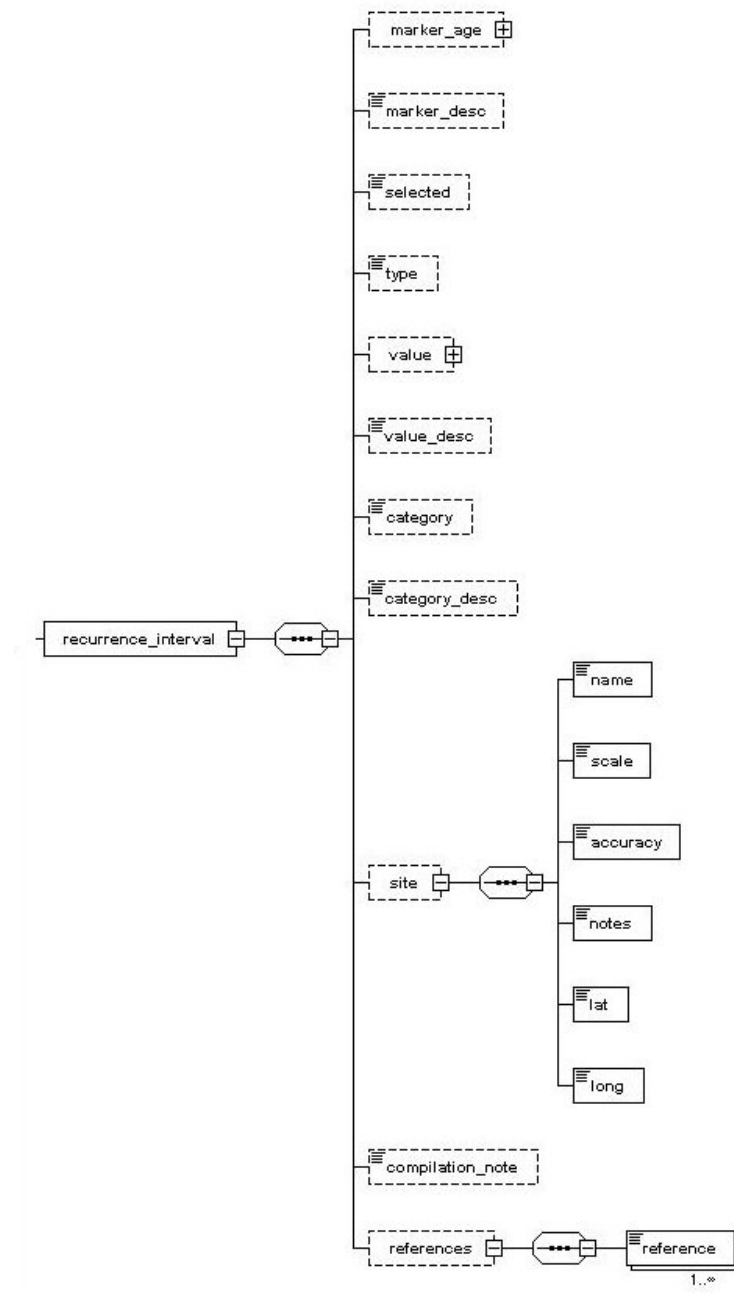


Figure 6.13 RecurrenceInterval observation element

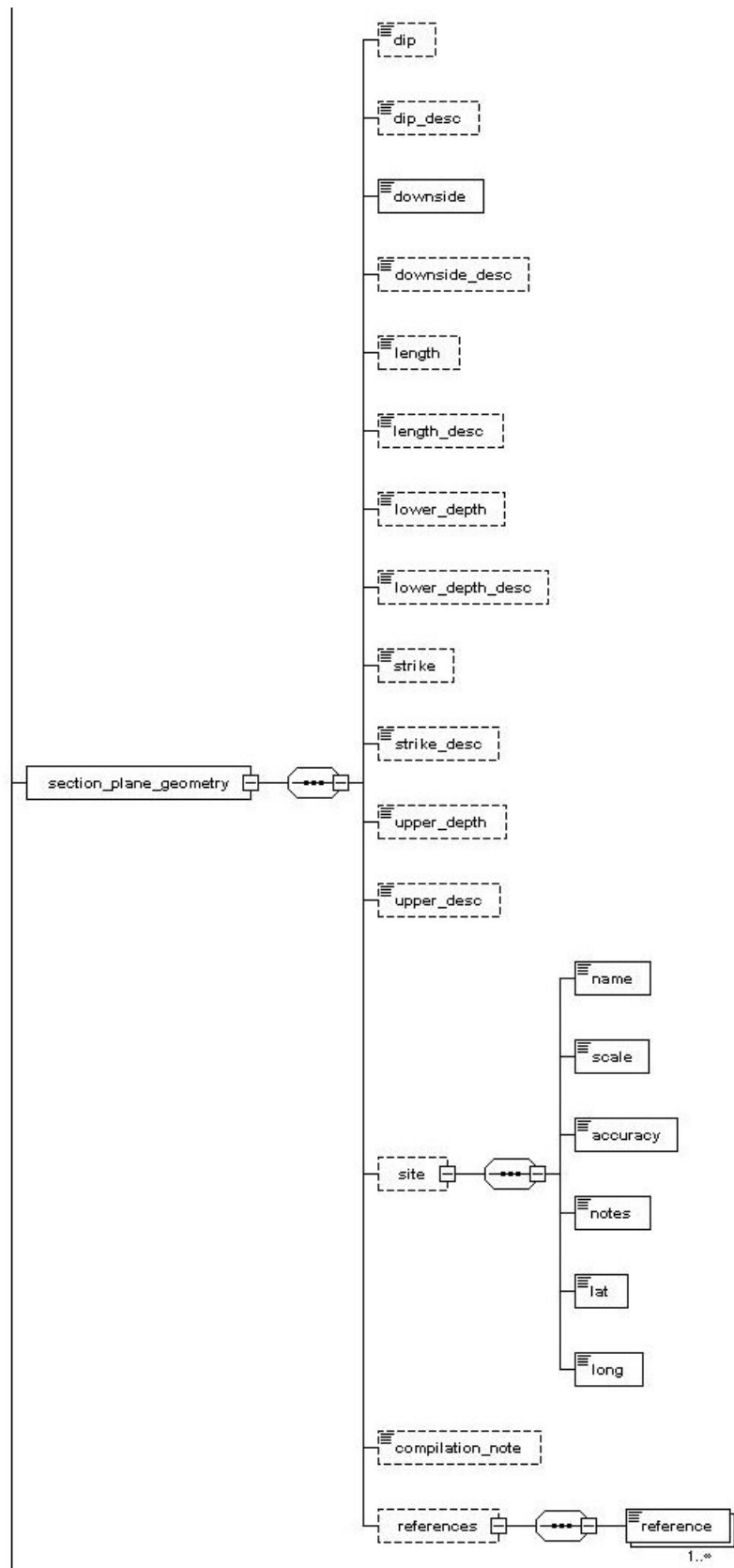


Figure 6.14 SectionPlaneGeometry observation element

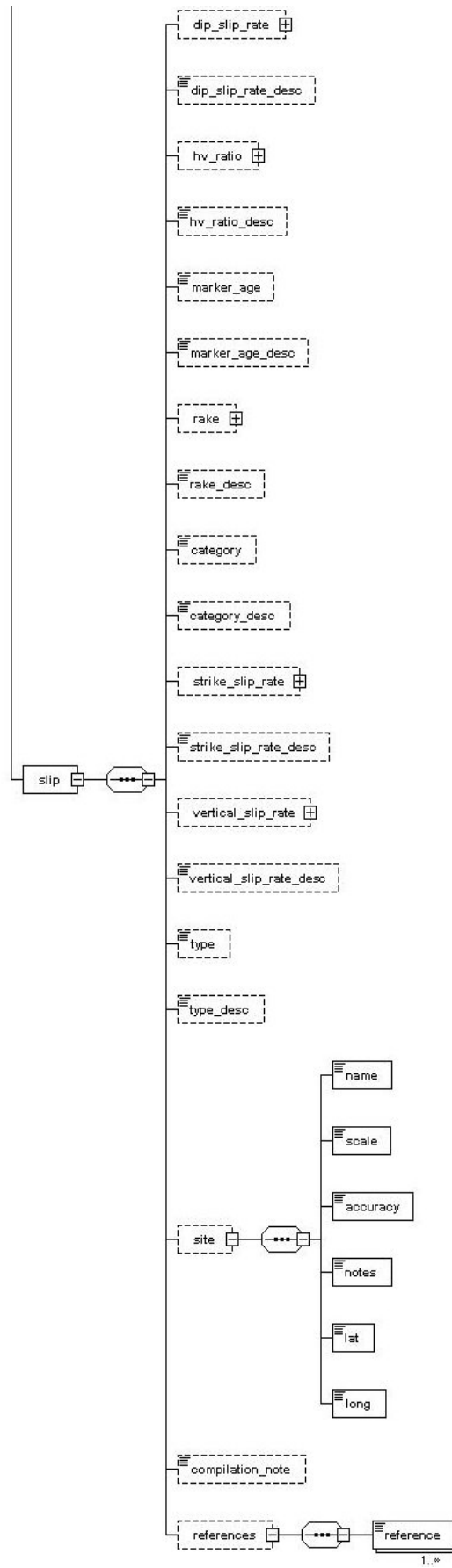


Figure 6.15 Slip observation element

7 Magnitude scaling relationships

This section is a reproduction of the magnitude-scaling relationship report by Stirling and Goded (2012) with minor adjustment to the section numbering, up-dating of the figures, and including the appendices as further sub-section. The results have since been published in the Bulletin of the Seismological Society of America (Stirling et al., 2013). The references are merged with the references in the other sections.

7.1 Introduction

A fundamentally important, but typically abbreviated part of seismic hazard modelling involves the selection of magnitude scaling relationships. These are typically regressions of historical earthquake datasets, in which magnitude is scaled to parameters such as fault rupture length and area. The mix of historical data from different tectonic environments, and the different forms of the regression equations can result in large differences in magnitude for a given fault rupture. Furthermore, regressions such as the extensively-used Wells and Coppersmith (1994) and Hanks and Bakun (2008) equations are liberally applied the world over, with little or no consideration as to their applicability to a particular environment. Figure 7.1 illustrates this issue by showing the significant underestimation of the M7.1 4 September 2010 Darfield (New Zealand) earthquake by the above regressions (the lower curves on the image). The objectives of this report are twofold: (1) compile a worldwide set of regressions into one document, and; (2) recommend the most suitable regressions for use in the range of tectonic regimes and fault slip types in existence around the world. This information is required by GEM, but is also a timely opportunity to provide general guidance for regression selection in seismic hazard modelling. Our compilation is limited to regressions of magnitude (or seismic moment) on source area or length. It is a representative but not exhaustive compilation of the available regressions around the world.

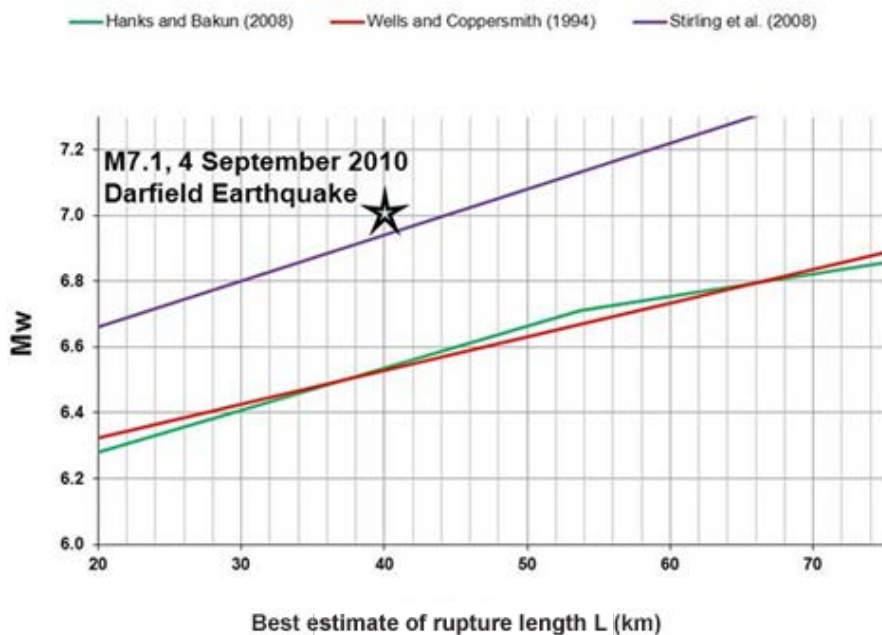


Figure 7.1 The Darfield earthquake compared to some commonly used regression relationships

7.2 Methodology

In the following sections we develop a physical framework for grouping regressions according to tectonic regime and fault slip type. We also provide an explanation of our basis for assigning Quality scores to regressions, followed by a tabulation and detailed description of the regressions recommended for use in GEM. The Appendix in Section 7.6 contains other regressions found in our compilation. We acknowledge the subjectivity of our overall assessment, but are nevertheless confident that it goes beyond methodologies for regression selection and application being practised in many parts of the world.

7.2.1 Tectonic Regime

The definition of tectonic regimes and grouping of regressions into these regimes are the result of our own assessment, using any guidelines or recommendations we could glean from the regression documents. However, the common lack of recommendations in the latter has required that we make our own assignment of tectonic regime to a particular regression on the basis of where the regression data were collected. Some regression datasets are restricted to specific regimes, whereas others are very wide-reaching. In the latter cases we assign these regressions to the tectonic environment responsible for most of the regression dataset. The following shows the categories of tectonic regime and fault type observed in our compilation:

Table 7.1 Tectonic regimes, sub regimes, and mechanisms (slip types) used as a basis for sorting regressions for appropriate use in seismic hazard studies. The IDs written in parentheses are for cross-referencing to Table 6.2, and have the following derivation: First character (A-D)=primary tectonic regime; second character (1-2)=tectonic sub-regime, and; third character (1-4)=mechanism or slip-type. For example, A11=plate boundary (A); fast (1); strike-slip mechanism (1)

Tectonic regime	Sub regime	Mechanism
A- Plate Boundary crustal	Fast Plate Boundary faults (> 10mm/year) (A1)	Strike-slip dominated (A11)
	Low Plate Boundary faults (< 10mm/year) (A2)	All faults (A21)
		Strike-slip (A22)
		Normal (A23)
B- Stable continental		Reverse (A24)
		Reverse (B1)
		Stroke-slip (B2)
C- Subduction	Continental	Thrust (C1)
	Marine	Thrust (C2)
	Intraslab	Normal (C3)
D- Volcanic	Thin Crust (< 10km)	Normal (D1)
	Thick Crust (> 10km)	Normal (D2)

7.2.2 Quality Score

A Quality score (1=best available, 2=good, 3=fair) is assigned according to the quality and quantity of the regression dataset. This is usually based on the size of the regression dataset and age of publication. Logically a regression that does not use the last 10 to 20 years of data, and has a small dataset (unless focussed on a specific environment) will not score as highly as one that is more data-rich and recent. To some extent, previous use is a criterion taken into consideration, although we are aware of widespread misuse of some

regressions (e.g., Wells and Coppersmith 1994 in intraplate areas). We also consider the scientific merit (e.g., inclusion of bilinear scaling etc.) in our assignment of a Quality score. The majority of regressions recommended for use in GEM logically have a Quality score of 1, but in some cases the limited availability of regressions for particular environments (e.g., stable continental) require the use of regressions with lower Quality scores.

7.3 Recommended Regressions

7.3.1 Regression Tabulation

In Table 6.2 we provide the regressions most applicable to the categories of tectonic environment and slip type listed in Table 1. These shortlisted regressions have generally been assigned a quality score of 1, although this is not always the case as some tectonic regimes and slip types are poorly represented in the literature. The Table is followed by our documentation of these regressions, which includes the equations, number and magnitude of events in the regression dataset, description of the regression in terms of equation form, the mix of data with respect to tectonic environment and geography, and any recommendations on use of the regression from the authors and ourselves. We also show the Quality score we have assigned to the regressions. Section 7.6 documents the remaining regressions in our compilation. These are not shortlisted as they do not satisfy our selection criteria to the same degree as our shortlisted regressions.

Table 7.2 Shortlisted regressions for each combination of tectonic environment, sub-environment and slip-type (underlined = highest priority). Underlined regressions correspond to the most suitable regressions for a given tectonic regime and/or slip type. The “Tectonic Regime” IDs shown in the left hand column relate to the IDs given in parentheses in Table 1 (see footnote for further explanation).

Tectonic regime	Name	Relationship	Units	Quality score	Comments
A11	<u>Hanks and Bakun (2008) – A ≤ 537km²</u>	$M_w = \text{Log}A + (3.98 \pm 0.03)$	A: Area (km ²)	1	Best represented by Hanks & Bakun regressions. Regression datasets are dominated by fast-slipping plate boundary faults. Regressions should be chosen according to the relevant fault area range.
	<u>Hanks and Bakun (2008) – A > 537km²</u>	$M_w = 4/3\text{Log}A + (3.07 \pm 0.04)$		1	
	UCERF2	$M_w = 4.2775A^{0.0726}$		1	
	Wesnousky (2008) – strike slip	$M_w = 5.56 + 0.87\text{Log}L$ sig=0.24 (in M _w)	L: surface rupture length (km)	1	
	Leonard (2010)	$W = C_1 L^\beta$ $\bar{D} = C_2 \sqrt{A}$ Mo=uLWD Mo=A ^{1.5} (see below for Leonard coefficients/explanation)	(*)	1	
A21	<u>Yen and Ma (2011) – all</u>	$\text{Log}A_e = -13.79 + 0.87\text{Log}M_o$ sig=0.41 (in A _e) $\text{Log}M_o = 16.05 + 1.5M$	A: effective area (km ²)	1	Best represented by Yen and Ma regression as datasets contain a mix of plate boundary

Tectonic regime	Name	Relationship	Units	Quality score	Comments
					earthquakes of strike-slip and dip-slip mechanisms.
A22	Hanks and Bakun (2008) – $A \leq 537\text{km}^2$	$M_w = \text{Log}A + (3.98 \pm 0.03)$	A: Area (km^2)	1	Larger magnitudes produced by Stirling et al. than by others (larger D-L scaling)
	<u>Stirling et al. (2008) (New Zealand – oblique-slip)</u>	$M_w = 4.18 + 2/3\text{log}W + 4/3\text{log}L$ sig=0.18 (in M_w)	L: subsurface rupture length (km) W: Width (km)	1	
	Wesnousky (2008) – strike slip	$M_w = 5.56 + 0.87\text{Log}L$ sig=0.24 (in M_w)	L: surface rupture length (km)	1	
	<u>Yen and Ma (2011) – strike slip</u>	$\text{Log}A_e = -14.77 + 0.92\text{Log}M_o$ sig=0.40(in A_e) $\text{Log}M_o = 16.05 + 1.5M_w$	A_e : effective area (km^2)	1	
A23	<u>Wesnousky (2008) – normal</u>	$M_w = 6.12 + 0.47\text{Log}L$ sig=0.27 (in M_w)	L: surface rupture length (km)	1	Basin & Range-rich normal-slip earthquake dataset
A24	Stirling et al. (2008) (New Zealand – oblique-slip)	$M_w = 4.18 + 2/3\text{log}W + 4/3\text{log}L$ sig=0.18 (in M_w)	W: Width (km) L: Subsurface rupture length (km)	1	Yen and Ma dip slip dataset dominated by reverse and thrust-slip earthquakes from wide area (Taiwan and east Asia)
	Wesnousky (2008) – reverse	$M_w = 4.11 + 1.88\text{Log}L$ sig=0.24 (in M_w)	L: surface rupture length (km)	1	
	<u>Yen and Ma (2011) – dip slip</u>	$\text{Log}A_e = -12.45 + 0.80\text{Log}M_o$ sig=0.43 (in A_e) $\text{Log}M_o = 16.05 + 1.5M_w$	A_e : effective area (km^2)	1	
B1	<u>Anderson et al. (1996)</u>	$M_w = 5.12 + 1.16\text{Log}L - 0.20\text{Log}S$ sig=0.26 (in M_w)	L: surface fault length (km) S: slip rate (mm/yr)	2	
	<u>Nuttli (1983)</u>	$\text{Log} M_o = 3.65\text{Log}L + 21.0$ $\text{Log}M_o = 16.05 + 1.5M_w$	M_o : seismic moment (dyne-cm) L: subsurface fault length (km)	3	Equal priority to Nuttli and Anderson et al. regressions. Nuttli regression is developed exclusively for stable continental regions (>500km from

Tectonic regime	Name	Relationship	Units	Quality score	Comments
					plate boundaries), but dataset is old. Anderson et al. dataset includes stable continental earthquakes, and negative coefficient on slip rate has a major influence on Mw
B2	<u>Anderson et al. (1996)</u>	$M_w = 5.12 + 1.16 \log L - 0.20 \log S$ sig=0.26 (in M_w)	L: surface fault length (km) S: slip rate (mm/yr)	2	As for B1
	<u>Nuttli (1983)</u>	$\log M_0 = 3.65 \log L + 21.0$ $\log M_0 = 16.05 + 1.5 M_w$	M_0 : seismic moment (dyne-cm) L: subsurface fault length (km)	3	
C1	<u>Strasser et al. (2010) Interface events</u>	$M_w = 4.441 + 0.846 \log_{10} (A)$ sig=0.286 (in M_w)	A: Rupture Area (km ²)	1	Diverse dataset and Mw dependence on interface area makes the Strasser et al. regression the most suitable for using on a wide variety of subduction "megathrusts"
C2	<u>Strasser et al. (2010) Interface events</u>	$M_w = 4.441 + 0.846 \log_{10} (A)$ sig=0.286 (in M_w)	A: Rupture Area (km ²)	1	As for C1
	<u>Blaser et al. (2010) Oceanic/subduction Reverse</u>	$\log_{10} L = -2.81 + 0.62 M_w$ $S_{xy} = 0.16$ (orthogonal standard deviation)	L: subsurface fault length (km)	1	
C3	<u>Ichinose et al. (2006)</u>	$\log_{10} (A_a) = 0.57 (\pm 0.06) M_0 - 13.5 (\pm 1.5)$ sig=16.1 (in A_a)	A_a : combined area of asperities M_0 =seismic moment (dyne-cm)	1	Only regression of relevance to intraslab earthquakes

Tectonic regime	Name	Relationship	Units	Quality score	Comments
D1	<u>Villamor et al. (2007)</u> (New Zealand – normal)	$M_w = 3.39 + 1.33\text{Log}A$ sig= 0.195 (in M_w)	A: Area (km ²)	1	Only regression of relevance to volcanic-normal earthquakes in thin crust (rift environments)
D2	<u>Wesnousky (2008) – normal</u>	$M_w = 6.12 + 0.47\text{Log}L$ sig=0.27 (in M_w)	L: surface fault length (km)	1	Basin & Range-rich normal-slip dataset

Explanation

Column 1: Tectonic regime IDs relate to Table 1. e.g., A11 signifies “Plate Boundary Crustal/Plate Boundary Fast Slipping/Strike-Slip Dominated”.

Column 2: Primary reference for regression

Column 3: Regression equations and standard deviations or standard errors (if available; applicable parameter in parentheses e.g., “in M_w ” means the standard deviation is for M_w). The standard Hanks and Kanamori 1979 equation is also provided in cases where seismic moment needs to be converted to moment magnitude

Column 4: Units

Column 5: Quality score

Column 6: Justification for shortlisting of regression into this Table.

(*) Leonard (2010). Description of parameters:

μ = shear modulus (MPa)

L = subsurface horizontal fault rupture length (km) (Note: surface rupture length has been used in the cases where this was the only length parameter available)

W = width (km)

D = depth (km)

$\beta=1$ for $M<5$

$\beta=2/3$ for $5<M<7.2$

$\beta=0$ for $M>7.2$

C_1, C_2 : constants (see table below)

Preferred values for C_1 and C_2 :

Data	C_1 (m ^{1/3})	$C_2 \times 10^5$	$\Delta\sigma$ (MPa)
Interplate dip-slip	17.5 (12-25)	3.8 (1.5-12)	3.0
Interplate strike-slip	15.0 (11-20)	3.7 (1.5-9.0)	3.0
SCR dip-slip	13.5 (11-17)	7.3 (5.0-10)	5.8

Methodology: First stage is solving for width W , then displacement D as a function of area A .

7.3.2 Hanks and Bakun (2008) relationship

$$M_w = \log A + (3.98 \pm 0.03)$$

for $A \leq 537 \text{ km}^2$

$$M_w = 4/3 \log A + (3.07 \pm 0.04)$$

for $A > 537 \text{ km}^2$

A=area (km^2)

Description: The regression is developed for continental strike-slip earthquakes. Based on a relatively small dataset of large earthquakes, and mainly suitable for large to great strike slip earthquakes in plate boundary settings (e.g., San Andreas, Alpine, North Anatolian).

Data: 88 continental strike-slip earthquakes. Includes historical earthquakes since 1857 and 12 new $M > 7$ events added to the Wells and Coppersmith (1994) dataset. Regions for the 7 new $M > 7$ events are: Japan (1), Turkey (2), California (1), China (2), Alaska (1). Magnitude range: 5-8 (M_w)

Application: Major plate boundary strike-slip faults. Not suitable for use on faults with slip rates less than $\sim 1 \text{ mm/yr}$. Widely used in major seismic hazard models around the world. Should be given high weighting in logic tree framework in the case of plate boundary strike-slip faults with high slip rates.

Tectonic regime and mechanism: A11

Quality score = 1

References: Wells and Coppersmith (1994); Hanks and Bakun (2008)

7.3.3 UCERF2 relationship

$$M_w = 4.2775A^{0.0726}$$

A=area (km^2)

Description: Developed by the scaling law team of UCERF2 as an alternative to Hanks and Bakun (2008) and Ellsworth B (WGCEP, 2008) relations, but using the combined dataset from these two regressions.

Data: Hanks and Bakun (2002, 2008) datasets: Hanks and Bakun (2002): strike-slip subset of the Wells and Coppersmith (1994) database, that contains 83 continental earthquakes of which 82 have magnitudes $M \geq 7.5$. Hanks and Bakun (2008): 88 continental strike-slip earthquakes. Includes historical earthquakes since 1857 and 12 new $M > 7$ events added to the Wells and Coppersmith (1994) dataset. Magnitude range: 7.0-8.5 (several types of magnitudes: mainly M_s but also some M_L and m_b)

Application: Relevant to strike-slip faults in all regions and for a wide magnitude range.

Tectonic regime and mechanism: A11

Quality score = 1

References: Hanks and Bakun (2002; 2008); Working Group on California Earthquake Probabilities (2008).

7.3.4 Wesnousky (2008) relationships

$$M_w = 5.30 + 1.02 \log L \quad \text{All events (37 events used)}$$

$$M_w = 5.56 + 0.87 \log L \quad \text{Strike-slip events (22 events used)}$$

$$M_w = 6.12 + 0.47 \log L \quad \text{Normal events (7 events used)}$$

$$M_w = 4.11 + 1.88 \log L \quad \text{Reverse events (8 events used)}$$

L= surface rupture length (km)

Description: The regressions have been developed from earthquakes associated with rupture lengths greater than about 15km, encompassing three slip types from both interplate and intraplate tectonic environments. The regression can therefore be widely applied to earthquake sources of lengths greater than 15km.

Data: dataset limited to the larger surface rupture earthquakes of length dimension greater than 15 km and for which there exist both maps and measurements of coseismic offset along the strike of the rupture. A total of 37 events have been used, limited to continental earthquakes. These include 22 strike-slip, 7 normal and 8 reverse-slip events. Regions: California (8), Turkey (7), Japan (5), Nevada (3), Australia (3), Iran (2), China (2), Mexico (1), Algeria (1), Philippines (1), Taiwan (1), Idaho (1), Montana (1) and Alaska (1). Magnitude range: 5.9-7.9 (M_w)

Application: All regions, for the relevant slip types but acknowledging that the regression dataset will be dominated by plate boundary earthquakes. Should be given reasonably strong weighting in logic trees. The author recommends giving more confidence to the relationship for strike slip events, as it is based on a larger data set.

Tectonic regime and mechanism: A11, A22 (strike-slip), A24 (reverse), A23, D2 (normal).

Quality score = 1

References: Wesnousky (2008)

7.3.5 Leonard (2010) relationships

$$W = C_1 L^\beta$$

$$\bar{D} = C_2 \sqrt{A}$$

$$M_0 = \mu L W D$$

$$M_0 = A^{1.5}$$

μ = shear modulus (MPa)

L = subsurface horizontal fault rupture length (km) (Note: surface rupture length has been used in the cases where this was the only length parameter available)

W = width (km)

D = depth (km)

$\beta=1$ for $M < 5$

$\beta=2/3$ for $5 \leq M < 7.2$

$\beta=0$ for $M \geq 7.2$

C_1, C_2 : constants (see table below)

Preferred values for C_1 and C_2 :

Data	C_1 ($m^{1/3}$)	$C_2 \times 10^5$	$\Delta\sigma$ (MPa)
Interplate dip-slip	17.5 (12-25)	3.8 (1.5-12)	3.0
Interplate strike-slip	15.0 (11-20)	3.7 (1.5-9.0)	3.0
SCR dip-slip	13.5 (11-17)	7.3 (5.0-10)	5.8

Description: Three regressions that collectively provide parameters for use in the “classic” equation for seismic moment M_0 . First stage is solving for width W , then displacement D as a function of area A . Leonard’s final step is to solve for seismic moment M_0 (M_0 can then be used to solve for M_w). The regressions are developed using worldwide data.

Data: Predominantly plate boundary earthquakes. Divided into two categories: a) interplate and plate boundary (classes I and II, Scholz et al., 1986) and b) stable continental region (SCR, i.e., intraplate continental crust that has not been extended by continental rifting) which includes midcontinental (class III, Scholz et al., 1986). Several datasets used: Wells and Coppersmith (1994), Henry and Das (2001), Hanks and Bakun (2002), Romanowicz and Ruff (2002) and Manighetti et al. (2007). For SCR events, Johnston (1994) database was used. Only data cited as good quality by the authors of the datasets have been considered. The 2004 Sumatra-Andaman earthquake is included, as well as 12 surface rupturing earthquakes. Data divided into strike-slip and dip-slip mechanism. Reverse and normal data combined.

Origin of each dataset:

- Wells and Coppersmith (1994): 244 continental crustal ($h < 40\text{km}$) earthquakes of all mechanism types, both interplate and intraplate.
- Henry and Das (2001): 64 shallow dip-slip and 8 strike-slip events in the period 1977–1996 plus 3 recent earthquakes: 1998 Antarctic plate, 1999 Izmit (Turkey), 2000 Wharton Basin. Events from all over the World. 27 strike-slip earthquakes from Pegler and Das (1996) also included (large earthquakes in the period 1977–1992 based on relocated 30-day aftershock zones). Wells and Coppersmith (1994) dataset extended to an order of magnitude greater in moment for dip-slip events. Subduction zone events included.
- Hanks and Bakun (2002): strike-slip subset of the Wells and Coppersmith (1994) database, that contains 83 continental earthquakes of which 82 have magnitudes $M \geq 7.5$.
- Romanowicz and Ruff (2002): they use different datasets: Pegler and Das (1996), standard collection of reliable M_0/L data for large strike-slip earthquakes since 1900 (e.g., Romanowicz, 1992), data for great central Asian events since the 1920’s (Molnar and Qidong, 1984), as well as data for recent large strike-slip events (e.g., Balleny Islands 1998; Izmit, Turkey 1999 and Hector Mines, CA, 1999) that have been studied using a combination of modern techniques (i.e., field observations, waveform modelling, aftershock relocation).
- Manighetti et al. (2007): 250 large ($M \geq \sim 6$), shallow (rupture width $\leq 40\text{ km}$, with an average value W_{mean} of 18 km), continental earthquakes of mixed focal mechanisms (strike-slip, reverse and normal), that have occurred in four of the most seismically active regions worldwide: Asia (broad sense), Turkey, West US and Japan.
- Johnston (1994): SCR database of 870 earthquakes where moment could be estimated from waveform or isoseismal data. Surface rupturing earthquakes included, such as the 3 1988 Tennant Creek events. Magnitude range: 4.2–8.5 (several types of magnitudes: mainly M_s but also some M_L and m_b)

Application: Wide application, including low seismicity/intraplate regions, but excluding normal faults regions (e.g., Great Sumatara Fault). The author suggests to use this relationship for all types of faults.

Tectonic regime and mechanism: A11

Quality score = 1

References: Molnar and Qidong (1984); Scholz *et al.* (1986); Romanowicz (1992); Johnston (1994); Wells and Coppersmith (1994); Pegler and Das (1996); Henry and Das (2001); Hanks and Bakun (2002); Romanowicz, and Ruff (2002); Manighetti *et al.* (2007); Leonard (2010).

7.3.6 Yen and Ma (2011) relationships

In terms of area:

$$\text{Log}A_e = -13.79 + 0.87\text{Log}M_0 \quad \text{All slip types}$$

$$\text{Log}A_e = -12.45 + 0.80\text{Log}M_0 \quad \text{Dip slip types}$$

$$\text{Log}A_e = -14.77 + 0.92\text{Log}M_0 \quad \text{Strike slip types}$$

In terms of length:

$$\text{Log}L_e = -7.46 + 0.47\text{Log}M_0 \quad \text{All slip types } (\sigma=0.19)$$

$$\text{Log}L_e = -6.66 + 0.42\text{Log}M_0 \quad \text{Dip slip types } (\sigma=0.19)$$

$$\text{Log}L_e = -8.11 + 0.50\text{Log}M_0 \quad \text{Strike slip types } (\sigma=0.20)$$

A_e =effective area (km²)

L_e =effective fault length (km)

M_0 =seismic moment (dyne-cm).

(Convert M_0 to M_w with the equation $\text{Log}M_0=16.05+1.5M_w$)

Description: Developed exclusively from earthquakes in a collisional tectonic environment. Equation has a bilinear form.

Data: 29 events used: 12 dip-slip and 7 strike-slip events in Taiwan, plus 7 large events worldwide (Wenchuan, China, 2008; Kunlun, Tibet, 2001; Sumatra 2004; Bhuj, India, 2001; 3 large thrust earthquakes from Mai and Beroza (2000) dataset. Magnitude range: 4.6-8.9 (M_w)

Application: Applicable to reverse to reverse-oblique faults in collisional environments. Use with high weighting in a logic tree framework relevant to collisional environments.

Tectonic regime and mechanism: A21 (all types), A22 (strike-slip), A24 (dip-slip).

Quality score = 1

References: Mai and Beroza (2000); Yen and Ma (2011).

7.3.7 Stirling *et al.* (2008) relationship (New Zealand oblique slip)

$$M_w = 4.18 + 2/3 \log W + 4/3 \log L$$

W =width (km)

L =subsurface rupture length (km)

Description: This regression has been developed for New Zealand strike-slip to reverse slip earthquakes. It produces magnitudes that are larger than those of Wells and Coppersmith (1994) and Hanks and Bakun (2008), and magnitudes that are appropriate for New Zealand fault sources based on expert judgement. The regression has been applied to numerous studies in New Zealand, and also in Australia in recent years. The regression is documented in a consulting report, but first published in the reference below.

Data: 28 New Zealand strike-slip to reverse earthquakes on low slip rate faults. The data were obtained from body-wave modelling studies of historical and contemporary earthquakes where fault mechanism, depth, source duration and seismic moment were obtained (Berryman *et al.*, 2002). Magnitude range: 5.6-7.8 (M_w).

Application: The authors recommend that the regression should be used for strike-slip-to-convergent-dip-slip faults, not for major plate boundary faults. Performs well for strike-slip to oblique-slip faults other than the primary plate boundary faults (e.g., Alpine Fault, San Andreas Fault) and for strike-slip to oblique-slip faults in low seismicity regions, i.e., larger magnitudes for given fault rupture lengths.

Tectonic regime and mechanism: A24

Quality score = 1

References: Berryman et al. (2002); Stirling et al. (2008).

7.3.8 Anderson et al. (1996) relationship

$$M_w = 5.12 + 1.16 \log L - 0.20 \log S$$

L = surface fault length (km)

S = slip rate (mm/yr)

Description: least-squares regression for a data set of 43 earthquakes where slip rates are available. The authors consider that regressions that ignore slip rates underestimate the magnitude of earthquakes under slow slip rates.

Data: worldwide data with slip rates information. Most of them from California. Other regions include Nevada (2), Missouri (1), Montana (1), Mexico (1), Philippines (1), Turkey (5), Japan (5), China (2) and New Zealand (3). Limited to regions with seismogenic depth from 15 to 20km. Magnitude range: 5.8-8.2 (M_w)

Application: interplate to intraplate environments where slip rate data are available. Although based on a relatively small earthquake dataset, the negative dependence of magnitude on slip rate makes this a potentially suitable regression for use in a wide variety of environments. However, the small size and age of the earthquake dataset should limit the weight placed on this regression in a logic tree framework.

Tectonic regime and mechanism: B1, B2

Quality score = 2

References: Anderson et al. (1996).

7.3.9 Nuttli (1983) relationship

$$\log M_0 = 3.65 \log L + 21.0$$

M_0 = seismic moment (dyne-cm)

L = subsurface fault length (km)

(Convert M_0 to M_w with the equation $\log M_0 = 16.05 + 1.5 M_w$)

Description: developed for mid-plate earthquakes (>500km from plate margins), both continental and oceanic. Magnitude-length relationships are obtained from derived fault lengths, not direct length measurements (empirical data are M_0 and magnitudes m_b and M_s).

Data: published data for 143 mid-plate earthquakes. Magnitude range: 0.4-7.3 (M_s)

Application: intraplate settings. Age of regression means some key earthquakes not included in regression database, but intraplate relevance makes this a valuable inclusion in this compilation.

Tectonic regime and mechanism: B1, B2.

Quality score = 3

References: Nuttli (1983).

7.3.10 Villamor *et al.* (2007) relationship (New Zealand normal slip)

$$M_w = 3.39 + 1.33 \log A$$

A=area (km²)

Description: This New Zealand-based regression has been developed from Taupo Volcanic Zone earthquakes for application to normal faults in volcanic and rift environments. It was developed for a consulting project, but first published in the reference below.

Data: 7 large earthquakes in the Taupo Volcanic Zone (3 strike-slip and 4 normal events), including the M_w 6.5 Edgcumbe 1987 earthquake. Magnitude range: 5.9-7.1 (M_w)

Application: Only for use with normal faults in thin weak crust (e.g., New Zealand's Taupo Volcanic Zone). Use in rift environments, but with careful examination of the results.

Tectonic regime and mechanism: D1

Quality score = 1

References: Villamor *et al.* (2007).

7.3.11 Strasser *et al.* (2010) relationships

a) In terms of length

$$M_w = 4.868 + 1.392 \log_{10}(L) \text{ Interface events (95 events used)}$$

$$M_w = 4.725 + 1.445 \log_{10}(L) \text{ Intraslab events (20 events used)}$$

b) In terms of area

$$M_w = 4.441 + 0.846 \log_{10}(A) \text{ Interface events (85 events used)}$$

$$M_w = 4.054 + 0.981 \log_{10}(A) \text{ Intraslab events (18 events used)}$$

L= surface rupture length (km)

A=rupture area (km²)

Description: for subduction zone events worldwide. They distinguish between interface and intraslab events. Relationship parameters are also available for width and length parameters as well as for area in terms of magnitude (instead of magnitudes in terms of area). Indicates that Wells and Coppersmith (1994) relationships are valid for shallow crustal events, excluding subduction zones. Intraslab events have similar scaling to crustal events in Wells and Coppersmith (1994). Interface events tend to have larger areas than the events in Wells and Coppersmith (1994) by a factor of up to 2 which increases with magnitude.

Predicted areas smaller than the ones in Somerville *et al.* (2002) and Mai and Beroza (2000) relationships for dip-slip events, but these two are based on a limited number of events and could be a sampling problem. In any case, it converges for large magnitudes. For events with M_w ≤ 7.0 the relations for interface events in this study have similar results than the ones for dip-slip events in Mai and Beroza (2000). It crosses at M=7.0 with Martin and Mai (2000) relationship.

Data: subduction events taken primarily from the SRCMOD database (Mai, 2004, 2007). 95 interface events (magnitude range M_w=6.3-9.4) and 20 intraslab events (magnitude range M_w=5.9-7.8).

Application: Subduction interfaces.

Tectonic regime and mechanism: C1, C2

Quality score = 1

References: Mai (2004, 2007), Strasser *et al.* (2010).

7.3.12 *Blaser et al. (2010) relationship*

Relationships for oceanic and subduction events:

- a) In terms of length
- $\text{Log}_{10}L = -2.81 + 0.62M_w$ Reverse slip (26 events used). Magnitude range: 6.1-9.5
- $\text{Log}_{10}L = -2.56 + 0.62M_w$ Strike-slip (16 events used). Magnitude range: 5.3-8.1
- $\text{Log}_{10}L = -2.07 + 0.54M_w$ All slip types (47 events used). Magnitude range: 5.3-9.5
- b) In terms of width
- $\text{Log}_{10}W = -1.79 + 0.45M_w$ Reverse slip (23 events used). Magnitude range: 6.1-9.5 (sxy=0.14)
- $\text{Log}_{10}W = -0.66 + 0.27M_w$ Strike-slip (14 events used). Magnitude range: 5.3-7.8 (sxy=0.21)
- $\text{Log}_{10}W = -1.76 + 0.44M_w$ All slip types (40 events used). Magnitude range: 5.3-9.5 (sxy=0.17)

L=subsurface fault length (km)

W: rupture width (km)

sxy: orthogonal standard deviation

(Note: only the relationships specific for oceanic/subduction events are shown)

Description: developed for subduction zones. Indicates that Wells and Coppersmith (1994) relationships are valid for all slip types except for thrust faulting in subduction zones. Based on a large dataset of 283 earthquakes. Most of the focal mechanisms are represented, but the analysis is focused on large subduction zones. For a given magnitude, this relationship has shorter but wider rupture areas than the Wells and Coppersmith (1994) relationships. The authors recommend the relationships using orthogonal regression. Exclusion of events prior to 1964 (when the WSSN was established) shows no saturation on rupture width for strike-slip earthquakes. Thrust relationships for pure continental and pure subduction zone rupture areas are almost identical. The authors recommend to use different scaling relationships depending on the focal mechanism.

Data: published data for 283 earthquakes. Database composed of 196 source estimates by Wells and Coppersmith (1994), 40 by Geller (1976), 25 by Scholz (1982), 31 by Mai and Beroza (2000), 36 by Konstantinou et al. (2005), and 31 by several other authors analysing single large events. Magnitude range (for oceanic/subduction zones): 5.3-9.5 (M_w)

Application: Subduction zones (especially oceanic).

Tectonic regime and mechanism: C2

Quality score = 1

References: Geller (1976), Scholz (1982), Wells and Coppersmith (1994), Mai and Beroza (2000), Konstantinou et al. (2005), Blaser et al. (2010).

7.3.13 *Ichinose et al. (2006) relationship*

$$\text{Log}_{10}(A_a) = 0.57 (\pm 0.06) M_0 - 13.5 (\pm 1.5)$$

A_a= combined area of asperities

M₀=seismic moment (dyne-cm)

(Convert M₀ to M_w with the equation $\text{Log}M_0 = 16.05 + 1.5M_w$)

Description: developed for intra-slab earthquakes at global scale, to distinguish them from shallow global strike-slip earthquakes. The authors have found that the combined area of asperities for intraslab earthquakes is smaller than for shallower strike-slip earthquakes with the same M_0 .

Data: data from the 3 events in Cascadia (1949 Olympia, Washington; 1965 Seattle-Tacoma and 2001 Nisqually) and several Japan (9 events taken from Asano et al., 2003 and Morikawa and Sasatani, 2004) and Mexico (14 events taken from Hernandez et al., 2001; Iglesias et al., 2002; Yamamoto et al., 2002 and Garcia et al., 2004) intraslab earthquakes (26 events in total). Magnitude range: 5.4-8.0 (Mw)

Application: Intraslab earthquake source modelling.

Tectonic regime and mechanism: C3

Quality score = 1

References: Hernandez et al. (2001), Iglesias et al. (2002), Yamamoto et al. (2002), Asano et al. (2003), Garcia et al. (2004), Morikawa and Sasatani (2004), Ichinose et al. (2006).

7.4 Conclusions

We have provided a compilation and evaluation of 72 magnitude-area and magnitude-length scaling relationships. Of these, 18 have been recommended for application in the Global Earthquake Model (GEM). The equations have been provided, as well as relevant dialogue and guidelines to assist with using the regressions in seismic hazard modelling. The recommended regressions have been sorted into four categories and eight subcategories of tectonic regime, four mechanism (slip-type) categories, and three levels of Quality score. The report will assist GEM Regional Programmes and Global Components in making appropriate choices of regressions for application in the GEM seismic hazard model.

7.5 Recommendations

Our efforts have been motivated by a need to assist scientists and practitioners in making the appropriate choice of regressions for seismic source modelling. We therefore make the following recommendations for future development and selection of regressions:

- Regression users must ensure that their choice of regression is as compatible as possible with the tectonic regime of interest. There has been frequent misuse of regressions in this respect, even in some very major seismic hazard projects.
- Regressions should not be used beyond the magnitude range of data used to develop the regression. Exceptions to this recommendation should be well justified.
- Regression users should, where possible, use a selection of regressions (e.g., by way of a logic tree framework), and carefully evaluate the consequences of the particular selection of regressions.
- Regression users should use regressions of Quality score = 1 whenever possible, although we acknowledge this may not be possible for some tectonic regimes (e.g., stable continental).
- Regression developers should strive to develop regressions for specific tectonic regimes, rather than combining all available earthquake data from an ensemble of tectonic regimes. The latter approach has obviously been the case for many of the regressions in existence today.
- Regression developers should provide clear recommendations regarding the tectonic regimes represented by their regressions.
- Regression developers should always provide standard deviations and/or standard errors for their regression equations.

7.6 Other Regressions

The following is a documentation of the regressions in our compilation that did not make the shortlist for reasons provided in the introductory sections of the report. The purpose of including these regressions in the report is to demonstrate that our compilation and evaluation has been a thorough procedure, in that it has captured all of the readily available published regressions in the literature. Furthermore, it allows access to all available regressions if need be.

7.6.1 Shaw (2009) relationship

$$M = \log A + \frac{2}{3} \log \frac{\max(1, \sqrt{\frac{A}{H^2}})}{[1 + \max(1, \frac{A}{H^2\beta})]^{1/2}} + \text{const.}$$

A= rupture area (km²)

H=seismogenic thickness (km)

$\beta=2\chi$, where $\chi = 3$

Const=constant

Description: Developed for worldwide earthquakes, both small and large. The regression has been developed to address the hypothesis that earthquake stress drops are constant from the smallest to the largest events (most other regressions assume non-constant stress drop scaling), combined with a thorough treatment of the geometrical effects of the finite seismogenic layer depth. The relationship has been tested for strike-slip events, because they are the ones with the largest aspect ratio L/W. For these events (see data below) the best fitting corresponds to H=15.6km and $\chi=6.9$.

Data: Strike-slip events taken from Hanks and Bakun (2008) data as well as Wells and Coppersmith (1994), Hanks and Bakun (2002) and WGCEP (2003). These datasets do not have error bars. The authors assume errors in logA are the same size as errors in magnitude. Magnitude range: 4.2-8.5 (several types of magnitudes: mainly Ms but also some ML and mb)

Origin of each dataset:

- Wells and Coppersmith (1994): 244 continental crustal (h<40km) earthquakes of all mechanism types, both interplate and intraplate.
- Hanks and Bakun (2002): strike-slip subset of the Wells and Coppersmith (1994) database, that contains 83 continental earthquakes of which 82 have magnitudes M≥7.5.
- Hanks and Bakun (2008): 88 continental strike-slip earthquakes. Includes historical earthquakes since 1857 and 12 new M>7 events added to the Wells and Coppersmith (1994) dataset.

Application: All kind of faults in all regions around the world. Has not been used greatly in seismic hazard studies, so careful examination of results is recommended. The author states that the scaling law fits the whole range of magnitude-area data.

Quality score = 2

References: Hanks and Bakun (2002; 2008); Working Group on California Earthquake Probabilities, (2003); Shaw (2009)

7.6.2 *Ellsworth-B relationship*

$$M_w = \log A + 4.2$$

A=fault area (km²)

Description: Simple magnitude-area scaling relationship applicable to all slip types in plate boundary areas (i.e., used extensively in WGCEP 2003 and 2008 i.e., UCERF2). No stand-alone reference exists for this relationship, but it has been used in the above studies and associated reports. Developed on the basis of worldwide earthquakes.

Data: continental strike-slip events from Wells and Coppersmith (1994) dataset with areas $A > 500 \text{ km}^2$ corresponding to $M > 6.5$. Magnitude range: 6.5-8.5 (several types of magnitudes: mainly Ms but also some ML and mb)

Application: Best applied to continental strike-slip faults, but can also be used in intraplate areas. Used by the WGCEP in the 2002 U.S. National Seismic Hazard Mapping Project with equal weight to the Hanks and Bakun (2008) relationship, indicating that it can be used with confidence in logic tree frameworks.

Quality score = 1

References: Wells and Coppersmith (1994); Working Group on California Earthquake Probabilities (2003; 2008)

7.6.3 *Bonilla et al. (1984) relationships*

$$M_s = 6.04 + 0.708 \log L \text{ All types of faults (45 events used)}$$

$$M_s = 5.71 + 0.916 \log L \text{ Reverse and reverse-oblique faults (12 events used)}$$

$$M_s = 6.24 + 0.619 \log L \text{ Strike-slip (23 events used)}$$

$$M_s = 5.58 + 0.888 \log L \text{ Plate margins (9 events used)}$$

$$M_s = 6.02 + 0.729 \log L \text{ Plate interiors (36 events used)}$$

$$M_s = 4.94 + 1.296 \log L \text{ US and China } k=1.75 \text{ attenuation region (9 events used)}$$

$$M_s = 4.88 + 1.286 \log L \text{ US } k=1.75 \text{ attenuation region (5 events used)}$$

$$M_s = 6.18 + 0.606 \log L \text{ Turkey (9 events used)}$$

$$M_s = 5.17 + 1.237 \log L \text{ Western North America (12 events used)}$$

L=surface rupture length (km)

Description: magnitude-length and/or displacement relationships obtained for 5 types of mechanisms: normal, reverse, normal oblique, reverse oblique and strike-slip. 100 published and unpublished events analyzed, 48 of them used to obtain the equation, which correspond to the ones with error estimations in reported length or displacement. Tests made for ordinary and weighted least-squares. Ordinary least-squares found to be the appropriate approach, due to the stochastic nature of the magnitude-fault length-displacement relations.

Data: 48 worldwide earthquakes taken from published and unpublished data. No subduction events included. Fault length 3-450km. Magnitude range: 6.5-8.3.

Application: worldwide application, although some relationships are specific for certain regions (US $k=1.75$ attenuation region, US and China $k=1.75$ attenuation region, Turkey, Western North America). No magnitude-length equations are available for normal mechanisms, but magnitude-displacement or displacement-length relations are available for these events. Age and size of the earthquake dataset limit the

applicability of these regressions, and they should therefore be given very low weighting if used in a logic tree framework. An additional recommendation from the author is that the equations should not be extrapolated beyond the range of the data set or applied to subduction zone sources.

Quality score = 3

References: Bonilla et al. (1984).

7.6.4 Stirling et al. (2002) relationship

$M_w = 5.88 + 0.80 \log L$ (50 events used)

L=surface rupture length (km)

Description: magnitude-length, magnitude-area and displacement-length relationships developed to compare preinstrumental (pre-1900) and instrumental events in order to understand why Wells and Coppersmith (1994) regressions tend to underestimate the magnitudes of many large worldwide earthquakes. Results show that these regressions produce significantly larger magnitudes than Wells and Coppersmith (1994) relationships.

Data: 389 worldwide events, 305 instrumental (post -1900) and 84 preinstrumental (pre-1900). Expanded and updated dataset from Wells and Coppersmith (1994). Magnitude range: 4.6-8.7 (Ms, ML and Mw)

Application: The authors did not intend this regression to be used in seismic hazard studies, so it should only be used if a large number of regressions are required for a logic tree framework. They further recommend that the regression only be used for the range of magnitudes, displacements and rupture lengths contained in the regression dataset.

Quality score = 2

References: Wells and Coppersmith (1994); Stirling et al. (2002).

7.6.5 Stock and Smith (2000) relationship

$\log M_0 = 3.1 \log L$ Small normal faults (32 events used)

$\log M_0 = 4.1 \log L$ Large normal faults (6 events used)

$\log M_0 = 2.9 \log L$ Small reverse faults (77 events used)

$\log M_0 = 2.9 \log L$ Large reverse faults (9 events used)

$\log M_0 = 3.2 \log L$ Dip-slip faults in Japan (21 events used)

$\log M_0 = 2.9 \log L$ Dip-slip events in Eastern Russia (16 events used)

$\log M_0 = 2.8 \log L$ Small strike-slip faults in California (27 events used)

$\log M_0 = 2.1 \log L$ Large strike-slip faults in California (9 events used)

$\log M_0 = 2.9 \log L$ Small strike-slip faults outside California (33 events used)

$\log M_0 = 2.3 \log L$ Large strike-slip faults outside California (25 events used)

M_0 =seismic moment (Nm)

L=average dislocation (rupture) subsurface length (km)

(Convert M_0 to M_w with the equation $\log M_0 = 16.05 + 1.5 M_w$)

Large=earthquakes rupturing the whole seismogenic layer

Small= earthquakes not rupturing the whole seismogenic layer

Description: scaling relationships obtained from a large dataset of more than 550 events from all over the world. The influence of the mechanism and the size in the scaling relationships has been analyzed. No differences in the scaling behaviour have been found between normal and reverse events, or between events from different regions for this type of mechanisms. No self-similarity breakdown has been found for dip-slip events, except for very large earthquakes, but in this case the data are too few to make it statistically significant. For strike-slip earthquakes, self-similarity breaks down for large events. This could be caused by the limitation in rupture width caused by the thickness of the seismogenic layer.

Data: database of more than 550 events obtained from several published papers (Kanamori and Anderson, 1975; Geller, 1976; Purcaru and Berckhemer, 1982; Scholz, 1982; Bonilla et al., 1984; Kanamori and Allen, 1986; Scholz et al., 1986; Shimazaki, 1986; Romanowicz, 1992; Wells and Coppersmith, 1994; Anderson et al., 1996; Yeats et al., 1997; Margaris and Boore, 1998). Magnitude range: 4.2-8.5 (several types of magnitudes: mainly Ms but also some ML and mb)

Application: Worldwide, although specific relationships have been developed from data in specific regions (California, Japan, and Eastern Russia). Regressions have not been widely used to date.

Quality score = 2

References: Kanamori and Anderson (1975); Geller (1976); Purcaru and Berckhemer (1982); Scholz (1982); Bonilla et al. (1984); Kanamori and Allen (1986); Scholz et al. (1986); Shimazaki (1986); Romanowicz (1992); Wells and Coppersmith (1994); Anderson et al. (1996); Yeats et al. (1997); Margaris and Boore (1998); Stock and Smith (2000)

7.6.6 *Vakov (1996) relationship*

$M_s = 4.442 + 1.448 \log L$ Slip faults (31 events used)

$M_s = 3.862 + 1.988 \log L$ Normal + reverse strike faults (13 events used)

$M_s = 4.171 + 1.949 \log L$ Strike-normal + strike-reverse faults (20 events used)

$M_s = 3.161 + 3.034 \log L$ Normal + reverse faults (18 events used)

$M_s = 4.524 + 1.454 \log L$ Strike-slip faults (44 events used)

$M_s = 4.323 + 1.784 \log L$ Oblique faults (33 events used)

$M_s = 4.270 + 1.947 \log L$ Dip-slip faults (38 events used)

$M_s = 4.805 + 1.348 \log L$ Strike-slip + oblique-slip faults (64 events used)

$M_s = 4.525 + 1.697 \log L$ Oblique + dip-slip faults (51 events used)

$M_s = 4.973 + 1.273 \log L$ All faults (82 events used)

L = surface rupture length (km)

Description: magnitude versus area/length/width analysed for worldwide events and different types of mechanisms. The authors have found dependence of the scaling relationships on the source mechanism but not on the regional setting. According to the authors, these relationships can be also used for the evaluation of earthquake mechanism types.

Data: database of 400 events worldwide taken from existing sources. Subduction events from Japan, New Zealand, Taiwan and Philippines have been excluded, as well as normal and thrust events with fault planes dipping less than 45°. ~~been finally used in the scaling laws.~~ Magnitude range: 4.5-8.5 (Ms)

Application: worldwide. Not widely used to date.

Quality score = 2

References: Vakov (1996)

7.6.7 *Stirling et al. (1996) relationships*

$M_0 = 1.22 \cdot 10^{18} \cdot L^{5.0}$ Strike-slip faults worldwide, $L < 50$ km

$M_0 = 2.37 \cdot 10^{24} \cdot L^{1.3}$ Strike-slip faults worldwide, $L > 50$ km

$M_0 = 2 \cdot 10^{23} \cdot L^{2.1}$ Large intraplate earthquakes in Japan

M_0 = seismic moment (dyne-cm)

L = surface or subsurface rupture length (km)

(Convert M_0 to M_w with the equation $\text{Log}M_0 = 16.05 + 1.5M_w$)

Description: the study analyses the shape of the magnitude-frequency relationships for strike-slip events worldwide. The authors obtain a specific scaling law for intraplate events in Japan.

Data: strike-slips events worldwide recorded in regional networks located in California, Mexico, New Zealand, Japan, China and Turkey. Data taken from published papers (Romanowicz, 1992; Wesnousky et al., 1983). Magnitude range: 5.7-7.8.

Application: The authors recommend use of this regression for strike-slip faults worldwide, and intraplate faults in Japan. Regression databases will now be significantly lacking with respect to the more modern earthquakes. Use only if logic tree framework requires a large number of regressions.

Quality score = 3

References: Wesnousky et al. (1983); Romanowicz (1992); Stirling et al. (1996).

7.6.8 *Mai and Beroza (2000) relationships*

In terms of area:

$\text{Log}A = -11.18 - 0.72 \text{log}M_0$ All events (18 events used)

$\text{Log}A = -8.49 - 0.57 \text{log}M_0$ Strike-slip events (8 events used)

$\text{Log}A = -11.90 - 0.75 \text{log}M_0$ Dip-slip events (10 events used)

In terms of length:

$\text{Log}L = -6.13 + 0.39 \text{log}M_0$ All events ($\square = 0.16$, in length)

$\text{Log}L = -6.31 + 0.40 \text{log}M_0$ Strike-slip events ($\square = 0.12$, in length)

$\text{Log}L = -6.39 + 0.40 \text{log}M_0$ Dip-slip events ($\square = 0.19$, in length)

A = area (km²)

L = subsurface length (km)

M_0 = seismic moment (Nm)

(Convert M_0 to M_w with the equation $\text{Log}M_0 = 16.05 + 1.5M_w$)

Description: Developed from finite-fault rupture models. The dataset lacks very large strike-slip events. The scaling laws produce very similar results to those of Wells and Coppersmith (1994).

Data: 18 earthquakes, of which 8 are large crustal strike-slip and 10 dip-slip earthquakes; regions: most of them in California (13), other regions: Idaho (USA, 1), Japan (2), Iran (1), Mexico (1). Magnitude range: 5.6-8.1 (M_w)

Application: To plate boundary environments. Small regression datasets potentially limit the stability of these regressions.

Quality score = 2

References: Mai and Beroza (2000).

7.6.9 Somerville et al. (1999) relationship

$$M_w = \log A + 3.95$$

A=rupture area (km²)

Description: Developed from crustal earthquakes. The relationships are constrained to be self-similar, and produce very similar results to those of Wells and Coppersmith (1994).

Data: 15 inland crustal earthquakes worldwide, most of them in California. Other regions are: Canada (2), Iran (1), Idaho (1) and Japan (1). Mechanisms: 1 normal, 6 thrust events, 6 strike-slip, 2 oblique earthquakes. Magnitude range: 5.7-7.2 (M_w)

Application: crustal earthquakes worldwide. Can be used with greatest confidence at moderate-to-large magnitudes. Departure from self-similar scaling may occur for very large crustal strike-slip earthquakes at very large magnitudes. Use with significant logic tree weighting when focus is on moderate-to-large magnitude earthquake sources.

Quality score = 2

References: Somerville et al. (1999).

7.6.10 Wells and Coppersmith (1994) relationships

$$M_w = 4.07 + 0.98\text{Log}A \quad \text{All slip types (148 events used)}$$

$$M_w = 3.98 + 1.02\text{Log}A \quad \text{Strike-slip faults (83 events used)}$$

$$M_w = 4.33 + 0.90\text{Log}A \quad \text{Reverse faults (43 events used)}$$

$$M_w = 3.93 + 1.02\text{Log}A \quad \text{Normal faults (22 events used)}$$

A=area (km²)

Description: These regressions are developed for worldwide earthquakes. Are still considered by many to be "industry standards" but in reality are out of date in terms of data. Magnitudes tend to be less than those estimated from the more modern regressions.

Data: 244 continental crustal (h<40km) earthquakes of all mechanism types, both interplate and intraplate, 127 are surface ruptures and 117 calculated subsurface ruptures. Taken from published results. Magnitude range: 4.2-8.5 (several types of magnitudes: mainly M_s but also some M_L and m_b)

Application: The regressions should not be used outside of active plate boundary regions, and in general should not be used if more modern regressions are available. Use with low weighting if it has to be used in a logic tree framework. The authors recommend that the all-slip types regression be used for most situations; the use of subsurface rupture length and area regressions may be appropriate where it is difficult to estimate the near-surface behaviour of faults, such as for buried or blind faults.

Quality score = 2

References: Wells and Coppersmith (1994).

7.6.11 Dowrick and Rhoades (2004) relationship

$$M_w = 4.39 + 2.0 \log L \quad L < 6.0 \text{ km}$$

$$M_w = 4.73 + 1.53 \log L \quad L \geq 6.0 \text{ km}$$

L = subsurface rupture length (km)

Description: developed for New Zealand events. Results have been compared to multiregional relationships, and significant differences have been found to regressions for California, Japan and China. Authors consider multiregional relationships to be a poor estimation for New Zealand data, as they underestimate New Zealand magnitudes (by 0.4 magnitude units when compared to Wells and Coppersmith, 1994, Somerville et al., 1999 and the lower part of the bilinear regression by Hanks and Bakun, 2002 relationships). The relations are influenced by structural restrictions placed on rupture width.

Data: 18 events in New Zealand. Magnitude range: 5.9-8.2 (M_w)

Application: New Zealand interplate. Use only in a logic tree framework with low weighting relative to other more widely used New Zealand-based regressions (e.g., Villamor et al., 2007; Stirling et al., 2008).

Quality score = 3

References: Dowrick and Rhoades (2004).

7.6.12 Wyss (1979) relationship

$$M_w = \log A + 4.15$$

A = fault area (km^2)

Description: Regressions have been developed for application to seismic risk studies. Author concludes that maximum magnitude values are more accurately obtained from magnitude-area relationships than magnitude-length relationships.

Data: worldwide events obtained from published databases. Some of the best data were collected by Kanamori and Anderson (1975). Magnitude range: 5.8-8.5 (M_s) (for the best data published in Kanamori and Anderson, 1975)

Application: $M > 5.6$ earthquakes worldwide. Age of regression is such that database will be significantly lacking with respect to more modern earthquakes. Only use if logic tree framework requires consideration of a large number of regressions.

Quality score = 3

References: Kanamori and Anderson (1975); Wyss (1979).

7.6.13 Somerville (2006) relationship

$$M_w = 3.87 + 1.05 \log(A)$$

A = area (km^2)

Description: Uses a uniform dataset of recent worldwide crustal earthquakes for which seismic inversions are available. Makes extensive use of teleseismic and strong motion inversions of coseismic slip. The relationship provides near identical estimates of M_w to self similar models (e.g., Wells and Coppersmith 1994) but with post 1994 data included.

Data: 16 large strike-slip events worldwide (USA, Japan, Tibet, Turkey). Magnitude range: 5.7-7.9 (M_w)

Application: For use on all fault types in interplate tectonic settings i.e., western North America, Indonesia, Caribbean/Central America, northern South America, New Zealand, Middle East, SE Asia. Paucity of

documentation for this relationship makes it difficult to assess the quality of this regression, so recommended usage in a logic tree framework is with relatively low weighting. Use in intraplate settings after verifying results make sense (e.g., comparison of predicted to observed earthquake magnitudes and rupture areas). Use with low weighting in logic tree framework on account of small regression dataset.

Quality score = 2

References: Working Group on California Earthquake Probabilities (2002); Somerville (2006); Somerville et al. (2006).

7.6.14 Ambraseys and Jackson (1998) relationship

$M_s = 5.13 + 1.14 \log L$ For historical and instrumental data

$M_s = 5.27 + 1.04 \log L$ For instrumental data

L = surface fault length (km)

Description: The regression has been developed from strike-slip, normal and thrust events in the Eastern Mediterranean region.

Data: collected from a variety of published and unpublished sources and field investigations, 25% collected by the first author. Both historical and instrumental data in the Eastern Mediterranean region and the Middle East. 150 events used to obtain the scaling relationship, all of them associated with coseismic surface faulting. Only 35 events are common to the Wells and Coppersmith (1994) database. For the instrumental data with high quality in the nature of the fault, 55% of the data are strike-slip events, 30% normal events and 15% thrust faults. Magnitude range: $M_s \geq 5.1$

Application: Eastern Mediterranean, Middle East and similar environments (i.e., Plate boundary transpressional to transtensional environments). Regression dataset is reasonably large and therefore makes the regressions suitable for application in eastern Mediterranean/Middle East.

Quality score = 1

References: Ambraseys and Jackson (1998).

8 Fault compilation tool

This section is a reproduction of Section 3 of the Guidelines report (Litchfield et al., 2013b) with minor adjustment to the section numbering.

8.1 Introduction and tool overview

A web-based fault compilation tool has been developed primarily for the purpose of entering new data into the GEM Faulted Earth database. The tool is designed for entering data for individual neotectonic faults and folds, and then deriving a fault source from an individual fault or fold. Traces for an individual section can be uploaded as a GIS shapefile, but the tool is not designed for bulk upload of multiple fault and fold datasets, which are uploaded into the GEM Faulted Earth database separately (Thomas, 2012; Litchfield et al., 2013a).

At the time of writing of this part of the report (May 2013), the tool has only been developed for input of neotectonic faults and fault sources (i.e., neotectonic folds are not included in the current version v1.12.11). Therefore, the remainder of this report only describes the currently available components.

The following sections are accompanied by screen shots of the version 1.12.11 of the tool, with features described denoted by red circles or ovals.

8.1.1 Access and login

The fault compilation tool (hereafter referred to as the tool) resides in the OpenQuake platform <https://platform.openquake.org/>

The OpenQuake platform is still under development (currently v1.12.11) and this report is based on:

<https://platform-sandbox.openquake.org/>

A user needs to be logged in to access the tool, so a username and password are required, which can be obtained by request from the GEM Foundation.

Once logged in, the tool can be accessed by clicking on the “CAPTURE” drop-down menu, and selecting “Active Faults” (Figure 7.1):

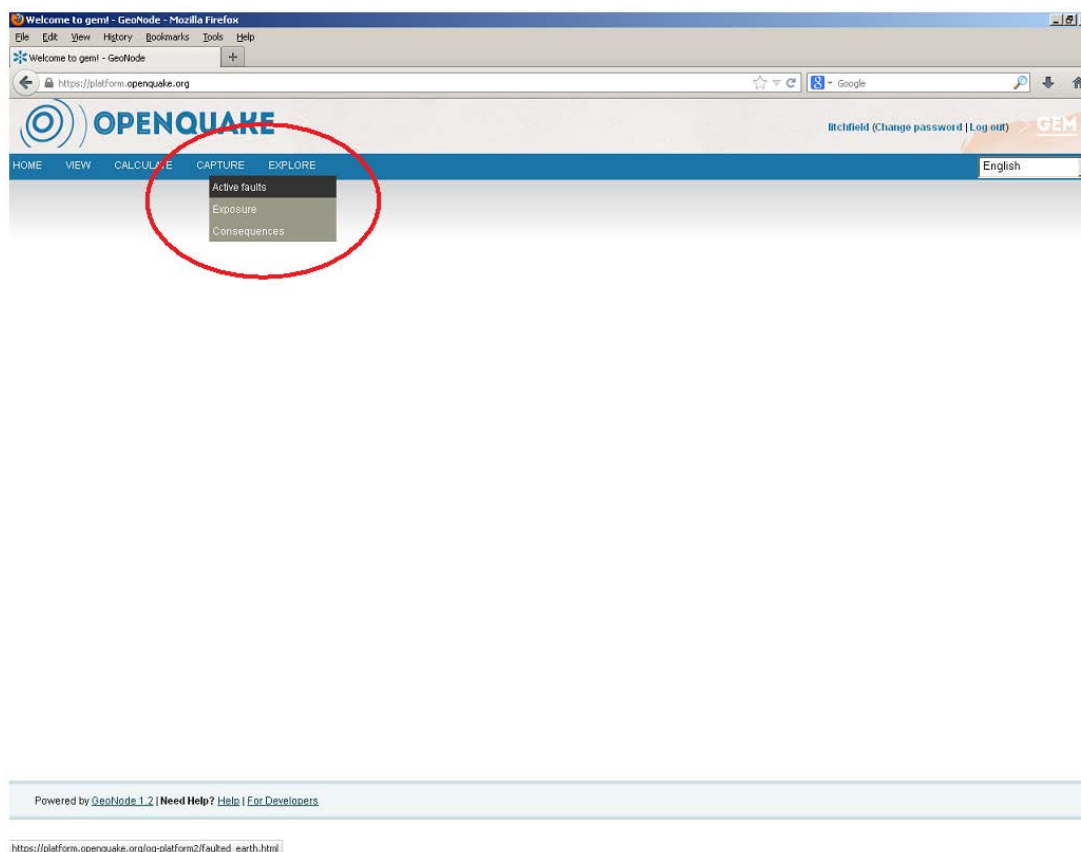


Figure 8.1 Accessing the tool on the OpenQuake website.

8.1.2 Tool design philosophy

The general design philosophy of the tool is a bottom-up or detailed to summary process (red arrows on Figure 3.1):

1. Draw or upload a series of fault traces.
2. Optional addition of site observations.
3. Join traces into a section and enter compulsory summary attributes.
4. Optional addition of additional attributes.
5. Combine sections into a fault and enter compulsory summary attributes.
6. Derive a fault source.

The tool layout is described in section 7.1.3, but in general the five main fault components (traces, fault section, site observations, fault, and fault source) are entered and edited in maps and tables, after selecting one of a series of buttons – “draw”, “upload” “modify”, “delete”, “join”, “generate”, “export”.

8.1.3 Tool layout

The tool consists of three main components (Figure 8.2):

1. Concertina (left hand side)
2. Map window (right hand side)
3. Grid (bottom)

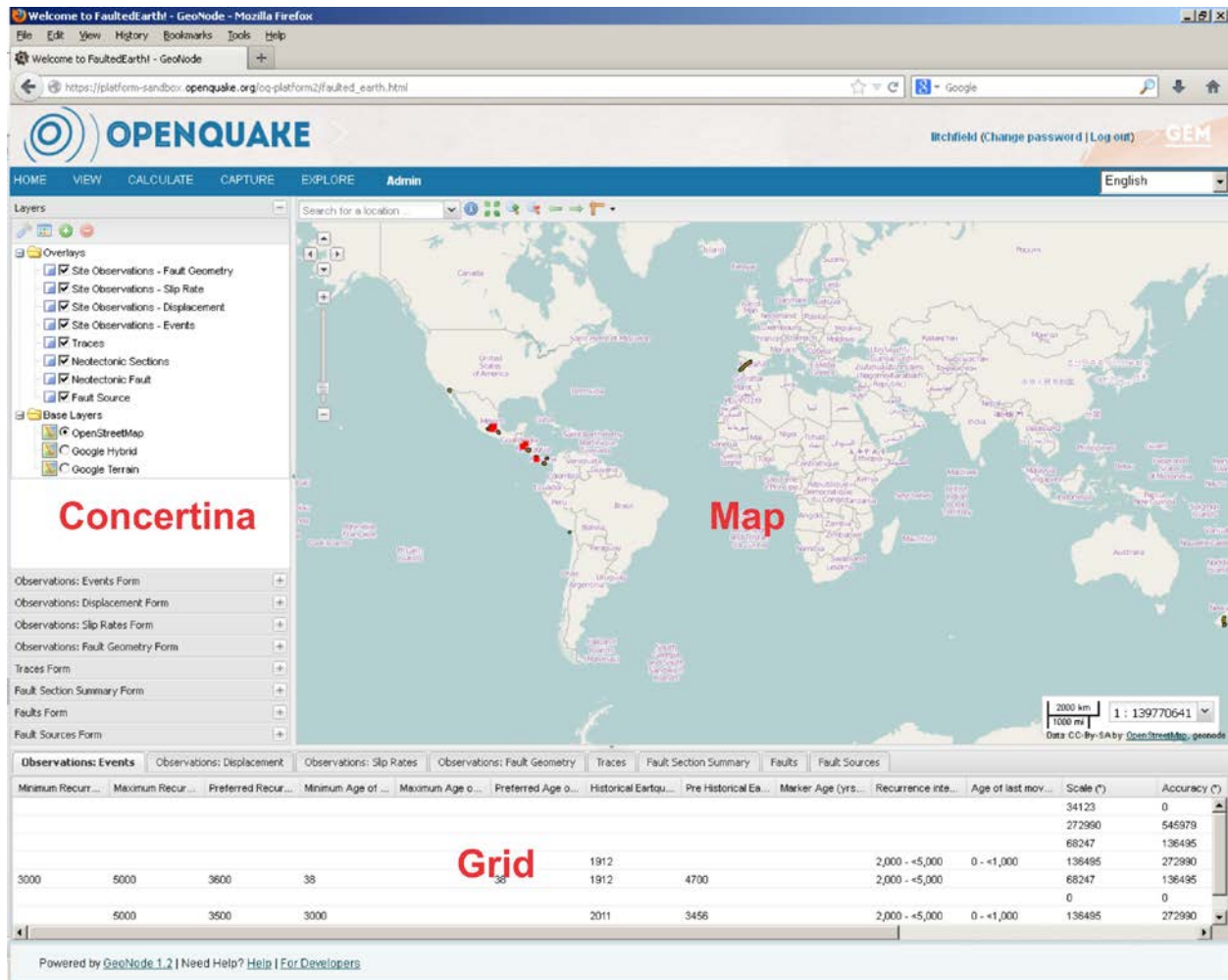


Figure 8.2 Layout of the tool with the three main panels labelled in red.

The **concertina** consists of a series of forms which can be expanded and subcontracted by either clicking on the form heading, or using the + or – symbols in the top right corner of each form. The *Layers* form controls the layers visible in the map window and these consist of 2 groups. These are:

1. **Overlays** – the GEM Faulted Earth database map layers. Traces and site observations are the only map layers that users can manually draw or edit; the remaining layers are automatically derived by joining traces or sections, or by calculations (generating fault sources).
2. **Base layers** – map layers to facilitate drawing or displaying data. The default map layers are Open Street Map and Google Hybrid and Terrain, but additional map layers can added or removed by selecting the “add layer” and “remove layer” buttons at the top of the layers form (see also section 7.1.4).

The *Traces*, *Fault section summary*, *Observation: Events*, *Observation: Displacement*, *Observation: Slip Rates*, *Observation: Fault Geometry*, *Faults*, and *Fault Sources* forms are the GEM Faulted Earth database forms and contain the operational buttons (draw, modify, join etc). They are ordered in the order of a typical workflow (section 7.2). An additional *Legend* form can be displayed by selecting the “show legend” button at the top. This form describes the symbols used for the GEM Faulted Earth database layers.

The **map window** is where the spatial data is displayed and edited. Layers can be turned on and off by selecting the tick boxes on the Layers form. Attribute tables also pop-up in the map window and help windows appear in the map window when an attribute is selected in the attribute tables. These are

descriptions of each attribute derived from the Data Dictionary (Litchfield et al., 2013a, and Section 4). Along the top of the map window are a series of tools including “search for a location”, “get feature info”, “measure” and various zoom tools. In the map window, you can also:

- pan by dragging and dropping
- zoom in using the slider on the left hand side, or hold the shift key and draw a box surrounding the area you want to zoom to.

The **grid** displays the contents of the GEM Faulted Earth database attribute tables. These cannot be edited (attributes are edited in pop-up windows in the map window), but can be used to select individual traces, sections, faults etc. They can be sorted by attribute and search functions in the concertina highlight rows in the grid tables.

More detailed descriptions of the tool features are contained in the user instructions in the section 7.2.

8.1.4 Adding and uploading base layers

The default base layers contained in the tool are Google Earth maps, but other maps (GeoTIFF and Shapefile) can be added by clicking on the “add layers” button at the top of the Layers form and selecting from the drop-down list. The tool automatically re-projects maps in projections other than WebMercator (Google).

Other maps in the format of Shapefile and GeoTIFF files can also be uploaded at <https://platform.openquake.org/data/> and clicking “Upload a new Layer” (Figure 8.3):

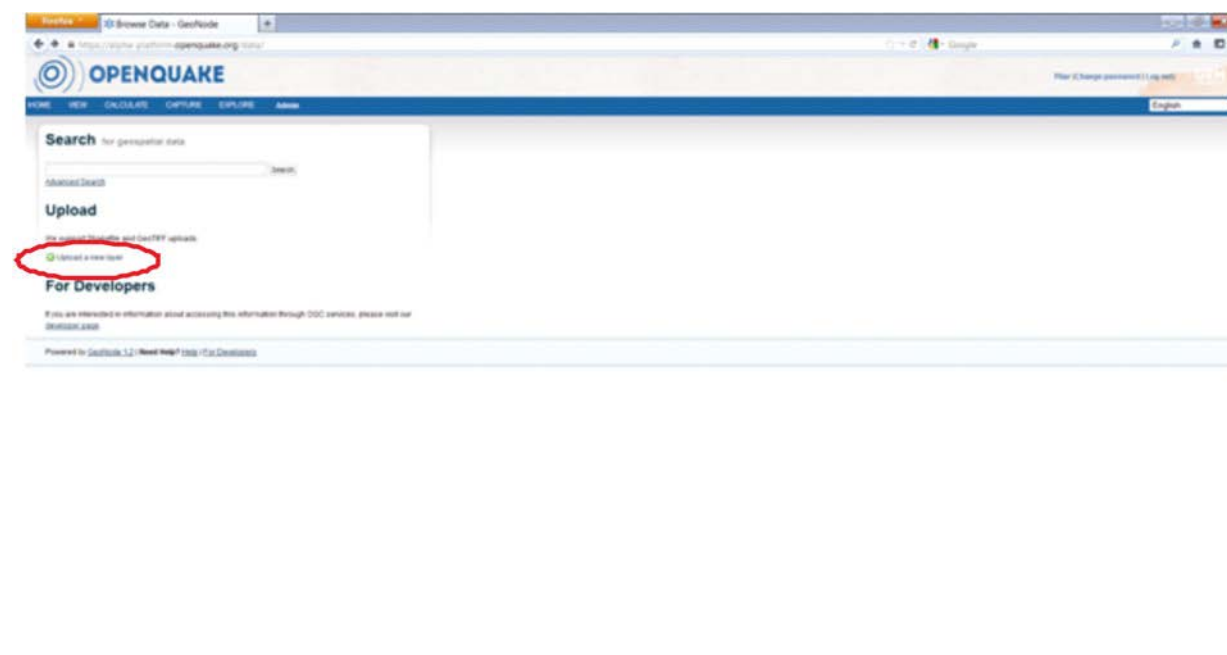


Figure 8.3 Upload a base map layer.

To upload a GeoTIFF map layer (Figure 8.4):

- Browse for your file
- Enter a title and brief description (Abstract)
- Select “Upload”
- Note that you can limit the access to this file to selected users in the “Permissions” box

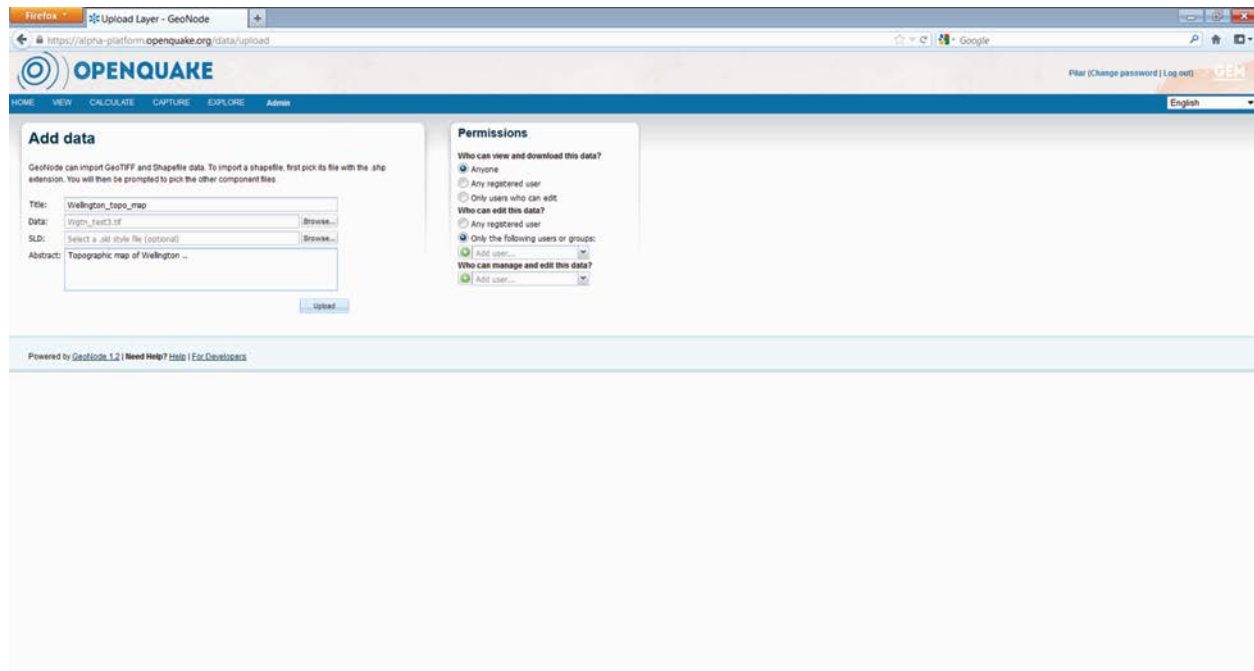


Figure 8.4 Upload a GeoTIFF base map layer.

To upload a Shapefile map layer (Figure 8.5):

- Browse for your file and open .shp file
- A list of file uploads are automatically displayed browse and open corresponding .dbf, .shx, .prj (optional), .sld (optional) files.
- Select “Upload”
- Note that you can limit the access to this file to selected users in the “Permissions” box

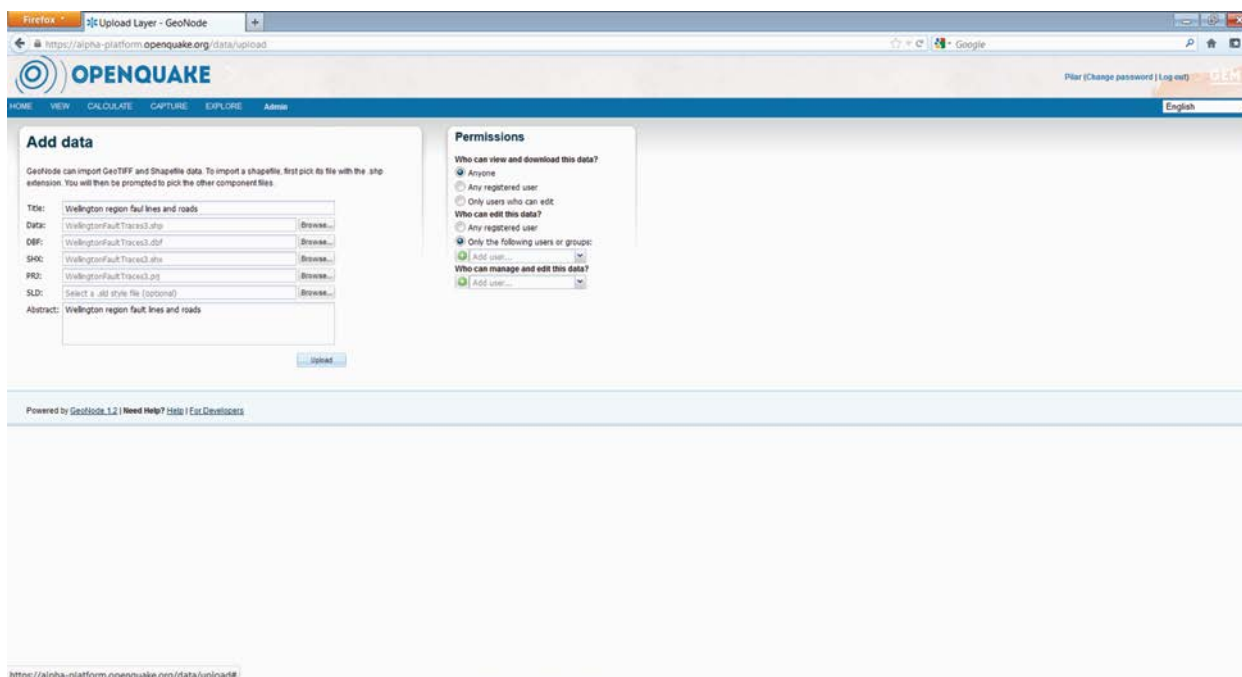


Figure 8.5 Upload a Shapefile base map layer.

To add metadata (Figure 8.6):

- After uploading GeoTIFFs and Shapefiles you will be asked to add more metadata information to the uploaded files
- Scroll down to display and enter all information.

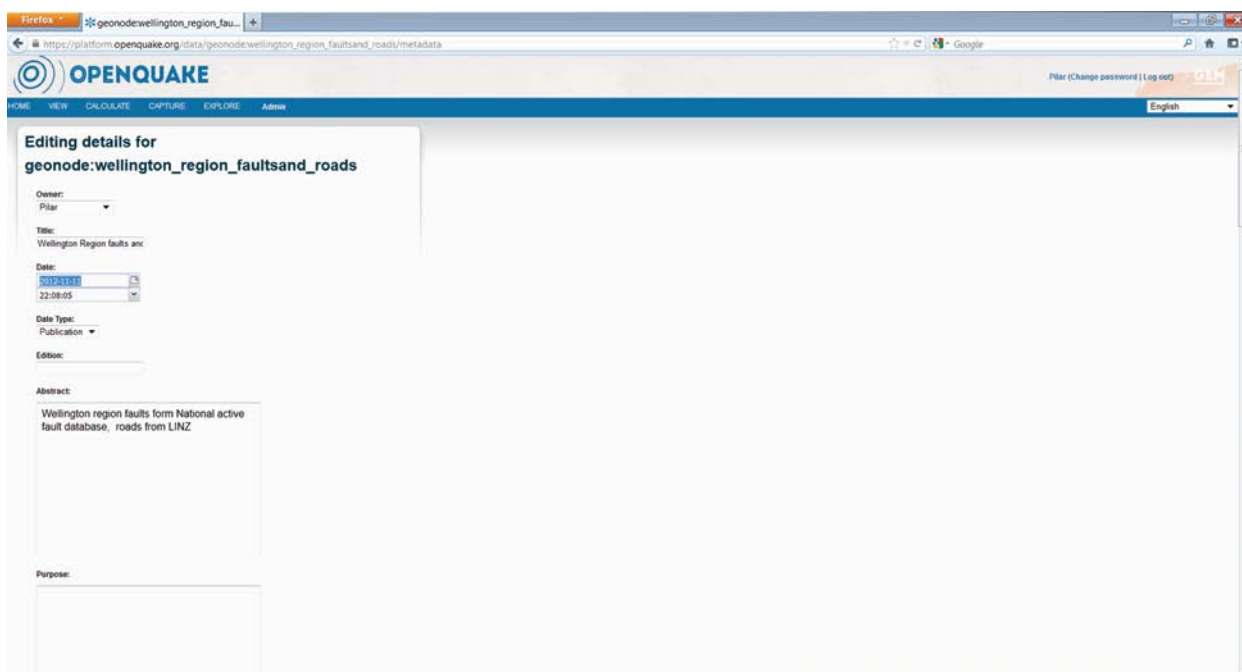


Figure 8.6 Add Metadata to a new base map layer.

To display an uploaded map (Figure 8.7):

- Return to the tool by choosing the “capture” drop-down menu and selecting “Active faults”
- Expand the “Layers” form
- Select the green “+” icon located at the upper left corner of the screen below the word “Layers” and add your layer

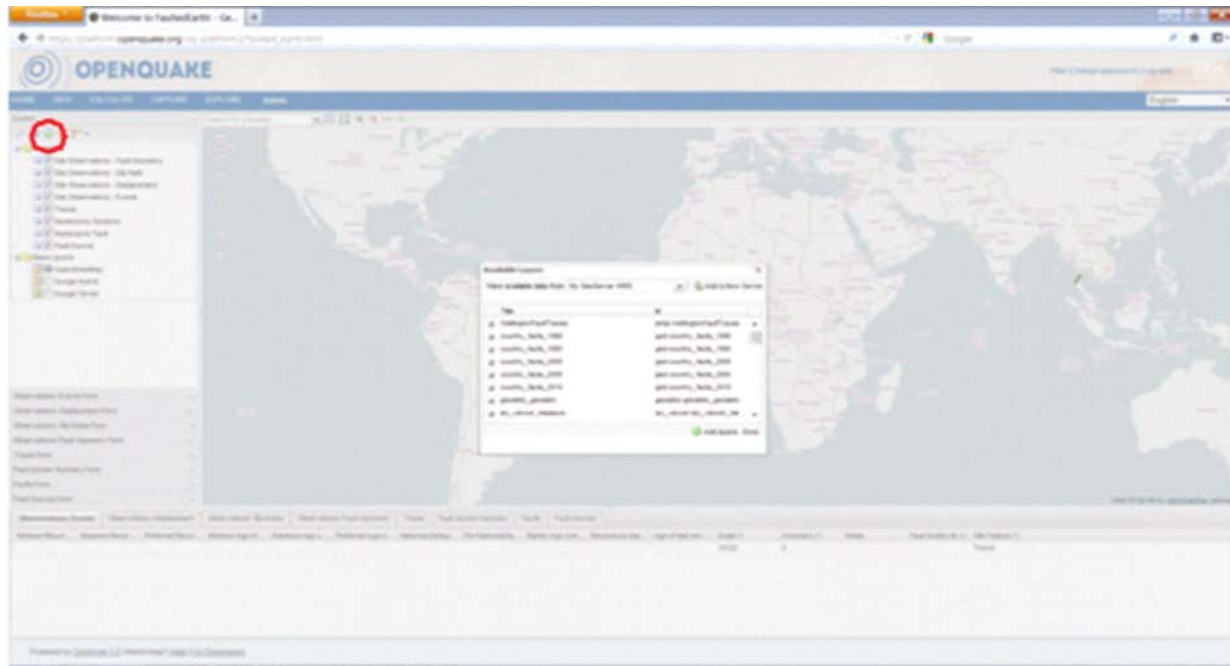


Figure 8.7 Display an uploaded base map layer in the map window.

8.2 Guidelines for entering new data

The following instructions are laid out in what are considered to be typical workflows of someone (likely to be a geologist) entering new neotectonic fault data and creating new fault sources. The compulsory steps (Traces – Sections – Faults – Fault Sources) are outlined first, followed by the optional step of compiling site observations.

8.2.1 Step 1 – Traces

This step involves either drawing or uploading (importing) traces and describing for each the scale and geomorphological features (spatial data attributes) which are being mapped. Editing and deleting traces is also described and traces can be exported as a zipped shapefile.

To draw a trace (Figure 8.8):

- Expand the *Traces* form in the concertina
- Select the “draw” button and draw a new trace on the map. Double click to finish.
- Enter compulsory attributes in the pop-up window that appears in the map. The scale and accuracy attributes are automatically populated from the current map scale once the user selects these attributes.

- Optional attributes (Notes, Location Method) can be entered by selecting the “more fields” button at the base of the pop-up window.
- Select the “save” button at the base of the pop-up window

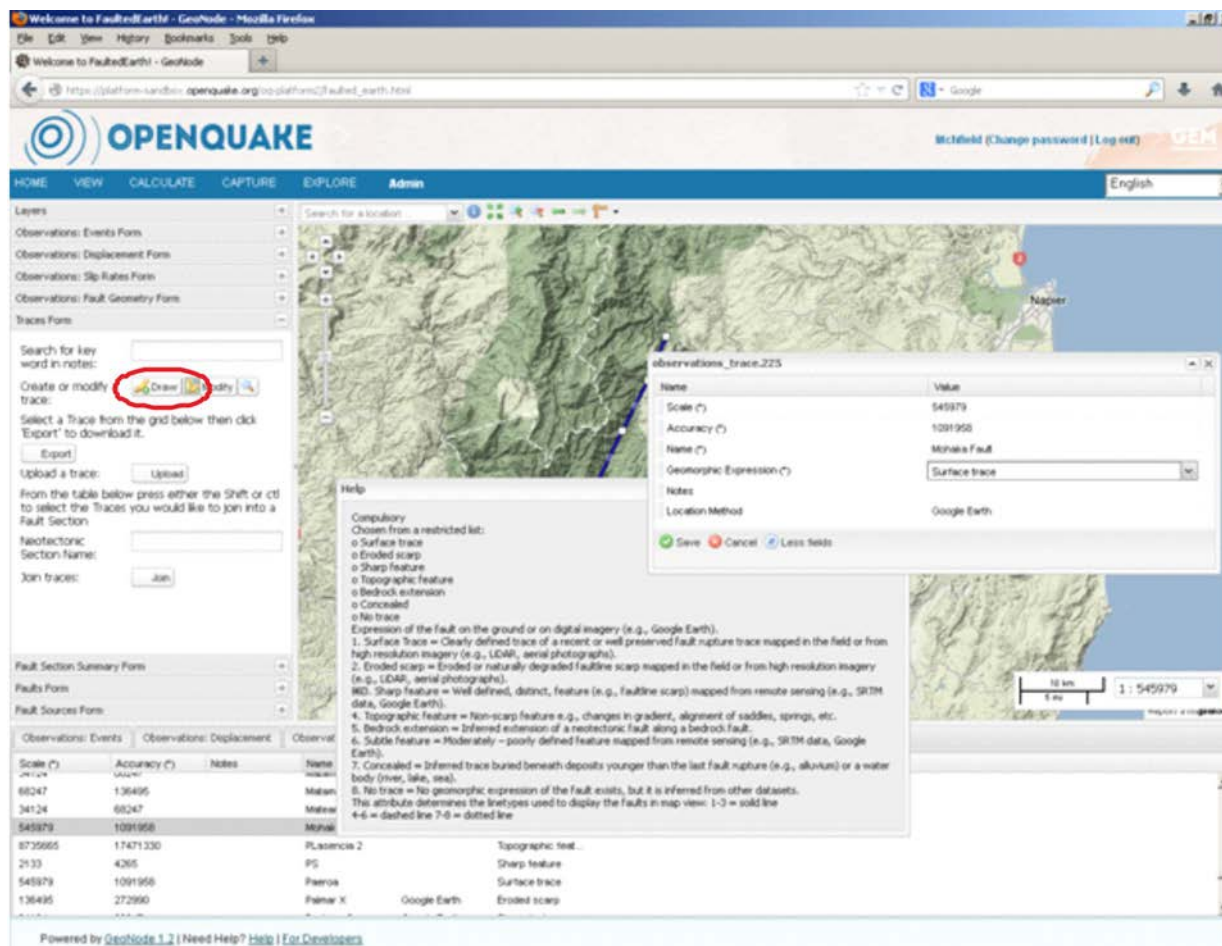


Figure 8.8 Draw a trace.

Traces can be uploaded individually, or as multiple traces which comprise one section. To upload traces (Figure 8.9):

- Expand the *Traces* form in the concertina
- Select the “upload” button in the concertina
- Browse to locate a zipped shapefile in the correct format
- Select “upload”

At the time of writing (May 2013) the upload function is not working correctly and a shapefile template cannot be downloaded.

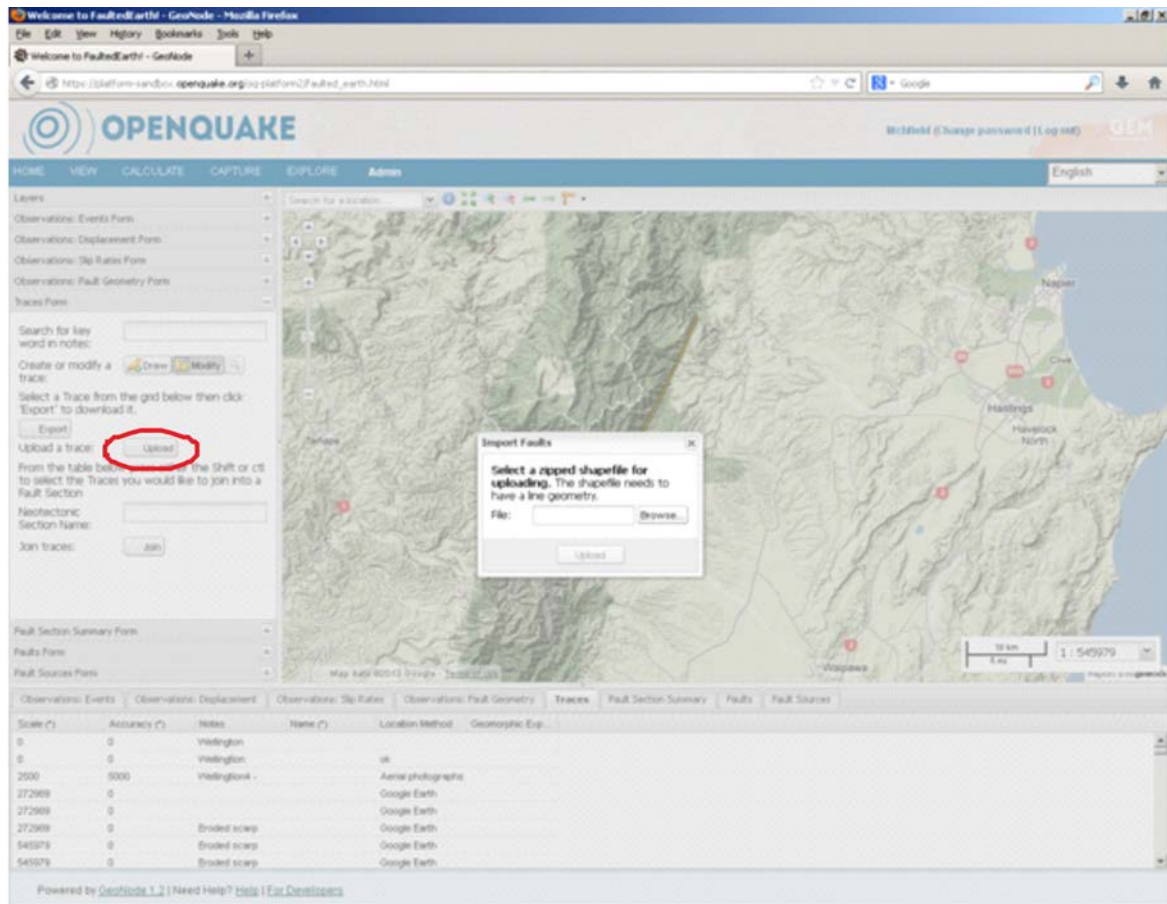


Figure 8.9 Upload traces.

To edit or delete traces (Figure 8.10):

- Expand the *Traces* form in the concertina
- Click on the “modify” button
- Select the trace from the map (not working correctly in tool v1.12.11) or “Traces” table in the grid. A trace can also be selected using the “Search for key word in notes” function in the *Traces* form
- Click on the “edit” or “delete” buttons on the base of the pop-up window
- Modify attributes, move or delete trace vertices on the map
- Save

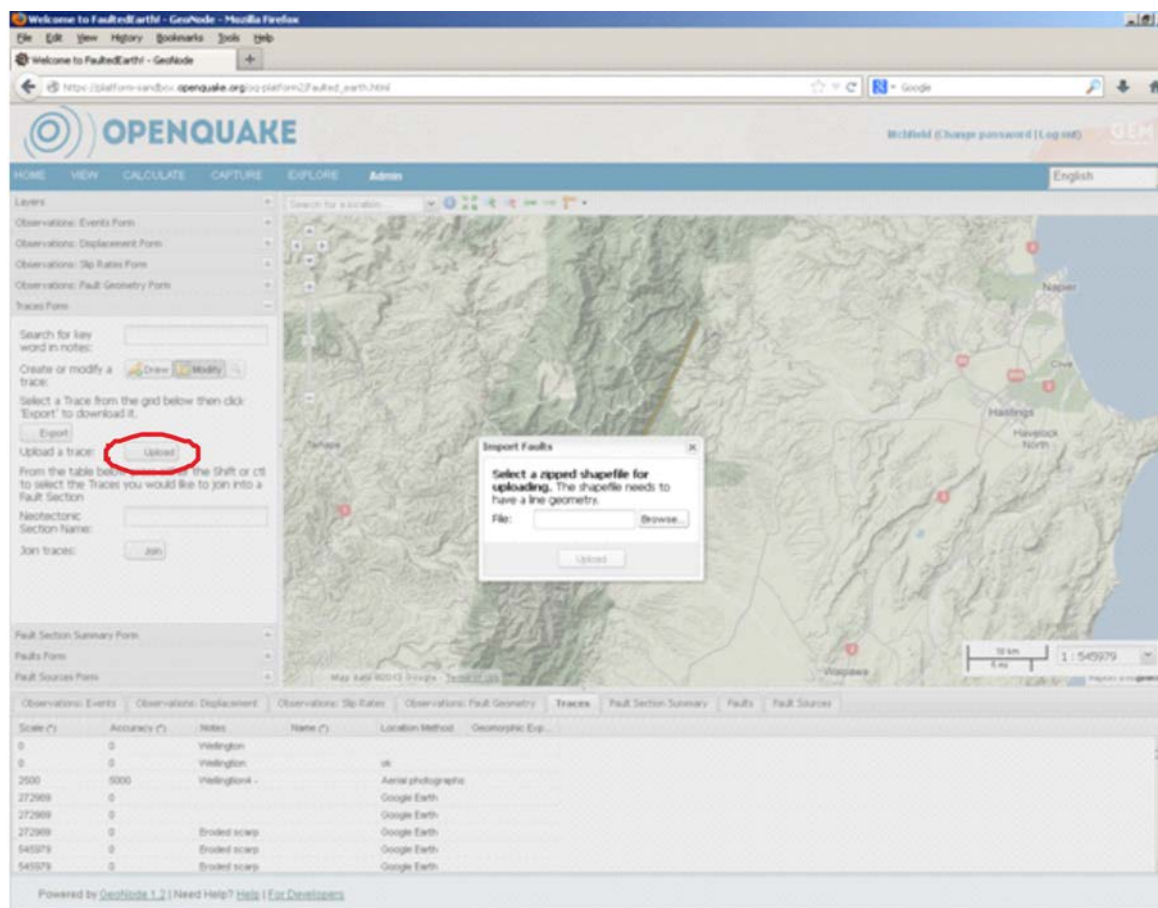


Figure 8.10 Edit or delete traces

8.2.2 Step 2 – Sections

Traces need to be combined into a neotectonic section before section summary attributes can be compiled. Even if a section only consists of one trace, the trace needs to be “joined” to create a section. Site observations (optional step section 7.2.6) can also be entered before creating a section, but if they are to be associated with a section then the section needs to be defined first. Sections can be edited, deleted, or exported.

To join traces to form a section (Figure 8.11):

- Expand the *Traces* form in the concertina
- Select 1 or more traces from the map (not working correctly in tool v1.12.11) or the “Traces” table in the grid
- Enter a neotectonic section name
- Click the “join” button (A “Fault Section created” information window should appear)

The screenshot shows the Openquake GeoNode web interface. The main map displays a topographic view of the Mohaka Fault area in New Zealand, with a blue line representing a trace. A pop-up window titled "observations_trace.225" is open, showing the following attributes:

Name	Value
Scale (*)	545979
Accuracy (*)	1091958
Name (*)	Mohaka Fault
Geomorphic Expression (*)	Surface trace

Below the map, there is a table of fault section data:

Scale (*)	Accuracy (*)	Notes	Name (*)	Location Method	Geomorphic Exp...
136495	272990		Matama Este 3		Sharp feature
68247	136495		Matama central 1		Sharp feature
34124	68247		Matama central 2		Sharp feature
34124	68247		Matama central 3		Concealed
68247	136495		Matama central 4		Bedrock extension
34124	68247		Matara noroeste	Google Earth	Surface trace
545979	1091958		Mohaka Fault	Google Earth	Surface trace

Figure 8.11 Join traces to form a section

To edit fault section attributes (Figure 8.12):

- Expand the *Fault Section Summary* form in the concertina
- Click on the “modify” button
- Select a section from the map (not working correctly in tool v1.12.11) or the Fault Section Summary table in the grid, for which a pop-up window will appear on the map (note to move this form around the screen the pin button on the top right needs to first be selected)
- Click on the “edit” button on the bottom left corner of the pop-up window
- Enter compulsory attributes in the summary table.
- Optional attributes can be entered by clicking on the “more fields” button at the base of the pop-up window.
- Save

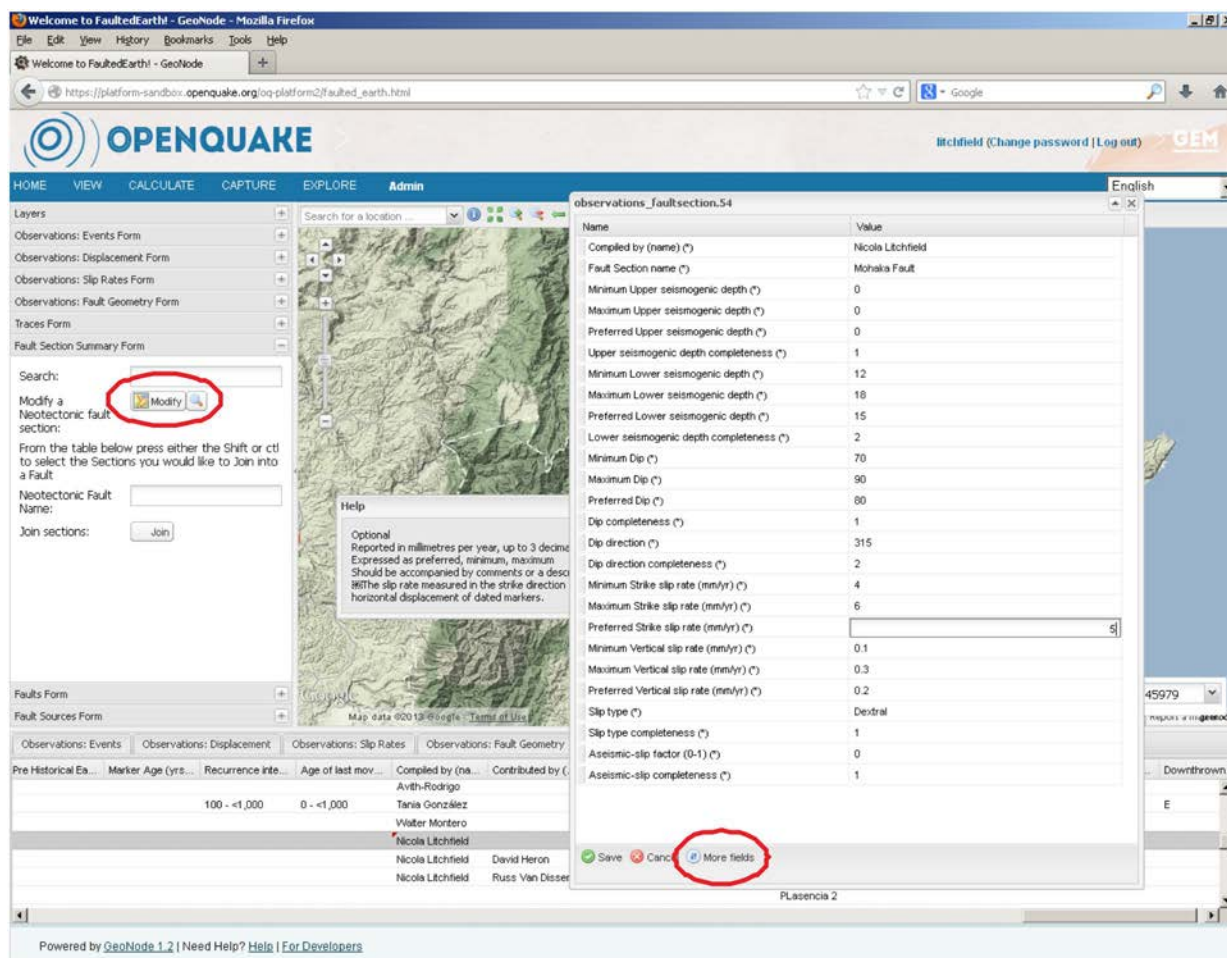


Figure 8.12 Edit section attributes.

8.2.3 Step 3 – Faults

Sections need to be combined together to form a fault. Even if a fault only consists of one section, the section needs to be “joined” to create a fault. Faults can be edited, deleted, or exported.

To join sections to form a fault (Figure 8.13):

- Expand the *Fault section summary* form in the concertina
- Select sections from the map (not working correctly in tool v1.12.11) or the Fault Section Summary grid
- Enter a fault name
- Click on the “join” button (A “Fault created” information window should appear)

The screenshot shows the Openquake GeoNode web application. The main interface includes a navigation menu (HOME, VIEW, CALCULATE, CAPTURE, EXPLORE, Admin), a search bar, and a map of New Zealand. A pop-up window titled 'observations_faultsection.54' is open over the map, displaying a table of seismicogenic depth parameters. In the left-hand 'Layers' panel, the 'Neotectonic Fault' form is active, showing a search for 'Mohaka Fault' and a 'Join sections' button circled in red.

Name	Value
Minimum Upper seismicogenic depth (°)	0.0
Maximum Upper seismicogenic depth (°)	0.0
Preferred Upper seismicogenic depth (°)	0.0
Upper seismicogenic depth completeness (°)	1.0
Minimum Lower seismicogenic depth (°)	12.0
Maximum Lower seismicogenic depth (°)	18.0

Earthquake	Pre Historical Earthquake	Marker Age (yrs)	Recurrence interval	Age of last movement	Compiled by (name)	Contributed by (name)	Created at (date)	Overall completeness	Fault Section name	Strike	Surface Dip	Episodic Behaviour	Do
			100 - <1,000	0 - <1,000	Avith-Rodrigo				Lajas				
					Tania González				Lirón Fault	20			
					Walter Montero				Matana Este				
					Nicola Litchfield				Mohaka Fault				
					Nicola Litchfield	David Heron	2012-04-11Z		Ohariu North				
					Nicola Litchfield	Russ Van Dissen	2012-04-10Z		Ohariu South				

Figure 8.13 Join sections to form a fault.

To enter fault attributes (Figure 8.14):

- Expand the *Faults* form in the concertina
- Click on the “modify” button
- Select a fault from the map (not working correctly in tool v1.12.11) or the Faults table in the grid
- Click on the “edit” button at the bottom left of the pop-up window on the map
- Enter compulsory attributes in the summary table.
- Optional attributes can be entered by clicking on the “more fields” button at the base of the pop-up window.
- Save

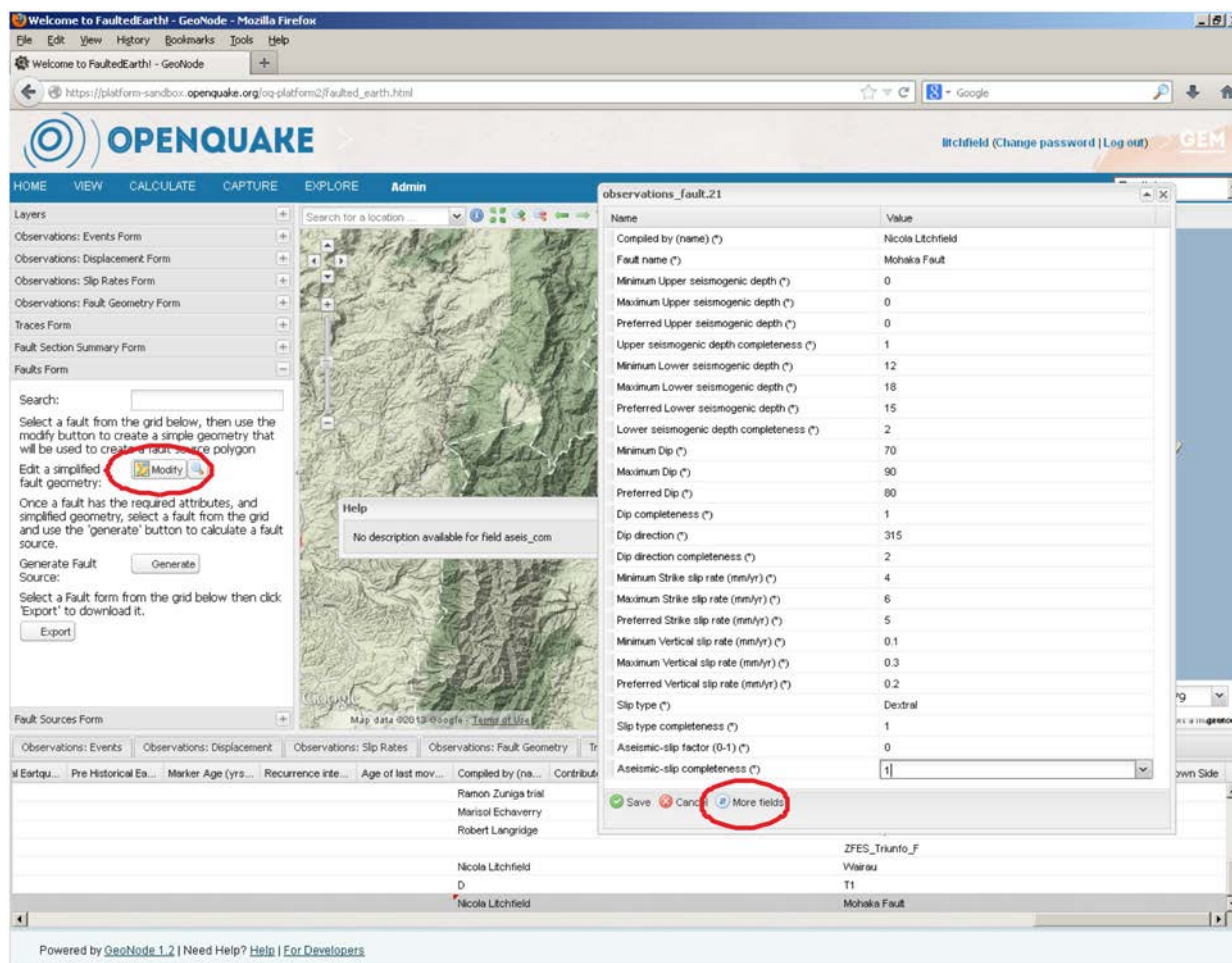


Figure 8.14 Enter fault attributes

8.2.4 Step 4 – Fault sources

A fault source is created (generated) from a fault. The fault source comprises a 2D polygon (a 3D polygon projected to the ground surface) with automatically populated or calculated attributes (calculations for magnitude and recurrence interval are described in the Data Dictionary; Litchfield et al., 2013). Fault source attributes cannot be edited (see section 8.2.5).

To generate a fault source (Figure 8.15):

- Expand the *Faults* form in the concertina
- Select a fault from the Faults table in the grid
- Click on the “generate” button (A “Fault source generated” information window should appear)
- To view the fault source polygon select the fault source from the Fault Sources table in the grid

h Age o...	Preferred Age o...	Historical Earthq...	Pre Historical Ea...	Marker Age (yrs...	Recurrence inte...	Age of last mov...	Compiled by (na...	Contributed by (...	Created at (date)	Overall complet...	fault_id	Fault name (*)
							Nicola Litchfield	Russ Van Dissen		31	3	Ohariu Fault
							PV				10	Placencia
							Marisol Echaverry				13	Pruebas1
							Robert Langridge				16	Acambay-Toma...
							D				18	T1
							Nicola Litchfield				19	Wairau
							Nicola Litchfield				21	Mohaka Fault

Figure 8.15 Generate a fault source

8.2.5 Step 5 – Review fault sources

The fault source attributes should now be reviewed. The fault source polygon can be edited by editing individual vertices in the map window (by clicking “modify” and then “edit”), but note that if the length is manually changed then the calculated length, area, and magnitude attributes will become incompatible. The attributes cannot be edited, but if they are incompatible with independent data (e.g., recurrence interval from field data), then some of the earlier entered information (e.g., traces, fault attributes) should be edited, or different sections could be combined. Fault sources can be exported.

8.2.6 Optional step – Site observations

Observations collected at a particular site (e.g., a trench, site where a slip rate or single event displacement has been obtained) can be entered once a section has been created (step 2; section 7.2.2). The site location can either be drawn on the map or uploaded (the latter is not working correctly in tool v1.12.11). The attributes are grouped into four forms: *Observations: Events*, *Observations: Displacement*, *Observations: Slip Rates*, *Observations: Fault Geometry* which correspond to boxes 4 on Figure 3.1. Site observations can be edited or deleted.

To draw a site (Figure 8.16):

- Expand the appropriate *Observations* form in the concertina
- Select the “draw” button and draw a site (point) on the map. A window will pop-up on the map.
- Enter attributes (all are optional).
- Attributes can also be edited by selecting the “modify” button on the *Observations* form and then the “edit” button on the bottom left corner of the window which pops up (Figure 8.17)
- To tie the site to a section, select the section name (Fault Section ID) from a drop-down menu. Note optional attributes can be entered by clicking on the “more fields” button at the base of the pop-up window.

The screenshot shows the OpenQuake web application interface. On the left sidebar, the 'Draw' button is highlighted with a red circle. A pop-up window titled 'observations_event.9' is open over a map, displaying a table of attributes and values. The table is as follows:

Name	Value
Scale (°)	545979
Accuracy (°)	1091958
Fault Section ID (°)	54
Site Feature (°)	
Minimum Recurrence Interval (yr)	
Maximum Recurrence Interval (yr)	
<input type="checkbox"/> Save <input type="checkbox"/> Cancel <input type="checkbox"/> Less fields	

At the bottom of the interface, there is a table with columns: Age of ..., Maximum Age o..., Preferred Age o..., Historical Earthqu..., Pre Historical Ea..., Marker Age (yrs.), Recurrence inte..., Age of last mov..., Scale (°), Accuracy (°), Notes, Fault Section ID (°), and Site Feature (°). The table contains several rows of data, including one row with a '54' in the 'Fault Section ID' column.

Figure 8.16 Draw a site and enter site observations

To upload a site (Figure 8.17):

- Expand the appropriate *Observations* form in the concertina
- Click on the “import” button and upload a GIS shapefile (not working correctly in tool v1.12.11)
- To review or edit attributes, select on the “modify” button on the *Observations* form
- Select the “edit” button on the bottom left corner of the window which pops up

- To tie the site to a section, select the section name (Fault Section ID) from a drop-down menu. Note optional attributes can be entered by clicking on the “more fields” button at the base of the pop-up window.

The screenshot displays the OpenQuake web application interface. The top navigation bar includes 'HOME', 'VIEW', 'CALCULATE', 'CAPTURE', 'EXPLORE', and 'Admin'. The left sidebar contains several observation forms, with 'Observations: Events Form' selected. The 'Create or modify a site observation' button and the 'Upload' button are circled in red. The main map area shows a topographic view of a region with a blue marker. A pop-up window titled 'observations_event.9' is open, showing a table of attributes and their values. The 'Edit' button at the bottom of this pop-up is also circled in red. Below the map is a table with columns for various observation parameters.

Minimum Recur...	Maximum Recur...	Preferred Recur...	Minimum Age of ...	Maximum Age o ...	Preferred Age o ...	Historical Earthq...	Pre Historical Ea...	Marker Age (yrs...	Recurrence inte...	Age of last mov...	Scale (°)	Accuracy (°)
						1912			2,000 - +5,000	0 - <1,000	68247	136495
3000	5000	3600	38		38	1912	4700		2,000 - +5,000	0 - <1,000	68247	136495
	5000	3500	3000			2011	3456		2,000 - +5,000	0 - <1,000	136495	272990
											68247	136495
											545979	1091958

Figure 8.17 Upload a site and edit site observations

9 Bulk upload of national and global databases

This section is a reproduction of the report on bulk upload of existing databases (Litchfield and Thomas, 2013) with minor adjustment to the section numbering, and including the appendices as sub-sections. No further bulk uploads have been undertaken since May 2013.

9.1 Introduction

This report summarises the bulk upload of national and global active fault and fault source databases into the GEM Faulted Earth global active fault, fold, and fault source database, as at 31 May 2013 (version 3.0.0; Figure 9.1). It does not include upload of global subduction thrusts (Section 10) or the Himalaya Frontal Thrust (Section 11), which have been compiled in a slightly different format to the GFE database and are being supplied to GEM independently.

The upload process generally involved some manual reformatting of each database to match the GFE database schema (Thomas et al., 2012), with the actual upload being undertaken using an XML interchange (Thomas, 2012). This report focuses on the manual reformatting, since the latter is supplied in logs accompanying supply of the databases to GEM.

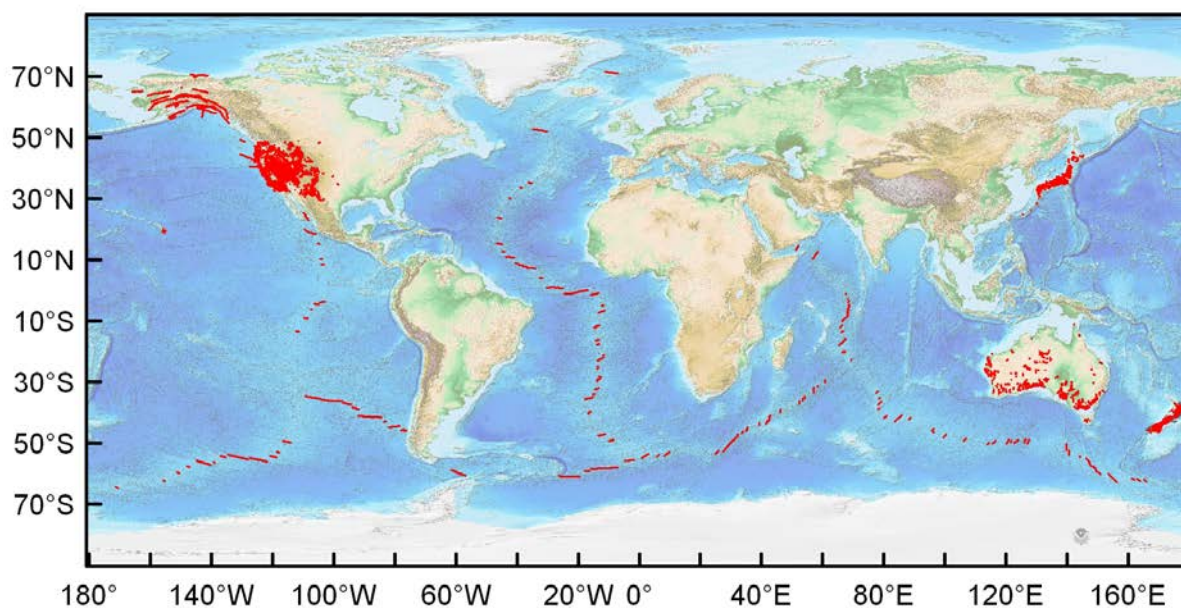


Figure 9.1 Active fault and fold traces, and fault source polygons (red) uploaded to the GFE database as at 31 May 2013

This report describes for each database uploaded to date: (1) the data (and format) obtained or supplied; (2) the data that was uploaded (or omitted); (3) mapping of attributes from the supplied database to the GFE database; (4) reformatting required; and (5) any additional data uploaded. Most of the details for (2) to (5) are contained in Sections 9.9 * 9.15. GFE attributes are defined by Litchfield et al. (2013a) but note some of the attribute names differ slightly between that and this report, as some of the names were modified during development of the fault compilation tool.

The order of the report is in the order the databases were uploaded. The uploading process generally required some minor changes to the GFE database, which were logged and supplied to GEM independently (R. Thomas email communication, May 2013).

9.2 New Zealand active faults database

The New Zealand active faults database [6] is a GIS database and was uploaded in March 2012.

12,580 fault traces (there are no folds in the database) were uploaded (Figure 9.2). These are grouped into 377 sections and 344 faults, but the remaining traces (3040) were also uploaded as sections, as in the original New Zealand database.

Not surprisingly, given the GFE database was primarily designed by the authors, most of the attributes mapped exactly from the New Zealand active faults database to the GFE database (Section 9.9).

Several attributes were not uploaded (e.g., net trend, earthquake depth), as they had been considered to be unnecessary detailed for inclusion in the GFE database, or are included in other GEM databases (e.g., Global Earthquake History). Most of the attributes not uploaded do not have data in the New Zealand database. Conversely, some extra attributes were added to the GFE database (e.g., aseismic-slip factor, upper seismogenic depth), which are not explicitly stored in the New Zealand active faults database.

Note a new, quality-checked and homogeneous scale (1:250,000) scale version of the database is currently in preparation and GNS Science would like to replace the version of the New Zealand active faults database loaded with this new version when it becomes available.

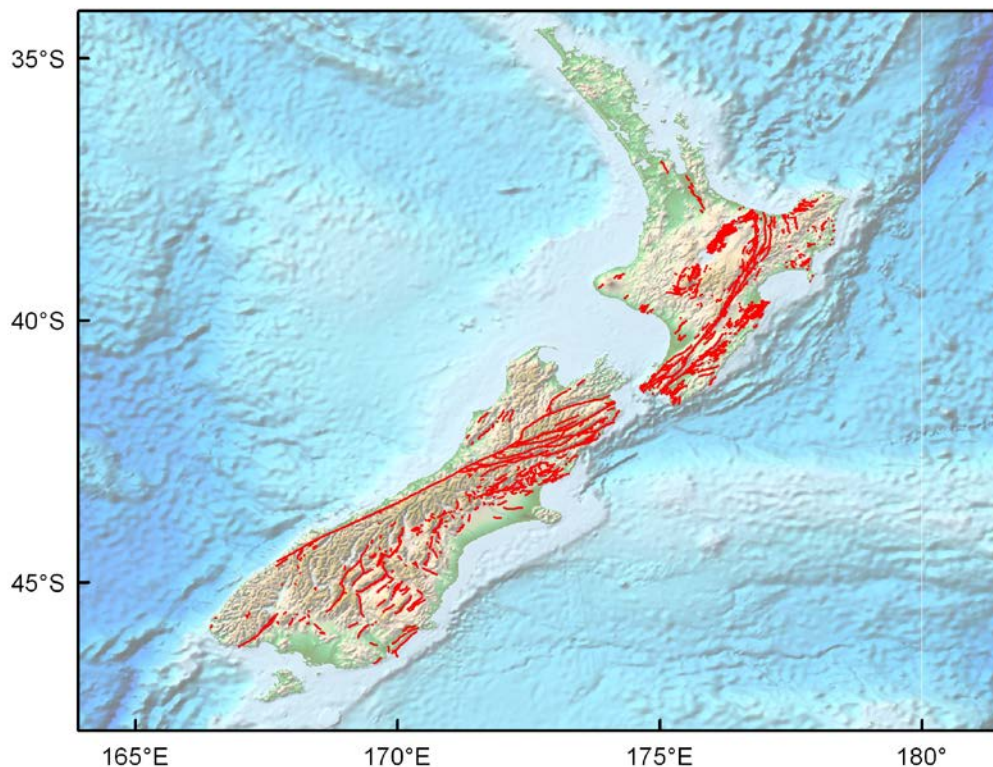


Figure 9.2 New Zealand active fault traces (red) uploaded to the GFE database

9.3 New Zealand National Seismic Hazard Model

The version of the New Zealand Seismic Hazard Model uploaded is the 2010 model published by Stirling et al. (2012). It was supplied in August 2011 as an excel spreadsheet (attributes) and shapefile of surface traces. The surface traces were then converted to polygons using code supplied by Roberto Basili and now included in the GFE fault compilation tool.

The model contained 537 sources (Figure 9.3), not including subduction zones, which were removed since subduction zones are being supplied to GEM independently.

As for the New Zealand active faults database, most attributes mapped exactly to GFE database attributes (Section 9.10).

Some attributes were not uploaded because there were problems with the original data (e.g., minimum and maximum Magnitude and Recurrence Interval have not been quality checked and are sometimes inconsistent with the preferred values), or they are not included as attributes in the GFE database (seismic moment, single event displacement). In this case, the values are calculated as part of another calculation (magnitude, recurrence interval), so don't need to be stored separately. Compiler and Contributor attributes were added.

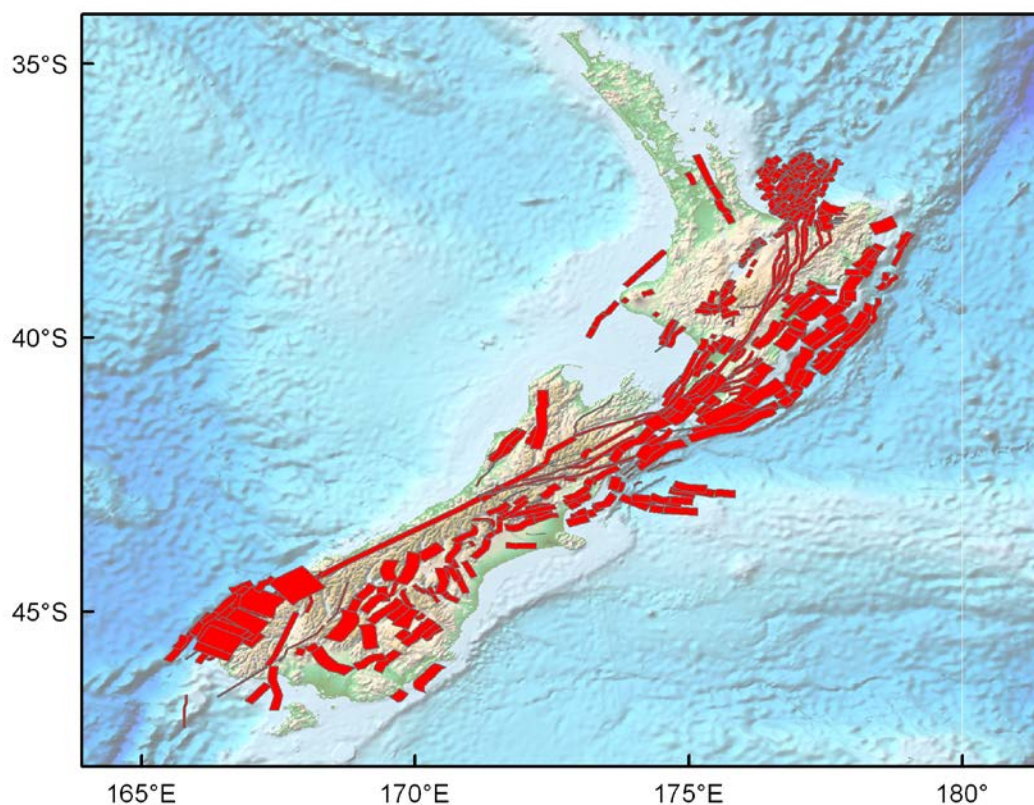


Figure 9.3 New Zealand fault source polygons (red) uploaded to the GFE database

9.4 Active fault database of Japan

The Active fault database of Japan [4] was supplied in December 2011 by email from Yoshioka Toshikazu, AIST (Geological Survey of Japan) to Kelvin Berryman. The database was supplied as an excel spreadsheet (attributes) and a Google Earth kmz file of fault polygons. The spreadsheet only contained key attributes; more attributes can be viewed on the database website [4].

The supplied database contained 559 fault sections, which were each mapped as a single polygon. All were uploaded and polygons were converted to surface traces (Figure 9.4). The sections were combined into 314 faults, as denoted by fault name. However, few attributes could be assigned to faults without significant input from the database owners. For example, slip rate was supplied for each section, but not for the whole fault, and so combining these would need input as to the appropriate combination method (e.g., averaging or assuming the highest slip rate).

Most of the mapping of the Japan database attributes to the GFE attributes was relatively straight forward (Section 9.11), with useful information on attribute definitions and formats obtained from the Japan database website [2]. Some format conversions were necessary (e.g., upthrown side to downthrown side, dip direction from a quadrant to a bearing).

Some attributes were not uploaded because there were no equivalents in the GFE database. Many of these were alternative values (e.g., of slip rate, recurrence interval), and because a preferred value was supplied, this is what was uploaded. No attributes were added.

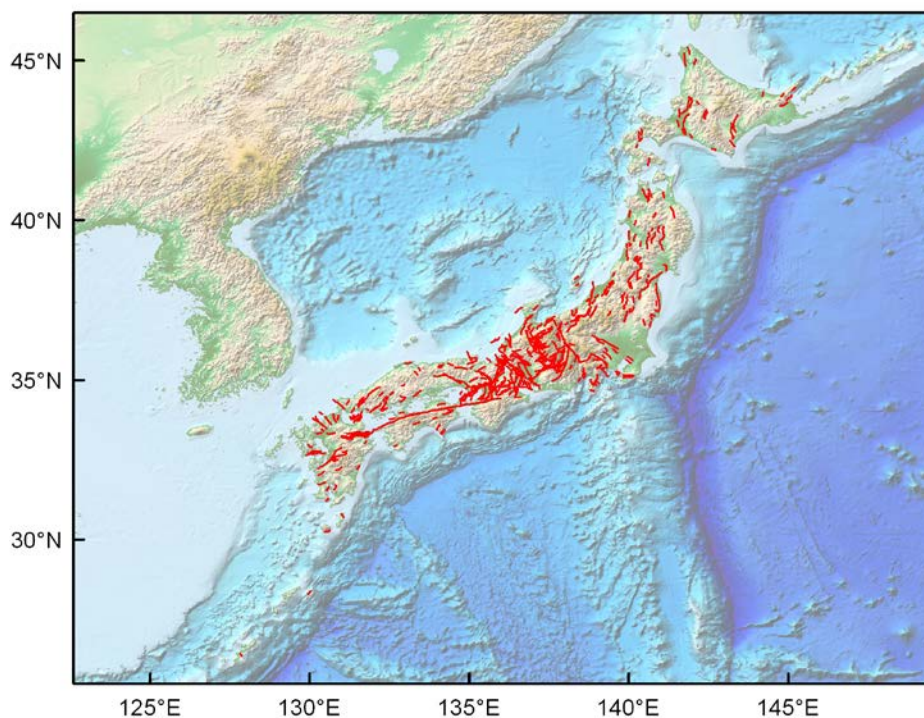


Figure 9.4 Active fault database of Japan traces uploaded to the GFE database

9.5 Alaska Quaternary faults and folds database

The Alaska Quaternary faults and folds database (Koehler et al., 2012) was downloaded from the database website [3] in August 2012. The data was in the format of a shapefile containing 1527 traces, with attributes for each trace. One fault cuts across the Canadian border.

The database contained subduction thrusts and seismic zones, which were not uploaded, since these are being supplied to GEM independently. The database also contained both faults and folds, and these were separated out using the name and Id number (NUM).

The remaining 1516 traces (Figure 9.4) were combined into 118 fault sections and 33 fold sections as defined by section names (given in brackets). The sections were then combined into 94 faults and 30 blind faults. Synclines were included as folds, but not as blind faults. Where individual traces of a section, or sections of a

fault, had different attributes, these were combined by: (1) assigning the most common value (dip, dip direction, slip type); (2) assigning the youngest value (age of last movement); or (3) the highest value (slip rate).

Most of the Alaska database attributes mapped reasonably readily to the GFE attributes, with some assistance from Richard Koehler (e.g., geomorphic expression) (Section 9.12). The exceptions were codes, which were not uploaded as codes are simply numbers derived from other attributes, and thus are duplicates. For example, the ACode is a number derived from Age, where 1 is <150, 2 is <15,000 etc. In this case Age, but not ACode was uploaded. Some format conversion was required (e.g., categories to values, spelling out abbreviations). Some attributes were added in consultation with Richard Koehler (e.g., upper seismogenic depth, aseismic-slip factor).

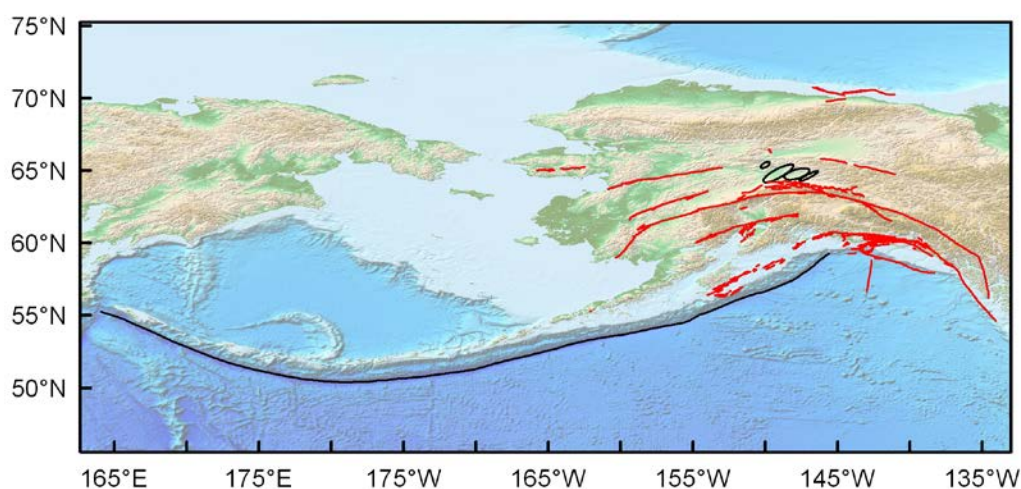


Figure 9.5 Alaska fault and fold traces (red) uploaded to the GFE database. Traces not uploaded are shown in black

9.6 USA Quaternary fault and fold database

The USA Quaternary faults and folds database (Machette et al., 2005) was downloaded from the database website [4] in February 2013. The website states that the data was last updated 3 November 2010. The format was the same as the Alaska database – a shapefile containing 10,021 traces, with attributes for each trace. Many traces were grouped together as multi-part features however, and so had to be ungrouped. The database covers the mainland USA (not including Alaska) and Hawaii (Figure 9.6). The data available for download on the website is not the entire contents of the USA database – there are additional information, particularly descriptions, available on the website.

The database contained the Cascadia subduction thrust, which was not uploaded (Figure 9.6), since subduction thrusts are being supplied to GEM independently. Fault areas were also not uploaded (Figure 9.6) as they were not included in the GFE database design and are considered to be included in other GEM databases (e.g., Global Instrumental Earthquake Catalogue). The database contained both faults and folds, and these were separated out using the name and Id number (NUM).

The remaining 10,005 traces (83,591 when ungrouped) were combined into 3188 fault sections and 35 folds using the ID number (NUM – letters denote sections). Where individual sections of a fault had different attributes, these were combined by either: (1) assigning the most common value (dip, dip direction, slip type); (2) assigning the youngest value (age of last movement); or (3) the highest value (slip rate). If was not possible to use these assumptions (e.g., there were commonly conflicting dip directions), then the attributes

were not uploaded. Combined attributes were also checked against the values reported on the database website.

The attribute mapping (Section 9.13) was essentially the same as for the Alaska database. However, in this case no single compiler could be added (i.e., the data were compiled by many un-named people), and so “USA compiler” was uploaded as a nominated person instead.

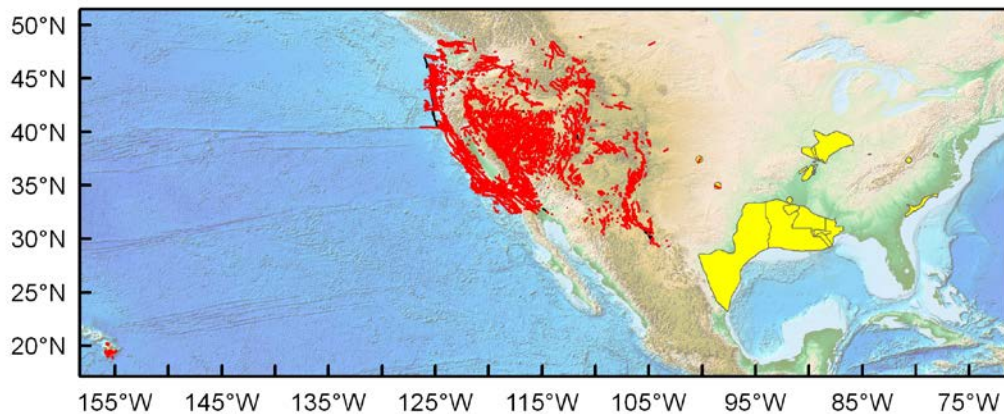


Figure 9.6 USA active fault and fold traces uploaded to the GFE database (red).

Traces not uploaded are shown in black, and fault areas not uploaded in yellow.

9.7 Australia neotectonic feature database

The Australia neotectonic feature database [5] was supplied in April 2013 by email from Andrew McPherson, Geoscience Australia, to Nicola Litchfield. The database consisted of an excel spreadsheet (attributes of each fault) and a shapefile of 1381 traces. The database is notable for having the greatest number of populated attributes of all those uploaded, including significant descriptions of many attributes. These included many more faults and attributes than are available on the website.

Two neotectonic features (Michelago sediment deformation and Narongo Fault) were removed from the database because, after consultation with Dan Clark (Geoscience Australia), they had a confidence level of none, meaning there is no evidence of activity.

1336 traces were uploaded (Figure 9.7). These were combined into 294 sections and 44 folds. No sections were identified in the original data, so sections were duplicated as faults.

Mapping of attributes was relatively straight forward (Section 9.14), although as noted above, the Australia database contains many descriptions, most of which had to be combined into notes or synopses. Some format conversion was needed, much of which was done in consultation with Dan Clark (e.g., converting geological periods into years before present, converting slip rate categories into minimum and maximum values). Aseismic slip factor and upper seismogenic depth were added in consultation with Dan Clark.

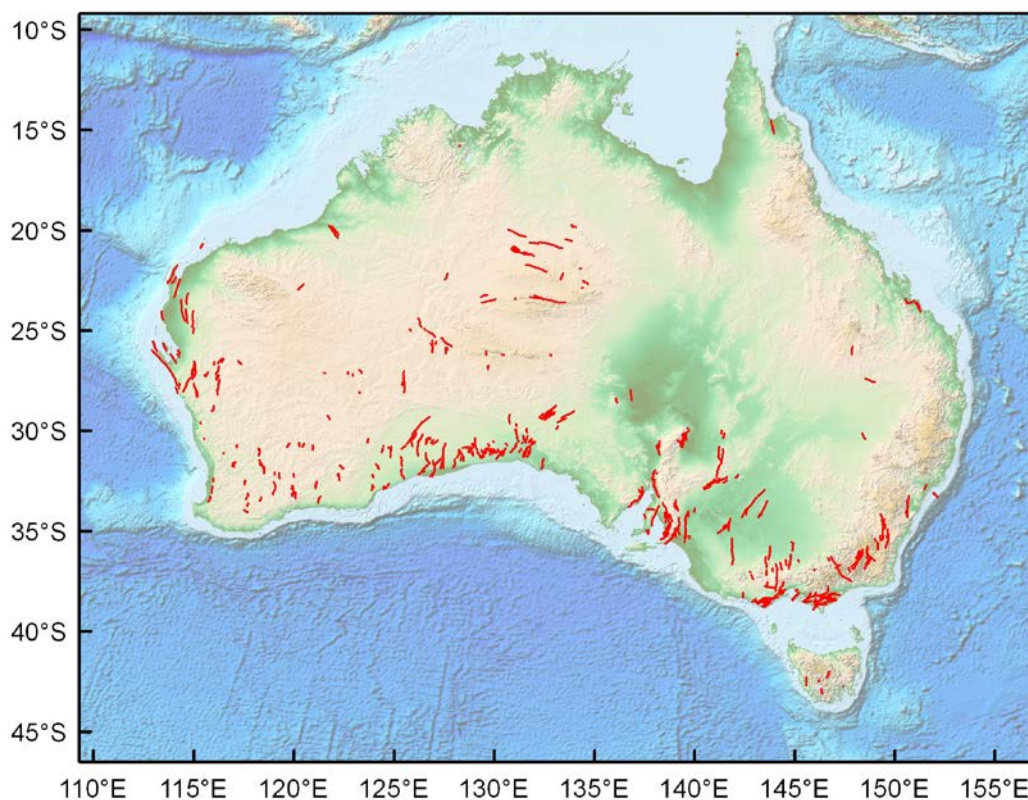


Figure 9.7 Australia active fault traces (red) uploaded to the GFE database

9.8 Mid-ocean ridge transform database

The global mid-ocean ridge transform database was supplied in April 2013 by email from Monica Wolfson-Schwehr, University of New Hampshire, to Nicola Litchfield. The database is an unpublished, updated version of that of Boettcher and Jordan (2004). The data format was an excel spreadsheet (attributes) and a shapefile of traces.

This database is considered to primarily be a fault source database, but some of the data was supplied as sections, so the data was uploaded as sections, faults, and fault sources. Sections were defined in the original database by highlighting and are defined as: if they are separated by an intra-transform offset that is shorter than either of the two adjacent fault segments and shorter than a maximum length of 50 km (Readme notes accompanying the database). 201 traces (Figure 9.8) were combined into 147 faults and 147 fault sources.

Attribute mapping was relatively straight forward (Section 9.15), with some reformatting required (e.g., spelling out tectonic regions). Several attributes were not uploaded because they were either not required (e.g., latitude, longitude) or are part of calculations (e.g., seismic moment). Several attributes were added from the notes supplied with the database (e.g., slip rate and recurrence interval description), or in consultation with Monica Wolfson-Schwehr (e.g., dip, magnitude description).

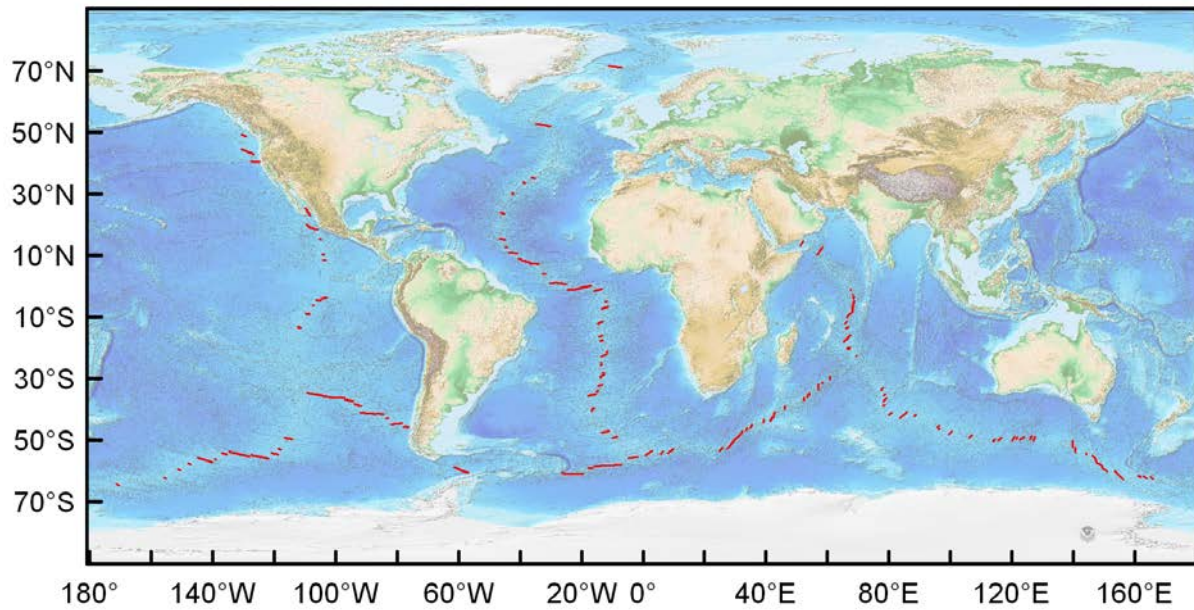


Figure 9.8 Mid-ocean ridge transform traces and sources (red) uploaded to the GFE database. Traces and sources appear identical because all are vertical.

9.9 New Zealand active faults database (afdb) – attribute mapping, formatting and upload

New Zealand afdb attribute	GFE database table	GFE database attribute	Comments
Feature ID	Section, Fault	Original ID	
Feature name	Trace, Section, Fault	Name	
Dominant sense	Section, Fault	Slip type	
Subordinate sense	Section, Fault	Slip type	Combined with dominant sense as a single attribute
Down Quadrant	Section, Fault	Downthrown side	
Dip	Section, Fault	Dip – pref, min, max	
Dip direction	Section, Fault	Dip direction	
Net trend			Not uploaded because no equivalent GFE attribute.
Net plunge			Not uploaded because no equivalent GFE attribute.
Strike displacement			Not uploaded because no equivalent GFE attribute.
Strike time			Not uploaded because no equivalent GFE attribute.
Strike slip rate	Section, Fault	Strike slip rate – pref, min, max	
Strike events			Not uploaded because no equivalent GFE attribute.
Strike single event displacement			
Vertical displacement			Not uploaded because no equivalent GFE attribute.
Vertical time			Not uploaded because no equivalent GFE attribute.
Vertical slip rate	Section, Fault	Vertical slip rate –	

New Zealand afdb attribute	GFE database table	GFE database attribute	Comments
		pref, min, max	
Vertical events			Not uploaded because no equivalent GFE attribute.
Vertical single event displacement			
Dip displacement			Not uploaded because no equivalent GFE attribute.
Dip time			Not uploaded because no equivalent GFE attribute.
Dip slip rate			
Dip events			Not uploaded because no equivalent GFE attribute.
Dip single event displacement			
Net displacement			
Net time			Not uploaded because no equivalent GFE attribute.
Net slip rate	Section, Fault	Net slip rate – pref, min, max	
Net events			
Net single event displacement	Section, Fault	Displacement – pref, min, max	
Recurrence interval	Section, Fault	Recurrence Interval – pref, min, max	
Last event	Section, Fault	Age of last movement – pref, min, max	
Bibliographic ID			
Method	Trace	Scale	
Method accuracy			Not uploaded because no equivalent GFE attribute.
Accuracy			Not uploaded because is incorporated into Geomorphic Expression.
Expression	Trace	Geomorphic expression	
Zone			Not uploaded because no equivalent GFE attribute.
Age			
Earthquake name			Not uploaded because no equivalent GFE attribute.
Earthquake date			Not uploaded because no equivalent GFE attribute.
Earthquake magnitude			Not uploaded because no equivalent GFE attribute.
Earthquake depth			Not uploaded because no equivalent GFE attribute.
Rupture type			Not uploaded because no equivalent GFE attribute.
Rupture length			Not uploaded because no equivalent GFE attribute.
Last event strike displacement			Not uploaded because no equivalent GFE attribute.
Last event dip displacement			Not uploaded because no equivalent GFE attribute.
Other information			

New Zealand afdb attribute	GFE database table	GFE database attribute	Comments
Date			
Source			
Owner			
-	Trace	Accuracy	
-	Section, Fault	Aseismic-slip factor	Added 0 for all sections/faults as there is no evidence of creep on any New Zealand active faults.
-	Section, Fault	Is active	Added t (true) for all sections/faults as all faults in the database are considered active.
-	Section, Fault	Is episodic	Added f (false) for all sections/faults as no faults in the database are considered episodic. This is not strictly true, as some Otago faults may be, but this data is incomplete and not compiled.
-	Section, Fault	Upper seismogenic depth – pref, min, max	Added 0 for all sections/faults as all faults in the database reach the ground surface.
-	Section, Fault	Created date	Added the date the upload was completed.
-	Section, Fault	Modified date	Added the date the upload was completed.
-	Section, Fault	Compiler	Added Nicola Litchfield as the compiler. Is not strictly true, but Nicola compiled most of the attributes when she was database administrator (2004-2008).

9.10 New Zealand National Seismic Hazard Model (NSHM) – attribute mapping, formatting and upload

New Zealand NSHM attribute	GFE database table	GFE database attribute	Comments
Fault	Source	Name	Expanded the abbreviated names
Sense	Source	Slip type	Spelled out: ss= dextral; nn=nv=normal; rv=reverse; sr=dextral-reverse; sn=dextral-normal; rs=reverse-dextral; ns=normal-dextral.
Sense index	Source		Not uploaded because no equivalent GFE attribute.
Length min	Source	Length – min	
Length pref	Source	Length – pref	
Length max	Source	Length – max	
Dip min	Source	Dip – min	
Dip pref	Source	Dip – pref	
Dip max	Source	Dip – max	
Dip direction	Source	Dip direction	
Depth min	Source	Lower seis depth – min	
Depth pref	Source	Lower seis depth – pref	
Depth max	Source	Lower seis depth – max	

New Zealand NSHM attribute	GFE database table	GFE database attribute	Comments
Top	Source	Upper seis depth – pref	
Slip rate min	Source	Net slip rate – min	
Slip rate pref	Source	Net slip rate – pref	
Slip rate max	Source	Net slip rate – max	
Width min	Source	Width – min	
Width pref	Source	Width – pref	
Width max	Source	Width – max	
Area min	Source	Area – min	
Area pref	Source	Area – pref	
Area max	Source	Area – max	
Magnitude min			Not uploaded because are some problems in the calculations in the original database.
Magnitude pref	Source	Maximum magnitude – pref	
Magnitude max			Not uploaded because are some problems in the calculations in the original database.
Moment min			Not uploaded because no equivalent GFE attribute (is part of a calculation).
Moment pref			Not uploaded because no equivalent GFE attribute (is part of a calculation).
Moment max			Not uploaded because no equivalent GFE attribute (is part of a calculation).
Single event displacement min			Not uploaded because no equivalent GFE attribute (is part of a calculation).
Single event displacement pref			Not uploaded because no equivalent GFE attribute (is part of a calculation).
Single event displacement max			Not uploaded because no equivalent GFE attribute (is part of a calculation).
Recurrence interval min			Not uploaded because are some problems in the calculations in the original database.
Recurrence interval pref	Source	Recurrence interval – pref	
Recurrence interval max			Not uploaded because are some problems in the calculations in the original database.
-	Source	Compiler	Added Nicola Litchfield as the compiler. Is not strictly true in that others were involved too, but Nicola was involved in compiling nearly all sources.
-	Source	Contributer	Added Mark Stirling as the contributor. Is not strictly true as there are many contributors to the 2010 model, but Mark undertook all calculations.

9.11 Active fault database (afdb) of Japan – attribute mapping, formatting and upload

Afdb Japan attribute	GFE database table	GFE database attribute	Comments
Fault no.	Fault	Original Id	
Fault name	Fault	Name	
Fault length	Fault	Length – pref	
Section name	Section	Name	
Section no.	Trace, Section	Original Id	
Section length	Section	Length – pref	
Seismic depth upper	Section	Upper seismogenic depth – pref	
Seismic depth lower	Section	Lower seismogenic depth – pref	
Strike N to E	Section	Strike	Converted to 0-360°
Dip degree	Section	Dip – preferred	
Dip direction	Section	Dip direction	Converted from a quadrant to a bearing in degrees: N = 0°, E = 90°, S = 180°, W = 270°. V (vertical) was left blank.
Slip type	Section	Slip type	Spelled out: N = normal, R = reverse, SL = sinistral, SR = dextral
Uprthrown side	Section	Downthrown side	Converted to opposite quadrant.
Slip rate vertical min	Section	Vertical slip rate – min	
Slip rate vertical max	Section	Vertical slip rate – max	
Slip rate horizontal min	Section	Strike slip rate – min	
Slip rate horizontal max	Section	Strike slip rate – maximum	
Slip rate net min	Section	Net slip rate – min	
Slip rate net max	Section	Net slip rate – max	
Slip rate net ave			Not uploaded in favour of Slip rate adopted.
Slip rate D/R			Not uploaded because no equivalent GFE attribute. Very few values supplied.
Slip rate geomorphic expression			Not uploaded because no equivalent GFE attribute available. Most values identical to Slip rate adopted values.
Slip rate adopted	Section	Net slip rate – pref	
Aseismic-slip factor	Section	Aseismic-slip factor	
Displacement min	Section	Displacement – min	
Displacement max	Section	Displacement – max	
Displacement ave			Not uploaded in favour of Displacement adopted.
Displacement surface rupture			Not uploaded because no equivalent GFE attribute. Most values identical to Displacement adopted values.

Afdb Japan attribute	GFE database table	GFE database attribute	Comments
Displacement S/R			Not uploaded because no equivalent GFE attribute. Most values identical to Displacement adopted values.
Displacement scaling law			Not uploaded because no equivalent GFE attribute. Most values identical to Displacement adopted values.
Displacement (adopted)	Section	Displacement – pref	
Recurrence interval min	Section	Recurrence interval – min	
Recurrence interval max	Section	Recurrence interval – max	
Recurrence interval ave			Not uploaded in favour of Recurrence interval adopted.
Recurrence interval D/S			Not uploaded because no equivalent GFE attribute. Most values identical to Recurrence interval adopted values.
Recurrence interval adopted	Section	Recurrence interval – pref	
Age of last movement oldest	Section	Age of last movement – max	Changed from AD/BC to a number relative to 1950 AD.
Age of last movement youngest	Section	Age of last movement – min	Changed from AD/BC to a number relative to 1950 AD.
Age of last movement historical record	Section	Age of last movement – pref	Changed from AD/BC to a number relative to 1950 AD.
Compiled by	Section, Fault	Compiled by	
Last updated	Section, Fault	Last updated	

9.12 Alaska Quaternary fault and fold database (Qffdb) – attribute mapping, formatting and upload

Alaska Qffdb attribute	GFE database table	GFE database attribute	Comments
Name	Fault trace, Fold trace, Section, Fault, Fold, Blind Fault	Name	Many names were accompanied by another name in brackets. Some were section names, so were separated out as such. Others were fault system or individual fault names, which were uploaded in notes. Blind fault names were created by adding “fault” after the associated fold name. Those parts of the Denali Fault and Toschunda sections which ruptured in 2002 had “2002 rupture” added to them.
Code			Not uploaded as is a duplicate (combination) of other codes (ACode, Slip Code, FCode), which in turn are duplicates or

Alaska Qffdb attribute	GFE database table	GFE database attribute	Comments
			other attributes
Num	Fault trace, Fold trace, Section, Fault, Fold, Blind Fault	Original Id	Some typos corrected. A few which had the same NUM and yet different names and were geographically separated, so were assigned new numbers.
Age	Section, Fault, Fold	Age of last movement – max	Did not upload “Class B” age
Acode			Not uploaded as is a duplicate of Age
Slip rate	Section, Fault, Fold, Blind fault	Section, Fault: Net slip rate – min, max Fold: Growth rate – vertical – min, max Blind Fault: Vertical slip rate – min, max	Converted from a category (<0.2, 1-2 etc) to min and/or max values. Because all the slip rates supplied for folds are vertical, these were duplicated as fold growth rate and vertical blind fault slip rate.
Slip code			Not uploaded as is a duplicate of slip rate
Slip sense	Fault, Section, Blind Fault	Slip type	Spelled out, assumed: LL = Left lateral; N = normal; R = Reverse, RL = Right lateral; SS = strike-slip; T = thrust; Unk = Unknown (left this blank).
Dip direction	Fault, Section	Dip direction	Converted from a quadrant to a bearing in degrees: North = 0°, East = 90°, South = 180°, West = 270° etc. Some had two dip directions, but were modified in consultation with Richard Koehler.
FCode			Not uploaded as is a duplicate of Ftype
Ftype	Trace (section/fault and fold)	Geomorphic expression	Ftpe (and FCode) reflect the accuracy of mapping of the original authors (1 = fault landforms are more continuous than discontinuous and mapping is accurate at given MAPPED SCALE (solid); 2 = fault landforms are more discontinuous than continuous and mapping is accurate at given MAPPED SCALE (dashed); 3 = location of fault is inferred (dotted) After consultation with Richard Koehler, mapped this to section/fault geomorphic expression: 1 = surface trace, 2 = eroded scarp, 3 = concealed. Richard Koehler provided some values for individual folds.
Mapped Scale	Trace	Scale	Spelled out abbreviated number by adding 3 zero’s to end.
Secondary sense			Combined with slip sense
-	Section, Fault, Fold, Blind Fault	Compiled by	Added Richard Koehlers name for all faults and folds after consultation with him
-	Section, Fault, Fold, Blind Fault	Last Updated	Added date downloaded for all faults and folds after consultation with Richard Koehler that there had been no updates since then.
-	Section, Fault,	References	Added Koehler et al. (2012) report reference for all folds and

Alaska Qffdb attribute	GFE database table	GFE database attribute	Comments
-	Fold, Blind Fault		faults.
-	Section, Fault	Upper seismogenic depth	Added after consultation with Richard Koehler
-	Section, Fault, Blind Fault	Aseismic-slip factor	Added after consultation with Richard Koehler, who said there is little data for creep on any Alaskan faults.
-	Fold	Fold type	Derived from the name
-	Blind Fault	Name	Added "fault" after the fold name (e.g., Beaver Creek Anticline "Fault")
-	Trace	Accuracy	Calculated by multiplying the scale by 2.

9.13 USA Quaternary fault and fold database (Qffdb) – attribute mapping, formatting and upload

USA Qffdb attribute	GFE database table	GFE database attribute	Comments
Name	Fault trace, Fold trace, Section, Fault, Fold, Blind Fault	Name	Note there are several faults with the same name. A very few were typos, but most are genuinely the same name (are geographically separated and have different Num = ID's).
Code			Not uploaded as is a duplicate (combination) of other codes
Num	Trace, Section, Fault, Fold	Original Id	Some typos corrected.
Age	Section, Fault, Fold	Age of last movement – max	Did not upload "Class B" age. Where different traces of the same section/fault have different values, chose the youngest.
Acode			Not uploaded as is a duplicate of Age
Slip rate	Section, Fault, Fold, Blind fault	Section, Fault: Net slip rate – min, max Fold: Growth rate – vertical – min, max Blind Fault: Vertical slip rate – min, max	Converted from a category (<0.2, 1-2 etc) to min and/or max values
Slip code			Not uploaded as is a duplicate of slip rate
Slip sense	Fault, Section, Blind Fault	Slip type	Spelled out, assumed: AC = Anticline; LL = Left lateral; MC = Monocline; N = normal; R = Reverse, RL = Right lateral; SC = Syncline; SS = strike-slip; T = thrust; Unk = Unknown (left this blank). Where different traces of the same section/fault have different values, chose the most common and/or checked the value on the website.
Dip direction	Fault, Section	Dip direction	Converted from a quadrant to a bearing in degrees: North = 0°, East = 90°, South = 180°, West = 270° etc. If traces dip in opposite directions, checked value on website or (especially if

USA Qffdb attribute	GFE database table	GFE database attribute	Comments
			a graben), deleted direction.
FCode			Not uploaded as is a duplicate of Ftype
Ftype	Trace (section/fault and fold)	Geomorphic expression	After consultation with Kathy Haller: For Sections/FaultsWell constrained = surface trace, Moderately constrained = subtle feature, Inferred = concealed. Folds assumed the same as the Alaska database.
Mapped Scale	Trace	Scale	
Secondary sense			Combined with slip sense
-	Section, Fault, Fold, Blind Fault	Last Updated	Added date noted on USGS website (3 Nov 2010).
-	Section, Fault, Fold, Blind Fault	References	Added USGS (2013) as instructed on the USGS website
-	Section, Fault	Upper seismogenic depth	Added assuming as for Alaska database
-	Fold	Fold type	Derived from the name
-	Blind Fault	Name	Added "fault" after the fold name (e.g., Beaver Creek Anticline "Fault")
-	Trace	Accuracy	Calculated by multiplying the scale by 2.

9.14 Australia neotectonic feature database (nfdb) – attribute mapping, formatting and upload

Australia nfdb attribute	GFE database table	GFE database attribute	Comments
Entity number	Fault trace, Fold trace, Section, Fault, Fold, Blind Fault	Original Id	
Name	Fault trace, Fold trace, Section, Fault, Fold, Blind Fault	Name	
Feature type			Not uploaded, but used to separate faults and folds
Originator	Section, Fault, Fold	Contributed by	
Compilation date	Section, Fault, Fold, Blind fault	Created date	
Compiler name	Section, Fault,	Compiled by	

Australia nfdb attribute	GFE database table	GFE database attribute	Comments
	Fold, Blind Fault		
Last update	Section, Fault, Fold, Blind fault	Last updated	
Updated by			Not uploaded because no equivalent GFE attribute.
QA date			Not uploaded because no equivalent GFE attribute.
QA by			Not uploaded because no equivalent GFE attribute.
QA status code			Not uploaded because no equivalent GFE attribute.
Access code			Not uploaded because no equivalent GFE attribute. Used by GA to denote which are shown on their website.
Activity code			Not uploaded because no equivalent GFE attribute.
Confidence level	Section, Fault, Fold	Data completion factor	Following consultation with Dan Clark, mapped these as: Definite = 1 (High); High = 2 (Moderate); Moderate = 3 (Low). Two features with confidence level none were deleted as discussed above.
Domain	Section, Fault, Fold	Notes	
Latitude			Not uploaded because faults and fold locations are denoted by their traces.
Longitude			Not uploaded because faults and fold locations are denoted by their traces.
Location method	Fault trace, Fold trace	Location method	
Location remark	Section, Fault, Fold	Synopsis	
Location precision	Fault trace, Fold trace		Not uploaded because no equivalent GFE attribute.
Synopsis	Section, Fault, Fold	Notes	
Geological setting	Section, Fault, Fold	Notes	
Geomorphic expression	Fault trace, Fold trace	Notes	
Length	Section, Fault, Fold	Length – pref	
Displacement	Section, Fault, Fold	Total displacement	Converted from metres to kilometres. Note this is a vertical, not a net displacement.
Sense of movement	Section, Fault, Fold	Slip type	
Average strike	Section, Fault, Fold	Strike	
Dip	Section, Fault,	Dip	

Australia nfdb attribute	GFE database table	GFE database attribute	Comments
	Blind fault		
Direction of dip	Section, Fault, Blind fault	Dip direction	Converted from a quadrant to a bearing in degrees: North = 0°, East = 90°, South = 180°, West = 270° etc.
Historic events	Section, Fault	Historical earthquake	Converted calendar date to number relative to 1950
Prehistoric events	Section, Fault, Fold	Pre-historical earthquake – min, max	Converted kiloyears (ka) into years BP and from a range to min and max values. Some were given as an incomplete range, but confirmed with Dan Clark that these are minimum values.
Seismicity remarks	Section, Fault, Fold	Event descriptions	
Largest single event displacement	Section, Fault	Displacement – pref	
Age of youngest deformed deposit	Section, Fault, Fold, Blind fault	Age of last movement – max	Converted into yrs BP from geological period using the IUGS ages as follows: Holocene = 11,700; Late Pleistocene = 126,000; Middle Pleistocene = 781,000; Pleistocene = 2,588,000; Quaternary = 2,588,000; Pliocene = 5,332,000; Early Pliocene = 5,332,000; Late Miocene = 11,608,000.
Deformed deposit description	Section, Fault, Fold	Marker age description	
Slip rate category	Section, Fault, Fold, Blind fault	Section, Fault: Net slip rate – min, max Fold: Growth rate – vertical – min, max Blind Fault: Vertical slip rate – min, max	Converted from a category (<0.01, 0.01-0.1 etc) to min and/or max values
Slip rate remarks	Section, Fault, Fold	Slip rate description	
Bibliographic references	Section, Fault, Fold	References	
-	Section, Fault, Blind Fault	Aseismic-slip factor	Added after consultation with Dan Clark that there is no evidence for creep on any faults or folds.
-	Fault, Section	Upper seismogenic depth – pref	Added after consultation with Dan Clark that all faults mapped in the database reach the ground surface.

9.15 Mid-ocean ridge transform database (Mortdb) – attribute mapping, formatting and upload

Mortdb attribute	GFE database table	GFE database attribute	Comments
Transform name	Trace, Section, Fault, Source	Name	Where sections were combined into faults, the fault was given a name combining the two sections – e.g., the combined “Tasman A” and “Tasman B” sections were renamed as the “Tasman A-B” fault and fault source.
Latitude			Not uploaded because fault locations are denoted by their traces.
Longitude			Not uploaded because fault locations are denoted by their traces.
MOR	Source	Tectonic region	Spelled out abbreviated names, assumed: AAR = America Atlantic Ridge; CIR = Central Indian Ridge; EPR = East Pacific Rise; MAR = Mid-Atlantic Ridge; PAR = Pacific Antarctic Ridge; SEIR = South East Indian Ridge; SSR = South Scotia Ridge; SWIR = South West Indian Ridge.
Start latitude			Not uploaded because fault locations are denoted by their traces.
Start longitude			Not uploaded because fault locations are denoted by their traces.
End latitude			Not uploaded because fault locations are denoted by their traces.
End longitude			Not uploaded because fault locations are denoted by their traces.
Length	Section, Fault, Source	Length – pref	Lengths were calculated for faults by summing the component section lengths.
Sinistral/Dextral	Section, Fault, Source	Slip type	
GRSM slip rate	Section, Source	Net slip rate – pref	
Seismogenic area			Not uploaded as is area for sections only, and area is not included as a section attribute in the GFE database.
Whole fault system seismogenic area	Source	Area – pref	
Max expected seismic moment			Not uploaded because is a step in magnitude calculation and is no equivalent GFE attribute.
Max expected Mw	Source	Maximum magnitude	
Expected repeat time	Source	Recurrence interval	
Scaling/Real	Source	Notes	
-	Section, Fault,	Compiled by	Added database administrators names

Mortdb attribute	GFE database table	GFE database attribute	Comments
-	Source	Last updated	Added date received (was updated immediately before delivery).
-	Section, Fault, Source	Upper seismogenic depth – pref	Added because all sections/faults were mapped from seafloor bathymetry (thus they reach the ground surface).
-	Source	Lower seismogenic depth – pref	Calculated from area divided by length (assuming all sources are vertical – see dip).
-	Source	Width	Added from area (assuming all sources are vertical – see dip).
-	Section, Fault, Source	Dip	Added 90° for all after confirming with Monica Wolfson that all are vertical.
-	Section	Slip rate description	Added from the readme notes supplied with the database.
-	Source	Seismogenic area description	Added from the readme notes supplied with the database.
-	Source	Magnitude description	Added from the readme notes supplied with the database and in consultation with Monica Wolfson.
-	Source	Recurrence interval description	Added from the readme notes supplied with the database.
-	Trace	Location method	Added description of location method from the readme notes supplied with the database.

10 Characterisation of subduction zones

This section is a reproduction of the report “The GEM Faulted Earth Subduction Interface Characterisation Project” by Berryman, Wallace, Hayes, Bird, Wang, Basili, Lay, Pagani, Stein, Sagiya, Rubin, Barreiros, Kreemer, Litchfield, Stirling, Gledhill, Haller, and Costa (2015) with minor adjustment to the section referencing. Appendix A and B are now Sections 10.5 and 10.6, respectively. The references are merged with the references in the other sections and are listed at the back of the report.

10.1 Introduction

As a component of the hazard models being developed by GEM (<http://www.globalquakemodel.org/>) our project (<http://www.globalquakemodel.org/what/global-projects/active-faults-database/>) has sought to develop a globally consistent characterisation of the world’s approximately 55,000 km of subduction interfaces as a basis for generating earthquake event sets for inclusion in earthquake hazard and risk modelling.

Subduction zones are where the majority of global seismic energy is released and, because of their dimensions, are where the largest and some of the most damaging earthquakes and associated tsunami have occurred. Recent examples include the Mw 9.2, December 26th, 2004 Sumatra earthquake and the Mw 9.0, March 11th, 2011 Tohoku earthquake. Thus, to underpin a global earthquake risk assessment, characterisation of subduction zones are crucial ingredients.

In December 2011 an invited group of scientists (the report authors) with extensive knowledge of subduction zones around the world met for four days to discuss the approach we should take to compile a database and also to begin populating the attributes of the 40 subduction zones identified (Figure 10.1). The process of attribution and discussion has continued to June 2014, refining the parameters and uncertainties. Note that the segments defined are not intended to represent rupture segments. They are largely chosen where plate motion rate or azimuth of subduction undergoes a change, or where there is a change in the plate pairs that are juxtaposed at the boundary. Where the segments link-up geometrically the possibility of multi-segment rupture must be included in the hazard model.

There is a rich scientific legacy of work on subduction zones globally, and a wealth of historical data to draw on, but the 2004 Sumatra earthquake, and more recently the Tohoku earthquake, have surprised many researchers in terms of the size of the event (see McCaffrey, 2008 for recent review). Many investigators have attempted to explain subduction seismogenesis by correlating the frequency and magnitude of earthquakes with geodynamic parameters, such as subduction rate, subducting plate age, subduction interface thermal structure, or the presence of subducting sediment (e.g., Uyeda and Kanamori, 1979; Ruff and Kanamori, 1980; Peterson and Seno, 1984; Kanamori, 1986; Ruff, 1989; Scholz and Campos, 1995, 2012; McCaffrey, 1997). However, recent large earthquakes, and further research, question the utility of some of the correlations as proxies for seismogenesis (e.g., Subarya et al., 2006; Stein and Okal, 2007; McCaffrey, 2008). In the Hikurangi subduction zone of New Zealand, Wallace et al. (2009b) suggest that there is a complex interplay between upper and lower plate structure, subducting sediment, thermal effects, regional tectonic stress regime, and fluid pressures, and all of these factors probably control the extent, and thus the possible maximum magnitude of subduction thrust earthquakes. In the Japan region there have been great

earthquakes in both the northeast where the incoming plate is old and the rate of subduction is fast (>80 mm/a) and in the southwest where the plate is young and the rate is only half of that in the northeast.

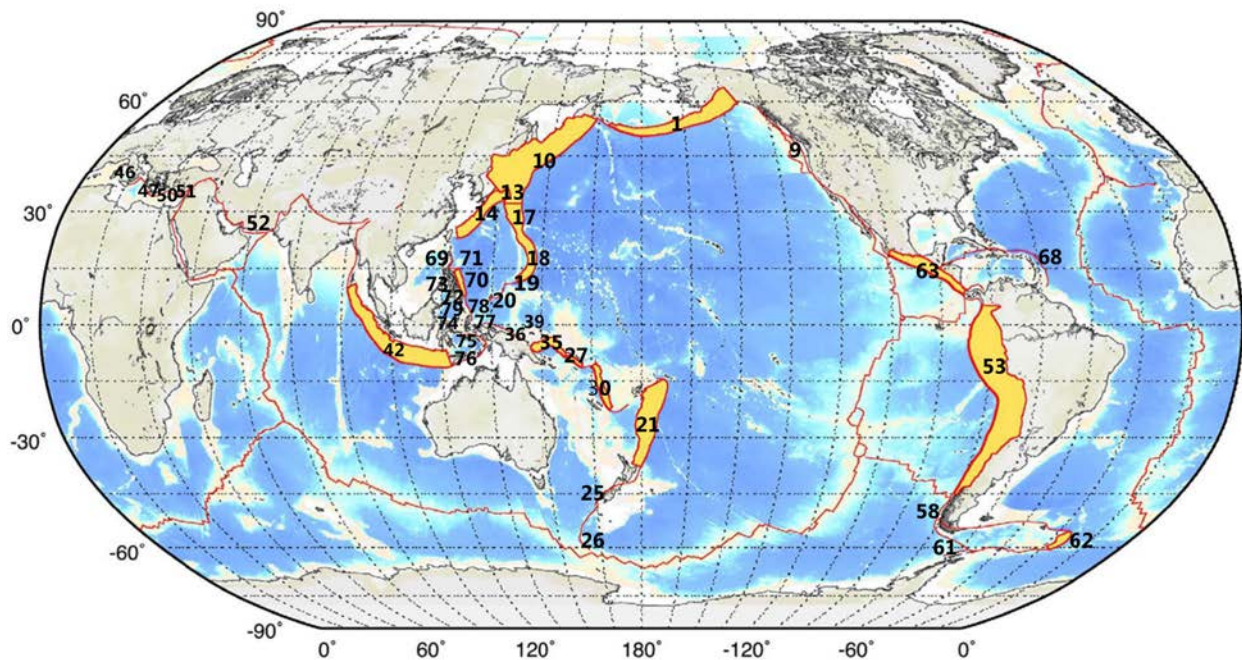


Figure 10.1 Location of the subduction zones identified in this database modified from Hayes et al. (2012) reproduced with permission of John Wiley and Sons. This is Figure 1 in the paper, 'Slab1.0: A three-dimensional model of global subduction zone geometries' by Hayes, Wald and Johnson published in the *Journal of Geophysical Research*, Volume 117, B01302, Copyright 2012. Several subduction zones are divided into segments. Therefore, the subduction zone labels are not sequential, and correspond with the listing in Table 10.1.

Given the obvious complexity of processes operating in subduction zones, and the recognition that the historical period is too short to provide a good basis for determining the frequency and maximum magnitude of earthquakes in any, let alone all of the Earth's subduction zones, there is a clear need to find a pragmatic approach that uses as much of the available knowledge as is possible, in a way that is neither too conservative nor too optimistic. The tools and techniques that we have used include improved understanding of the geometry of most of the global subduction zones via the SLAB1.0 model (Hayes et al., 2012), plate motions incorporating upper plate rotations and backarc motions (e.g., Bird, 2003; Bird et al., 2009), historical event catalogues (e.g., Heuret et al., 2011), increasingly robust plate models built from GPS velocities (e.g., DeMets et al., 2010), and the widely used, but nevertheless debated methods of earthquake hazard assessment (e.g., Stein et al., 2012; Hanks et al., 2012).

In this report we assess the parameters associated with the plate interface itself and do not include seismicity within the down-going plate or overriding plate. To accurately estimate the total hazard associated with subduction zones, one also needs to consider plate-bending earthquakes and earthquakes associated with deformation of the down-going plate before it enters the subduction zone – so-called 'outer rise' events, as well as events occurring in the upper plate. These are outside of the scope of this report. In characterising the subduction interface we adopt some aspects of the approach presented by McCaffrey (2008), including a procedure for prescribing length-limited estimates of maximum magnitude. In the absence of adequately long records of earthquakes for most subduction zones, and the occurrence of

unexpectedly large and long ruptures in Indonesia and Japan, we conclude that earthquake magnitude is probably only limited by available subduction length. The approach presented here provides a basis for developing earthquake event sets for the subduction zones of the World on a consistent basis using an up-to-date synthesis of available published data. We assign the maximum magnitude to each subduction zone based on its total length. If the total length of the subduction zone exceeds what can realistically rupture with the generally accepted maximum magnitude of Mw 9.6 then we propose that the earthquake events should 'float' along the whole subduction zone, using the available seismic moment respecting the maximum magnitude and the Gutenberg and Richter b value, in the manner developed by Parsons et al. (2012) for the Nankai Trench in Japan. The key, and perhaps most contentious assumption in this approach is that any subduction zone may rupture a surprisingly long segment along strike regardless of its geological conditions, but the recurrence time of such events will vary dramatically between subduction zones according to those geological conditions. A recent example of a subduction event rupturing through what had previously been considered a segment boundary is the 2007 Mw 8.1 earthquake on the Solomon Islands subduction zone (Taylor et al., 2008a). The recurrence time for all earthquakes in the subduction zone further depends on the fraction of the plate motion convergence rate that is released as earthquakes, the so-called coupling coefficient. A very conservative treatment is to assume all relative plate motion is converted to seismic moment release (i.e., 100% coupling) but observations have shown this to be an unlikely end-member model. The initial assessment of subduction zones into "Chilean type" and "Mariana type" (Uyeda & Kanamori, 1979) still demonstrates some first-order coherence in terms of variations in seismic coupling among subduction zones. Together with other data, particularly the interpretation of campaign and continuous GPS velocities (see Appendix B), these observations provide a basis for assessments of seismic coupling that ranges from near to 90% in Cascadia and Nankai to as low as 15% at the Manila trench. Despite this low coupling in subduction zones like the Manila Trench, following the assumption of McCaffrey (2008), very large events can still occur there because the subduction zone is sufficiently long. What makes the short-term hazard low at the Manila trench is the extremely long recurrence time of full-margin rupture.

Determination of the Gutenberg & Richter b-value (the long-term ratio of small to large events that comprise the co-seismic component of plate motion measured over the duration of a seismic cycle) is a key requisite for calculating hazard. The b-value is an important driver of seismicity rate calculations, and seemingly small changes to the b-value can result in significant differences in hazard estimates, an observation directly attributable to the log-linear relationship between frequency and magnitude. For example, a distributed seismicity source model with a b-value range of 0.6 to 1.0 (all else held constant) produces hazard estimates (e.g., peak ground accelerations) that vary by about 30%. In continental settings the b-value is observed to fall in the range of about 0.6 to 1.5. Bird and Kagan (2004) deduced a global average subduction b-value of 0.96 with a 95% confidence interval of 0.90 to 1.02, but this includes plate-bending earthquakes in the downgoing plate as well as interface events. Suckale and Grünthal (2009) reported a lower b-value of 0.71 from historical events in the New Hebrides region. On closer inspection the historic events upon which these assessments have been made should more correctly be termed b-values from the subduction zone region, as they often include only sparse events from the locked part of the interface, as well as crustal and plate-bending events in the downgoing plate. Thus, for characterising likely future major events on the locked part of the interface these studies may not be the most appropriate.

A long record of large interface events has been obtained by Goldfinger et al. (2012) using paleoseismic methods in the Cascadia margin of western North America. Studies in this region suggest a paucity of moderate magnitude events in this region but the data are almost certainly incomplete. Nevertheless it appears that some subduction zones are highly productive while others are "quiet" suggesting that much of

the available seismic moment on the locked part of the interface is released in infrequent large events. At these margins the b-value is likely to be lower over complete seismic cycles than for productive regions such as the New Hebrides. Heuret et al. (2011) examined seismicity rates specifically on the thrust interface of subduction zones (Figure 10.2) and identified low rates of $\geq M_w 5.5$ events on the Hikurangi, Caribbean, southern Chile, western and eastern Aleutians, Java, and the Makran interface zones. For these unproductive zones the b-value is likely to be substantially lower than the global average b-value which has been obtained from locations where there has been significant activity in the instrumental period. Conversely, Heuret et al. (2011) also identify some margins where the rate of interface events of $\geq M_w 5.5$ is high which are those regions where the 'global average' of Bird and Kagan (2004) is likely to be representative.

To further illustrate likely variability in b-values at subduction zones, we have compiled a list of published b-values (Table 10.2). At individual subduction zones (such as the Tonga Trench), estimated b-values can vary by as much as 0.5 or more between studies. The lowest b-values in Table 10.2 are ~ 0.6 (New Hebrides, Solomon Islands), while the highest ones are ~ 1.5 (Marianas). To encompass this uncertainty, we assume a minimum b-value for all subduction zones of 0.7, and a maximum of 1.2. In cases where published studies have estimated b-values that are less than 0.7, or exceed 1.2, we use the published values to inform the minimum or maximum value in our table. In addition to these three principal parameters of seismogenesis – maximum magnitude, seismic coupling coefficient, and b-value – we also need to define the potential upper and lower extent of rupture in future interface earthquakes to position the rupture plane with respect to the land surface above, as input to hazard and risk calculations.

When implemented in a seismic hazard model, the procedure should be to generate earthquakes of appropriate size and frequency within a subduction zone that uses the available seismic moment as defined for that region. Here, we define the maximum magnitude for each subduction zone, and the moment from earthquakes in a seismic hazard model should be balanced over the entire fault surface, similar to that proposed for the fault slip component of a California hazard model developed by Hiemer et al. (2013), and by the 'earthquake simulator developed by Parsons et al. (2012) for the Nankai subduction zone.

In the database we constrain lower bound maximum magnitudes in each subduction segment as the largest earthquake that has occurred in the instrumental record as defined in most recent literature. In some places, such as for the 1960 rupture in Chile this may narrow the range of M_{max} because the 1960 $M_w 9.5$ is close to the theoretical maximum magnitude proposed by McCaffrey (2008) of $M_w 9.6$. Where no great earthquakes ($M_w > 8$) have occurred in the instrumental period the range applied to M_{max} is often at least one magnitude unit. By capturing some estimate of uncertainty in many of the key parameters the database lends itself to creating alternate event sets for each subduction segment via Monte Carlo sampling, and for frequent updating as new data come to hand.

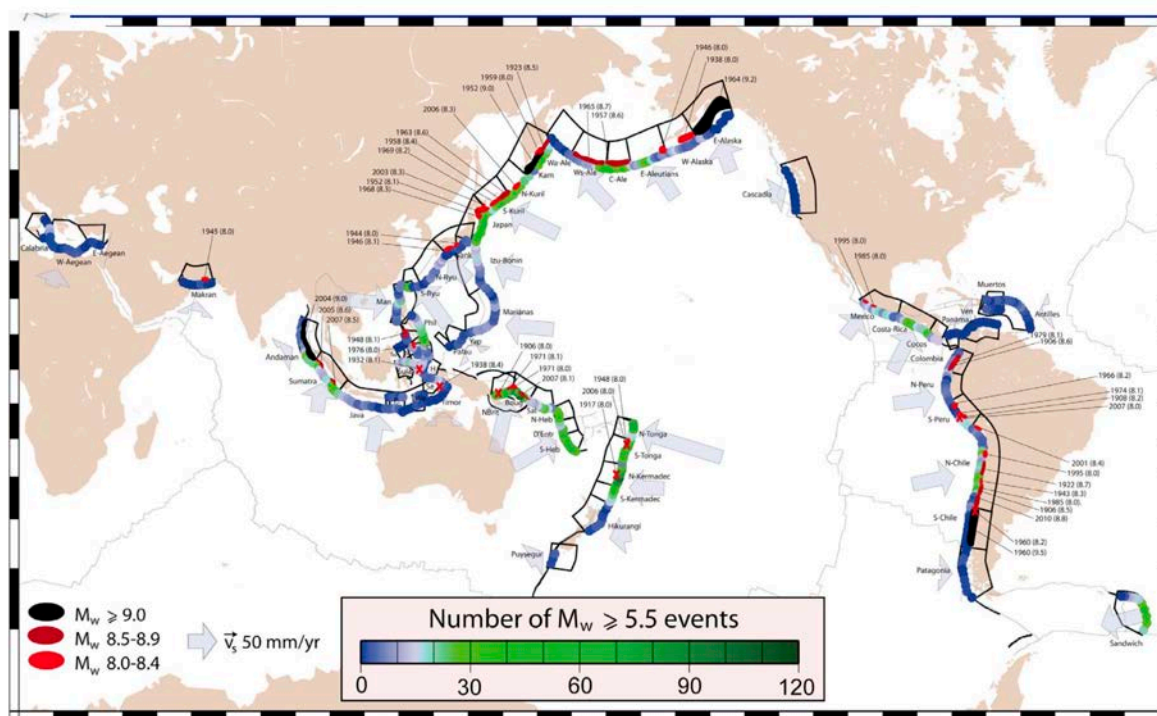


Figure 10.2 Subduction zone interface seismicity and trench segmentation, from Heuret et al. (2011) reproduced with permission of John Wiley and Sons. This is Figure 1 in the paper ‘Physical characteristics of subduction interface type seismogenic zones revisited’ by Heuret, Lallemand, Funiciello, Piromallo and Faccenna published in *Geochemistry, Geophysics, Geosystems* 12: Q01004, Copyright 2011. The figure and part of the following caption are reproduced with permission of John Wiley & Sons. The rupture area of the $M_w \geq 8.0$ subduction interface events (1900–2007) is represented by red and black ellipses. The rupture areas were taken from McCann et al. (1979), Kanamori (1986), Schwartz et al. (1989), Byrne et al. (1992), Tichelaar and Ruff (1993), Johnson et al. (1994), Ishii et al. (2005), Fedotov et al. (2007), Ruppert et al. (2007), Bilek (2010), and Madariaga et al. (2010). Red crosses are used here to indicate $M_w \geq 8.0$ events that did not have available rupture area data. Colored dots represent, by each 1° of trench, the number of $M_w \geq 5.5$ subduction interface events (1976–2007). Subduction velocities (Heuret, 2005) are represented by blue arrows, although in this study we use velocities from more recent geodetic studies (see Section 10.6) and Bird (2003), rather than the ones shown here. In this study we relax the segmentation model delimited by Heuret et al. (as black lines in this figure), and propose to ‘float’ earthquakes along the whole subduction zone as discussed in the text.

10.2 Procedure

To populate the database we have firstly defined subduction zones, and in some cases segments, where there is a change in kinematics at the subduction zone (usually due to the juxtaposition of different plate pairs and/or major changes in plate boundary orientation). These segments are largely defined for kinematic convenience when calculating the plate rates at the segment endpoints, but in some cases these segments represent possible rupture segments (as in the Alaska case; Wesson et al., 2007). In the database, we record the plate pairs at each subduction segment, define the segment coordinate endpoints, the average dip of the seismogenic portion of the interface, the dip direction, and the trench depth. Most of these values are inferred from observations. The down-dip geometry of subduction zones are those identified in the SLAB 1.0 model of Hayes et al. (2012) which is available on-line from US Geological Survey (see:

<http://earthquake.usgs.gov/data/slab/>). The geometry of zones in Slab 1.0 is determined from careful examination of instrumental seismicity. In subduction zones where there is little seismicity this basis for defining geometry is not available and so we have assigned estimates of dip angle from the literature. Uncertainty in the dip angle could also be incorporated into the estimate of fault area and maximum magnitude, but for this study we consider this to be relatively well constrained and uncertainty will have a relatively small impact on hazard compared with uncertainty in coupling coefficients and b-values.

Important judgments are then made for the maximum up-dip extent of ruptures, including uncertainty estimates (min, preferred, max), and the down-dip extent of ruptures, again with uncertainty (min, preferred, max). The down-dip rupture width can then be calculated. Another parameter requiring considerable judgement is the coupling coefficient in the particular subduction segment and again we assign uncertainty (min, preferred, max). We outline the rationale behind our choice of coupling coefficients for each subduction zone in Appendix B. For all segments, we assume a range of M_{max} values, with the largest possible M_{max} based on rupture length of the entire segment (or combination of segments), using scaling relationships between subduction zone (or segment) length and magnitude in McCaffrey (2008). The minimum M_{max} value is taken as the largest earthquake observed in the historical record on that segment. As a default for the preferred value, we take the average of the minimum and maximum M_{max} values. The b-value for the subduction zone is also a significant judgement as discussed above, and so considerable uncertainty is applied to this parameter also.

With all of these parameters defined or calculated, a series of earthquake event sets can then be calculated for each subduction segment defining the frequency-magnitude distribution and the recurrence of each earthquake. Monte Carlo sampling of the range of event sets can determine uncertainty statistics for each event set.

10.3 Results

A wide range of possible earthquakes have been identified in this project, reflecting widely varying parameters (Table 10.1). Subduction segment lengths range from as little as 229 km (Halmahera segment in the Molucca Sea) to 6536 km for the South American margin. The dip on the seismogenic interface ranges from 6° in the Prince William Sound segment of the Alaska subduction zone to 28° in a segment of the New Hebrides subduction zone. The up-dip extent of rupture is often thought to be 5-10 km below the seafloor, although in many places the possibility of rupture to the trench is given some weight. The down-dip limit of rupture is also expected to vary significantly – as shallow as 15 km in the Yakataga segment of Alaska or as deep as 50 km in Japan and Chile. With these wide ranges of dip and rupture limits, the rupture widths vary from as little as 40 km in the Yakataga segment of Alaska and parts of the New Hebrides region, to as much as 240 km in the shallowly-dipping Prince William Sound segment of the Alaska subduction margin.

The wide range of segment lengths and widths is responsible for the range of maximum earthquake magnitudes expected in global subduction zones (Figure 10.3). The preferred maximum magnitude earthquakes expected in the Hjort (south of New Zealand), Calabria, and east Luzon subduction zones are only M_w 7.8, and, while at the other end of the spectrum a M_w 9.5 is the calculated preferred estimate for central Chile, and in several subduction zones the available length in the subduction zone cannot preclude the occurrence of the generally accepted global maximum M_w 9.6 event. Accepting uncertainties in the estimated parameters, and in delineation of segments of subduction zones, we find that maximum magnitude earthquakes of M_w 9.6 appear possible in 10 of the 79 subduction zones or their segments as defined in this project, and a maximum of M_w 9.0 to 9.5 is possible in an additional 36 of the 79 subduction zones or their segments (Table 10.1).

Figure 10.3 shows that there is a clear positive correlation between magnitude and area ($R=0.81$), and a weaker but positive correlation between magnitude and coupling coefficient ($R=0.51$) (red and orange symbols tend to sit above blue symbols). There appears to be a weaker or no correlation ($R=0.28$) between maximum magnitude and average velocity across the plate interface (larger symbols tend to fall in the lower magnitude and lower area quadrants of the plot). Similarly, there is poor correlation between coupling coefficient and area ($R=0.27$). The correlation between magnitude and area is expected because magnitude is derived in large part from the area. A positive correlation between coupling coefficient and magnitude may also be understood as higher friction on the fault plane resulting in larger locked patches and resultant larger earthquakes. The finding that relative plate velocity is poorly correlated with magnitude is somewhat surprising, but it may be that higher velocities result in more fracturing and break-up of the down-going plate and therefore smaller area of locked patches. Higher velocities could also lead to less fault healing and hence lower coupling.

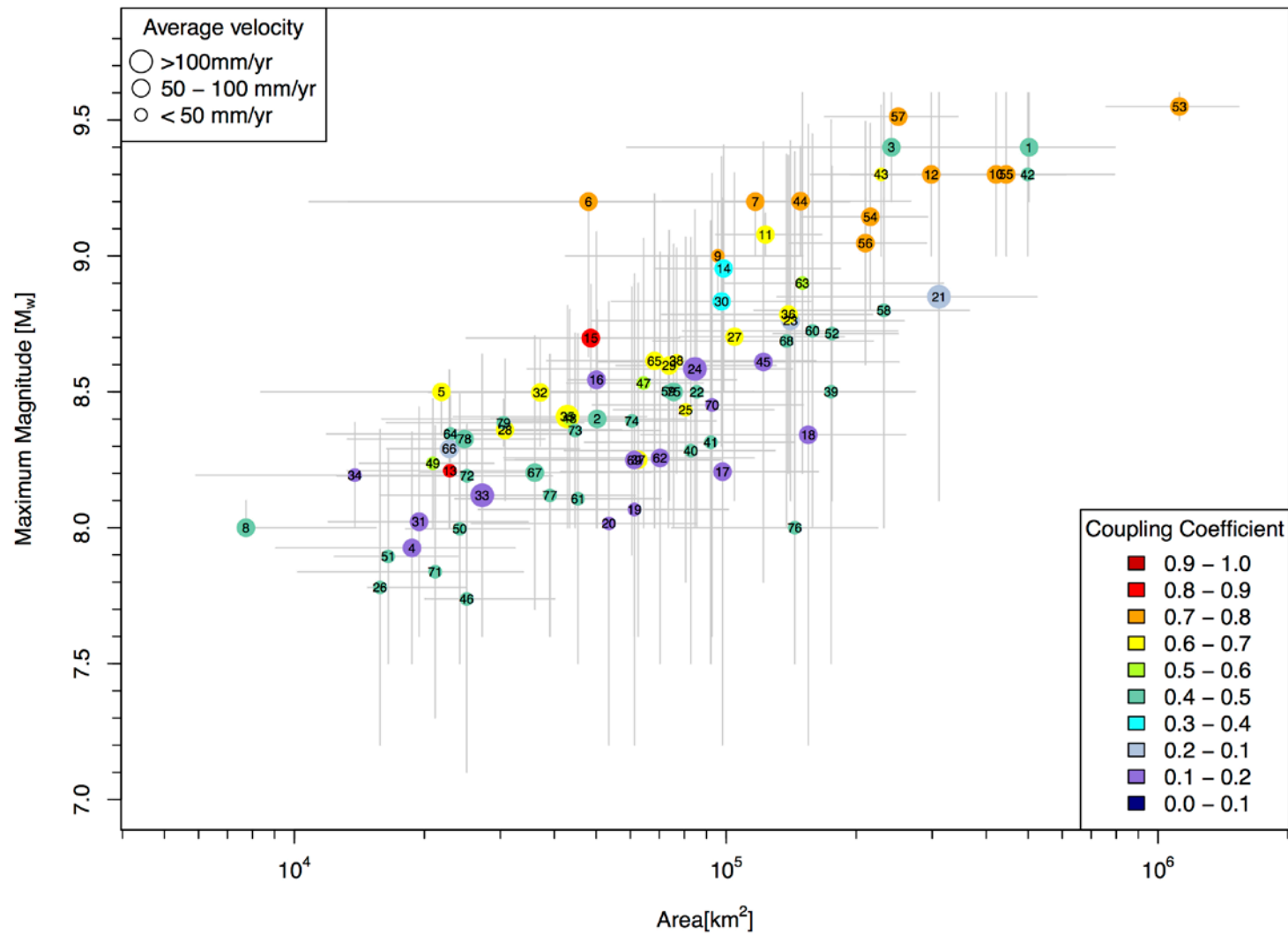


Figure 10.3 Plot showing relationships between maximum magnitude, rupture area, coupling coefficient and relative velocity across the interface for each of the 79 subduction interface zones and their possible segments considered in this study.

Table 10.1 Subduction Interface Zone Parameters as defined in Section 10.5.

*Note all subduction zones divided into segments (Alaska, Central America, much of the South American margin) are considered to be plausible segments based on trench geometry and kinematics. However, an alternative and recommended treatment of these very long subduction zones is to define a maximum magnitude and allow earthquakes to ‘float’ along the total length with the earthquake event set determined by plate convergence rates, coupling coefficient and b-value of the interface source zone. The abbreviated names of the overriding/subducting plates follow those defined in Bird (2003) (see table 1 in that publication).

No.	Subduction Zone	Segment	Plate pairs	Left_E_ LONG	Left_N_L AT	Left_REL_V EL (mm/yr)	Left_REL _AZI (°)	Right_E_ LONG	Right_N_ LAT	Right_REL _VEL (mm/yr)	Right_REL_ AZI (°)	Length (km)
1	Alaska/ Aleutians	Whole margin	PA\NA	164.066	55.209	74.6	311	-140.128	60.381	49.0	350	4130
2	Alaska	Komandorski	PA\NA	164.066	55.209	74.6	311	170.700	52.498	74.3	313	531
3	Alaska	Western Aleutians	PA\NA	170.700	52.498	74.3	313	-162.413	53.367	64.0	329	1963
4	Alaska	Shumagin	PA\NA	-162.413	53.367	64.0	329	-157.986	54.101	61.0	332	302
5	Alaska	Semidi	PA\NA	-157.986	54.101	61.0	332	-154.160	55.239	58.4	336	279
6	Alaska	Kodiak	PA\NA	-154.160	55.239	58.4	336	-149.220	56.925	55.0	340	361
7	Alaska	Prince William Sound	PA\NA	-149.220	56.925	55.0	340	-144.316	59.918	51.4	347	444
8	Alaska	Yakataga	PA\NA	-144.316	59.918	51.4	347	-140.128	60.381	49.0	350	250
9	Cascadia		JF\NA	-130.850	51.612	47.8	58	-124.742	40.313	32.7	58	1415
10	Japan/Kurile	Whole margin	PA\OK	141.992	34.666	93.0	294	164.066	55.209	78.7	308	2965
11	Japan/Kurile	Japan Trench	PA\OK	141.992	34.666	93.0	294	144.454	40.847	91.1	295	742
12	Japan/Kurile	Kurile-Kamchatka	PA\OK	144.454	40.847	90.9	296	164.066	55.209	78.7	308	2223
13	Kanto		PS\OK	138.674	35.034	36.0	317	141.883	34.213	34.1	312	312
14	Nankai/Ryukyu	Whole margin	PS\AM, PS\ON	122.501	23.643	134.0	314	138.674	35.034	44.4	310	2202
15	Nankai/Ryukyu	Nankai	PS\AM	132.824	30.754	55.7	310	138.674	35.034	44.4	310	762
16	Nankai/Ryukyu	Ryukyu	PS\ON	122.501	23.643	134.0	314	132.824	30.754	58.0	311	1440
17	Izu-Bonin		PA\PS	143.522	24.391	47.1	292	141.883	34.213	61.4	284	1128
18	Marianas		PA\MA	143.503	11.494	76.3	277	143.522	24.391	49.1	281	1822

No.	Subduction Zone	Segment	Plate pairs	Left_E_LONG	Left_N_LAT	Left_REL_VELOCITY (mm/yr)	Left_REL_AZI (°)	Right_E_LONG	Right_N_LAT	Right_REL_VELOCITY (mm/yr)	Right_REL_AZI (°)	Length (km)
19	North Yap		PA\PS	138.359	9.379	3.0	297	143.097	11.569	9.0	311	690
20	Palau-South Yap		CL\PS	134.521	6.990	1.6	318	138.359	9.379	7.1	324	554
21	Hikurangi-Tonga-Kermadec	Whole margin	PA\HF, KE,TO	175.503	-42.059	19.5	236	-173.407	-14.584	269.5	256	3412
22	H-T-K	Hikurangi	PA\HF	175.503	-42.059	19.5	236	179.838	-37.476	65.5	247	660
23	H-T-K	Kermadec	PA\KE	179.838	-37.476	45.3	258	-174.985	-23.750	98.1	257	1627
24	H-T-K	Tonga	PA\TO	-174.985	-23.750	112.6	248	-173.407	-14.584	269.5	256	1125
25	Puysegur		AU\PA	168.770	-44.021	36.6	68	163.235	-50.079	29.9	51	834
26	Hjort		see notes	157.615	-57.474	25.2	19	161.228	-61.457	18.9	342	493
27	Solomons	Whole margin	WL\PA, AU\PA	153.083	-5.750	91.1	49	164.612	-10.892	88.4	80	1460
28	Solomons	Northwest	WL\PA	153.083	-5.750	91.1	49	156.296	-8.174	107.0	47	465
29	Solomons	Southeast	AU\PA	156.296	-8.174	98.1	75	164.612	-10.892	88.4	80	995
30	New Hebrides	Whole margin	AU\PA, NH,MH	164.612	-10.892	94.7	78	174.277	-22.667	45.8	7	1923
31	New Hebrides	North	AU\PA	164.612	-10.892	94.7	78	166.106	-13.634	90.7	79	400
32	New Hebrides	Central	AU\NH	166.106	-13.634	33.7	74	167.350	-18.022	102.3	74	500
33	New Hebrides	South	AU\NH	167.350	-18.022	102.3	74	169.954	-22.325	174.9	68	560
34	New Hebrides	Matthew-Hunter	AU\MH	169.954	-22.325	49.1	8	174.277	-22.667	45.8	7	463
35	New Britain		WL\SB	147.283	-7.000	48.7	21	153.083	-5.750	160.0	-3	660
36	New Guinea Trench	Whole margin	PA\NGH, CL\BH	143.743	-3.200	92.6	251	132.515	0.017	22.1	183	1364
37	NGT	east	PA\NGH	143.743	-3.200	92.6	251	138.793	-1.159	84.1	259	600
38	NGT	west	CL\BH	138.793	-1.159	28.1	185	132.515	0.017	22.1	183	764
39	Manus Trench	Whole margin	PA,CL\NB	154.955	-4.550	10.0	181	142.246	-2.693	8.7	141	1709
40	Manus	East	PA\NB	154.955	-4.550	10.0	181	149.270	-0.650	6.9	162	809

No.	Subduction Zone	Segment	Plate pairs	Left_E_ LONG	Left_N_L AT	Left_REL_V EL (mm/yr)	Left_REL _AZI (°)	Right_E_ LONG	Right_N_ LAT	Right_REL _VEL (mm/yr)	Right_REL_ AZI (°)	Length (km)
41	Manus	West	CL\NB	149.270	-0.650	16.9	152	142.246	-2.693	8.7	141	900
42	Sunda Trench	Whole margin	AU\BU,SU	92.068	13.715	12.4	178	120.886	-11.493	69.3	8	4874
43	An-Sunda Tr.	Andaman	IN or AU\BU	92.068	13.715	12.4	178	96.202	1.345	50.8	90	1579
44	An-Sunda Tr.	Sumatra	AU\SU	96.202	1.345	46.4	1	104.576	-8.167	55.7	11	1438
45	An-Sunda Tr.	Java	AU\SU	104.576	-8.167	55.7	11	120.886	-11.493	69.3	8	1857
46	Calabria		AF\EU	15.775	37.282	2.0	306	17.415	39.071	2.0	306	245
47	Hellenic Trench	Whole margin	AF\AS	19.912	37.731	23.0	26	28.726	36.579	10.0	37	1032
48	Hellenic Tr.	western segment	AF\AS	19.912	37.731	23.0	26	25.288	34.202	35.0	35	620
49	Hellenic Tr.	eastern segment	AF\AS	25.228	34.202	10.0	37	28.726	36.579	10.0	37	412
50	Cyprus	western segment	AF\AT	28.726	36.579	14.0	30	32.254	34.729	9.0	30	380
51	Cyprus	eastern segment	AF\AT	32.160	34.604	7.0	40	35.169	34.824	7.0	40	276
52	Makran		AR\EU	57.057	26.049	19.5	14	65.028	24.382	19.5	17	941
53	South America	Whole margin	NZ\SA,ND	-78.646	7.337	53.0	80	-76.006	-45.659	78.7	80	6526
54	S. America	Ecuador-Colombia	NZ\ND	-78.646	7.337	53.0	80	-81.599	-3.245	60.9	83	1329
55	S. America	Peru	NZ\SA or AP	-81.599	-3.245	70.0	82	-71.307	-21.965	63.9	78	2502
56	S. America	North Chile	NZ\SA	-71.307	-21.965	79.5	77	-73.246	-34.290	80.5	78	1394
57	S. America	Central Chile	NZ\SA	-73.246	-34.290	80.5	78	-76.006	-45.659	78.7	80	1301
58	Patagonia	Whole margin	AN\SA,SC	-76.006	-45.659	21.3	93	-56.925	-60.565	10.8	94	2308
59	Patagonia	N. Patagonia	AN\SA	-76.006	-45.659	21.3	93	-76.483	-52.068	19.3	93	731
60	Patagonia	S. Patagonia	AN\SC	-76.483	-52.068	15.1	85	-56.925	-60.565	10.8	94	1577
61	South Shetland		AN\SL	-56.925	-60.565	10.0	150	-63.969	-62.422	10.0	156	435
62	South Sandwich		SA\SW	-26.071	-60.391	84.1	262	-28.647	-55.005	66.3	266	791
63	Mexico/Central America	Whole margin	RI,CO\NA,CA,PM	-106.890	21.799	13.6	21	-82.875	7.366	79.1	29	3185
64	Mexico/CA	Jalisco	RI\NA	-106.890	21.799	13.6	21	-105.247	18.762	36.3	50	396

No.	Subduction Zone	Segment	Plate pairs	Left_E_LONG	Left_N_LAT	Left_REL_VEL (mm/yr)	Left_REL_AZI (°)	Right_E_LONG	Right_N_LAT	Right_REL_VEL (mm/yr)	Right_REL_AZI (°)	Length (km)
65	Mexico/CA	Michoacan-Guatemala	CO\NA	-105.247	18.762	44.0	36	-90.898	12.584	78.8	33	1710
66	Mexico/CA	El Salvador-Nicaragua	CO\CA	-90.898	12.584	71.3	21	-86.648	10.235	80.0	23	546
67	Mexico/CA	Costa Rica-west Panama	CO\PM	-86.648	10.235	70.8	27	-82.875	7.366	79.1	29	533
68	Antilles		SA or NA\CA	-58.157	10.160	20.1	263	-63.360	19.691	17.0	263	1400
69	Manila		SU\PS	120.452	21.632	92.0	118	119.255	16.556	97.8	116	610
70	Philippine Trench		see notes	129.197	1.059	43.0	255	124.891	14.704	29.4	256	1633
71	East Luzon Trough		see notes	122.263	15.633	14.2	257	123.483	18.067	11.9	247	290
72	Cotabato Trench		see notes	123.500	7.000	18.8	76	125.150	5.600	18.2	78	250
73	Sulu Trench		see notes	122.500	8.660	18.9	72	119.607	6.333	19.4	76	445
74	Minahassa Trench		see notes	123.430	2.006	19.1	184	119.249	0.714	51.6	170	591
75	Seram Trough		BH\BS	132.717	-4.440	74.2	257	126.167	-2.750	66.1	267	815
76	Timor		BS\TI	132.689	-6.681	23.4	132	120.543	-7.812	35.4	149	1382
77	Manokwari Trench		PS\BH	132.515	0.017	21.8	206	129.197	1.059	15.0	210	389
78	Halmahera		MS\BH	126.426	1.706	100.9	116	125.969	-0.278	89.6	117	229
79	Kepulauan Sangihe		MS\SU	125.263	-0.446	16.5	288	126.426	1.706	5.0	264	282

Table 10.1 Continued.

No.	Subduction Zone	Segment	Dip (°)	Trench depth (km)	Updip_ pref (km)	Updip – min (km)	Updip – max (km)	Down-dip depth – pref (km)	Down-dip depth – min (km)	Down-dip depth – max (km)	Width – pref (km)	Width – min (km)	Width – max (km)	Coupling coefficient – pref
1	Alaska/Aleutians	Whole Margin	14	6	12	6	24	40	26	48	122	30	192	0.55
2	Alaska/Aleutians	Komandorski	15	5.5	10.5	5.5	24	35	25	45	95	30	153	0.5
3	Alaska/Aleutians	Western Aleutians	18	7	12	7	27	50	30	55	123	30	155	0.5
4	Alaska/Aleutians	Shumagin	14	6	11	6	16	26	20	32	62	30	107	0.2
5	Alaska/Aleutians	Semidi	14	6	11	6	24	30	25	50	79	30	182	0.7
6	Alaska/Aleutians	Kodiak	8	4.5	9.5	4.5	24.5	28	25	50	133	30	327	0.8
7	Alaska/Aleutians	Prince William Sound	6	4.5	14.5	4.5	24.5	42	25	50	263	30	435	0.8
8	Alaska/Aleutians	Yakataga	15	4	9	4	9	15	10	20	30	30	62	0.5
9	Cascadia		15	2.5	7.5	2.5	12.5	25	20	30	68	30	106	0.8
10	Japan/Kurile	Whole Margin	16	8	12	8	14	50	40	61	142	97	197	0.77
11	Japan/Kurile	Japan	15	7	7	7	7	50	40	65	166	128	224	0.7
12	Japan/Kurile	Kurile-Kamchatka	16	8	13	8	16	50	40	60	134	87	189	0.8
13	Kanto		15	1	6	1	9	25	20	30	73	43	112	0.9
14	Nankai/Ryukyu	Whole Margin	15	5	10	5	13	22	17	27	45	31	83	0.44
15	Nankai/Ryukyu	Nankai	15	3.5	8.5	3.5	11.5	25	20	30	64	33	102	0.9
16	Nankai/Ryukyu	Ryukyu	15	6	11	6	14	20	15	25	35	30	73	0.2
17	Izu-Bonin		15	7.5	12.5	7.5	15.5	35	25	45	87	37	145	0.2
18	Marianas		15	8	13	8	16	35	25	45	85	35	143	0.2
19	North Yap		15	7	12	7	15	35	25	45	89	39	147	0.2
20	Palau-South Yap		15	5	10	5	13	35	25	45	97	46	155	0.2
21	Hikurangi-Tonga-Kermadec	Whole margin	13	6	11	6	15	32	20	41	91	38	154	0.31

No.	Subduction Zone	Segment	Dip (°)	Trench depth (km)	Updip_ pref (km)	Updip – min (km)	Updip – max (km)	Down-dip depth – pref (km)	Down-dip depth – min (km)	Down-dip depth – max (km)	Width – pref (km)	Width – min (km)	Width – max (km)	Coupling coefficient – pref
22	H-K-T	Hikurangi	10	2.5	7.5	2.5	12.5	30	25	35	130	72	187	0.54
23	H-K-T	Kermadec	12	7	12	7	15	30	15	40	87	30	159	0.3
24	H-K-T	Tonga	17	8	13	8	16	35	25	45	75	31	127	0.2
25	Puysegur		15	5	10	5	13	35	30	45	97	66	155	0.7
26	Hjort		22	6	11	6	14	20	15	25	30	30	51	0.5
27	Solomons	Whole margin	26	3.6	8.6	3.6	11.6	40	35	60	72	53	129	0.70
28	Solomon	Northwest	26	6	11	6	14	40	35	60	66	48	123	0.7
29	Solomon	Southeast	26	2.5	7.5	2.5	10.5	40	35	60	74	56	131	0.7
30	New Hebrides	Whole Margin	24	6.0	11	6	14	31	25	35	51	33	74	0.37
31	New Hebrides	North	23	6	11	6	14	30	25	40	49	30	87	0.25
32	New Hebrides	Central	23	6	11	6	14	40	30	45	74	41	100	0.7
33	New Hebrides	South	23	6	11	6	14	30	25	40	49	30	87	0.25
34	New Hebrides	Matthew-Hunter	28	6	11	6	14	25	20	30	30	13	51	0.25
35	New Britain		26	6.5	11.5	6.5	14.5	40	30	50	65	35	99	0.7
36	New Guinea Trench	Whole Margin	15	3.6	8.6	3.6	11.6	35	25	45	102	52	160	0.70
37	NGT	East	15	3	8	3	11	35	25	45	104	54	162	0.7
38	NGT	West	15	4	9	4	12	35	25	45	100	50	158	0.7
39	Manus Tr.	Whole Margin	15	3.5	8.5	3.5	11.5	35	25	45	102	52	160	0.50
40	Manus Tr.	East	15	3.5	8.5	3.5	11.5	35	25	45	102	52	160	0.5
41	Manus Tr.	West	15	3.5	8.5	3.5	11.5	35	25	45	102	52	160	0.5
42	Andaman-Sunda Trench	Whole Margin	14	4.4	7.6	4.4	12.3	32	26	45	102	57	163	0.54
43	An-Sunda Tr.	Andaman	14	3	5	3	11	40	35	45	145	99	174	0.7
44	An-Sunda Tr.	Sumatra	14	5	10	5	13	35	25	50	103	50	186	0.8

No.	Subduction Zone	Segment	Dip (°)	Trench depth (km)	Updip_ pref (km)	Updip – min (km)	Updip – max (km)	Down-dip depth – pref (km)	Down-dip depth – min (km)	Down-dip depth – max (km)	Width – pref (km)	Width – min (km)	Width – max (km)	Coupling coefficient – pref
45	An-Sunda Tr.	Java	15	5	8	5	13	25	20	40	66	30	135	0.2
46	Calabria		20	4	10	4	12	45	40	60	102	82	164	0.5
47	Hellenic Tr.	Whole Margin	35	24	17	2.4	10.4	45	40	50	50	53	86	0.60
48	Hellenic	western segment	30	2	17	2	10	45	40	50	56	60	96	0.6
49	Hellenic	eastern segment	42	3	17	3	11	45	40	50	42	43	70	0.6
50	Cyprus	western segment	39	2	10	2	10	50	40	60	64	48	92	0.5
51	Cyprus	eastern segment	42	2	10	2	10	50	40	60	60	45	87	0.5
52	Makran		8	3	9	3	11	35	30	40	187	137	266	0.5
53	S. America	Whole Margin	14	5	10	5	13	50	40	60	172	116	236	0.80
54	S. America	Ecuador-Colombia	15	3	8	3	11	50	40	60	162	112	220	0.8
55	S. America	Peru	13	5	10	5	13	50	40	60	178	120	244	0.8
56	S. America	N. Chile	15	6	11	6	14	50	40	60	151	100	209	0.8
57	S. America	Central Chile	12	5	10	5	13	50	40	60	192	130	265	0.8
58	Patagonia	Whole Margin	15	4	9	4	12	35	25	45	100	50	158	0.5
59	Patagonia	North	15	4	9	4	12	35	25	45	100	50	158	0.5
60	Patagonia	South	15	4	9	4	12	35	25	45	100	50	158	0.5
61	South Shetland		15	3	8	3	11	35	25	45	104	54	162	0.5
62	South Sandwich		15	7	12	7	15	35	25	45	89	39	147	0.2
63	Mexico/Central America	Whole Margin	35	2.4	17	2.4	10.4	45	40	50	50	53	86	0.60
64	Mexico/CA	Jalisco	16	4	9	4	12	25	20	35	58	30	112	0.5
65	Mexico/CA	Michoacan-Guatemala	16	4	9	4	12	20	15	30	40	30	94	0.7

No.	Subduction Zone	Segment	Dip (°)	Trench depth (km)	Updip_ pref (km)	Updip – min (km)	Updip – max (km)	Down-dip depth – pref (km)	Down-dip depth – min (km)	Down-dip depth – max (km)	Width – pref (km)	Width – min (km)	Width – max (km)	Coupling coefficient – pref
66	Mexico/CA	El Salvador-Nicaragua	21	5	10	5	13	25	20	35	42	30	84	0.3
67	Mexico/CA	Costa Rica-west Panama	15	2.5	7.5	2.5	10.5	25	20	35	68	37	126	0.5
68	Antilles		15	4.5	9.5	4.5	12.5	35	25	45	99	48	156	0.5
69	Manila		15	4	9	4	12	35	25	45	100	50	158	0.15
70	Philippine		25	6	11	6	14	35	25	45	57	30	92	0.25
71	East Luzon Trough		20	5	10	5	13	35	25	45	73	35	117	0.5
72	Cotabato Trench		15	4	9	4	12	35	25	45	100	50	158	0.5
73	Sulu Trench		15	4	9	4	12	35	25	45	100	50	158	0.5
74	Minahassa Trench		15	3.5	8.5	3.5	11.5	35	25	45	102	52	160	0.5
75	Seram Trough		15	6	11	6	14	35	25	45	93	43	151	0.5
76	Timor		15	3	8	3	11	35	25	45	104	54	162	0.5
77	Manokwari Trench		15	4	9	4	12	35	25	45	100	50	158	0.5
78	Halmahera		15	2	7	2	10	35	25	45	108	58	166	0.5
79	Kepulauan Sangihe		15	2	7	2	10	35	25	45	108	58	166	0.5

Table 10.1 Continued.

No	Subduction Zone	Segment	Coupling coefficient – min	Coupling coefficient – max	Mmax – pref	Mmax – min	Mmax – max	B-value – pref	B-value – min	B-value – max
1	Alaska/Aleutians	Whole Margin	0.42	0.77	9.40	9.20	9.60	0.93	0.67	1.20
2	Alaska/Aleutians	Komandorski	0.30	0.70	8.40	8.00	8.80	0.95	0.70	1.20
3	Alaska/Aleutians	Western Aleutians	0.30	0.70	9.40	9.20	9.60	0.92	0.63	1.20
4	Alaska/Aleutians	Shumagin	0.10	0.70	7.93	7.50	8.35	0.95	0.70	1.20
5	Alaska/Aleutians	Semidi	0.60	0.90	8.50	8.34	8.50	0.95	0.70	1.20
6	Alaska/Aleutians	Kodiak	0.90	1.00	9.20	8.63	9.20	0.95	0.70	1.20
7	Alaska/Aleutians	Prince William Sound	0.90	1.00	9.20	9.00	9.20	0.95	0.70	1.20
8	Alaska/Aleutians	Yakataga	0.30	0.70	8.10	8.00	8.10	0.95	0.70	1.20
9	Cascadia		0.70	0.90	9.00	8.80	9.20	0.95	0.70	1.20
10	Japan/Kurile	Whole Margin	0.67	0.90	9.30	9.00	9.60	0.91	0.62	1.20
11	Japan/Kurile	Japan Trench	0.60	0.90	9.08	9.00	9.16	0.91	0.61	1.20
12	Japan/Kurile	Kurile-Kamchatka	0.70	0.90	9.30	9.00	9.60	0.92	0.63	1.20
13	Kanto		0.80	1.00	8.21	8.00	8.42	0.95	0.70	1.20
14	Nankai/Ryukyu	Whole Margin	0.34	0.80	8.95	8.50	9.41	0.91	0.61	1.20
15	Nankai		0.80	1.00	8.70	8.50	8.90	0.91	0.61	1.20
16	Ryukyu		0.10	0.70	8.54	8.00	9.09	0.91	0.61	1.20
17	Izu-Bonin		0.10	0.70	8.21	7.20	9.21	0.95	0.70	1.20
18	Marianas		0.10	0.70	8.34	7.20	9.48	1.08	0.68	1.47
19	North Yap		0.10	0.70	8.07	7.20	8.93	0.95	0.70	1.20
20	Palau-South Yap		0.10	0.70	8.02	7.20	8.83	0.95	0.70	1.20
21	Hikurangi-Kermadec-Tonga	Whole Margin	0.21	0.72	8.85	8.10	9.60	0.95	0.70	1.21
22	H-K-T	Hikurangi	0.40	0.70	8.50	8.00	9.00	0.95	0.70	1.20
23	H-K-T	Kermadec	0.20	0.75	8.76	8.10	9.42	0.96	0.70	1.21

No	Subduction Zone	Segment	Coupling coefficient – min	Coupling coefficient – max	Mmax – pref	Mmax – min	Mmax – max	B-value – pref	B-value – min	B-value – max
24	H-K-T	Tonga	0.10	0.70	8.58	8.00	9.17	0.96	0.70	1.21
25	Puysegur		0.50	0.80	8.43	7.80	9.07	0.95	0.70	1.20
26	Hjort		0.30	0.70	7.78	7.20	8.36	0.95	0.70	1.20
27	Solomon	Whole Margin	0.60	0.80	8.70	8.10	9.31	0.90	0.60	1.20
28	Solomon	Northwest	0.60	0.80	8.36	8.10	8.62	0.90	0.60	1.20
29	Solomon	Southeast	0.60	0.80	8.60	8.10	9.09	0.90	0.60	1.20
30	New Hebrides	Whole Margin	0.27	0.73	8.83	8.30	9.37	0.90	0.60	1.20
31	New Hebrides	North	0.15	0.70	8.02	7.60	8.44	0.90	0.60	1.20
32	New Hebrides	Central	0.6	0.80	8.50	8.30	8.70	0.90	0.60	1.20
33	New Hebrides	South	0.15	0.70	8.12	7.60	8.64	0.90	0.60	1.20
34	New Hebrides	Matthew-Hunter	0.15	0.70	8.19	8.00	8.39	0.90	0.60	1.20
35	New Britain		0.60	0.80	8.41	8.00	8.82	0.90	0.60	1.20
36	New Guinea Trench	Whole Margin	0.60	0.80	8.78	8.20	9.37	0.95	0.70	1.20
37	New Guinea Trench	East	0.60	0.80	8.25	7.60	8.90	0.95	0.70	1.20
38	New Guinea Trench	west	0.60	0.80	8.61	8.20	9.03	0.95	0.70	1.20
39	Manus	Whole Margin	0.30	0.70	8.50	7.50	9.50	0.95	0.70	1.20
40	Manus	East	0.30	0.70	8.28	7.50	9.07	0.95	0.70	1.20
41	Manus	West	0.30	0.70	8.31	7.50	9.13	0.95	0.70	1.20
42	Andaman-Sunda Trench	Whole Margin	0.44	0.79	9.30	9.00	9.60	0.94	0.67	1.20
43	Andaman-Sunda	Andaman	0.60	0.80	9.30	9.00	9.55	0.94	0.67	1.20
44	Andaman-Sunda	Sumatra	0.70	0.90	9.20	9.00	9.40	0.94	0.67	1.20
45	Andaman-Sunda	Java	0.10	0.70	8.61	7.80	9.42	0.94	0.67	1.20
46	Calabria		0.30	0.70	7.74	7.10	8.38	0.95	0.70	1.20
47	Hellenic Trench	Whole margin	0.20	1.00	8.50	8.00	9.00	0.95	0.69	1.20
48	Hellenic	western segment	0.20	1.00	8.37	8.00	8.74	0.95	0.69	1.20

No	Subduction Zone	Segment	Coupling coefficient – min	Coupling coefficient – max	Mmax – pref	Mmax – min	Mmax – max	B-value – pref	B-value – min	B-value – max
49	Hellenic	eastern segment	0.20	1.00	8.21	8.00	8.42	0.95	0.69	1.20
50	Cyprus	western segment	0.30	0.70	8.00	7.50	8.49	0.95	0.70	1.20
51	Cyprus	eastern segment	0.30	0.70	7.89	7.50	8.29	0.95	0.70	1.20
52	Makran		0.30	0.70	8.71	8.10	9.33	0.95	0.69	1.20
53	South America	Whole Margin	0.70	0.90	9.55	9.50	9.60	0.88	0.56	1.20
54	S. America	Ecuador-Colombia	0.70	0.90	9.14	8.80	9.49	0.95	0.70	1.20
55	S. America	Peru	0.70	0.90	9.30	9.00	9.60	0.87	0.53	1.20
56	S. America	N. Chile	0.70	0.90	9.05	8.60	9.49	0.87	0.53	1.20
57	S. America	Central Chile	0.70	0.90	9.51	9.50	9.53	0.87	0.53	1.20
58	Patagonia	Whole Margin	0.30	0.70	8.80	8.00	9.60	0.95	0.70	1.20
59	Patagonia	North	0.30	0.70	8.50	8.00	9.00	0.95	0.70	1.20
60	Patagonia	South	0.30	0.70	8.72	8.00	9.45	0.95	0.70	1.20
61	South Shetland		0.30	0.70	8.11	7.50	8.71	0.95	0.70	1.20
62	South Sandwich		0.10	0.70	8.26	7.50	9.01	1.09	0.70	1.48
63	Mexico/Central America	Whole Margin	0.37	0.81	8.90	8.20	9.60	0.91	0.62	1.20
64	Mexico/CA	Jalisco	0.30	0.70	8.34	8.20	8.49	0.89	0.58	1.20
65	Mexico/CA	Michoacan-Guatemala	0.50	0.90	8.61	8.00	9.23	0.89	0.58	1.20
66	Mexico/CA	El Salvador-Nicaragua	0.10	0.70	8.29	8.00	8.58	0.95	0.70	1.20
67	Mexico/CA	Costa Rica-west Panama	0.30	0.70	8.20	7.70	8.71	0.95	0.69	1.20
68	Antilles		0.30	0.70	8.69	8.00	9.37	0.92	0.64	1.20
69	Manila		0.05	0.70	8.25	7.60	8.90	0.95	0.70	1.20
70	Philippine		0.10	0.75	8.45	7.60	9.30	0.94	0.68	1.20
71	East Luzon Trough		0.30	0.70	7.84	7.30	8.38	0.95	0.70	1.20
72	Cotabato Trench		0.30	0.70	8.19	8.00	8.38	0.95	0.70	1.20

No	Subduction Zone	Segment	Coupling coefficient – min	Coupling coefficient – max	Mmax – pref	Mmax – min	Mmax – max	B-value – pref	B-value – min	B-value – max
73	Sulu Trench		0.30	0.70	8.36	8.00	8.72	0.95	0.70	1.20
74	Minahassa Trench		0.30	0.70	8.39	7.90	8.89	0.95	0.70	1.20
75	Seram Trough		0.30	0.70	8.50	8.00	9.04	0.95	0.70	1.20
76	Timor		0.30	0.70	8.00	7.50	9.38	0.95	0.70	1.20
77	Manokwari Trench		0.30	0.70	8.12	7.60	8.64	0.95	0.70	1.20
78	Halmahera		0.30	0.70	8.33	8.30	8.35	0.95	0.70	1.20
79	Kepulauan Sangihe		0.30	0.70	8.39	8.30	8.47	0.95	0.70	1.20

Table 10.2 Compilation of published subduction interface zone b-values.

“Bayrak” values are from Bayrak et al. (2002), “Hayes” values were calculated by Gavin Hayes (USGS) as part of this GEM exercise, and the superscripts on the b-values in the “other” column refer to the following papers: ¹Power et al. (2012); ²Cao and Gao (2002), ³Suckale and Grünthal (2009); ⁴Ghosh et al. (2008), ⁵Bird and Kagan (2004) (which uses all shallow seismicity including plate-bending earthquakes); ⁶Molchan et al. (1997) (note on Molchan et al. (1997); we use the b-values determined from mainshocks only, see their Table 1).

Subduction Zone	Bayrak	Hayes	other
Aleutian Trench	0.63	0.94	
Middle America Trench/Mexico	0.58	0.69	
Antilles Trench	0.64		
Peru-Chile Trench	0.53	0.71	
Tonga Trench	0.72	1.21	
Kermadec Trench		1.21	1.12 ¹
South Sandwich Trench	0.74	1.48	
Hellenic Trench	0.69		
Makran Trench	0.78		
Sunda Trench (Sumatra-Java)	0.67	0.69	
Philippine Trench	0.68	0.84	
Nankai Trough/Ryukyu Trench	0.61	0.9	
Kurile Trench	0.63	0.81	
Japan Trench	0.61	0.81	0.73-0.86 ²
Mariana Trench	0.68	1.47	
New Hebrides	0.6	0.95	0.71 ³
Solomon Islands/New Britain	0.6	0.95	
Costa Rica		0.69	1.06 ⁴
Global Subduction Zones			0.96 ⁵
Global Subduction zones (<15 km)			0.93 ⁶
Global Subduction zones (16-33 km)			0.63 ⁶
Global Subduction zones (34-70 km)			0.83 ⁶

10.4 Discussion and Conclusions

Subduction zone earthquakes release approximately 90% of the long-term seismic moment outside of collision belts (Bird and Kagan, 2004). Here, we have reported on the development of a globally consistent characterisation of the world's subduction plate boundary interfaces. This can be used by seismic hazard analysts as a basis for generating earthquake event sets for inclusion in earthquake hazard and risk modelling.

In this report we assess the parameters associated with the plate interface itself and do not include seismicity within the down-going plate or overriding plate. To accurately estimate the total hazard associated with subduction zones, one also needs to consider plate-bending earthquakes and earthquakes associated with deformation of the down-going plate before it enters the subduction zone – so-called 'outer rise' events, as well as events occurring in the upper plate. These are outside of the scope of this report.

Using geophysical data, supplemented by the past history of earthquakes in subduction zones, a database has been developed to derive earthquake event sets on any segment of the globe's 55,000-km-long subduction interface zones. We have defined the likely maximum magnitude earthquake that could occur, the ratio of small to large earthquakes typical of each region (the Gutenberg-Richter b-value), a seismic coupling coefficient, and the relative plate velocity. Event sets for any subduction zone can then be created from these, consistently-derived, simple parameters.

The maximum magnitude of each subduction zone is based on its total length (McCaffrey, 2008). If the total length of the subduction zone exceeds what can realistically rupture with the generally accepted maximum magnitude around Mw 9.6 (e.g., Kagan and Jackson, 2013; Rong et al., 2014) then the Mmax is capped at this. When implemented, we propose that the earthquake event sets should 'float' along the whole subduction zone in the manner developed by Parsons et al. (2012) for the Nankai Trench in Japan, with the moment rate balanced against the convergence rates, coupling coefficients.

In this database we have defined suitably large uncertainties to encompass the plausible range of values to the input parameters and thus envelope the hazard posed by the subduction interface seismic zones. The database thus derived suggests that earthquakes above Mw 9 could be expected in as many 50% of the global subduction zones and their possible segments, consistent with the growing awareness that the historic period has been too short to accurately characterise the largest earthquakes on many of the subduction interface zones worldwide.

10.5 Definition of Database Parameters

Subduction Zone: Name of subduction zone

Segment: Name of segment of the subduction zone. Note that these segments are not necessarily intended to represent rupture segments. They are largely chosen where a change in plate motion rate and azimuth undergoes a change, due to a change in the plate pairs that are juxtaposed at the boundary. The main exception to this is Alaska, where we define segments similar to the most recent USGS seismic hazard model for Alaska (Wesson et al., 2007).

Plate pairs: These are the plate pairs used in the calculation of convergence rate and azimuth on the subduction zone. In all cases, except where specified with an asterisk (*) in Table 10.1 the plate abbreviations conform to the tectonic model of Bird (2003), referred to as PB2002 for the remainder of these notes. Where there are exceptions, we detail those within the supplementary notes.

Left_E_LONG, Right_E_LONG: The longitude of the left- and right-hand sides (respectively) of the trench for the segment in this row. NOTE: The left and right hand endpoints of the trench are defined with an arbitrary

convention such that when the subduction zone is rotated so that the trench is at the bottom, the volcanic arc is at the top, and the subducting plate moves relatively upward on the map.

Left_N_LAT, Right_N_Lat: The Latitude of the left- and right-hand sides (respectively) of the trench for this segment.

Left_REL_VEL, Right_REL_VEL: Horizontal relative plate velocity in mm/yr, on the left- and right-hand sides (respectively) of the trench, using the Plate pairs described in the Plate pairs column of Table 10.1. Unless otherwise noted (in the following notes) these relative plate velocities are derived from PB2002. If a source other than PB2002 is used, we detail the source in these notes.

Left_REL_AZI, Right_REL_AZI: Azimuth of relative plate convergence (on the left- and right-hand sides, respectively) assuming a fixed overriding plate. Azimuths are listed in degrees clockwise from local north. Unless otherwise noted in Appendix B these relative convergence azimuths are derived from PB2002. If a source other than PB2002 is used, we detail the source in these notes.

Length: Distance along trench between segment endpoints (in km).

Dip: Average dip angle for the seismogenic portion of the segment. Unless otherwise noted (see additional notes in Appendix B), the dips are determined from Hayes et al. (2012) database of global subduction zone geometries. Where we have no information about the dip angle, we use a default value of 15°.

Trench depth: Vertical distance (in km) of the trench from mean sea level.

Up-dip depth (Pref, Min, Max): Vertical distance (in km below sea level) to the up-dip limit of seismic rupture on the subduction interface (with preferred, minimum, and maximum values). In all cases, we use the intersection of the trench with the Earth's surface as a default "Up-dip depth-min" estimate, to account for the possibility that rupture to the trench cannot be ruled-out anywhere. We use 5 km below the intersection of the subduction interface and the seafloor as a default preferred value, and 8 km as a default maximum value where no other information is available. Where we use values that depart from these assumptions, we explain our choices in these notes. Where possible we use depths below sea level derived from Hayes et al. (2012) database of global subduction zone geometries.

Down-dip depth (Pref, Min, Max): Vertical distance (in km below sea level) to the down-dip limit of seismic rupture on the subduction interface (with preferred, minimum, and maximum values). For subduction zones where we do not have knowledge of this, we assume a default value of 35 ± 10 km. Where we use a value that departs from this assumption, we justify this in these notes. Where possible we use depths below sea level derived from Hayes et al. (2012) database of global subduction zone geometries.

Down-dip width (Pref, Min, Max): is the width along the dip of the interface (in km) of the seismogenic portion of the subduction interface. This is calculated using the interface dip, up-dip depths, and down-dip depths in previous columns.

Coupling Coefficient (Pref, Min, Max): is the seismic coupling coefficient (preferred, minimum, and maximum values) for the subduction interface segment. Coupling coefficient is the proportion of relative plate motion that will be eventually accommodated as seismic slip. Ideally, this is best determined from the knowledge of historic and prehistoric subduction interface ruptures, but the short records for most subduction zones do not allow a meaningful determination in this fashion. Therefore, where the megathrust locking ratio (the ratio of slip deficit rate to plate convergence rate) is available from interpretation of geodetic measurements (see Appendix B for delineation of which margins geodetic coupling estimates are available for), we use this value as a proxy for the seismic coupling coefficient. We are mindful of the fact that the physical meaning of the locking ratio and its relationship with the long-term seismic coupling coefficient is still uncertain, but we are not aware of other, better

ways of defining the coupling coefficient at present. For each subduction zone we outline the sources of data used for the choice of coupling coefficients. At many subduction zones, it is not possible to determine coupling coefficients, either due to a lack of geodetic data, and/or a lack of sufficient historical seismicity data. We assign reasonably large uncertainties to those coupling coefficients. For subduction zones where the coupling coefficient is highly uncertain, we use a default value of 0.5 ± 0.2 . We also do not allow the maximum coupling coefficient for any subduction zone to be less than 0.7, even when independent data (geodetic, historical seismicity) exists to help constrain this. This is to help incorporate our current lack of understanding of the relevance of contemporary estimates of coupling (from geodetic and historic seismicity studies) to the long-term subduction plate interface earthquake behaviour.

Mmax (Pref, Min, Max): the Maximum Magnitude earthquake expected for the subduction segment. For all segments, we assume a default maximum Mmax based on rupture length of the entire segment (or combination of segments), using the relationship between segment length and magnitude in McCaffrey (2008). The minimum Mmax value is taken as the largest earthquake observed in the historical record on that segment. For the preferred value, we take the average of the minimum and maximum Mmax values. For subduction zones where little or no seismicity or paleoseismological data exist to constrain Mmax, we generally assume 7.5 as a minimum Mmax. For all magnitudes discussed here, we use the moment magnitude scale of Hanks and Kanamori (1979).

b-value (Pref, Min, Max): Our understanding of b-values at subduction megathrusts is incomplete, and estimates from individual subduction zones range from ~ 0.6 to >1.2 (see Table 10.1). To encompass this uncertainty, we assume a minimum b-value for all subduction zones of 0.7, and a maximum of 1.2. In cases where published studies have estimated b-values that are less than 0.7, or exceed 1.2, we use the published values to inform the minimum or maximum value in our table.

10.6 Additional notes on parameter choices for specific subduction zones/segments

*Note that the subduction zones/segments are not necessarily ordered in an identical manner as Table 10.1.

10.6.1 Alaska/Aleutian

Most of the parameter values we use in the spreadsheet are derived from Wesson et al. (2007). However, the coupling coefficients, dips, and down-dip limits for the Shumagin, Semidi, and Kodiak segments are derived directly from geodetic studies of Fournier and Freymueller (2007; their fault planes 3 and 4 combine to form the Shumagin segment, while plane 2 is the Semidi segment and plane 1 is the western part of the Kodiak segment). For the maximum down-dip limit we assume the maximum value in Wesson et al. (2007), and for the Kodiak and Semidi segments we assume a sigma on the coupling coefficient of 0.1. For the Prince William Sound segment, we base the minimum and maximum seismogenic depths (and their uncertainties) on the Mw 9.2 1964 Prince William Sound earthquake. Due to this segment's propensity to produce megathrust earthquakes Mw > 9.0 , we assign a high coupling coefficient for this segment as well. Note that the segments are largely defined for kinematic and plate boundary geometry purposes; multiple segment rupture is possible and will be considered in any model.

The Wesson et al. (2007) report precedes the recent subduction margin studies which entertain the possibility of larger earthquakes than has been observed historically (e.g., McCaffrey, 2008). Therefore, in this report, we suggest it is prudent to allow for the possibility of larger ruptures than have occurred historically, which largely forms the basis of the Wesson et al. (2007) study. We indicate this in Table 10.1 as 'whole margin' rupture, but in fact the total length of the margin is longer than reasonably associated with the upper bound Mmax of 9.6. Therefore, we recommend that hazard analysts consider a logic tree approach and provide some weight to a model where earthquakes up to Mw 9.6 could occur anywhere along the

Alaska-Aleutian subduction zone, and event sets respect the available seismic moment noting variation in coupling coefficient, convergence rates and small variation in b-value along the length of the subduction zone.

10.6.2 Cascadia

For down-dip depth and M_{max} , we use values consistent with Frankel and Petersen (2007), and references therein. Based on geodetic evidence for high interseismic coupling coefficients on the megathrust (relevant studies discussed in Frankel and Petersen, 2007), we assign a high coupling coefficient (0.8 ± 0.1).

10.6.3 Japan

The coupling coefficients and seismogenic depths are based on interseismic modelling of geodetic data (Nishimura et al., 2004a; Hashimoto et al., 2009), and the updip limit and minimum M_{max} values are based on the recent Mw 9.0 Tohoku earthquake.

10.6.4 Kanto

The coupling coefficients and down-dip limit of the seismogenic zone are based on interseismic modelling of geodetic data (Nishimura et al., 2007), and the maximum rupture depth of the 1923 M 7.9 Kanto earthquake (e.g., Wald and Somerville, 1995). The minimum M_{max} value is based on the estimated M 8.0 Genroku earthquake in 1703.

10.6.5 Nankai

The down-dip limit of the Nankai Trough seismogenic zone is based on models of rupture in previous great earthquakes there (Ando, 1975; Sagiya and Thatcher, 1999) and models of interseismic coupling (Ito and Hashimoto, 2004). High coupling coefficients are justified on the basis of the interseismic coupling models from GPS and the large amount of plate boundary slip required in historic great earthquakes at the Nankai Trough. The minimum M_{max} (8.5) is based on the largest historic events observed at the Nankai Trough, which involved simultaneous rupture of all segments of the Nankai Trough in a single event (Ando, 1975).

10.6.6 Kurile

Due to the propensity of this subduction zone to produce Mw 8.0 -9.0 earthquakes, we assign a high coupling coefficient. A minimum M_{max} of 9.0 is used based on the largest historical earthquake on this subduction zone (the 1952 earthquake). However, due to the great length of this subduction zone, it certainly may be capable of generating larger events.

10.6.7 Ryukyu

Despite the very high convergence rates at the Ryukyu Trench (up to 130 mm/yr) no large historical earthquakes have occurred here (e.g., larger than Mw 8.0). Thus, we assign a relatively low coupling coefficient to the Ryukyu Trench. GPS measurements from Kyushu and the Ryukyu arc also suggest little or no interseismic coupling on the Ryukyu Trench (Nishimura et al., 2004b; Wallace et al., 2009a), although this is particularly difficult to resolve for most of the Ryukyu Trench due to the distance of land-based geodetic studies from portions of the thrust that could undergo interseismic locking (Ando et al., 2009). The largest historic earthquake thought to be on interface occurred in 1911 and is estimated to be M 8.0 (Utsu, 1989). The upper plate is rifted continental margin crust so we also include a relatively shallow down-dip limit to the seismogenic zone.

10.6.8 Izu-Bonin

No historic earthquakes larger than Mw 7.2 have been observed on the Izu-Bonin Trench. Due to the lack of significant historical subduction thrust events (and a prevalence of more frequent moderate magnitude events), we assign a low coupling coefficient (0.2 ± 0.1).

10.6.9 Mariana

No historic underthrusting earthquakes larger than Mw ~ 7.2 have been observed along the Mariana Trench. Due to the lack of significant historical subduction thrust events (and a prevalence of more frequent moderate magnitude events), we assign a low coupling coefficient (0.2 ± 0.1).

10.6.10 North Yap, and Palau/South Yap

Little is known about the seismogenic potential of these trenches. We assign similar values as for the Izu-Bonin-Marianas Trench. Convergence rates used are from DeMets et al. (2010), which has a more up to date Philippine Sea Plate model.

10.6.11 Hikurangi

The parameters for the Hikurangi subduction zone are largely derived from Wallace et al. (2004a; 2009b) and from the inputs for the Hikurangi subduction source to the updated New Zealand national seismic hazard model (Stirling et al., 2012). Although we treat the Hikurangi Trough as a single source in this spreadsheet, in the New Zealand seismic hazard model, it is treated as 3 segments, where the southern Hikurangi segment has a higher coupling coefficient than the central and northern segments. For the purposes of this study, we average the coupling coefficients over the length of the margin. The M_{\max} preferred is based on a plausible scenario where rupture of the entire southern Hikurangi segment occurs, which is currently interseismically coupled over a large area. The maximum M_{\max} is based on a scenario where rupture of the entire Hikurangi margin occurs in a single event, which would produce an Mw ~ 9.0 (Wallace et al., 2009b; Stirling et al., 2012). Convergence rates at each end of the trench are derived from the relative motion between the forearc blocks of the Hikurangi margin relative to the subducting Pacific Plate (Wallace et al., 2004a, 2009b).

10.6.12 Kermadec

Most of the values for the Kermadec Trench are taken from Power et al. (2011). The convergence rates at the Kermadec Trench are for the Kermadec Arc relative to the Pacific Plate, and are based on elastic block modelling of a GPS velocity from a site in the Kermadec Islands (Raoul Island) and earthquake slip vectors and transform orientations from events on the Kermadec Trench and in the Havre Trough (respectively) (Power et al., 2011). The preferred down-dip limit of rupture and the maximum coupling coefficient (0.8) are based on the depth of interseismic coupling on the megathrust in the Kermadec Islands (locking on the down to 30 km depth is required to fit GPS data from Raoul Island) (Power et al., 2011). We use a lower preferred coupling coefficient (0.3), given the possibility that the coupling observed from GPS data at Raoul Island is not representative of coupling on the Kermadec Trench elsewhere. The dip is based on the average dips of the interface estimated from seismic surveys of the Kermadec Trench (Scherwath et al., 2008). The minimum M_{\max} of 8.1 is based on the estimated magnitude of the largest historical event on the Kermadec Trench, occurring in May 1917 (see Power et al., 2011).

10.6.13 Tonga

The convergence rates we prescribe for the Tonga Trench reflect motion between the Tonga arc and the subducting Pacific plate; these are based on results from elastic block modelling of GPS velocities and earthquake slip vectors (Wallace et al., 2005b). Despite the very high convergence rates at the Tonga Trench (up to 250 mm/yr) no earthquakes larger than Mw 8.0 have occurred here and abundant Mw 6.0-8.0 events have occurred on the subduction interface. Thus, we assign a relatively low preferred coupling coefficient to the Tonga Trench. The largest historical earthquake on the Tonga Trench was an Mw 8.0 in 2009 (Beavan et al., 2010b; Lay et al., 2010), so we use this as a minimum M_{max} value, given that the historical record is short and it is likely that earthquakes larger than Mw 8.0 are possible.

10.6.14 Puysegur

The Mw 7.8 Dusky Sound earthquake in July 2009 is the largest subduction thrust event recorded at the Puysegur Trench. We base our preferred down-dip rupture limits on GPS observations that show slip down to 35 km depth in the event (Beavan et al., 2010). We use an upper limit on the rupture depth of 45 km, where postseismic slip was observed following the 2009 earthquake (Beavan et al., 2010a). For the minimum M_{max} value, we assume Mw 7.8 based on the Dusky Sound earthquake. High interseismic coupling was observed on the Puysegur Trench in the region of the Dusky Sound earthquake prior to that event (Wallace et al., 2007), so we assume a relatively high coupling coefficient, but acknowledge that this has a large uncertainty due to the short historical record and the lack of geodetic coverage above much of the Puysegur subduction zone.

10.6.15 Hjort

Subduction of the Macquarie Plate beneath the Pacific Plate is accommodated at the Hjort Trench. Relative motion between the Macquarie Plate and the Pacific Plate is low, and we use the estimates of DeMets et al. (2010). Meckel et al. (2005) divide the trench into two portions: Northern Hjort (55.5°S-57.5°S) and Southern Hjort (57.5S-59.5S). Meckel et al. (2003) postulate a low angle oblique-slip fault at the Hjort Trench (between 55-58°S), dipping $\sim 10^\circ$, at least down to 10 km (based on gravity data and seismic reflection data). Below 10 km, it is likely that the geometry of the fault steepens. At the southernmost part of the Hjort trench (59.5 deg S), Meckel et al. (2003) suggest that the Trench likely steepens (to $\sim 45^\circ$). We assume 22° average dip to encompass this range of steep to shallow dip values. Meckel et al. (2003; 2005) suggest that there has only been a small amount of underthrusting of the Macquarie Plate, so we restrict the down-dip limit of any ruptures to ~ 20 km depth. Very little historical seismicity has been observed in the region of the Hjort Trench, with no events larger than Mw 7.2.

10.6.16 Northwest Solomon

This segment comprises the eastern end of the New Britain Trench adjacent to Bougainville, and north of the triple junction between the Woodlark, Pacific, and Australian Plates. Clusters of Mw 7.3-8.1 earthquakes have been observed in the northwest Solomons approximately every 30 years for the last century (Lay and Kanamori, 1980). More recently, the 2007 Mw 8.1 earthquake ruptured the southern half of this segment (as well as the northern part of the San Cristobal Trench, south of the triple junction.) We define a minimum M_{max} of 8.1, consistent with historical seismicity. We use relatively high coupling coefficients for this subduction source (0.7 ± 0.1) based on the large (Mw >8.0) that occur along this trench on a relatively regular basis.

10.6.17 Southeast Solomon

This segment comprises the San Cristobal Trench, east of the triple junction between the Woodlark, Pacific, and Australian Plates. The eastern boundary of this source is where a 90° turn is taken in the orientation of the trench near Vanuatu. Overall, we use similar values for this subduction segment to those used for the northwest Solomons. Possibilities for simultaneous rupture across northwest and southeast Solomons segments must also be accounted for, as was observed to occur during the 2007 Mw 8.1 earthquake (Taylor et al., 2008a).

10.6.18 New Hebrides

The New Hebrides Trench is divided into four segments, northern, central, southern, and the Matthew-Hunter segment. Scenarios involving rupture across the first three segments should be considered. The relative motion at the New Hebrides trench is determined by elastic block modelling of GPS velocities and earthquake slip vectors (Power et al., 2011). The relative motion at the central and southern New Hebrides segments are the New Hebrides forearc/arc blocks relative to the subducting Australian Plate, while the relative motion at the Matthew-Hunter segment reflects the motion of the Matthew and Hunter Islands relative to the Australian Plate. The northern segment reflects motion between the Australian and Pacific Plates. GPS models of interseismic coupling suggest deep, high interseismic coupling along the northern New Hebrides segment, while interseismic coupling appears lower on the southern New Hebrides segment. The degree of interseismic coupling on the Matthew Hunter segment is not well-resolved. We use the down-dip limit of interseismic coupling on the central New Hebrides segment (Power et al., 2011) to define our preferred down-dip limit in that area. We make the down-dip limit on the southern and northern segment slightly shallower due to the lack of geodetic evidence for deep interseismic coupling. Much of the upper plate for the Matthew Hunter segment is recently rifted oceanic crust (related to north Fiji Basin development), so the depth to the down-dip limit of possible rupture is likely to be lower than for the north and south New Hebrides segments. Using subduction thrust events on the Matthew Hunter segment, Power et al. (2011) estimate a b-value of 0.74, which we use as the minimum value for this segment. The largest historical earthquake on the Matthew Hunter segment (in 1901) is estimated at Mw 8.4, although the data are somewhat ambiguous (see review in Power et al., 2011), so we use this for our preferred Mmax value and Mw 8.0 as our minimum Mmax value. The Mmax in a PSHA model developed for Vanuatu (Suckale and Grünthal, 2009) is Mw 8.3 for the northern segment, and Mw 7.6 for the southern segment. These Mmax values are based on historical data, so we adopt these as our minimum Mmax value. The slab is difficult to define in the Matthew Hunter segment due to the relatively lower level of seismicity there, so we adopt an average dip of 28° for the Matthew Hunter segment, following the slab geometry model developed by Power et al. (2011).

10.6.19 New Britain

We consider the western end of the New Britain Trench as the point where the Ramu Markham Fault goes offshore near Lae, Papua New Guinea. The eastern end is the cusp in the New Britain Trench where it bends strongly to the southeast near 153°E. Convergence rates at the New Britain Trench reflect motion of the Woodlark Plate relative to the South Bismarck Plate using poles of rotation from Wallace et al. (2004b). This subduction zone is very seismically active, with frequent moderate to large events. The largest historical subduction interface earthquakes that have occurred on the New Britain Trench have been Mw ~8.0 (e.g., Park and Mori, 2007), so we use this as our minimum Mmax estimate. Due to the occurrence of some subduction thrust events down to ~40 km depth (Park and Mori, 2007) we use this as the preferred down-dip

limit of seismogenic zone. Due to the similarities in the level of seismicity and tectonic setting as the San Cristobal Trench offshore the Solomon Islands, we use the same coupling coefficients.

10.6.20 New Guinea

The eastern half of the New Guinea Trench accommodates southwest subduction of the Pacific, North Bismarck, and/or Caroline Plates (note that the motion of all three plates is very similar) beneath the north coast of the island of New Guinea. To determine the rate of convergence on the eastern half, we use the pole of rotation of the Pacific Plate relative to the New Guinea Highlands (NGH) plate from Wallace et al. (2004b). The relative motion in western half of the New Guinea Trench reflects motion between the Caroline Plate and the Bird's Head Block (e.g., Bird, 2003). We thus divide the New Guinea trench into two segments reflecting this. The largest historic event on the eastern part of the New Guinea Trench was Mw 7.6 in 2002 (Tregoning and Gorbatov, 2004), while the largest historic event on the western segment was the Biak earthquake in 1996 (Mw 8.2). The shallow geometry of the slab subducting at the New Guinea Trench is not well known. We assume a 30 km maximum down-dip limit for seismogenesis, and an average dip of 15°.

10.6.21 Manus (east and west)

The Manus trench accommodates very slow southward subduction of the Pacific and Caroline Plates beneath the north Bismarck Plate. Very little is known about the seismogenic potential of this feature, and whether or not it is truly a subduction zone. Thus, we largely use default values to parameterize this source. In absence of any major historical subduction thrust earthquakes on this trench, we assume a minimum M_{max} of 7.5 here.

10.6.22 Andaman

We base many of our Andaman source parameters on geodetic and seismological studies of coseismic slip in the 2004 Mw 9.0-9.3 earthquake that ruptured along much of the Andaman Trench. The 2004 earthquake is the largest earthquake documented along the Andaman trench. We assign the northern and southern boundaries of this source coincide with the limits of rupture in the 2004 earthquake. We assume average dips (14°) and widths (~150 km), and depths (~40 km) of the source that are consistent with GPS studies of coseismic deformation in the earthquake (Subaraya et al., 2006). Based on the large tsunami produced in this event, we assume the updip limit of rupture to be within 2 km seafloor, with a maximum value of 5 km depth. We also assume a relatively high coupling coefficient, given the proven ability of this trench to produce large slip that helps to accommodate a major proportion of the plate motion budget.

10.6.23 Sumatra

Abundant seismological, paleoseismic and geodetic data (see reviews in Subaraya et al., 2006; McCaffrey, 2009; and Prawirodirdjo et al., 2010) exist to help constrain the source we use for the thrust accommodating subduction of the Indo-Australian Plate beneath Sumatra. The largest observed historical earthquake on this source segment was a Magnitude 9.0 in 1833, which we use as a minimum estimate for our M_{max} . Depending on the geometry of the subduction thrust, maximum interseismic coupling depths (and we assume maximum rupture depths) are 25-50 km depth (Prawirodirdjo et al., 2010). Interseismic coupling values from geodetic studies are close to one, so we assume high interseismic coupling for this segment in this study.

10.6.24 Java

The largest historic subduction thrust events to occur at the Java Trench were the 1994 and 2006 Mw 7.8 earthquakes (Abercrombie et al., 2001; Ammon et al., 2006), the former caused a much larger tsunami than expected from its magnitude. The main slip in the 1994 earthquake occurred at ~20 km depth, which we assume as a minimum estimate for the down-dip limit of slip in earthquakes on this segment. We assume a slightly deeper depth (25 km) as our preferred down-dip limit estimate, and account for the possibility that even deeper rupture could occur (by assuming a maximum down-dip limit of 40 km). Much of the Java Trench is thought to be dominated by aseismic creep, rather than deep interseismic coupling (in contrast to Sumatra), so we assume a low coupling coefficient for this source. Fujii and Satake (2006) estimate very shallow propagation of the 2006 rupture, based on interpretation and modelling of tsunami observations from that event, justifying our choice of a shallow updip limit for the seismogenic zone.

10.6.25 Calabria

Most geometric and kinematic parameters of this source are drawn from the European Database of Seismogenic Faults (EDSF) (Basili et al., 2013a) and literature review by Basili et al. (2013b). According to GPS velocities and current plate models, relative motion between the subducting Africa plate and the European plate at the Calabria margin results in a convergence rate of 2-5 mm/y (D'Agostino and Selvaggi, 2004; Devoti et al., 2008; Serpelloni et al., 2010; D'Agostino et al., 2011). Very little is known about the seismogenic potential of the slab interface in the Calabrian arc. We largely use default seismic values for this source. However, there was a historic earthquake in 1905 with Mw 7.1, doubtfully associated with the subduction, which we take as the lower end of our Mmax range.

10.6.26 Hellenic

Most geometric and kinematic parameters of this source are drawn from the EDSF (Basili et al., 2013 a) and literature review by Basili et al. (2013b). According to GPS velocities and current plate models (e.g., Reilinger et al., 2006; Ganas and Parsons, 2009), in the western part of the arc relative motions result in a convergence rate of 35 mm/y. In the eastern part, where relative plate motion is oblique, the lateral component is of about 10 mm/y. GPS velocities of the Aegean plate progressively decrease toward the northwest, where the subduction zone approaches its lateral termination in the Ionian Islands (Hollenstein et al., 2008). Very little is known about the seismogenic potential of the Hellenic subduction zone from the instrumental period. Much controversy exists over whether or not this subduction thrust is dominated by aseismic creep (Reilinger et al., 2006; Shaw and Jackson, 2010) or if it has a very high coupling coefficient (Ganas and Parsons, 2009). Thus, we assume a broad range of possible coupling coefficients. Shaw and Jackson (2010) observe shallowly dipping thrust events on or near the interface between 15 km and 45 km depth, so we assume 45 km depth as our preferred down-dip limit of the seismogenic zone. Some studies suggest that a magnitude 8.4 earthquake that caused uplift at Crete in AD 365 occurred on the subduction interface (Ganas and Parsons, 2009), while others suggest that it was on an upper plate fault (Shaw and Jackson, 2010). If this event occurred on the subduction interface, the maximum rupture depth would have been 68 km, which we assume as a constraint for the down-dip limit of the seismogenic zone. We use the AD 365 possible subduction thrust event as our preferred Mmax. A magnitude 8.0 earthquake in eastern Crete in 1303 (Guidoboni and Comastri, 1997), could also be thought to represent rupture of the subduction interface. Also note the shallow portion of the Hellenic Trench dips at a very low angle.

10.6.27 Cyprus

Most geometric and kinematic parameters of this source are drawn from the EDSF (Basili et al., 2013a). According to GPS velocities and current plate models, relative motions result in an orthogonal convergence of about 18 mm/y (Reilinger et al., 2006) or 14 mm/y in the western part of the arc, decreasing eastwards to 7-9 mm/y, where relative motion becomes oblique (Wdowinski et al., 2006). The Paphos Fault is thought to accommodate about 10 mm/y of differential velocity between the eastern and western segments of the arc. Little is known about the subduction thrust earthquake potential of the Cyprus Arc, so we largely use default seismic values here. However, the largest historic earthquakes in the Cyprus area thought to have occurred on the subduction thrust are the 342 AD and 1222. Magnitude estimates vary a lot for both, Mw 6.6 to 7.4 for the first one (Guidoboni et al., 2007; Cagnan and Tanircan, 2010) and Mw 6 to 7.5 for the second (Guidoboni et al., 2007; Guidoboni and Comastri, 2005; Yolsal et al., 2007). We use the largest (Mw=7.5) of these estimates as our minimum value for Mmax.

10.6.28 Makran

The largest subduction thrust event on the Makran Trench was an Mw 8.1 in 1945 that triggered a large tsunami, killing up to 4000 people (Heidarzadeh et al., 2008). Vernant et al. (2004) show from GPS measurements that convergence rates at the Makran Trench are 19.5 ± 2 mm/yr. Seismic reflection profiles across the Makran Trench show a dip angle between 2 and 8° (Koppa et al., 2000; Schluter et al., 2002), so we assume an average dip of 8°, which is at the upper end of this range to also account for the possibility that the slab steepens up with depth (beyond the range of seismic reflection imaging). The Makran system has a very thick incoming sedimentary package (up to 7 km thick; Koppa et al., 2000), and the trench is not well-defined morphologically (Schluter et al., 2002), so we assume a somewhat deeper updip limit of seismogenic rupture compared to other places. Following the overview of historical seismicity at Makran in Heidarzadeh et al. (2008), we assume 35 km as a preferred down-dip limit of the seismogenic zone.

10.6.29 Ecuador/Columbia segment of the Andean margin

The largest historical earthquake in this segment was an Mw 8.8 in 1906 (see review in Bilek, 2010). We assume relatively high coupling coefficients for all of the Andean margin segments, due to the seismically productive nature of this subduction system.

10.6.30 Peru segment of the Andean margin

The largest historical earthquake in this segment was an Mw 8.4 in 2004 (see review in Bilek, 2010).

10.6.31 Northern Chile segment of the Andean margin

The largest historical earthquake in this segment was an Mw 8.6 in 1906 (see review in Bilek, 2010).

10.6.32 Central Chile segment of the Andean margin

The largest historical earthquake in this segment was an Mw 9.5 in 1960 (see review in Bilek, 2010; Cifuentes and Silver, 1989). Using the length limited approach to assessing the maximum possible Mmax, we also calculate 9.5.

10.6.33 Patagonia (north and south segments)

The convergence rates at the far southern end of the Chile Trench are much slower (10-20 mm/yr) compared to further north. No significant historical seismicity has occurred on this segment of the Chile Trench. This

may be due to the low convergence rates in the segment of the subduction zone, and we cannot rule out the possibility that large subduction thrust earthquakes occur here. Due to our lack of knowledge about the behavior of the subduction thrust in this portion of the Andean margin, we largely use default values and assume a minimum M_{\max} of 8.0.

10.6.34 South Shetland Islands

Very little is known about historical seismicity at this subduction zone. Convergence rates are very low at this trench (<10 mm/yr; Taylor et al., 2008b), so the historical record is not likely to be representative of the seismogenic potential of this subduction margin. Due to our lack of knowledge about the behaviour of this subduction zone, we largely assign default values.

10.6.35 South Sandwich

Very little is known about the potential for large subduction thrust earthquakes subduction zone. Convergence rates are reasonably high (70-90 mm/yr) and historical subduction thrust earthquakes larger than M_w 7.0 have rarely been observed here, leading some to suggest that subduction here is largely aseismic (Frankel and McCann, 1979). The exception is the far southern end of the trench (south of 59°S), where earthquakes up to M_w 7.4 have been observed (Frankel and McCann, 1979). Based on this, we assign a low preferred coupling coefficient (0.2 ± 0.1) to this subduction source. Due to our lack of knowledge about the behaviour of this subduction zone, we largely assign default values to the other parameters.

10.6.36 Jalisco segment of Middle America

The largest historic subduction thrust event to rupture this portion of the Middle America Trench was the 1932 M_w 8.2 earthquake. More recently, an M_w 8.0 earthquake occurred on this segment of the Middle America Trench in 1995. Slip in the 1995 earthquake was largely focused shallower than 20 km depth, so we assume 25 km depth as our maximum down-dip limit of rupture. Interpretation of GPS velocities from the Jalisco region can fit the data assuming 50% coupling coefficient on the Middle America Trench (Selvans et al., 2010), so we assume 0.5 ± 0.2 for our coupling coefficient.

10.6.37 Michoacan to Guatemala portion of Middle America

A well-documented array of historical subduction thrust earthquakes have occurred on this portion of the Middle America Trench. Based on the distribution of those events (see overview of previous studies in Pacheco and Singh, 2010) as well as observations of interseismic coupling and slow slip events in the Oaxaca and Guerrero regions, we assign a preferred down-dip limit of coupling as 25 ± 5 km. The largest historic earthquake on this segment was an M_w 8.0 in 1985. In general, the down-dip limit of rupture in these historical earthquakes is ~ 25 km, and slow slip event behaviour appears to occur down to ~ 35 -40 km depth (Larson et al., 2004). Due to the high seismic productivity of this portion of the Middle American Trench, and high interseismic coupling estimates from campaign GPS (Larson et al., 2004) we assume a coupling coefficient of 0.7 ± 0.2 .

10.6.38 Middle America – El Salvador to Nicaragua

This portion of the Middle America Trench frequently experiences moderate sized subduction thrust earthquakes (M_w 6.0-7.4), but rarely experiences really large earthquakes. The 2 September 1992 (M_w 7.6) Nicaragua tsunami earthquake established the potential for shallow rupture to the trench. There is a suspected M 8 subduction thrust event in 1915 (Ambraseys and Adams, 2001). GPS data suggest that if

interseismic coupling occurs on this portion of the Middle America Trench it must be shallow (<20 km depth, La Femina et al., 2009) and that the coupling ratio is likely to be low. Thus, we assume a down-dip limit to the seismogenic zone of 20 ± 5 , and 0.3 for the preferred coupling coefficient.

10.6.39 Middle America – Costa Rica to west Panama

This segment of the Middle America Trench produces Mw 6-7.5 earthquakes on a regular basis, approximately every decade or so. The largest historic subduction thrust event on this portion of the trench was a Mw 7.7 earthquake beneath the Nicoya Peninsula in 1950. GPS studies of interseismic coupling (Norabuena et al., 2004; LaFemina et al., 2009) on the Middle America Trench suggest interseismic locking down to 20 km depth, and possibly deeper in some places. LaFemina et al. (2009) obtain an average interseismic coupling coefficient of 0.5.

10.6.40 Lesser Antilles

Subduction of North America beneath the Caribbean Plate occurs at the Antilles Trench. Little is known about the seismogenic potential of this feature, and the largest historic subduction thrust event is the 1843 Magnitude 7.5-8.0 earthquake at the northern end of the trench (Bernard and Lambert, 1988). Virtually nothing else is known about the seismogenic zone geometry and potential for subduction earthquake occurrence at this subduction zone, so we largely use default values for this source.

10.6.41 Manila

Galgana et al. (2007) use GPS to estimate low interseismic coupling (near zero) on the Manila Trench, so we assume a coupling coefficient of 0.15 ± 0.1 . Results of Beavan et al. (2001) also suggest largely aseismic deformation on the Manila Trench. Although data on historic subduction interface earthquakes at the Manila Trench is sparse, Hamburger et al. (1983) noted two large earthquakes in 1934 and 1948 (magnitudes 7.6 and 7.2, respectively), which they suggest could represent interplate thrust events. Given the lack of significant historic subduction thrust seismicity on the Manila Trench, we know very little about the depth to the down-dip limit of the seismogenic zone, and other relevant parameters, so we largely use default values for these.

10.6.42 Philippine

We use the motion of the southeast Luzon block relative to the Philippine Sea Plate from Galgana et al. (2007) to determine the rate and azimuth of convergence on the Philippine Trench. The largest historic event on the Philippine Trench was the 1907 M 7.0-7.6 earthquake (Hamburger et al., 1983). Little is known about the earthquake potential of the Philippine Trench, and published GPS studies in the region of the Philippine Trench are sparse. However Galgana et al. (2007) see some evidence for elastic strain accumulation on the northern end of the Philippine Trench and estimate a coupling coefficient of 0.27.

10.6.43 East Luzon

The east Luzon Trough is the northward continuation of the Philippine Trench, and is thought to be accommodating incipient subduction of the Philippine Sea Plate (Hamburger et al., 1983). Galgana et al. (2007) estimate 9-15 mm/yr of convergence at the southern end of this feature. To calculate the rates of motion on this feature we use the pole of rotation for northeastern Luzon relative to the Pacific Plate from Galgana et al. (2007). The Luzon Trough seismogenic potential is not well-understood, although there are a number of historic events with underthrusting focal mechanisms (Hamburger et al., 1983). Seismicity defines

a 20° dipping plate down to ~50 km depth (Hamburger et al., 1983). The largest historical earthquake thought to be associated with the Luzon Trough was a magnitude 7.3 in 1968 (Hamburger et al., 1983). Due to our lack of understanding of the Luzon Trough as a subduction earthquake source we use default values for the other parameters defining this feature.

10.6.44 Cotabato

This inferred subduction zone accommodates subduction of the Celebes Sea crust beneath southwest Mindanao, and has generated major earthquakes and tsunamis over the last 40 years. The largest historic event on this feature was the 1976 Mw 8.0 Moro Gulf earthquake, which caused a devastating tsunami in the region. Although GPS coverage in the southern Philippines is sparse, we use the pole of rotation for Mindanao relative to Sunda calculated by Galgana et al. (2007) to estimate convergence rates at the Cotabato Trench. For most of the other parameters, we assume default values due to our lack of detailed knowledge about this feature. We assume a dip of 15° for the subduction thrust, based on typical dips for similar subduction zones.

10.6.45 Sulu

This inferred subduction zone accommodates subduction of the Sulu Basin beneath western Mindanao, and is thought to have generated a major subduction thrust event in 1897 (magnitude ~8.0). Although GPS coverage in the southern Philippines is sparse, we use the pole of rotation for Mindanao relative to Sunda calculated by Galgana et al. (2007) to estimate convergence rates at the Sulu Trench. For most of the other parameters, we assume default values due to our lack of detailed knowledge about this feature. We assume a dip of 15° for the subduction thrust, based on typical dips for similar subduction zones.

10.6.46 Minahassa

The Minahassa Trench along the north coast of Sulawesi accommodates subduction of the Celebes Basin beneath the northern arm of Sulawesi. This feature produces significant subduction thrust earthquakes; the largest historic event was an Mw 7.9 earthquake in 1996, which was followed by an eastward propagating sequence of moderate to large subduction thrust events over the following year or two (Vigny et al., 2002). To estimate convergence rates at the western end of the Minahassa Trench we use Socquet et al.'s (2006) pole of rotation for the Sunda block relative to the north Sula block. For the eastern end of the Trench we use Socquet et al.'s (2006) pole for the Manado block relative to the Sunda block. We assume an average dip of 15° for the subduction thrust, based on typical dips for similar subduction zones.

10.6.47 Seram

The largest historic earthquake in the region was an Mw 8.5 earthquake in 1938. Okal and Reymond (2003) suggest a thrust mechanism at ~60 km depth. Although Okal and Reymond (2003) suggest that the earthquake was either within the subducting slab, or within the mantle wedge (due to its depth and the fact that it is ~100 km from the Seram Trough), we consider the possibility that this event occurred along the deeper part of the seismogenic zone on the plate interface, so assume this as our preferred Mmax, with a minimum Mmax of 8.0. Very little else is known about the subduction thrust earthquake potential of the Seram Trough, so we largely use default values.

10.6.48 Timor

The Timor Trough is thought to have recently ceased activity due to the impingement of the Australian continental margin, with most of the relative plate motion transferred onto reverse faults in the back-arc, such as the Wetar and Flores thrusts. It is not known if this continues to accommodate active tectonic motion. The historical seismicity on the Timor Trough is very sparse. Due to our lack of knowledge about the seismogenic potential of the plate interface at the Timor Trough, we largely assign default values, and assume Mw 8.0 for preferred Mmax, with Mw 7.5 as a minimum Mmax.

10.6.49 Manokwari

The largest historic underthrusting earthquake at the Manokwari Trench was a Mw 7.6 on 3 January 2009. Very little else is known about the subduction thrust earthquake potential of the Manokwari Trench, so we largely use default values.

10.6.50 Molucca Sea

The largest historic event in this region was the 14 May 1932 magnitude 8.3. Beyond that, we know very little about the seismogenic potential of this complex region, and resort to default values to parameterize these sources.

11 Characterisations of the Himalaya frontal thrust system

This section is a reproduction of the report Berryman, Ries and (2014) with minor adjustment to the section referencing. The references are merged with the references in the other sections.

11.1 Introduction

The 2500 km long Himalaya Frontal Thrust (HFT) fault system is one of the great fault systems of the world with many attributes similar to oceanic subduction zones. Seminal work by Nakata (1972, 1989), Yeats and Lillie (1991), and Yeats et al. (1992) established the framework for later more detailed fault and paleoseismic studies. Considerable information on the damage and seismological characteristics of the large to great historical earthquakes of the Himalayan front in 1505, 1555, 1883, 1905, 1934, and 1950 (see figure 11.1 and references in the figure caption) have also been collected, but these early studies did not generally identify the causative faults.

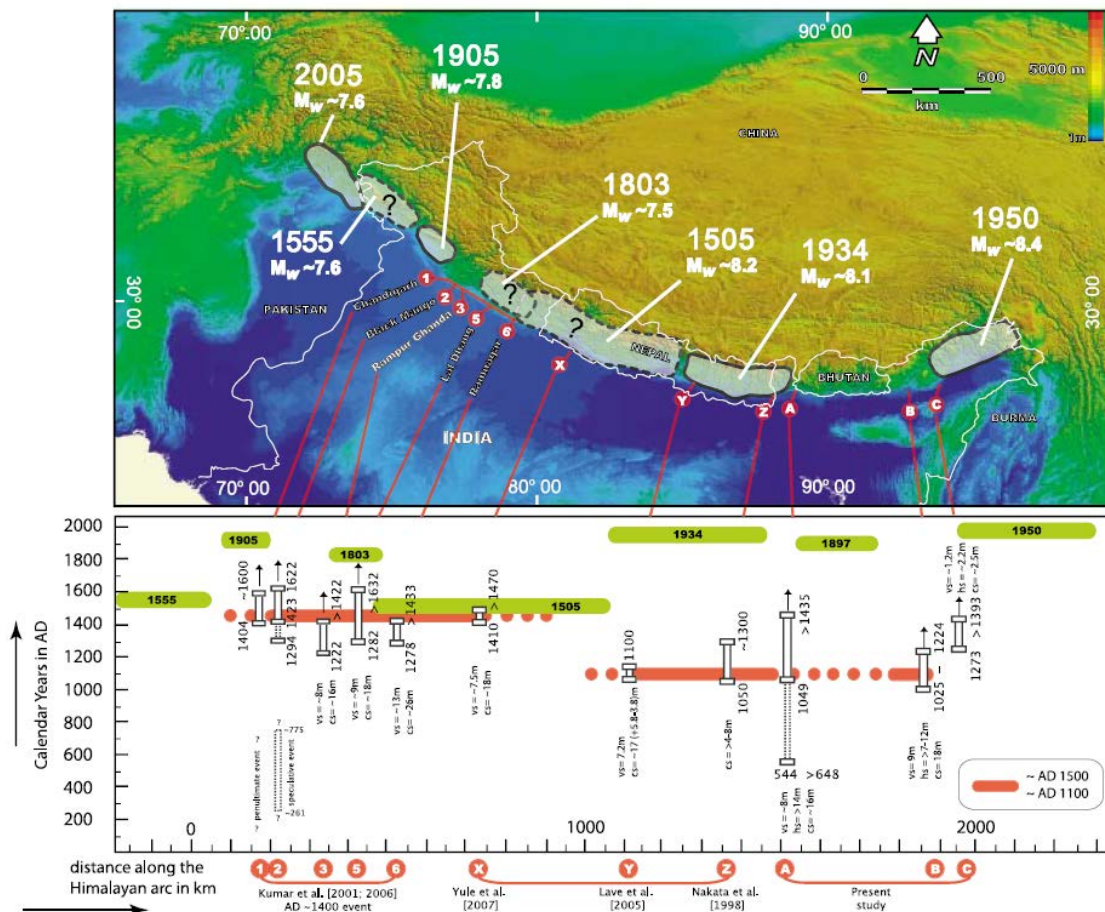


Figure 11.1 Synopsis of historical and paleoseismic history along the HFT from Kumar et al. (2010) reproduced with permission of John Wiley and Sons. This is Figure 12 in the paper ‘Paleoseismological evidence of surface faulting along the northeastern Himalayan front, India: Timing, size, and spatial extent of great earthquakes’ by Kumar, Wesnousky, Jayangondaperumal, Nakata, Kumahara, and Singh, published in the Journal of Geophysical Research, Volume 115,

B12422, Copyright 2010. The figure and the following caption are reproduced with permission of John Wiley & Sons.

(top) Digital topography is from 90 m Shuttle Radar Topography Mission (SRTM) data (<http://glcf.umiacs.umd.edu/data/srtm/>). Shaded areas with bold outline or dotted line in map view correspond to areas of strong ground shaking associated with historical earthquakes. Each is labelled with the corresponding age and magnitude of the earthquake. Solid circles with numbers and letters are location of trench studies described here for sites A through C in the northeast Himalaya, along with previously reported at sites 1–6 in the northwest Himalaya and sites X through Z in Nepal (Kumar et al., 2001; Kumar et al., 2006; Lavé et al., 2005; Nakata et al., 1998; Upreti et al., 2000; Yule et al., 2006). (bottom) Space-time diagram showing radiocarbon constraints on timing of surface rupture earthquakes documented at each site. Vertical axis is time in calendar years A.D.; horizontal axis is kilometers. The location of each site is also labelled by a solid circle below the horizontal axis with lines connecting to respective site on overlying map. The horizontal scales of overlying digital topographic map and space-time diagram are the same. The vertical bars and upward pointing arrows at each study site reflect radiocarbon ages that bracket the age of surface in calendar years A.D. or B.C. (2σ standard deviation of the ^{14}C calendar ages). The vertically pointing arrows above some sites indicate the brackets encompass only the uncertainty of the youngest radiocarbon age in displaced deposits and thus the upper bound of the age of the last earthquake displacement may be younger (see text for discussion). The coseismic slip (cs), vertical separation (vs), and horizontal shortening (hs) of the corresponding earthquake are also shown in meters. The rupture extents of known large to great earthquakes within the study area are provided as a long box with the year of the rupture annotated within. Inferred rupture length is based on revised and expanded Medvedev-Sponheuer-Karnik (MSK) intensity (Ambraseys and Bilham, 2000; Ambraseys and Jackson, 2003; Ambraseys and Douglas, 2004; Bilham, 1995; Bilham, 2004; Bilham and Ambraseys, 2005; Chander, 1989; Molnar and Pandey, 1989; Pandey and Molnar, 1988; Wallace et al., 2005a). Long bold and solid horizontal lines without ages annotated are speculated rupture lengths of earthquakes in \sim A.D. 1100 and \sim A.D. 1500 resulting from interpretation of timing and size of surface displacements observed in trench exposures (dotted where inferred in absence of paleoseismic data). Mapping the surface trace of the HFT has proven difficult because of the 2500 km total length, the low dip of the fault which frequently results in surface folds and warps rather than discrete scarps, and because the HFT often occurs at the juncture between bedrock and alluvium such that late Quaternary scarps are quite discontinuous. Driven by a desire to link large historic earthquakes to causative faults, and to understand the earthquake cycle of strain accumulation and release, and what proportion might be accommodated aseismically, has resulted in a decade of fairly intensive paleoseismic study. These have concentrated effort at a relatively detailed scale at perhaps a dozen sites (see Kumar et al., 2010; Sapkota et al., 2012; Kumahara and Jayangondaperumal, 2013, for review), and made good progress in connecting historic events with sections of the HFT and have identified evidence for the penultimate event at several locations.

There has been no systematic mapping of the trace of the HFT since early efforts by Nakata (1972) produced hand-drawn maps at 1:100,000 scale, and little work on long term slip rates except as inferred from geodetic study (Ader et al., 2012), and no assessment of possible segmentation of the 2500 km long system except as inferred from the rupture dimensions of individual earthquakes.

With these few data we cannot attribute the fault according to the GEM Faulted Earth database format (Litchfield et al., 2013). However, because the HFT has many similarities with oceanic subduction zones, we have developed a data attribute table more akin to that developed by Berryman et al. (2014) for global subduction zones. The key to developing earthquake event sets in these situations is defining the likely maximum magnitude earthquake that could occur; define the appropriate frequency-magnitude b-value; and

the slip rate on the fault. Event sets for any sector of the HFT can then be created from these simple parameters.

Using GIS technology and global imagery data we have mapped the position of the HFT using a combination of Shuttle Radar Topographic Mission (SRTM) and Advanced Spaceborne Thermal Emission and Reflection Radiometer (ASTER) imagery downloaded from the Global Land Cover Facility web site (<http://glcf.umiacs.umd.edu/data/srtm/>), supplemented with Google Earth imagery. This report covers only the HFT. There are active faults within the hanging wall of the Himalaya (e.g., Karakoram fault; Houlié and Phillips, 2013), but these are not included in the current compilation. Similarly, faults on the margins of the Shillong Plateau near the eastern syntaxis of the Himalaya are not included.

11.2 Method

Our method consisted of three steps: (1) digitising and characterising the HFT trace, (2) defining and characterising segments, and (3) defining and characterising floating segment to be used for hazard and risk modelling. We describe each step in more detail below.

11.2.1 Digitising and characterising the HFT trace

We developed the delineation of fault traces for the HFT using published data and interpretation of Shuttle Radar Topographic Mission (SRTM) (USGS, 2006) and Advanced Spaceborne Thermal Emission and Reflection Radiometer (ASTER) elevation and hillshade models (USGS and Japan ASTER Program, 2003), supplemented with global satellite and airborne imagery provided as part of the Esri ArcGIS software package. We used the trace attributes of the GEM Faulted Earth database (Litchfield et al., 2013) as defined below:

Location method

This attribute identifies the mapping method or basemap on which the trace was digitised (e.g., GPS surveying, LiDAR data, aerial photographs, topographic map, Google Earth).

Scale

This attribute represents the average scale at which a trace is digitised. It is reported as a number – i.e., 1:200000 is reported as 200000.

Accuracy

This attribute represents the location accuracy of the trace on the ground surface. A conservative definition is to calculate it from twice the scale at which the trace was mapped. For example, if a trace was mapped at 1:100000 scale then the accuracy is calculated to be 1:200000.

Geomorphic Expression

This attributes identifies the expression of the fault on the ground or on digital imagery. The data dictionary (Litchfield et al., 2013) defines eight options:

1. Surface Trace = Clearly defined trace of a recent or well preserved fault rupture trace mapped in the field or from high resolution imagery (e.g., LiDAR, aerial photographs).
2. Eroded scarp = Eroded or naturally degraded faultline scarp mapped in the field or from high resolution imagery (e.g., LiDAR, aerial photographs).
3. Sharp feature = Well defined, distinct, feature (e.g., faultline scarp) mapped from remote sensing (e.g., SRTM data, Google Earth).
4. Topographic feature = Non-scarp feature e.g., changes in gradient, alignment of saddles, springs, etc.
5. Bedrock extension = Inferred extension of a neotectonic fault along a bedrock fault.

6. Subtle feature = Moderately – poorly defined feature mapped from remote sensing (e.g., SRTM data, Google Earth).
7. Concealed = Inferred trace buried beneath deposits younger than the last fault rupture (e.g., alluvium) or a water body (river, lake, sea).
8. No trace = No geomorphic expression of the fault exists, but it is inferred from other datasets.

The attribute determines the line type used to display the faults in map view: Solid line for 1 to 3, dashed line for 4 to 6, and dotted line for 7 and 8.

11.2.2 Defining and characterising segments

We subdivide the HFT based on changes in rate and orientation of convergence identified by Drukpa et al. (2012), and Ader et al. (2012) into three segments. Each segment is characterised using the attributes of the subduction zone sources (Berryman et al., 2014), which are briefly defined in Table 11.1.

Table 11.1 Definition of the subduction zone parameters used for characterising the HFT segments

Attribute	Definition
Segment	Geographic Name
Plate pairs	<p>These are the plate pairs used in the calculation of convergence rate and azimuth on the subduction zone.</p> <p>Along the HFT the plate pair is consistently India-Asia.</p>
Coordinates of segment end points	<p>Left_E_LONG – The longitude of the west side of the segment</p> <p>Left_N_LAT – The latitude of the west side of the segment</p> <p>Left_REL_VEL – Horizontal relative plate velocity in mm/yr, on the west side of the segment, using the respective plate</p> <p>Left_REL_AZI – Azimuth of relative plate convergence (on the west side) assuming a fixed Asia plate. Azimuths are listed in degrees clockwise from local north.</p> <p>Right_E_LONG – The longitude of the east side of the the segment</p> <p>Right_N_LAT – The latitude of the east side of the segment.</p> <p>Right_REL_VEL – Horizontal relative plate velocity in mm/yr on the east side of the segment, using therespective plate pair</p> <p>Right_REL_AZI – Azimuth of relative plate convergence (on the east side) assuming a fixed Asia plate. Azimuths are listed in degrees clockwise from local north.</p>
Dip	Average dip angle for the segment
Dip direction	Average direction of segment dip (in down-dip direction) in degrees clockwise from north
Up-dip limit	Vertical distance (in km below ground surface) to the up-dip limit of seismic rupture
Down-dip depth	Vertical distance (in km below ground surface) to the down-dip limit of seismic rupture

Coupling Coefficient	Proportion of relative plate motion that will be eventually accommodated as seismic slip.
Mmax	The magnitude of the largest earthquake expected to occur on a segment
b-value	Parameter of the magnitude-frequency relation of earthquakes that describes the relative frequency of small to large earthquake.

11.2.3 Defining and characterising floating segment

The procedure we have used to define a floating rupture segment was to first define maximum rupture length from the available paleoseismic record. It appears permissive that a 900 km long rupture occurred around AD 1500 in the western Himalaya and around A.D 1100 in the eastern Himalaya (Figure 1.1) and we accept this as the longest likely rupture along the HFT. There are relatively few data on which to base this determination but implications for maximum earthquake magnitude of possible longer ruptures based on geometric considerations are presented below in Table 11.3. From the 900 km length it is possible to calculate the likely associated earthquake magnitude from equations 1 and 2;

$$M_w^{max} = 2/3 \log_{10}(M_o^{max} - 9.1) \quad (\text{McCaffrey, 2008}) \quad (1)$$

and

$$M_o^{max} = \mu L W D \quad (\text{Aki \& Richards, 2002}) \quad (2)$$

where μ is rigidity (30 GPa), L is length in m, W is the width of the locked interface in m, and D is average fault slip in m.

For the HFT the estimated width of the locked interface has been investigated by Ader et al. (2012) and determined to be about 100 km (Figure 3.2). Using the above equations and accepting a length of 900 km, a width of 100 km, and standard values of crustal rigidity, it is possible to investigate possible average displacement values and resulting maximum earthquake magnitudes. From recent field studies (see summary by Kumar et al., 2010) the largest co-seismic surface displacements from several localities along the HFT (which we presume to be correlative with the largest earthquakes) are in the range of 18-26 m. If we accept a midpoint of this range of 22 m then the corresponding earthquake magnitude is Mw 9.1.

11.3 Results

11.3.1 HFT traces

Mapping the surface trace of the HFT has proven difficult because of cultural modification of the landscape, rapid rates of erosion and deposition at the range front which obliterates recently-formed scarps, the low dip of the fault which frequently results in surface folds and warps rather than discrete scarps. Driven by a desire to link large historic earthquakes to causative faults, and to understand the earthquake cycle of strain accumulation and release, and what proportion might be accommodated aseismically, has resulted in a decade of fairly intensive paleoseismic study that has resulted in relatively detailed scale mapping of fault traces at perhaps a dozen sites (see Kumar et al., 2010; Sapkota et al., 2012; Kumahara and Jayangondaperumal, 2013, for review). At these locations good progress has been made in connecting historic events with sections of the HFT and in identifying evidence for the penultimate event.

A total of 661 HFT traces have been mapped, from ~85 km southeast of Islamabad (west) to ~25 km northwest of Roing (east) (Figure 11.2A). The traces range from ~85 m to 61 km in length and primarily cross alluvial fans along the range-front, with a few extending out into the Indo-Gangetic Plain. Some are sharp or eroded traces, but the majority are topographic breaks in slope at the foot of the ranges (Figure 11.2B, C). Many concealed traces have also been inferred beneath riverbeds.

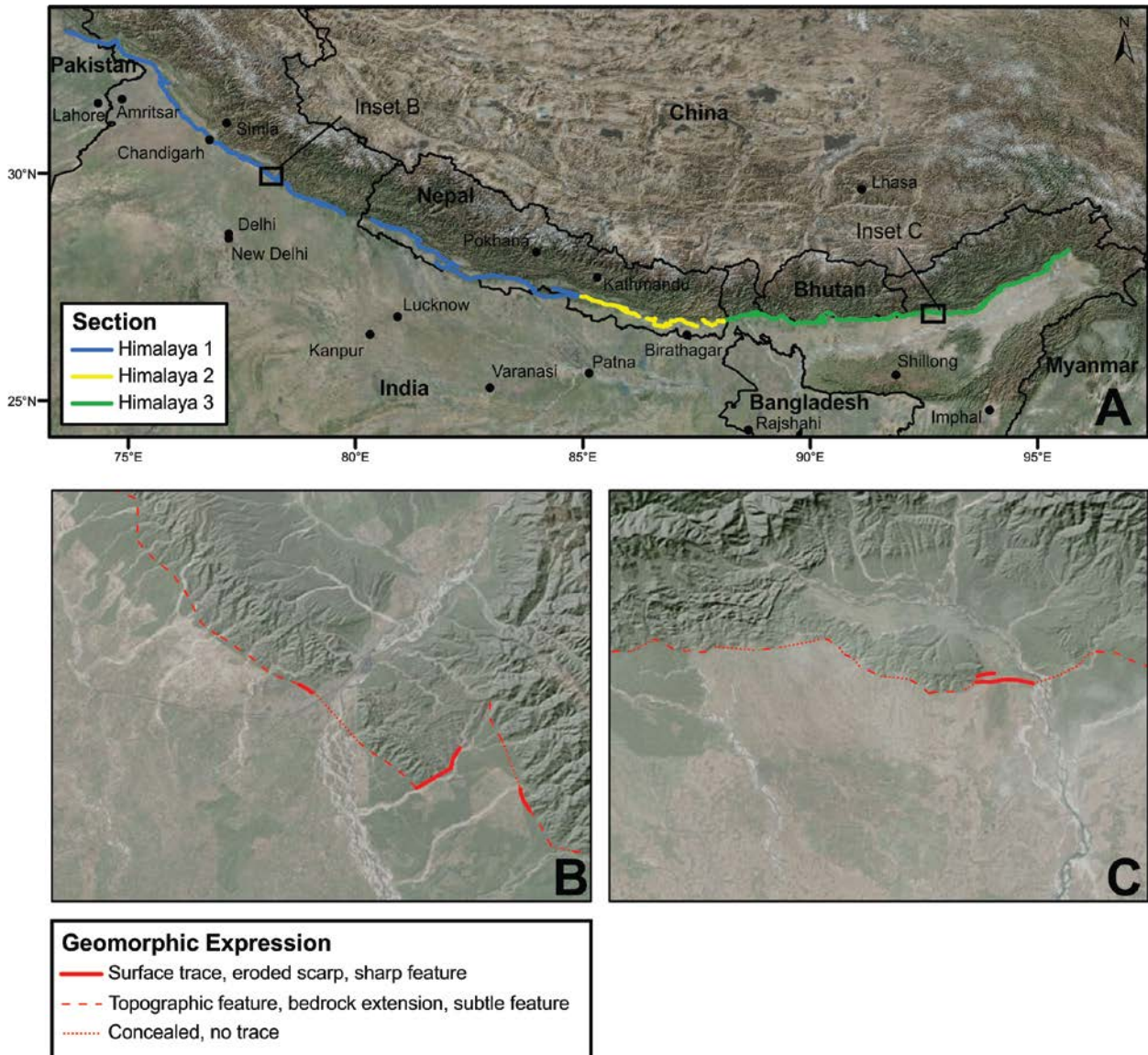


Figure 11.2 Overview of the mapped traces. Figure A. Traces of the HFT derived from published data and our interpretation of remote sensing imagery. Geometric fault segments of the HFT are colour-coded (note these are not likely to represent rupture segments). Segment boundaries are chosen where a change in plate motion rate and azimuth occurs, or between Himalaya 2 and 3 in eastern Nepal where the Tista fault (Nakata and Kumahara, 2002) may coincide with a small decrease in the amount of slip on the HFT. Insets of areas shown in more detail in B and C are shown. The GIS shape file showing attributes of the traces at a scale appropriate for use at 1:400,000 is available from the GEM secretariat on request. B. Example of fault trace delineation near Haridwar at 1:1,000,000 scale C. Example of fault trace delineation at 1:1,000,000 scale (based on field mapping shown by Kumar et al. (2010) in their figure 7.

11.3.2 Segment characterisation

We subdivide the HFT based on changes in rate and orientation of convergence identified by Drukpa et al. (2012), and Ader et al. (2012) into three segments: from the northwestern syntaxis to eastern Nepal, from eastern Nepal to western Bhutan, and from western Bhutan to the eastern syntaxis (Figure 11.2). Table 11.2 shows the attributes that we assigned to each segment. Below we provide our rationale for the chosen dip, dip direction, up-dip limit, down-dip depth, down-dip width, coupling coefficient, M_{max} and b -value.

Table 11.2 Attributes of the three HFT segments

Segment	Himalaya 1	Himalaya 2	Himalaya 3
Left E long	73.642	84.889	88.101
Left N_lat	33.125	27.281	26.745
Left rel_vel	20.5	18	18
Left rel_azimuth	18	18	12
Right E_long	84.889	88.101	95.679
Right N_lat	27.281	26.745	28.324
Right rel_vel	20.5	18	20
Right rel_azimuth	18	12	10
length (km)	1300	330	800
dip	10	10	10
dip direction	18	12	0
downdip_pref	17	17	17
downdip_min	15	15	15
downdip_max	20	20	20
width_pref	98	98	98
width_min	86	86	86
width_max	115	115	115
coupling_pref	0.95	0.95	0.95
coupling_min	0.80	0.80	0.80
coupling_max	1.0	1.0	1.0
SED (m) whole seg	32.5	8.25	20
Mmax_pref	9.33	8.53	9.05
b value_pref	1.0	1.0	1.0
b value_min	0.8	0.8	0.8
b value_max	1.2	1.2	1.2

Dip

Average dip angle for the segment. Unless otherwise noted the dips are determined from Ader et al. (2012) who use GPS, seismicity at the down-dip edge of the locked HFT and thermal arguments similar to those from subduction tectonics to determine an average dip of 10° to 15-20 km depth (a down-dip width of 86-115 km).

Dip direction

Average direction of segment dip (in down-dip direction) in degrees clockwise from north. Unless otherwise noted the dip directions are determined from Ader et al. (2012) whose study area extended from 78-88° east longitude, and from Drukpa et al. (2012) in their study area that extended from 86-93° east longitude.

Up-dip limit

This parameter is uncertain for subduction zones, and while there may well be major events on the HFT that do not extend to the surface trace, many events have been shown to do so (Kumar et al., 2010; Sapkota et al., 2012; Kumahara and Jayangondaperumal, 2013) and therefore, in this study we presume all ruptures extend to the surface trace.

Down-dip depth

Vertical distance (in km below ground surface) to the down-dip limit of seismic rupture on the HFT (with preferred, minimum, and maximum values) is based on Ader et al., (2012) (see Figure 11.3).

Down-dip width

The width along the dip of the fault plane (in km) of the seismogenic portion of the HFT. This is calculated using the fault dip, and the down-dip length of the fault from previous columns.

Coupling Coefficient

The coupling coefficient (preferred, minimum, and maximum values) for the HFT. Coupling coefficient is the proportion of relative plate motion that will be eventually accommodated as seismic slip and for the HFT has been addressed by Ader et al., (2012), which we present here as Figure 11.3. For the HFT the best estimates from Figure 11.3 range from 0.8 to 1.0 along a transect across the Himalaya where the data are best resolved. We apply these estimates to the whole length of the fault system. Ader et al. (2012) address the question of coupling along the HFT and show that in the interseismic period the GPS data suggest the fault is currently highly locked (Figure 11.3). The authors speculate that there may be some post-seismic creep but there are no data to support this at present, and thus we assume the current interseismic coupling ratios apply to the whole seismic cycle.

Mmax

The maximum magnitude earthquake M_{max} expected for each Himalaya segment has been defined using the relationship between segment length and magnitude developed for subduction zones by McCaffrey (2008). The segments we have defined vary from 300 to 1300 km long, but limited paleoseismic data over the past 2-3 events suggests a maximum rupture length of around 900 km (Kumar et al., 2010).

b-value

Based on an analysis of international catalogues such as NSC and CMT, Ambraseys and Douglas (2004) and Ader et al. (2012) conclude that the best-fit to the historical and instrumental data is a b-value of 1.0. We have not undertaken a formal assessment of the uncertainty on the b-value but recommend the use of ± 0.2 to allow for significant uncertainty in the seismicity characteristics of the region.

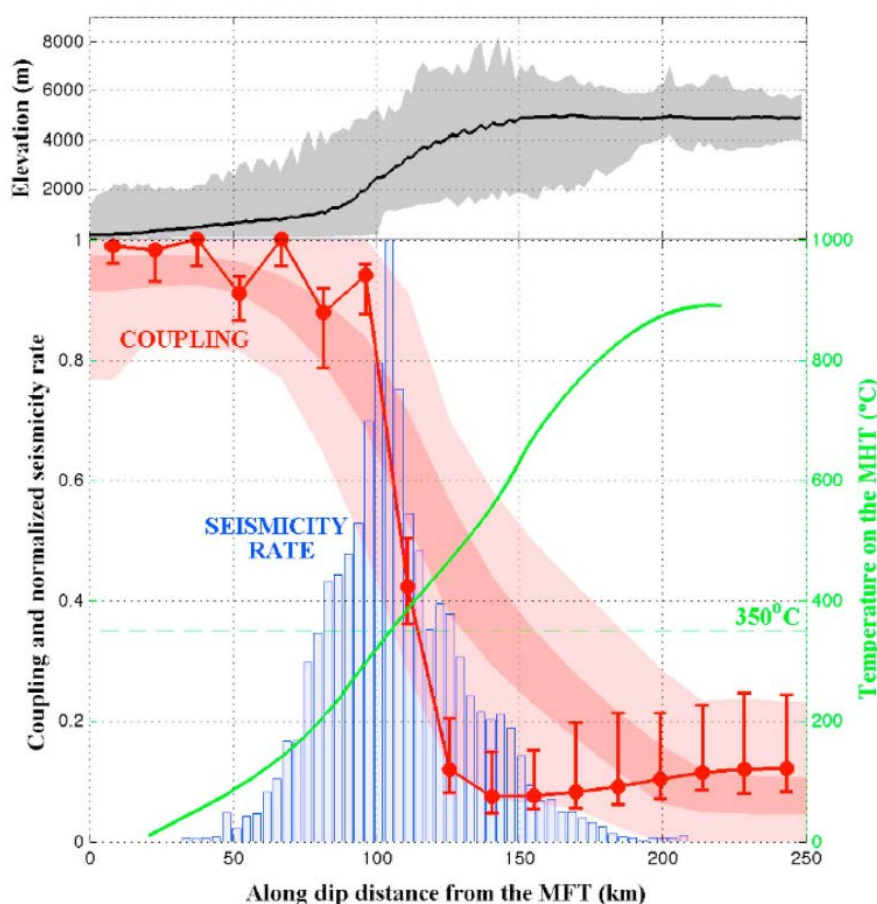


Figure 11.3 Elevation, coupling coefficient, seismicity rate, temperature on the main Himalayan Thrust (MHT) HFT from Ader et al. (2012) reproduced with permission of John Wiley and Sons. This is Figure 6 in the paper ‘Convergence rate across the Nepal Himalaya and interseismic coupling on the Main Himalayan Thrust: Implications for seismic hazard’ by Ader, Avouac, Liu-Zeng, Lyon-Caen, Bollinger, Galetzka, Genrich, Thomas, Chanard, Sapkota, Rajaure, Shrestha, Ding, and Flouzat published in the Journal of Geophysical Research, Volume 115, B12422, Copyright 2012. (top) Elevation profile. The thick black line represents the mean elevation of the Himalaya in the sector from 78-88° east longitude, while the shaded grey area represents the whole elevation swath. Bottom – comparison between the coupling, temperature and seismicity rate along the slip direction. The red line with the error bars corresponds to the coupling underneath the transect where the resolution is best. The shaded red curve in the background is the stack of the coupling on the whole fault. The darker red shaded area represents the 1 σ scatter of coupling and the lighter red shaded area shows the whole scatter of coupling with respect to the distance to the HFT. The blue histogram shows the seismicity rate, normalised to a maximum value of 1. The green curve shows the temperature variation along a frontal thrust plane dipping at 10°, determined by Herman et al. (2010). The thin dashed green line indicates the critical temperature of 350°C, above which frictional sliding is generally thought to be dominantly rate-strengthening, promoting stable sliding (Blankpied et al., 1995; Marone, 1998).

11.3.3 HFT Paleoseismology

From the available data, largely from isoseismal maps for historic large earthquakes, supplemented by limited paleoseismic data, it is very difficult to further segment the 2500 km long HFT. Here, we suggest that

by analogy with recent observations from oceanic subduction zones, the possibility of very long ruptures such as the 26 December 2004 Andaman-Sumatra earthquake or the rupture associated with the 11 March 2011 Great East Japan earthquake, should not be discounted (see McCaffrey 2008 for discussion).

Kumar (2010) illustrated the likelihood that the penultimate rupture on the western part of the HFT in ~AD 1400 was much larger than in the most recent events of AD 1803 and AD 1905 (Figure 11.1). The AD 1555 event in the western Himalaya is inferred to be a different event to the much larger ~AD 1500 event but there are few data to constrain a preferred model. Therefore, we explore the possibility that the whole ~1300 km long western part of the HFT could rupture in a single event (Himalaya 1 segment of Table 11.2) and provide other fault parameters consistent with such a long rupture.

We also take the c. 900 km long possible rupture in the penultimate event in the eastern Himalaya (Figure 11.1) as a potential maximum magnitude and calculate other parameters consistent with this rupture. The associated earthquake magnitude is Mw 9.1, but there is significant uncertainty, probably ± 0.2 magnitude units judging by the alternate magnitudes corresponding to longer geometric segments characterised in Table 11.2. Surface displacement consistent with a Mw 9.1 event is 22.5 m (Table 11.2). This surface displacement is consistent with field data in the range of 16-26 m from several localities along the HFT (Figure 11.1).

Based on these data we suggest the best estimate maximum magnitude anywhere along the HFT is a Mw 9.1 ± 0.2 event associated with c. 900 km long surface rupture and 21 ± 4 m of surface slip. The most recent series of historical events from A.D. 1505 – 2005 appear to be substantially smaller than apparent for the penultimate earthquake based on geologic data (Figure 11.1) and this suggests a lack of stable segments or self-similarity in repeated ruptures. Therefore, for earthquake hazard analysis we advocate assembling an earthquake event set balancing the available seismic moment, and constrained by the Mmax of Mw 9.1 ± 0.2 and a Gutenberg and Richter b-value in the range of 1.0 ± 0.2 . We suggest the resulting Gutenberg-Richter magnitude frequency distribution should be truncated at a lower bound of Mw 7 as events smaller than this probably do not contribute to surface slip rate on the HFT.

Table 11.3 Attributes of the segment HFT Paleoseismology

Attribute	HFT Paleoseis
dip	10
dip direction	n/a
downdip_pref	17
downdip_min	15
downdip_max	20
width_pref	98
width_min	86
width_max	115
coupling_pref	0.95
coupling_min	0.80
coupling_max	1.0
SED (m)_whole seg	22.5
Mmax_pref	9.12
B value_pref	1.0
B value_min	0.8
B value_max	1.2

11.4 Conclusions

We have completed a reconnaissance mapping exercise of the traces of the HFT from remote sensing imagery, supplemented and validated at a few locations by published detailed field mapping. We have compiled the traces at a scale of 1:200,000 and, because of uncertainty in accurate delineation of the traces, recommend its usage at no larger scale than 1:400,000. The GIS dataset can be obtained from the GEM Foundation Secretariat on request. We have also summarised characteristics of the fault which are required to develop an earthquake event set that can be used for earthquake hazard and risk studies. These parameters are developed for possible geometric segments of the fault, but caution that these are not likely to represent stable rupture segments. Instead we recommend an approach for developing an earthquake event set by defining a maximum magnitude earthquake that could occur anywhere along the HFT, allow these earthquakes to 'float' along the length of the fault and be supplemented with smaller events down to Mw7 whose fault area is scaled with magnitude, and activity rate determined by the Gutenberg – Richter 'b value', the convergence rate across the fault, and the proportion of the convergence that could be released without seismic energy release (the aseismic slip factor). The parameters for these truncated Gutenberg-Richter magnitude frequency distributions are all defined and presented in this report.

12 Towards new neotectonic fault data

This section in parts reproduces the report Towards new active fault data (Villamor, Ornthammarath, Zúñiga, Horspool, Christophersen, and Langridge (2013) which mainly describes two workshops that were held in Southeast Asia in November 2012 and Central America in April 2013. We have modified the introduction and exclude the details on the workshop preparation as well as the detailed feedback received by the participants. In addition we discuss the challenges of compiling data in other regions of the world.

12.1 Overview of the two regional workshops

The Southeast Asia workshop was held in Bangkok, Thailand, in November 2012 and was hosted locally by RIMES, the Regional Integrated Multi-Hazard Early Warning System for Africa and Asia, and AIT, the Asian Institute of Technology. 26 participants from nine countries attended the Southeast Asia workshop. The Central America workshop was held in Querétaro, Mexico, in April 2013, and was hosted locally by UNAM (Universidad Nacional Autónoma de México), Centro de Geociencias de Juriquilla. 31 participants from eight countries attended the Central America workshop.

The workshops were designed to:

- Introduce the Active fault database concept and structure at regional and national level.
- Introduce (when necessary) the data dictionary concepts, in particular those attributes that are compulsory in the database.
- Train researchers in the OpenQuake Platform Active fault database webtool.
- Get feedback from participants on the Active fault database structure and the OpenQuake webtool.
- Discuss active fault database parameters and their uncertainties in the different countries.
- Facilitate the beginning of compilation of active faults by the participating researchers.
- Help create regional working groups or support groups in active faulting studies.

Each workshop consisted of presentations of the goals and concepts of GEM and GFE, an explanation of the structure of the database, a presentation on the status of active faults in each of the participating countries, training on the webtool and plenty of time for discussion. Below is an overview of the status of active faults in the participating countries.

12.2 Overview of the status of active faults in the participating countries in Southeast Asia

12.2.1 Thailand

After the 1994 Pan earthquake, ML 5.1, in northern Thailand, the Department of Mineral Resources (DMR), the Geological Survey of Thailand, has begun conducting systematic investigation of major active faults in Thailand. As a consequence, the active fault map of the country is relatively well constrained and compiled into GIS. There are numerous specific active faulting studies with characterisation of seismic parameters by DMR, other universities and consultants. Studies are of great quality and have assessed recurrence intervals for fault rupture around 10,000 + years. Main difficulties found to characterise fault are related to the urban development of extensive areas. Faults have been incorporated into national seismic hazard studies by Asian

Institute of Technology, and it has been adopted in national seismic design code in 2009. In the GEM meeting, discussion took place about centralising the input to the GEM database through the Department of Mineral Resources (DMR), the Geological Survey of Thailand. Currently, the centralising input to the GEM database project has been proposed to local funding agency (e.g., Thailand Research Fund) by local researchers at Thai universities.

12.2.2 Vietnam

Vietnam is an area of moderate to low seismicity. However, distributed active faulting in the high populated area Hanoi is a potential major hazard. Faulting in that area is an extension of the Red River Fault from the north. The Red River fault is clearly active in China with slip rate 2-5 mm/yr. The fault opens in to several splays in Vietnam. The Institute of Geological Sciences (Vietnam Academy of Science and Technology) has mapped numerous active faults based on topographic expression, and remote sensing image. Some fault immediately offshore show evidence for active faulting. However, the actual active fault rates are not constrained. Geodetic information can be used as proxy for slip rate on potential mapped faults.

12.2.3 Myanmar

The Myanmar Earthquake Committee is promoting active faulting studies in Myanmar. The Seismotectonics Research Division of the Myanmar Earthquake Committee has produced an internal map of the active faults of the country and there is also a published tectonic map produced by the Myanmar Geosciences Society. There are a few high quality paleoseismic studies along some of the most active faults (slip rates ~ 10-20 mm/yr) close to large populations. Some faults crossing the border with Thailand have been mapped by Thai researchers. At the workshop, it was discussed that fault parameters on these faults need to be reconciled across the border. Fault parameters have been incorporated into national PSHA maps.

12.2.4 The Philippines

The Philippines has a long history of compilation of active fault locations and fault parameters, and as a consequence The Philippines has the most complete database (compiled in GIS) of the countries represented at the workshop. As consequence of the 1990 Luzon Earthquake (Philippines Fault Zone; with a slip rate of 20-30 mm/yr), an active fault mapping and paleoseismology program started led by PHIVOLCS. In the last 20 years, most of the detailed mapping and paleoseismic studies have concentrated on The Philippines Fault Zone and the Marakina Fault (in close proximity to Manila city). Other active faults have been mapped using interpretation of remote sensing images, occasionally verified by field mapping. The national active fault database is structured similar to existing databases and contains most of the attribute fields that are compulsory for GFE active fault database.

12.2.5 Indonesia

Most of Indonesia's seismicity and active faulting studies are dominated by the Sumatran Subduction Zone. However, because of its great extension and location among fast moving tectonic plates, there are also numerous onshore active faults. Lab Earth – LIPI (Indonesian Institute of Sciences), together with G.R.E.A.T (Graduate Research on Earthquake and Active Tectonics, Institute of Technology Bandung) and AIFDR (Australian Indonesia Facility for Disaster Reduction) have concentrated on characterising the seismic hazard nationwide. Also the Geological Agency of the Ministry of Energy and Mineral Resources has identified earthquake prone areas and has stated assessing the seismic hazard of those areas, with current efforts focussed don Sulawesi Island. As a consequence there is a relatively complete preliminary compilation of the

location of the main faults. For most faults there is a preliminary assessment of earthquake parameters and national and regional PSH maps have been built. However, only a few onshore faults have been studied in detail with paleoseismic techniques given the large number of faults and the small number of active faulting researchers.

12.2.6 Papua New Guinea

PNG lies among highly complex and fast moving plate boundaries. Numerous faults have been identified and published in international journal papers. Port Moresby Geophysical Observatory (PMGO) of the Department of Mineral Policy & Geohazards Management (DMPGM) has attempted to assign historical earthquakes to fault lines. However, detail fault mapping and fault activity rates have not been studied or compiled into an active fault database.

12.3 Overview of the status of active faults in the participating countries in Central America

Several initiatives, including the “World Map of Major Active Faults” (Trifionov and Machette, 1993), and ILP initiative, in the late 90’s to early 2000s, have compiled relevant information on active faults for some countries in Central America. However, for the majority of faults there are no paleoseismic studies that characterise the seismic potential. In some areas, not all active faults have even been mapped. Rates of tectonic activity in some areas are still not very well known because the number of seismic stations in some countries is very low (see Table 1; Rose et al., 2004). Also rates of deformation from geodetic measurements are only starting to be available in the last ~ 5 years. We describe next the main status of active faulting studies in Central America. Note that we lack information for Belize, since we could not find any researcher in that country to attend the workshop. From 1990 to 1996 every country of Central America received seismograph equipment from a project sponsored by Scandinavian countries. In 1998, the Central America Seismological Centre was opened at the Universidad de Costa Rica.

Table 12.1 Seismic stations and accelerometers in Central America (Rose et al., 2004)

Country	Short-period stations	Broadband stations	Accelerometers
Guatemala	12	1	8
El Salvador	36	1	15
Honduras	3	1	1
Nicaragua	36	1	20
Costa Rica	54	3	53
Panama	13	1	10
Total	154	8	107

12.3.1 Mexico

Mexico’s seismicity is dominated by subduction zone events but there are also numerous faults onshore in different seismotectonic regions that have ruptured historically. In some of the areas affected by earthquakes in the last century, such as the area of Acambay visited during the GEM workshop fieldtrip, the population is currently growing fast. There are relatively few high quality paleoseismologic studies for the number of faults, and they have concentrated on the central section of the Transmexican Volcanic Belt and the northwest region of Mexico (southern extension of the San Andreas system into Baja California). Several teams working on paleoseismology are fast developing and collaborating among themselves and are enriched through collaboration with more experienced teams from abroad. Discussions took place to

centralize the Mexican Active fault database in the UNAM, Centro de Geociencias, to feed into GEM. Mexico is currently training various students in paleoseismology. A recent digital version of the general tectonic map of Mexico compiled by a group from the Engineering School of UNAM and including major faults (with somehow limited precision), has recently been made available through the server at <http://www.datapages.com/AssociatedWebsites/GISOpenFiles/TectonicMapMexico.aspx>.

12.3.2 Guatemala

Guatemala's seismic activity is dominated by the onshore extension of the Swan Islands oceanic transform fault approaching from the north and the subduction offshore to the west. Onshore, the transform fault splays into highly active faults (e.g., Motagua and Polochic faults) with slip rates ranging from ~1.5 to 6 mm/yr. Sound compilations of historic earthquakes demonstrate the high seismic activity of the country. However, there is no local or regional map of active fault lines and scarce paleoseismic studies even on the most active ones. The mentioned active fault lines are located in areas of high population density. This is one of the Central America countries hampered by limited information on active fault lines.

12.3.3 Honduras

While seismicity rates and geodetic strain rates are somewhat lower than in neighboring countries, the areas of moderate to high seismicity in Honduras correspond to areas of high population. Faults associated with the Swan Island transform system affect the north western areas of the country. In the rest of the country, distributed normal faulting affects different regions including the capital. While historic seismicity (from sources offshore and onshore) has produced casualties and damage, there is to date no clear understanding of real rates of current tectonic activity. Very few active faults have been mapped at reasonable detail during the compilation of detailed geological maps, but detailed geological maps do not cover all the country. There is no national seismic network and no paleoseismic studies, and thus seismic parameters of known active fault are not characterized. There is no local research team undertaking paleoseismic studies. However, recent geodetic studies can be used to acquire a first approximation of deformation rates along specific fault or fault systems and to identify critical areas for future research.

12.3.4 El Salvador

Active faulting studies started after the devastating 2001 Earthquakes. Most of the mapping so far has concentrated on the El Salvador Fault (along the volcanic region) and surrounding areas. Paleoseismic information is only available for sections of the El Salvador Fault. Active faulting studies have been undertaken by overseas institutions (Spain, NZ, Italy) in collaboration with Servicio Nacional de Estudios Territoriales (*SNET*). These studies have identified a large number of distributed faults but there are still many gaps in the mapping and scarce active faulting studies for the density of faults. However, recent published and on-going GPS studies are currently used to assess a first proxy fault slip rate for some faults. One of the major issues is that El Salvador does not have a University Faculty of Geology, and thus overseas initiatives have not been able to train local geologists in active faulting studies.

12.3.5 Nicaragua

In Nicaragua, a high quality map of active faults for the metropolitan areas of Managua (INETER, 2012: and update of Cowan et al., 2000) was funded by Red Cross and the local emergency Institution and is currently used as a tool for land use planning. There are numerous faults in that area and specific active faulting studies are commonly undertaken, especially in the urban areas for land planning. All those studies are

reviewed and logged by INETER. The Centro de Investigaciones Geocientíficas from Universidad Nacional Autónoma de Nicaragua (CIGEO-UNAN) undertakes high quality research on active faults, as well as other international researchers. While not complete, the active fault database of Nicaragua is quite robust, in particular for the Managua metropolitan area. Academic and research institute resources are scarce to characterize active faults.

12.3.6 Costa Rica

Costa Rica has a complex tectonic structure because of the interaction between the Cocos Ridge and the overriding Panama Block. A high quality active fault map of the whole country shows this complexity (Montero et al., 1998). This map can be used as a base for the active fault database. However, seismic parameters are lacking for most faults. Some recent journal papers have characterized a few faults. At this stage, there is no Institution that has started to compile an active fault database per se. Additional research related to faults has been carried out by the Institute of Electricity (ICE) and Universidad de Costa Rica (UCR). There are at least two regional seismic networks (controlled by Universidad de Costa Rica and by Universidad Nacional) monitoring seismicity.

12.3.7 Panama

Panama has a complex active tectonic structure surrounded offshore by actively deforming belts. Numerous onshore active faults have been compiled on a map of active faults in Panama (Cowan et al., 1998). Recent studies have confirmed and characterized Holocene activity along several faults close to the Panama Canal (consultants and US academics). Those studies have confirmed moderate to large slip rates (3 to 7 mm/yr). There are scarce active faulting studies in the rest of the country. Active tectonics studies with limited resources by Instituto de Geociencias, Universidad de Panamá, are concentrating on correlating historical seismicity to active fault in the south of the country, but actual fault slip rates are still not known.

12.4 Conclusions and recommendations resulting from the workshops

The GFE workshops on the active fault database and its OpenQuake webtool have achieved the following outcomes:

- They have served as a basis to create a working group on active faults for two regions of the world, Southeast Asia and Central America.
- The host countries had the largest number of participants, and in both cases there were discussions to centralize the active fault database input into GEM on one of the leading Institutions. This seems to be a great achievement towards future collaboration and agreement on parameters that need to be input into GEM.
- They have provided training on the conceptual aspects of the parameters that are required for hazard assessment and their uncertainties.
- They have provided training into the GEM database structure, parameters and the OpenQuake active fault database tool.
- Feedback from participants on the GEM philosophy, activities and, in particular, on the active fault database has been received by GEM and incorporated into the reporting and the development of the webtool and associated resources.
- The participants and the leaders have acquired a clear picture of the status of the active faulting studies in the two regions.

- Dictionary and users guide were distributed and have proven to be very useful based on participants' feedback.
- A few active faults have been input into the database

The GFE workshops have also identified the following gaps:

- While the approximate location of most of the major active fault lines in the two regions is well known, most of the faults are poorly characterized through paleoseismic studies due to lack of resources (e.g., large country and not many geologists; lack of financial resources; or lack of fault expression due to urbanization, vegetation and/or difficult access). In a few cases, active fault lines are not even mapped.
- Most of the geologists focusing on paleoseismic studies are not used to “best guess” a fault parameter, e.g., fault slip rate. The lack of familiarity to the use of large uncertainty ranges when data is lacking could hamper data inputs to the database. However, hazard assessment requires this type of evaluations through the application of appropriate uncertainty estimates.
- Unknown fault parameters in hazard assessment can be derived from other data sets such as geodetic rates, seismic moment rates, etc. However, this approach has not been used by many of the participants. Also literature on how to derive these parameters and how to assess the uncertainty is not available through the traditional academic resources.
- The GFE workshops have also identified potential impediments for constructing a relatively complete GFE active fault database in the two region such as: the lack of resources mentioned above can leave some gaps in the maps (e.g., Guatemala, Honduras, PNG); and input of data is labour intensive and the upload of existing datasets is currently not working thought an uploading tool.
- Both workshop participants used a prototype tool still in development. There were issues relating to stability, and other aspects under development that participants have not learned yet.

12.4.1 Recommendations going forward

The GFE workshops have certainly achieved very valuable outcomes but there is a need to continue working towards the goal of creating a homogenous complete worldwide active fault database. We recommend the following:

- Our strongest recommendation is that the working groups are maintained through future meetings and activities.
- Future workshops are needed once the tool is live and stable to assist the participants to upload their data. These first workshops planted the seed and got them thinking; future workshops could focus on inputting data. We strongly believe that momentum will snowball after then. If there is no follow up, we fear that not much data will be inputted. We strongly suggest that we avoid an “out-of-sight out-of-mind” situation.
- A compilation meeting will also help discussions on controversial fault parameters and finalize the regional database. This can be and should be undertaken within the Regional Component, as it is of importance that other researchers (seismologists, geodesist) take part in these discussions.
- To assist geologists deal with scarce datasets or lack of data, some wider training to earthquake geologists about making best estimates, using auxiliary data, and even a better understanding that it is possible to include fault parameters with large uncertainties is possible in PSHA could help. We

believe this will then give users confidence to include faults in the GEM-FE that have little information.

- A forum/chat board is also recommended. This could be done through NEXUS. This would help create a user community which is critical for people gathering momentum.
- On the technical side, we strongly recommend that the webtool is implemented so that fault traces can be uploaded from GIS format, because there is already a large amount of data in GIS form. Also scientist will be more encouraged to contribute with data if there is an automatic upload of attribute information from an xls. and the possibility of copying attributes from fault section.
- A natural follow up from this first meeting is to provide the participants with templates of shape files to upload the traces that are already digitized and, if possible, an .xls template for section attributes. If this is provided, the researchers can start working towards building the database while the webtool is finalized.
- Once the OpenQuake tool is fully working and the server maintained, the researchers with no GIS facilities can start loading their datasets.
- As new training material we suggest the use of recorded webinars and screen grabs and their distribution.

13 Summary and outlook

GFE has developed a modern neotectonic fault database structure and a unique graphical interface for the compilation of new fault data that is a generational advance on previous databases. In addition, national databases that have been made available to the project have been uploaded to the OpenQuake Platform. Several regional or fault specific coverages, including all subduction zones, mid-ocean fault zones, and the Himalaya Frontal [Thrust](#) Fault have been characterised and parameters developed that enable the derivation of earthquake event sets to underpin earthquake hazard assessment across these regions, on a consistent basis. Achieving global coverage has been challenging for many reasons, including the timeframe of the project being too short when in-country expertise has been lacking and training is required before fault mapping and characterisation can begin. For parts of the world with no, or partial coverage of neotectonic fault data, we recommend the establishment of national programmes to map, compile and synthesise neotectonic fault data under the auspices of a database manager. In this way, consistently compiled neotectonic fault data can contribute to seismic hazard assessment. The availability of international standards will help collaboration across national borders, leading to consistently compiled neotectonic fault data, and a consistent basis for seismic hazard assessment, when combined with seismological, geodetic, and ground motion data.

REFERENCES

Document References

- Abercrombie, R.E., M. Antolik, K. Felzer, and G. Ekstrom (2001), The 1994 Java tsunami earthquake: Slip over a subducting seamount, *J. Geophys. Res.*, 106, 6595–6607.
- Ader, T., J.-P. Avouac, J. Liu-Zeng, H. Lyon-Caen, L. Bollinger, J. Galetzka, J. Genrich, M. Thomas, K. Chanard, S.N. Sapkota, S. Rajaure, P. Shrestha, L. Ding, and M. Flouzat (2012), Convergence rate across the Nepal Himalaya and interseismic coupling on the Main Himalayan Thrust: Implications for seismic hazard, *J. Geophys. Res.*, 117, B04403, doi:10.1029/2011JB009071.
- Aki, K., and P.G. Richards (2002), *Quantitative seismology* (2 ed.). University Science Books.
- Aki, K., and P.G. Richards. (1980), *Quantitative Seismology: Theory and methods*. W. H. Freeman, San Francisco, California, USA.
- Albini, P., R.M.W. Musson, A.A. Gomez Capera, M. Locati, A. Rovida, M. Stucchi, and D. Viganò (2013), Global Historical Earthquake Archive and Catalogue (1000–1903), GEM Technical Report 2013-01 V1.0.0, 202pp., GEM Foundation, Pavia, Italy, doi: 10.13117/GEM.GEGD.TR2013.01.
- Ambraseys, N.N. and R.D. Adams (2001), *The Seismicity of Central America*, Imperial College Press, London, 309 pp.
- Ambraseys, N., and R. Bilham (2000), A note on the Kangra Ms = 7.8 earthquake of 4 April 1905, *Curr. Sci.*, 79: 45–50.
- Ambraseys, N., and J. Douglas (2004), Magnitude calibration of north Indian earthquakes, *Geophys. J. Int.*, 159: 165–206.
- Ambraseys, N., and D. Jackson (2003), A note on early earthquakes in northern India and southern Tibet, *Curr. Sci.*, 84: 571–582.
- Ambraseys, N.N. and J.A. Jackson (1998), Faulting associated with historical and recent earthquakes in the Eastern Mediterranean region. *Geophys. J. Int.*, 133 (2), 390–406.
- Ammon, C.J., H. Kanamori, T. Lay, and A.A. Velasco (2006), The 17 July 2006 Java tsunami earthquake, *Geophys. Res. Lett.*, 33, L24308, doi:10.1029/2006GL028005.
- Anderson, J.G., S.G. Wesnousky and M.W. Stirling (1996), Earthquake size as a function of fault slip rate. *Bull. Seism. Soc. Am.*, 86 (3), 683–690.
- Ando, M., (1975), Source mechanisms and tectonic significance of historical earthquakes along the Nankai Trough, Japan, *Tectonophys.*, v. 27(2), 119-140.
- Ando, M., M. Nakamura, T. Matsumoto, M. Furukawa, K. Tadokoro, and M. Furumoto (2009), Is the Ryukyu subduction zone in Japan coupled or decoupled? – The necessity of seafloor crustal deformation observation, *Earth Planets and Space*, 61, 1031-1039.

- Asano, K., T. Iwata and K. Irikura (2003), Source characteristics of shallow intraslab earthquakes derived from strong motion simulations, *Earth Planets Space*, 55, e5–e8.
- Audemard, F.A., M.N. Machette, J.W. Cox, R.L. Dart, K.M. Haller (2000), Map and database of Quaternary faults in Venezuela and its offshore regions, *United States Geological Survey Open-File Report* 00-018.
- Basili, R., and V. Kastelic (2011), D3.4 – Database of active faults and seismogenic sources, Seismic Hazard Harmonization in Europe Deliverable Report, Istituto Nazionale de Geofisica e Vulcanologia (INGV).
- Basili, R., V. Kastelic, M.B. Demircioglu, D. Garcia Moreno, E.S. Nemser, P. Petricc, S.-P. Sboras, G.M. Besana-Ostman, J. Cabral, T. Camelbeeck, R. Caputo, L. Danciu, H. Domac, J. Fonseca, J. García-Mayordomo, D. Giardini, B. Glavatovic, L. Gulen, Y. Ince, S. Pavlides, K. Sesetyan, G. Tarabusi, M.M. Tiberti, M. Utkucu, G. Valensise, K. Vanneste, S. Vilanova, and J. Wössner (2013), The European Database of Seismogenic Faults (EDSF) compiled in the framework of the Project SHARE. <http://diss.rm.ingv.it/share-edsf/>. doi: 10.6092/INGV.IT-SHARE-EDSF.
- Basili, R., V. Kastelic, G. Valensise and DISS Working Group 2009 (2009), Guidelines for compiling records of the Database of Individual Seismogenic Sources, version 3, DISS tutorial series, Istituto Nazionale di Geofisica e Vulcanologia.
- Basili, R., M.M. Tiberti, V. Kastelic, F. Romano, A. Piatanesi, J. Selva, S. Lorito (2013b), Integrating geologic fault data into tsunami hazard studies. *Nat. Hazards Earth Syst. Sci.*, 13(4), 1025-1050, doi: 10.5194/nhess-13-1025-2013.
- Basili, R., G. Valensise, P. Vannoli, P. Burrato, U. Fracassi, S. Mariano, M.M. Tiberti, and E. Boschi (2008), The Database of Individual Seismogenic Sources (DISS), version 3: summarizing 20 years of research on Italy's earthquake geology, *Tectonophysics*, Vol. 453, pp. 20–43.
- Bayrak, Y., A. Yilmazturk, S. Ozturk (2002), Lateral variations of the modal (a/b) values for the different regions of the world, *Journal of Geodynamics*, 34, 653-666.
- Beavan, J., S. Samsonov, P. Denys, R. Sutherland, N. Palmer, and M. Denham (2010a), Oblique slip on the Puysegur subduction interface in the 2009 July Mw 7.8 Dusky Sound earthquake from GPS and InSAR observations; implications for the tectonics of southwestern New Zealand, *Geophys. J. Int.*, 183, 1265-1286.
- Beavan, J., D. Silcock, M. Hamburger, E.G. Ramos, C. Thibault, and R. Feir, (2001), Geodetic constraints on postseismic deformation following the 1990 Ms 7.8 Luzon earthquake and implications for Luzon tectonics and Philippine Sea plate motion, *Geochem. Geophys. Geosyst.*, vol. 2.
- Beavan, J., X. Wang, C. Holden, K. Wilson, W. Power, G. Prasetya, M. Bevis, and R. Kautoke (2010b), Near-simultaneous great earthquakes at Tongan megathrust and outer rise in September 2009, *Nature*, 466, doi:10.1038/nature09292.
- Bernard, P. and J. Lambert (1988), Subduction and seismic hazard in the northern Lesser Antilles: Revision of the historical seismicity, *Bull. Seism. Soc. America*, 78, 1965-1983.
- Berryman, K., C. Costa, K. Sieh, and R.S. Yeats (2010), GEM Faulted Earth: A proposal for a Global Active Fault and Seismic Source Database.

- Berryman K., L. Wallace, G. Hayes, P. Bird, K. Wang, R. Basili, T. Lay, M. Pagani, R. Stein, T. Sagiya, C. Rubin, S. Barreintos, C. Kreemer, N. Litchfield, M. Stirling, K. Gledhill, K.M. Haller, C. Costa (2015) The GEM Faulted Earth Subduction Interface Characterisation Project, Version 2.0, April 2015, GEM Faulted Earth Project], available from <http://www.nexus.globalquakemodel.org/gem-faulted-earth/posts>.
- Berryman, K., T. Webb, N. Hill, M. Stirling, D. Rhoades, J. Beavan and D. Darby (2002). Seismic loads on dams, Waitaki system. Earthquake Source Characterisation. Main report. GNS client report 2001/129, 56 p.
- Bilek, S. (2010), Seismicity along the South American subduction zone: Review of large earthquakes, tsunamis, and subduction zone complexity, *Tectonophys*, doi:10.1016/j.tecto.2009.02.037.
- Bilham, R. (1995), Location and magnitude of the 1833 Nepal earthquake and its relation to the rupture zones of contiguous great Himalayan earthquakes, *Curr. Sci.*, 69: 155–187.
- Bilham, R. (2004), Earthquakes in India and the Himalaya: Tectonics, geodesy and history. *Ann. Geophys.* 47: 839–858.
- Bilham, R., and N. Ambraseys (2005), Apparent Himalayan slip deficit from the summation of seismic moments for Himalayan earthquakes, 1500–2000, *Curr. Sci.*, 88(10): 1658–1663.
- Bird, P. (2003), An updated digital model of plate boundaries, *Geochemistry, Geophysics, Geosystems*, Vol. 4, No. 3, 1027, doi:10.1029/2001GC000252.
- Bird, P., and Y.Y. Kagan (2004), Plate tectonic analysis of shallow seismicity: Apparent boundary width, beta, corner magnitude, coupled lithosphere thickness, and coupling in seven tectonic settings, *Bull. Seis. Soc. America*, 94(6), 2380-2399.
- Bird, P., Y.Y. Kagan, D.D. Jackson, F.P. Schoenberg, and M.J. Werner (2009), Linear and nonlinear relations between relative plate velocity and seismicity, *Bull. Seismol. Soc. Am.*, 99, 3097–3113, doi:10.1785/0120090082.
- Blanpied, M.L., D.A. Lockner, and J.D. Byerlee (1995), Frictional slip of granite at hydrothermal conditions. *J. Geophys. Res.*, 100, 13,045–13,064.
- Blaser, L., F. Krüger, M. Ohrnberger, and F. Scherbaum (2010), Scaling Relations of Earthquake Source Parameter Estimates with Special Focus on Subduction Environment, *Bull. Seismol. Soc. Am.*, 100 (6), 2914–2926.
- Boettcher, M.S., and T.H. Jordan (2004) Earthquake scaling relations for mid-ocean ridge transform faults, *Journal of Geophysical Research*, Vol. 109, B12302, doi:10.1029/2004JB003110.
- Bonilla, M.G., R.K. Mark and J.J. Lienkaemper (1984), Statistical relations among earthquake magnitude, surface rupture length, and surface fault displacement. *Bull. Seism. Soc. Am.*, 74 (6), 2379–2411.
- Byrne, D.E., L.R. Sykes, and D.M. Davies (1992), Great thrust earthquakes and aseismic slip along the plate boundary of the Makran subduction zone, *J. Geophys. Res.*, 97(B1), 449–478, doi:10.1029/91JB02165.
- Cagnan, Z., and G. Tanircan (2010), Seismic hazard assessment for Cyprus, *J. Seismol.*, 14, 2, 225-246, 10.1007/s10950-009-9163-1.
- Cao, A., and S.S. Gao, 2002, Temporal variation of seismic b-values beneath the northeastern Japan island Arc, *Geophysical Research Letters*, 29(9), 1334, doi: 10.1029/2001GL013775

- Casa, A., M. Yamin, E. Wright, C. Costa, M. Ceppelechhia, and M. Cegarra (2011), *Deformaciones Cuaternarias de la Republica Argentina, Sistema de Informacion Geografica, Instituto de Geologia y Recursos Minerales, Servicio Geologico Minero Argentina, Publicacion No. 171, v 1.0 en format DVD.*
- Chander, R. (1989), Southern limits of major earthquake ruptures along the Himalaya between 15 deg. E and 90 deg. E, *Tectonophysics*, 170: 115–123.
- Cifuentes, I. L., and P. G. Silver (1989), Low-frequency source characteristics of the great 1960 Chilean earthquake, *J. Geophys. Res.*, 94(B1), 643–663, doi:[10.1029/JB094iB01p00643](https://doi.org/10.1029/JB094iB01p00643).
- Cornell, C.A. (1968), Engineering seismic risk analysis. *Bull. Seismol. Soc. Am.*, 58, 1583–1606.
- Costa, C., M.N. Machette, R.L. Dart, H.E. Bastias, J.D. Paredes, L.P. Perucca, G.E. Tello, and K.M. Haller (2000), Map and database of Quaternary faults and folds in Argentina, *United States Geological Survey Open-File Report 00-0108*.
- Cowan, H., M.N. Machette, X. Amador, K.S. Morgan, R.L. Dart, and L-A. Bradley (2000), Map and database of Quaternary faults in the vicinity of Managua, Nicaragua, *United States Geological Survey Open-File Report 00-437*.
- Cowan, H., M.N. Machette, K.M. Haller, and R.L. Dart (1998), Map and database of Quaternary faults and folds in Panama and its offshore regions, *United States Geological Survey Open-File Report 98-779*.
- Crowley H., R. Pinho, M. Pagani, and N. Keller (2013), Assessing global earthquake risks: the Global Earthquake Model (GEM) initiative. *Handbook of Seismic Risk Analysis and Management of Civil Infrastructure Systems* 815–838. doi: 10.1533/9780857098986.5.815.
- D'Agostino, N., E. D'Anastasio, A. Gervasi, I. Guerra, M.R. Nedimovic, L. Seeber, and M. Steckler (2011), Forearc extension and slow rollback of the Calabrian Arc from GPS measurements, *Geophys. Res. Lett.*, 38, 17, L17304, [10.1029/2011GL048270](https://doi.org/10.1029/2011GL048270).
- D'Agostino, N., and G. Selvaggi (2004), Crustal motion along the Eurasia-Nubia plate boundary in the Calabrian Arc and Sicily and active extension in the Messina Straits from GPS measurements, *J. Geophys. Res.*, 109, B11402, [10.1029/2004JB002998](https://doi.org/10.1029/2004JB002998).
- DeMets, C., R.G. Gordon, and D.F. Argus (2010), Geologically current plate motions, *Geophys. J. Int.*, Vol. 181, pp. 1–80.
- Devoti, R., F. Riguzzi, M. Cuffaro and C. Doglioni (2008), New GPS constraints on the kinematics of the Apennines subduction. *Earth Planet. Sc. Lett.*, 273, 163-174.
- Dowrick, D., and D.A. Rhoades (2004), Relations between Earthquake Magnitude and Fault Rupture Dimensions: How Regionally Variable Are They? *Bull. Seism. Soc. Am.*, 94 (3), 776–788.
- Drukpa, D., P. Pelgay, A. Bhattacharya, P. Vernant, W. Szeliga, and R. Bilham (2012), GPS constraints on Indo-Asian convergence in the Bhutan Himalaya: Segmentation and potential for a 8.2<Mw<8.8 earthquake, HKT meeting, Kathmandu, Nepal November 2012. *Journal of Nepal Geological Society*, Vol. 45, Special Issue, 43–44.

- Eguez, A., A. Alvarado, H. Yepes, M.N. Machette, C. Costa, and R.L. Dart (2003), Database and map of Quaternary faults and folds of Ecuador and its offshore regions" *United States Geological Survey Open-File Report 03-289*.
- Fedotov, S.A., A.V. Solomatin, and S.D. Chernyshev (2007), Long-term earthquake prediction for the Kuril-Kamchatka arc for 2006–2011 and successful prediction for the Middle Kuril Island earthquake, 15.11.2006, $M_s = 8.2$, *J. Volcanol. Seismol.*, 1(3), 143–163, doi:10.1134/S0742046307030013.
- Fournier, T.J., and J.T. Freymueller (2007), Transition from locked to creeping subduction in the Shumagin region, Alaska, *Geophys. Res. Lett.*, 34, L06303, doi:10.1029/2006GL029073.
- Frankel, A. and W. McCann (1979), Moderate and large earthquakes in the South Sandwich Arc: Indicators of tectonic variation along a subduction zone, *J. Geophys. Res.*, 84 (B10), 5571-5577.
- Frankel, A.D., and M.D. Petersen (2007), Cascadia Subduction Zone, U. S. Geol. Surv. Open File Rep. 2007-1437-L.
- Fujii, Y., and K. Satake (2006), Source of the July 2006 West Java tsunami estimated from tide gauge records, *Geophys. Res. Lett.*, 33, L24317, doi:10.1029/2006GL028049.
- Galgana, G., M. Hamburger, R. McCaffrey, E. Corpuz, Q. Chen (2007), Analysis of crustal deformation in Luzon, Philippines using geodetic observations and earthquake focal mechanisms, *Tectonophysics*. 432, 63-87.
- Ganas, A., and T. Parsons (2009), Three-dimensional model of Hellenic Arc deformation and origin of the Cretan uplift, *J. Geophys. Res.*, 114, B06404, doi:10.1029/2008JB005599.
- Garcia, D., S.K. Singh, M. Herraiz, J.F. Pacheco, and M. Ordaz (2004), Inslab earthquakes of central Mexico: Q, source spectra, and stress drop, *Bull. Seismol. Soc. Am.* 94 (3), 789–802.
- Geller, R.J. (1976), Scaling relations for earthquake source parameters and magnitudes. *Bull. Seismol. Soc. Am.*, 66 (5), 1501–1523.
- Ghosh, A., A.V. Newman, A.M. Thomas, and G.T. Farmer (2008), Interface locking along the subduction megathrust from b-value mapping near Nicoya Peninsula, Costa Rica, *Geophys. Res. Lett.*, 35, L01301, doi:10.1029/2007GL031617.
- Goldfinger, C., C.H. Nelson, A.E. Morey, J.R. Johnson, J. Patton, E. Karabanov, J. Gutierrez-Pastor, A.T. Eriksson, E. Gracia, G. Dunhill, R.J., Enkin, A. Dallimore, and T. Vallier (2012), Turbidite event history—Methods and implications for Holocene paleoseismicity of the Cascadia subduction zone: U.S. Geological Survey Professional Paper 1661–F, 170 p, 64 figures, available at <http://pubs.usgs.gov/pp/pp1661/f>.
- Guidoboni, E., and A. Comastri (1997), The large earthquake of 8 August 1303 in Crete: seismic scenario and tsunamis in the Mediterranean, *J. Seismol.*, 1, 55–72.
- Guidoboni, E., and A. Comastri (2005), Catalogue of earthquakes and tsunamis in the Mediterranean area from the 11th to the 15th century. Istituto Nazionale di Geofisica e Vulcanologia – SGA, Bologna, 1037 pp.
- Guidoboni, E., G. Ferrari, D. Mariotti, A. Comastri, G. Tarabusi, and G. Valensise (2007), CFTI4Med, Catalogue of Strong Earthquakes in Italy (461 B.C.-1997) and Mediterranean Area (760 B.C.-1500). INGV-SGA. Available from <http://storing.ingv.it/cfti4med/>.

- Haller, K.M., and Basili, R. (2011), Developing seismogenic source models based on geologic fault data, *Seismological Research Letters*, Vol. 82, pp. 519–525.
- Haller, K.M., M.N. Machette, and R.L. Dart (1993), Maps of major active faults, Western Hemisphere International Lithosphere Program (ILP) Project II-2: Guidelines for U.S. Database and Map, *USGS Open-File Report*, Vol. 93–338.
- Hamburger, M.W., R.K. Cardwell, and B.L. Isacks, Seismotectonics of the northern Philippine island arc, in *The Tectonic and Geologic Evolution of Southeast Asian Seas and Islands: Part 2*, *Geophys. Monogr. Ser.*, vol. 27, edited by D. Hayes et al., pp. 1 – 22, AGU, Washington, D. C., 1983.
- Hanks, T.C., and W.H. Bakun (2002), A bilinear source-scaling model for M-log A observations of continental earthquakes, *Bull. Seismol. Soc. Am.*, 92 (5), 1841–1846.
- Hanks, T.C., and W.H. Bakun (2008), M-log A observations of recent large earthquakes. *Bull. Seismol. Soc. Am.*, 98 (1), 490–494.
- Hanks, T.C., G.C. Beroza, and S. Toda (2012), Have recent earthquakes exposed flaws in or misunderstandings of probabilistic seismic hazard analysis? *Seismol. Res. Lett.*, 83, 759-764.
- Hanks, T.C., and H. Kanamori (1979), A moment magnitude scale. *J. Geophys. Res.*, Vol. 84, pp. 2348–2350.
- Hashimoto, C., A. Noda, T. Sagiya, and M. Matsu'ura (2009), Interplate seismogenic zones along the Kuril–Japan trench inferred from GPS data inversion, *Nature Geoscience*, 2, 141-144.
- Hayes, G.P., and D.J. Wald (2009), Developing framework to constrain the geometry of the seismic rupture plane on subduction interfaces a priori – a probabilistic approach, *Geophys. J. Int.*, Vol. 176, pp. 951–964, doi:10.1111/j.1365-246X.2008.04035.x
- Hayes, G.P., D.J. Wald, and R.L. Johnson (2012), Slab1.0: A three-dimensional model of global subduction zone geometries, *J. Geophys. Res.*, 117, B01302, doi:10.1029/2011JB008524.
- Heidarzadeh, M., Pirooz, M.D., Zaker, N.H., Yalciner, A.C., Mokhtari, M., Esmaeily, A. (2008), Historical tsunami in the Makran Subduction Zone off the southern coasts of Iran and Pakistan and results of numerical modelling, *Ocean Engineering*, 35 (774-786).
- Henry, C. and S. Das (2001), Aftershock zones of large shallow earthquakes: Fault dimensions, aftershock area expansion and scaling relations. *Geophys. J. Int.*, 147 (2), 272–293.
- Hernandez, B., N.M. Shapiro, S.K. Singh, J.F. Pacheco, F. Cotton, M. Campillo, A. Iglesias, V. Cruz, J.M. Comez, and L. Alcantara (2001), Rupture history of September 30, 1999 intraplate earthquake of Oaxaca, Mexico ($M_w=7.5$) from inversion of strong-motion data, *Geophys. Res. Lett.*, 28 (2), 363–366.
- Heuret, A. (2005), *Dynamique des zones de subduction: Etude statistique globale et approche analogique— Subduction zones dynamics: Global statistical study and experimental modelling*, Ph.D. thesis, Univ. Montpellier II, Montpellier, France. (Available at <http://tel.archives-ouvertes.fr/tel-00108728/en/>)

- Heuret, A., S. Lallemand, F. Funiciello, C. Piromallo, and C. Faccenna (2011), Physical characteristics of subduction interface type seismogenic zones revisited. *Geochemistry, Geophysics, Geosystems* 12: Q01004, doi:10.1029/2010GC003230.
- Hiemer, S., D.D. Jackson, Q. Wang, Y.Y. Kagan, J. Woessner, J.D. Zechar and S. Wiemer (2013), A stochastic forecast of California earthquakes based on fault slip and smoother seismicity. *BSSA* 103: 799-810.
- Hollenstein, Ch., M.D. Müller, A. Geiger and H.-G. Kahle (2008), Crustal motion and deformation in Greece from a decade of GPS measurements, 1993–2003, *Tectonophy.*, 449, 17–40, 10.1016/j.tecto.2007.12.006.
- Houlié, N., and R.J. Phillips (2013), Quaternary rupture behavior of the Karakoram Fault and its relation to the dynamics of the continental lithosphere, NW Himalaya–western Tibet. *Tectonophysics*, 599, 1–7.
- Ichinose, G.E., H.K. Thio and P.G. Somerville (2006), Moment Tensor and Rupture Model for the 1949 Olympia, Washington, Earthquake and Scaling Relations for Cascadia and Global Intraslab Earthquakes, *Bull. Seismol. Soc. Am.* 96 (3), 1029–1037.
- Iglesias, A., S.K. Singh, J.F. Pacheco and M. Ordaz (2002), A source and wave propagation study of the Copalillo, Mexico, earthquake of 21 July 2000 (M_w 5.9): implications for seismic hazard in Mexico City from intraslab earthquakes. *Bull. Seismol. Soc. Am.* 92 (3), 1060–1071.
- Ishii, M., P.M. Shearer, H. Houston, and J.E. Vidale (2005), Extent, duration and speed of the 2004 Sumatra-Andaman earthquake imaged by Hi-Net array, *Nature*, 435, 933–936, doi:10.1038/nature03675.
- Ito, T., and M. Hashimoto (2004), Spatiotemporal distribution of interplate coupling in southwest Japan from inversion of geodetic data, *J. Geophys. Res.*, 109, B02315, doi:10.1029/2002JB002358.
- Johnston, A.C. (1994), Seismotectonic interpretations and conclusions from the stable continental region seismicity database, in *The Earthquake of Stable Continental Regions. Volume 1: Assessment of Large Earthquake Potential*, A. C. Johnston, K. J. Coppersmith, L. R. Kanter and C. A. Cornell (Editors), Electric Power Research Institute.
- Johnson, J. M., Y. Tanioka, L. J. Ruff, K. Satake, H. Kanamori, and L. R. Sykes (1994), The great Aleutian earthquake, *Pure Appl. Geophys.*, 142, 3–28, doi:10.1007/BF00875966.
- Jongens, R., and G. Dellow (2003), The active faults database of New Zealand: Data dictionary, *Institute of Geological & Nuclear Sciences science report*, Vol. 2003/17.
- Kagan, Y.Y., and D.D. Jackson (2013), Tohoku Earthquake: A Surprise?. *BSSA* 103: 1181 -1194.
- Kanamori, H. (1986), Rupture process of subduction-zone earthquakes, *Annu. Rev. Earth Planet. Sci.*, 14, 293–322, doi:10.1146/annurev.ea.14.050186.001453.
- Kanamori, H., and C.R. Allen (1986), Earthquake repeat time and average stress drop. In *Earthquake source mechanics*, eds. Das, S., J. Boatwright and C.H. Scholz. *Geophys. Monogr.*, 37, 227–235.
- Kanamori, H., and D.L. Anderson (1975), Theoretical basis of some empirical relations in seismology. *Bull. Seism. Soc. Am.*, 65 (5), 1073–1095.

- Koehler, R.D., R.-E. Farrell, P.A.C. Burns, and R.A. Combellick (2012), Quaternary faults and folds in Alaska: A digital database. *Alaska Division of Geological & Geophysical Surveys Miscellaneous Publication*, Vol. 141.
- Konstantinou, K.I., G.A. Papadopoulos, A. Fokaefs, and K. Orphanogiannaki (2005), Empirical relationships between aftershock area dimensions and magnitude for earthquakes in the Mediterranean sea region, *Tectonophysics*, 403 (1–4), 95.115.
- Koppa, C., J. Fruehn., E.R. Flueh., C. Reichert., N. Kukowski., J. Bialas., D. Klaeschen (2000), Structure of the Makran subduction zone from wide-angle and reflection seismic data, *Tectonophysics*. 329, 171–191.
- Kreemer, C., G.E. Klein, Z.-K. Shen, M. Wang, L. Estey, S. Wier, and F. Boler (2014), Global Geodetic Strain Rate Model, GEM Technical Report 2014-07 V1.0.0, 129pp., GEM Foundation, Pavia, Italy, doi: 10.13117/GEM.GEGD.TR2014.07.
- Kumahara, Y., and R. Jayangondaperumal (2013), Paleoseismic evidence of a surface rupture along the northwestern Himalayan Frontal Thrust (HFT), *Geomorphology*, 180, 47–56.
- Kumar, S., S.G. Wesnousky, R. Jayangondaperumal, T. Nakata, Y. Kumahara, and V. Singh (2010), Paleoseismological evidence of surface faulting along the northeastern Himalayan front, India: Timing, size, and spatial extent of great earthquakes, *J. Geophys. Res.*, 115, B12422, doi:10.1029/2009JB006789.
- Kumar, S., S.G. Wesnousky, T.K. Rockwell, R.W. Briggs, V.C. Thakur, and R. Jayangondaperumal (2006), Paleoseismic evidence of great surface-rupture earthquakes along the Indian Himalaya, *J. Geophys. Res.*, 111, B03304, doi:10.1029/2004JB003309.
- Kumar, S., S.G. Wesnousky, T.K. Rockwell, D. Ragona, V.C. Thakur, G.G. Seitz (2001), Earthquake recurrence and rupture dynamics of Himalayan Frontal Thrust, India, *Science*, 294(5550), 2328–2331.
- LaFemina, P., T.H. Dixon, R. Govers, E. Norabuena, H. Turner, A. Saballos, G. Mattioli, M. Protti, and W. Strauch (2009), Fore-arc motion and Cocos Ridge collision in Central America, *Geochem. Geophys. Geosyst.*, 10, Q05S14, doi:10.1029/2008GC002181.
- Larson, K., A.R. Lowry, V. Kostoglodov, W. Hutton, O. Sanchez, K. Hudnut, and G. Suarez (2004), Crustal deformation measurements in Guerrero, Mexico, *J. Geophys. Res.*, 109(B04409).
- Lavé, J., D. Yule, S. Sapkota, K. Basant, C. Madden, M. Attal, and R. Pandey (2005), Evidence for a great medieval earthquake (~1100 A.D.) in the Central Himalayas, Nepal, *Science*, 307, 1302-1305.
- Lavenu, A., R. Thiele, M.N. Machette, R.L. Dart, L.-A. Bradley, and K.M. Haller (2000), Maps and database of Quaternary faults in Bolivia and Chile, *United States Geological Survey Open-File Report* 00-283.
- Lay, T., C.J. Ammon, H. Kanamori, L. Rivera, K.D. Koper, and A.R. Hutko, (2010), The 2009 Samoa-Tonga great earthquake triggered doublet, *Nature*, 466, 964-968.
- Lay, T., and H. Kanamori (1980), Earthquake doublets in the Solomon Islands, *Phys. Earth Planet. Int.*, 21, 283-304.
- Leonard, M. (2010), Earthquake Fault Scaling: Relating Rupture Length, Width, Average Displacement, and Moment Release, *Bull. Seismol. Soc. Am.*, 100 (5A), 1971–1988.

- Litchfield N., K. Berryman, R. Stein, and M. Willis (2011), Inventory of existing fault databases and data attributes, GEM Faulted Earth, Available from www.nexus.globalquakemodel.org/gem-faulted-earth/posts/
- Litchfield, N., K. Berryman, and R. Thomas (2013a), *Data Dictionary*, GEM Faulted Earth, Available from www.nexus.globalquakemodel.org/gem-faulted-earth/posts/.
- Litchfield, N., and R. Jongens (2006), Active Faults Database of New Zealand, *Proceedings of the New Zealand Earthquakes and urban development, New Zealand Geotechnical Society 2006 Symposium*, Nelson, New Zealand, pp. 327–340.
- Litchfield N., and R. Thomas (2013), Bulk upload of national and global databases, Available from www.nexus.globalquakemodel.org/gem-faulted-earth/posts/.
- Litchfield N., B. Wyss, A. Christophersen, R. Thomas, K. Berryman, P. Henshaw, P. Villamor, and M. Pagani (2013b), Guidelines for compilation of neotectonic faults, folds, and fault sources, Available from www.nexus.globalquakemodel.org/gem-faulted-earth/posts/.
- Machere, J., C.H. Fenton, M.N. Machette, A. Lavenu, C. Costa, R.L. Dart (2003), “Database and map of Quaternary faults and folds in Peru and its offshore region” *United States Geological Survey Open-File Report* 03-451.
- Machette, M.N., K.M. Haller, and L. Wald (2004), Quaternary Fault and Fold Database for the Nation, *United States Geological Survey Fact Sheet*, Vol. 2004–3033.
- Madariaga, R., M. Metois, C. Vigny, and J. Campos (2010), Central Chile finally breaks, *Science*, 328(5975), 181–182, doi:10.1126/science.1189197.0.
- Mai, P.M. (2004), SRCMOD – Database of finite-source rupture models. Annual meeting of the Southern California Earthquake Center (SCEC), Palm Springs, September 2004 (abstract).
- Mai, P.M. (2007), SRCMOD – Database of finite-source rupture models. Available online at: <http://www.seismo.ethz.ch/srcmod>.
- Mai, P.M., and G.C. Beroza (2000), Source Scaling Properties from Finite-Fault-Rupture Models. *Bull. Seismol. Soc. Am.* 90 (3), 604–615.
- Manighetti, I., M. Campillo, S. Bouley, and F. Cotton (2007), Earthquake scaling, fault segmentation, and structural maturity, *Earth Planet. Sci. Lett.*, 253 (3–4), 429–438.
- Margaris, B.N., and D.M. Boore (1998), Determination of $\Delta\sigma$ and κ_0 from response spectra of large earthquakes in Greece, *Bull. Seismol. Soc. Am.*, 88 (1), 170–182.
- Marone, C. (1998), Laboratory-derived friction laws and their application to seismic faulting, *Annual Reviews of Earth and Planetary Sciences*, 26, 643–696.
- McCaffrey, R. (1997), Influences of recurrence times and fault zone temperature on the age-rate dependence of subduction zone seismicity, *J. Geophys. Res.*, 102, 22,839–22,854, doi:10.1029/97JB01827.
- McCaffrey, R. (2008), Global frequency of magnitude 9 earthquakes, *Geology*, 36.3, 263–266.
- McCaffrey, R. (2009), The tectonic framework of the Sumatran Subduction Zone, *Annual Rev. Earth Planet. Sci.*, 37, 346–366.

- McCalpin, J.P. (2009), *Paleoseismology*, International Geophysics Series 95, Academic Press Inc., Sand Diego, USA.
- McCann, W.R., S.P. Nishenko, L.R. Sykes, and J. Krause (1979), Seismic gaps and plate tectonics: Seismic potential for major boundaries, *Pure Appl. Geophys.*, 117, 1082–1147, doi:10.1007/BF00876211.
- Meckel, T.A., M.F. Coffin, S. Mosher, P. Symonds, G. Bernardel, and P. Mann (2003), Underthrusting at the Hjort Trench, Australian-Pacific plate boundary: Incipient subduction?, *Geochem. Geophys. Geosyst.*, 4(12), 1099, doi:10.1029/2002GC000498.
- Meckel, T. A., P. Mann, S. Mosher, and M. F. Coffin (2005), Influence of cumulative convergence on lithospheric thrust fault development and topography along the Australian-Pacific plate boundary south of New Zealand, *Geochem. Geophys. Geosyst.*, 6, Q09010, doi:10.1029/2005GC000914.
- Molchan, G., T. Kronrod, and G.F. Panza (1997), Multi-scale seismicity model for seismic risk, *Bull. Seismol. Soc. of America*, 87(5), 1220-1229.
- Molnar, P., and D. Qidong (1984), Faulting associated with large earthquakes and the average rate of deformation in central and eastern Asia, *J. Geophys. Res.*, 89 (B7), 6203– 6227.
- Molnar, P., and M.R. Pandey (1989), Rupture zones of great earthquakes in the Himalaya region, *Earth Planet. Sci.*, 98, 61–70.
- Montero, W., P. Denyer, R. Barquero, G.E. Alvarado, H. Cowan, M.N. Machette, K.M. Haller, and R.L. Dart (1998), Map and database of Quaternary faults and folds in Costa Rica and its offshore regions *United States Geological Survey Open-File Report* 98–481.
- Morikawa, N., and T. Sasatani (2004), Source models of two large intraslab earthquakes from broadband strong ground motions, *Bull. Seismol. Soc. A.*, 94 (3), 803–817.
- Nakata, T. (1972), *Geomorphic History and Crustal Movements of Foothills of the Himalaya*, Sendai Institute of Geography, Tohoku University, Japan, 77pp.
- Nakata, T. (1989), Active faults of the Himalaya of India and Nepal, in *Tectonics of the Western Himalayas*, edited by L.L. Malinconico Jr. and R.J. Lillie, pp. 243–264, *Geol. Soc. of Am.*, Boulder, Colo.
- Nakata, T., and Y. Kumahara (2002), Active faulting across the Himalaya and its significance in the collision tectonics. *Active Fault Research* 22 (2002): 7–16.
- Nakata, T., K. Kumura, and T. Rockwell (1998), First successful paleoseismic trench study on active faults in the Himalaya, *Eos Trans. AGU*, 79(45), Fall Meet Suppl., Abstract S22A-18.
- Nishimura, S., M. Hashimoto, and M. Ando (2004b), A rigid block rotation model for the GPS derived velocity field along the Ryukyu arc, *Phys. Earth Planet. Inter.*, 142, 185–203, doi:10.1016/j.pepi.2003.12.014.
- Nishimura, T., T. Hirasawa, S. Miyazaki et al. (2004a), Temporal change of interplate coupling in northeastern japan during 1995–2002 estimated from continuous GPS observations, *Geophys. J. Int.*, 157, 901–916.
- Nishimura, T., T. Sagiya, and R.S. Stein (2007), Crustal block kinematics and seismic potential of the northernmost Philippine Sea plate and Izu microplate, central Japan, inferred from GPS and leveling data, *J. Geophys. Res.*, 112, B05414, doi:10.1029/2005JB004102.

- Norabuena, E., et al. (2004), Geodetic and seismic constraints on some seismogenic zone processes in Costa Rica, *J. Geophys. Res.*, 109, B11403, doi:10.1029/2003JB002931.
- Nuttli, O. (1983), Average seismic source-parameter relations for mid-plate earthquakes. *Bull. Seism. Soc. Am.*, 73 (2), 519–535.
- Okal, E.A., and D. Reymond (2003), The mechanism of the great Banda Sea earthquake of 01 February 1938: Applying the method of Preliminary Determination of Focal Mechanism to a historical event, *Earth Planet. Sci. Letts.*, 216, 1-15.
- Pacheco, J. F., and S.K. Singh (2010), Seismicity and state of stress in Guerrero segment of the Mexican subduction zone, *J. Geophys. Res.*, 115, B01303, doi:10.1029/2009JB006453.
- Pandey, MR., and P. Molnar (1988), The distribution of intensity of the Bihar-Nepal earthquake of 15 January 1934 and bounds on the extent of the rupture zone, *J. Geol. Soc. Nepal*, 5, 22–44.
- Paris, G., M.N. Machette, R.L. Dart, and K.M. Haller (2000), Map and database of Quaternary faults and folds in Colombia and its offshore regions *United States Geological Survey Open-File Report 00-0284*.
- Park, S.-C., and J. Mori (2007), Are asperity patterns persistent? Implication from large earthquakes in Papua New Guinea, *J. Geophys. Res.*, 112, B03303, doi:10.1029/2006JB004481.
- Parsons, T., Console, R., Falcone, G., Murru, M., and Yamashita, K. (2012), Comparison of characteristic and Gutenberg-Richter models for time-dependent $M \geq 7.9$ earthquake probability in the Nankai-Tokai subduction zone, Japan, *Geophys. J. Int.* 190, 1673-1688, doi: 10.1111/j.1365-246X.2012.05595.x
- Pegler, G. and S. Das (1996), Analysis of the relationship between seismic moment and fault length for large crustal strike-slip earthquakes between 1977–92, *Geophys. Res. Lett.*, 23 (9), 905–908.
- Petersen, M.D., A.D. Frankel, S.C. Harmsen, C.S. Mueller, K.M. Haller, R.L. Wheeler, R.L. Wesson, Y. Zeng, O.S. Boyd, D.M. Perkins, N. Luco, E.H. Field, C.J. Wills, and K.S. Rukstales (2008), Documentation for the 2008 update of the National Seismic Hazard Maps, USGS Open-file Report, Vol. 2008–1128.
- Peterson, E. T., and T. Seno (1984), Factors affecting seismic moment release rates in subduction zones, *J. Geophys. Res.*, 89, 10,233–10,248, doi:10.1029/JB089iB12p10233.
- Pinho, R. (2012) GEM: a participatory framework for open, state-of-the-art models and tools for earthquake risk assessment worldwide. In: *Proceedings of the 15th world conference on earthquake engineering*, Lisbon, Portugal.
- Power, W.L., L.M. Wallace., X. Wang., M.E. Reyners (2011), Tsunami hazard posed to New Zealand by the Kermadec and southern New Hebrides subduction margins: an assessment based on plate boundary kinematics, interseismic coupling, and historical seismicity. *Pure and applied geophysics*, doi:10.1007/s00024-011-0299-x.
- Prawirodirdjo, L., R. McCaffrey, C.D. Chadwell, Y. Bock, and C. Subarya (2010), Geodetic observations of an earthquake cycle at the Sumatra subduction zone: Role of interseismic strain segmentation, *J. Geophys. Res.*, 115, B03414, doi:10.1029/2008JB006139.

- Proyecto Multinacional Andino: Geociencia para les Comunidades Andinas (2008), Atlas de deformaciones cuaternarias de los Andes. *Servicio Nacional de Geología y Minería, Publicación Geológica Multinacional*, No. 7, 320 pp, 1 mapa en CD-ROM.
- Purcaru, G., and H. Berckhemer (1982), Quantitative relations of active source parameters and a classification of earthquakes. *Tectonophysics*, 84 (1), 57–128.
- Reilinger, R., et al. (2006), GPS constraints on continental deformation in the Africa-Arabia-Eurasia continental collision zone and implications for the dynamics of plate interactions, *J. Geophys. Res.*, 111, B05411, doi:10.1029/2005JB004051.
- Romanowicz, B. (1992), Strike-slip earthquakes on quasi-vertical transcurrent faults: Inferences for general scaling relations, *Geophys. Res. Lett.*, 19 (5), 481–484.
- Romanowicz, B., and L.J. Ruff (2002), On moment-length scaling of large strike slip earthquakes and the strength of faults, *Geophys. Res. Lett.*, 29 (12), 45–1 to 45–4.
- Rong, Y., D.D. Jackson, H. Magistrale, and C. Goldfinger (2014), Magnitude limits of subduction zone earthquakes. *Bull. Seismol. Soc. Am.* 104(5):2359-2377. doi:10.1785/0120130287.
- Ruff, L.J. (1989), Do trench sediments affect great earthquake occurrence in subduction zones?, in *Subduction Zones Part I*, edited by L. J. Ruff and H. Kanamori, *Pure Appl. Geophys.*, 129, 263–282.
- Ruff, L.J., and H. Kanamori (1980), Seismicity and the subduction process, *Phys. Earth Planet. Inter.*, 23, 240–252, doi:10.1016/0031-9201(80)90117-X.
- Ruleman, C.A., A.J. Crone, M.N. Machette, K.M. Haller, and K.S. Rukstales (2007), Map and database of probable and possible Quaternary faults in Afghanistan, *USGS Open-File Report*, Vol. 2007–1103.
- Ruppert, N.A., J.M. Lees, and N.P. Kozyreva (2007), Seismicity, earthquakes and structure along the Alaska-Aleutian and Kamchatka-Kurile subduction zones: A review, in *Volcanism and Subduction: The Kamchatka Region*, *Geophys. Monogr. Ser.*, vol. 172, edited by J. Eichelberger et al., pp. 129–144, doi:10.1029/172GM12,AGU,Washington,D.C.
- Saadi, A., M.N. Machette, K.M. Haller, R.L. Dart, L.-A. Bradley, and A.M.P.D. de Souza (2002), Map and database of Quaternary faults and lineaments in Brazil, *United States Geological Survey Open-File Report* 02-230.
- Sagiya, T., and W. Thatcher (1999), Coseismic slip resolution along a plate boundary megathrust: The Nankai Trough, southwest Japan, *J. Geophys. Res.*, 104(B1), 1111-1129.
- Sapkota, S.N., L. Bollinger, Y. Klinger, P. Tapponnier, Y. Gaudemer, and D. Tiwari (2013), Primary surface ruptures of the great Himalayan earthquakes in 1934 and 1255. *Nature Geosci.*, 2013, 6, 71–76; doi: 10.1038/ngeo1669
- Scherwath, M., H. Kopp., E.R. Flueh., S.A. Henrys., and R. Sutherland (2008), Structure and Deformation of the Hikurangi-Kermadec Subduction Zone – Transitions Revealed by Seismic Wide-angle Data. *Eos Trans. AGU*, 2008 Fall Meeting. Suppl., Abstract T23A-1997.
- Schluter, H.U., A. Prexl., Ch. Gaedicke., H. Roeser., Ch. Reichert., H. Meyer., C. von Daniels (2002). The Makran accretionary wedge: sediment thicknesses and ages and the origin of mud volcanoes. *Mar. Geol.* 185, 219–232.

- Scholz, C.H. (1982), Scaling laws for large earthquakes: consequences for physical models, *Bull. Seismol. Soc. Am.*, 72 (1), 1–14.
- Scholz, C.H., C.A. Aviles and S.G. Wesnousky (1986), Scaling differences between large interplate and intraplate earthquakes. *Bull. Seismol. Soc. Am.*, 76 (1), 65–70.
- Scholz, C.H., and J. Campos (1995), On the mechanism of seismic decoupling and back-arc spreading at subduction zones, *J. Geophys. Res.*, 100, 22,103–22,115, doi:10.1029/95JB01869.
- Scholz, C.H., and J. Campos (2012), The seismic coupling of subduction zones revisited, *J. Geophys. Res.* 117, doi:10.1029/2011JB009003.
- Schwartz, S.Y., T. Lay, and L.J. Ruff (1989), Source process of the great 1971 Solomon Islands doublet, *Phys. Earth Planet. Inter.*, 56(3–4), 294–310, doi:10.1016/0031-9201 (89)90164-7.
- Selvans, M., J. Stock, C. DeMets, O. Sanchez, and B. Marquez-Azua (2010), Constraints on Jalisco Block motion and tectonics of the Guadalajara Triple Junction from 1998-2001 campaign GPS data, *PAGEOPH*, DOI: 10.1007/s00024-010-0201-2, 201
- Serpelloni, E., R. Burgmann, M. Anzidei, P. Baldi, B. Mastrolembo Ventura, and E. Boschi (2010), Strain accumulation across the Messina Straits and kinematics of Sicily and Calabria from GPS data and dislocation modeling. *Earth Planet. Sc. Lett.*, 298, 3-4, 347-360, 10.1016/j.epsl.2010.08.005.
- Sesetyan, K. (2011), EMME – Earthquake Model of the Middle East Region: Hazard, Risk Assessment, Economics & Mitigation A GEM Regional Project, *GEM Outreach Meeting*. Beijing, China.
- Shaw, B.E. (2009), Constant Stress Drop from Small to Great Earthquakes in Magnitude-Area Scaling, *Bull. Seismol. Soc. Am.*, 99 (2A), 871–875.
- Shaw, B., and Jackson, J. (2010), Earthquake mechanisms and active tectonics of the Hellenic subduction zone. *Geophys. J. Int.*, 181: 966–984. doi: 10.1111/j.1365-246X.2010.04551.x
- Shimazaki, K. (1986), Small and large earthquakes: the effects of the thickness of seismogenic layer and the free surface. In *Earthquake source mechanics*, eds. Das, S., J. Boatwright and C.H. Scholz. *Geophys. Monogr.*, 37, 209–216.
- Shyu, J.B.H., K. Sieh, Y.-G. Chen, and C.-S. Liu (2005), Neotectonic architecture of Taiwan and its implications for future large earthquakes, *J. Geophys. Res.*, 110, B08402, doi:10.1029/2004JB003251.
- Socquet, A., W. Simons, C. Vigny, R. McCaffrey, C. Subarya, D. Sarsito, B. Ambrosius, and W. Spakman (2006), Microblock rotations and fault coupling in SE Asia triple junction (Sulawesi, Indonesia) from GPS and earthquake slip vector data, *J. Geophys. Res.*, 111, B08409, doi:10.1029/2005JB003963.
- Somerville, P.G. (2006), Review of magnitude-area scaling of crustal earthquakes, *Rep. to WGCEP*, 2006.
- Somerville, P.G., N. Collins, and R. Graves (2006), Magnitude-rupture area scaling of large strike-slip earthquakes, Final Technical Report Award No. 05-HQ-GR-0004, USGS.

- Somerville, P., K. Irikura, R. Graves, S. Sawada, D. Wald, N. Abrahamson, Y. Iwasaki, T. Kagawa, N. Smith, and A. Kowada (1999), Characterizing crustal earthquake slip models for the prediction of strong ground motion. *Seism. Res. Lett.*, 70 (1), 59–80.
- Stein, S., R.J. Geller, and M. Liu (2012), Why earthquake hazard maps often fail and what to do about it. *Tectonophysics*, 562-563, 1-25.
- Stein, S., and E.A. Okal (2007), Ultralong period seismic study of the December 2004 Indian Ocean earthquake and implications for regional tectonics and the subduction process, *Bull. Seismol. Soc. Am.*, 97(1A), S279–S295, doi:10.1785/0120050617.
- Stirling, M.W., M.C. Gerstenberger, N.J. Litchfield, G.H. McVerry, W.D. Smith, W.D., J. Pettinga, J., and P. Barnes (2008), Seismic hazard of the Canterbury region, New Zealand: new earthquake source model and methodology. *Bulletin of the New Zealand Society for Earthquake Engineering*, 41, 51–67.
- Stirling, M.W., and T. Goded (2012), *Magnitude scaling relationships*. GEM Faulted Earth, Available from www.nexus.globalquakemodel.org/gem-faulted-earth/posts/
- Stirling, M., T. Goded, T., K. Berryman, and N. Litchfield (2013), Selection of Magnitude Scaling Relationships for Seismic-Hazard Analysis, *Bull. Seism. Soc. Am.*, 103, pp. 2993–3011.
- Stirling, M.W., G.H. McVerry, and K.R. Berryman (2002), A new seismic hazard model for New Zealand, *Bull. Seism. Soc. Am.*, 92, pp. 1878–1903.
- Stirling, M.W., G.H. McVerry, M. Gerstenberger, N.J. Litchfield, R. Van Dissen, K.R. Berryman, R.M. Langridge, A. Nicol, W.D. Smith, P. Villamor, L. Wallace, K. Clark, M. Reyners, P. Barnes, G. Lamarche, S. Nodder, J. Pettinga, B. Bradley, D. Rhoades, and K. Jacobs (2012), National Seismic Hazard Model for New Zealand: 2010 Update. *Bull. Seismol. Soc. Am.* 102(4), 1514-1542.
- Stirling, M.W., D.A. Rhoades, and K. Berryman (2002), Comparison of earthquake scaling relations derived from data of the instrumental and preinstrumental era, *Bull. Seism. Soc. Am.*, 92(2), 812–830.
- Stirling, M.W., S.G. Wesnousky, and K.R. Berryman (1998), Probabilistic seismic hazard analysis of New Zealand, *New Zealand Journal of Geology and Geophysics*, 41, pp. 355–375.
- Stirling, M.W., S.G. Wesnousky, and K. Shimazaki (1996), Fault trace complexity, cumulative slip, and the shape of the magnitude-frequency distribution for strike-slip faults: a global survey, *Geophys. J. Int.*, 124(3), 833–868.
- Storchak D.A., D. Di Giacomo, I. Bondár, J. Harris, E.R. Engdahl, W.H.K. Lee, A. Villaseñor, P. Bormann, and G. Ferrari (2012), ISC-GEM Global Instrumental Earthquake Catalogue (1900–2009), GEM Technical Report 2012-01 V1.0.0, 128 pp., GEM Foundation, Pavia, Italy, doi: 10.13117/GEM.GEGD.TR2012.01.
- Stock, S., and E.G.C. Smith (2000), Evidence for different scaling of earthquake source parameters for large earthquakes depending on fault mechanism, *Geophys. J. Int.*, 143 (1), 157–162.
- Strasser, F.O., M.C. Arango, and J.J. Bommer (2010), Scaling of the Source Dimensions of Interface and Intraslab Subduction-zone Earthquakes with Moment Magnitude, *Seism. Res. Lett.*, 81 (6), 941–950.

- Subarya, C., M. Chlieh, L. Prawirodirdjo, J.-P. Avouac, Y. Bock, K. Sieh, A.J. Meltzner, D.H. Natawidjaja, and R. McCaffrey (2006), Plate boundary deformation associated with the great Sumatra-Andaman earthquake, *Nature*, 440(7080), 46–51, doi:10.1038/nature04522.
- Suckale, J., and G. Grünthal (2009), A probabilistic seismic hazard model for Vanuatu, *Bull. Seis. Soc. Am.*, 99, 4, 2108-2126.
- Taylor, F.W., M.G. Bevis, I.W.D. Dalziel, R. Smalley Jr., C. Frohlich, E. Kendrick, J. Foster, D. Phillips, and K. Gudipati (2008b), Kinematics and segmentation of the South Shetland Islands-Bransfield basin system, northern Antarctic Peninsula, *Geochem. Geophys. Geosyst.*, 9, Q04035, doi:10.1029/2007GC001873.
- Taylor, F.W., R.W. Briggs, C. Frohlich, A. Brown, M. Hornbach, A.K. Papabatu, A.J. Meltzner, and D. Billy, (2008a), Rupture across arc segment and plate boundaries in the 1 April 2007 Solomons earthquake, *Nature Geoscience*, 1, 253-257
- Thomas, R. (2012), GEM Faulted Earth Database XML Interchange, GEM Faulted Earth, Available from www.nexus.globalquakemodel.org/gem-faulted-earth/posts/.
- Thomas, R., N. Litchfield, A. Christophersen (2012), GEM Faulted Earth database design, Available from www.nexus.globalquakemodel.org/gem-faulted-earth/posts/.
- Tichelaar, B.W., and L.J. Ruff (1993), Depth of seismic coupling along subduction zones, *J. Geophys. Res.*, 98, 2017–2037, doi:10.1029/92JB02045.
- Tregoning, P., and A. Gorbato (2004), Evidence for active subduction at the New Guinea Trench, *Geophys. Res. Lett.*, 31, L13608, doi:10.1029/2004GL020190.
- Upreti, B.N., et al. (2000), The latest active faulting in Southeast Nepal, paper presented at Proceedings Active Fault Research for the New Millennium, Hokudan Int. Symp. and Sch. on Active Faulting, Awaji Island, Hyogo, Japan.
- USGS (2006), Shuttle Radar Topography Mission, Global Land Cover Facility, University of Maryland, College Park, Maryland, February 2000.
- USGS, and Japan ASTER Program (2003), USGS, Sioux Falls.
- Utsu, T., Table of destructive earthquakes in the world, <http://iisee.kenken.go.jp/utsu/>, 1989.
- Uyeda, S., and H. Kanamori (1979), Back-arc opening and the mode of subduction, *J. Geophys. Res.* 84, 1049-1061.
- Vakov, A.V. (1996), Relationships between earthquake magnitude, source geometry and slip mechanism. *Tectonophysics*, 261 (1–3), 97–113.
- Vernant, P., and 11 co-authors, (2004), Present-day crustal deformation and plate kinematics in the Middle East constrained by GPS measurements in Iran and northern Oman, *Geophys. J. Int.*, 157, 381-398.
- Vigny, C., and 16 co-authors (2002), Migration of seismicity and earthquake interactions monitored by GPS in SE Asia triple junction: Sulawesi, Indonesia, *J. Geophys. Res.*, 107(B10), 2231, doi:10.1029/2001JB000377.

- Villamor, P., R. Van Dissen, B.V. Alloway, A.S. Palmer, and N. Litchfield (2007), The Rangipo Fault, Taupo Rift, New Zealand: An example of temporal slip-rate and single-event displacement variability in a volcanic environment. *GSA Bulletin*, 119, 529–547.
- Wald, D.J., and P.G. Somerville (1995), Variable-slip rupture model of the great 1923 Kanto, Japan earthquake: Geodetic and body-waveform analysis, *Bull. Seismol. Soc. Am.*, 85, 159–177.
- Wallace, L.M., R.J. Beavan, R. McCaffrey, K.R. Berryman, and P. Denys (2007), Balancing the plate motion budget in the South Island, New Zealand using GPS, geological and seismological data. *Geophys. J. int.*, 168(1): doi:10.1111/j.1365-246X.2006.03183.
- Wallace, L.M., J. Beavan., R. McCaffrey, and D. Darby (2004a), Subduction zone coupling and tectonic block rotations in the North Island, New Zealand: *J. Geophys. Res.*, v. 109, no. B12406, p. doi:10.1029/2004JB003241.
- Wallace, K., R. Bilham, F. Blume, V.K. Gaur, and V. Gahalaut (2005a), Surface deformation in the region of the 1905 Kangra Mw = 7.8 earthquake in the period 1846–2001, *Geophys. Res. Lett.*, L15307, doi:10.1029/2005GL022906.
- Wallace, L.M., S. Ellis., K. Miyao, S. Miura, J. Beavan, and J. Goto (2009a), Enigmatic, highly active left-lateral shear zone in southwest Japan explained by aseismic ridge collision, *Geol.*, 37(2), 143–146, doi:10.1130/G25221A.1.
- Wallace, L.M., R. McCaffrey, J. Beavan, and S. Ellis (2005b), Rapid microplate rotations and back-arc rifting at the transition between collision and subduction, *Geology*, 33(11), 857-860.
- Wallace, L.M., C. Stevens, E. Silver, R. McCaffrey, W. Loratung, S. Hasiata, R. Stanaway, R. Curley, R. Rosa, and J. Taugaloidi (2004b), GPS and seismological constraints on active tectonics and arc-continent collision in Papua New Guinea: Implications for mechanics of microplate rotations in a plate boundary zone, *J. Geophys. Res.*, 109, B05404, doi:10.1029/2003JB002481.
- Wallace, L.M., and 21 co-authors (2009b), Characterizing the seismogenic zone of a major plate boundary subduction thrust: Hikurangi Margin, New Zealand, *Geochem. Geophys. Geosyst.*, 10.
- Wdowinski, S., Z. Ben-Avraham, R. Arvidsson and G. Ekström (2006) Seismotectonics of the Cyprian Arc. *Geophys. J. Int.*, 164, 1, 176-181, 10.1111/j.1365-246X.2005.02737.x
- Wells, D.L., and K.J. Coppersmith (1994), New empirical relationships among magnitude, rupture length, rupture width, rupture area, and surface displacement, *Bull. Seismol. Soc. Am.*, 84 (4), 974–1002.
- Wesnousky, S.G. (2008), Displacement and geometrical characteristics of earthquake surface ruptures: Issues and implications for seismic-hazard analysis and the process of earthquake rupture, *Bull. Seismol. Soc. Am.*, 98 (4), 1609–1632.
- Wesnousky, S.G., C.H. Scholz, K. Shimazaki, and T. Matsuda (1983), Earthquake frequency distribution and the mechanics of faulting, *J. Geophys. Res.*, 88(B11), 9331–9340
- Wesson, R.L., O.S. Boyd, C.S. Mueller, C.G. Bufe, A.D. Frankel, and M.D. Petersen (2007), Revision of Time-Independent Probabilistic Seismic Hazard Maps for Alaska, USGS Open File Report 2007-1043.

- Working Group on California Earthquake Probabilities (WGCEP, 2003), Earthquake Probabilities in the San Francisco Bay Region: 2002–2031, *U.S. Geol. Surv. Open File Rep. 03-214* (<http://pubs.usgs.gov/of/2003/of03-214/>).
- Working Group on California Earthquake Probabilities (WGCEP, 2008), The Uniform California Earthquake Rupture Forecast, Version 2 (UCERF2). USGS Open File Report 2007–1437, CGS Special Report 203, SCEC Contribution #1138. Appendix D: Earthquake Rate Model 2 of the 2007 Working Group for California Earthquake Probabilities, Magnitude–Area Relationships By Ross S. Stein
- Wyss, M. (1979), Estimating maximum expectable magnitude of earthquakes from fault dimensions. *Geology*, 7 (7), 336–340.
- Yamamoto, J.L., Quintanar, C.J. Rebollar, and Z. Jimenez (2002), Source characteristics and propagation effects of the Puebla, Mexico, earthquake of 15 June 1999, *Bull. Seismol. Soc. Am.*, 92(6), 2126–2138.
- Yeats, R. (2012), *Active faults of the world*, Cambridge University Press, Cambridge, England.
- Yeats, R.S., and R.J. Lillie (1991), Contemporary tectonics of the Himalayan frontal fault system: folds, blind thrusts and the 1905 Kangra earthquake, *Journal of Structural Geology*, 13, 215–225.
- Yeats, R.S., T. Nakata, A. Farah, M. Fort, M.A. Mira, M.R. Pandey, and R.S. Stein (1992), The Himalayan frontal fault system, *Ann. Tecton.*, 6: S85–S98.
- Yeats, R.S., K. Sieh, and C.R. Allen (1997), *The Geology of Earthquakes*, Oxford University Press, New York, USA.
- Yen, Y.-T., and K.-F. Ma (2011), Source-Scaling Relationship for M 4.6–8.1 Earthquakes, Specifically for Earthquakes in the Collision Zone of Taiwan, *Bull. Seism. Soc. Am.*, 101(2), 464–481.
- Yolsal, S., T. Taymaz, and A.C. YalÄşiner (2007), Understanding tsunamis, potential source regions and tsunami-prone mechanisms in the Eastern Mediterranean. *Geol. Soc. Spec. Publ.*, 291, 1, 201, 10.1144/SP291.10.
- Yoshioka, T., Y. Awata, Y. Shimokawa, and Y. Fusejima (2005), Explanatory text of the Rupture Probability Map of Major Active Faults in Japan, Tectonic Map Series 14, Geological Survey of Japan, AIST, Japan.
- Yule, D., S. Dawson, J. Lavé, S. Sapkota, and D. Tiwari (2006), Possible evidence for surface rupture of the Main Frontal Thrust during the great 1505 Himalayan earthquake, far-western Nepal, *Eos Trans. AGU*, 87(52), Fall Meet. Suppl., Abstract S33C-05.

Website references

1. Istituto Nazionale di Geofisica e Vulcanologia (INGV)

Database of Individual Seismogenic Sources (DISS) – Italy seismogenic source database

[Available at <http://diss.rm.ingv.it/diss/>]

2. United States Geological Survey (USGS)

Quaternary Faults and Folds Database – US active fault database

[Available at <http://earthquake.usgs.gov/hazards/qfaults/>]

3. United States Geological Survey (USGS)*National Seismic Hazard Maps – US seismogenic source database*[Available at http://gldims.cr.usgs.gov/webapps/cfusion/Sites/hazfaults_search/hf_search_main.cfm]**4. National Institute of Advanced Industrial Science and Technology (AIST)***RIO-DB Active Fault Database of Japan – Japan active fault database*[Available at http://riodb02.ibase.aist.go.jp/activefault/index_e.html]**5. National Research Institute for Earth Science Disaster Prevention (NIED)***Japan Seismic Hazard Information Station – Japan seismogenic source database (In Japanese)*[Available at <http://www.j-shis.bosai.go.jp/>]**6. GNS Science***New Zealand active fault database*[Available at <http://data.gns.cri.nz/af/>]**7. United States Geological Survey (USGS)***Slab models for global subduction zones – SLAB1.0*[Available at <http://earthquake.usgs.gov/research/data/slab/>]**8. Seismic Hazard Harmonization in Europe (SHARE)***SHARE project overview*[Available at <http://www.share-eu.org/node/70>]**9. Seismic Hazard Harmonization in Europe (SHARE)***Euro-Mediterranean seismogenic source database (access available to SHARE partners only)*[Available at <http://diss.rm.ingv.it/SHARE/>]**10. Earthquake Model in the Middle East Region (EMME)***Middle East active fault and seismogenic source database*[Available at <http://www.emme-gem.org/>]**11. New Zealand active faults database**[Available at http://riodb02.ibase.aist.go.jp/activefault/index_e.html]**12. Active fault database of Japan**[Available at http://riodb02.ibase.aist.go.jp/activefault/index_e.html]**13. Alaska Quaternary faults and folds**[Available at <http://www.dggs.alaska.gov/pubs/id/24956>]**14. USA Quaternary faults and folds**

[Available at <http://earthquake.usgs.gov/hazards/qfaults/>]

15. Australia neotectonic features

[Available at <http://www.ga.gov.au/earthquakes/staticPageController.do?page=neotectonics>]

THE GLOBAL EARTHQUAKE MODEL

The mission of the Global Earthquake Model (GEM) collaborative effort is to increase earthquake resilience worldwide.

To deliver on its mission and increase public understanding and awareness of seismic risk, the GEM Foundation, a non-profit public-private partnership, drives the GEM effort by involving and engaging with a very diverse community to:

- Share data, models, and knowledge through the OpenQuake platform
- Apply GEM tools and software to inform decision-making for risk mitigation and management
- Expand the science and understanding of earthquakes

GEM Foundation

Via Ferrata 1
27100 Pavia, Italy
Phone: +39 0382 5169865
Fax: +39 0382 529131
info@globalquakemodel.org
www.globalquakemodel.org

Copyright © 2015 GEM Foundation,
Christophersen, A., Berryman, K., Litchfield, N



Except where otherwise noted, this work is licensed under a **Creative Commons Attribution 3.0 Unported License**

APRIL 2015



GEM
GLOBAL EARTHQUAKE MODEL
working together to assess risk

The logo features a stylized circular icon with concentric lines to the left of the bold letters 'GEM'. Below this, the full name 'GLOBAL EARTHQUAKE MODEL' is written in a smaller, bold font, followed by the tagline 'working together to assess risk' in a regular font.